Oxidative Medicine and Cellular Longevity

Redox Signaling and Neural Control of Cardiovascular Function

Guest Editors: Hanjun Wang, Adam J. Case, Wei-Zhong Wang, Patrick J. Mueller, and Scott A. Smith

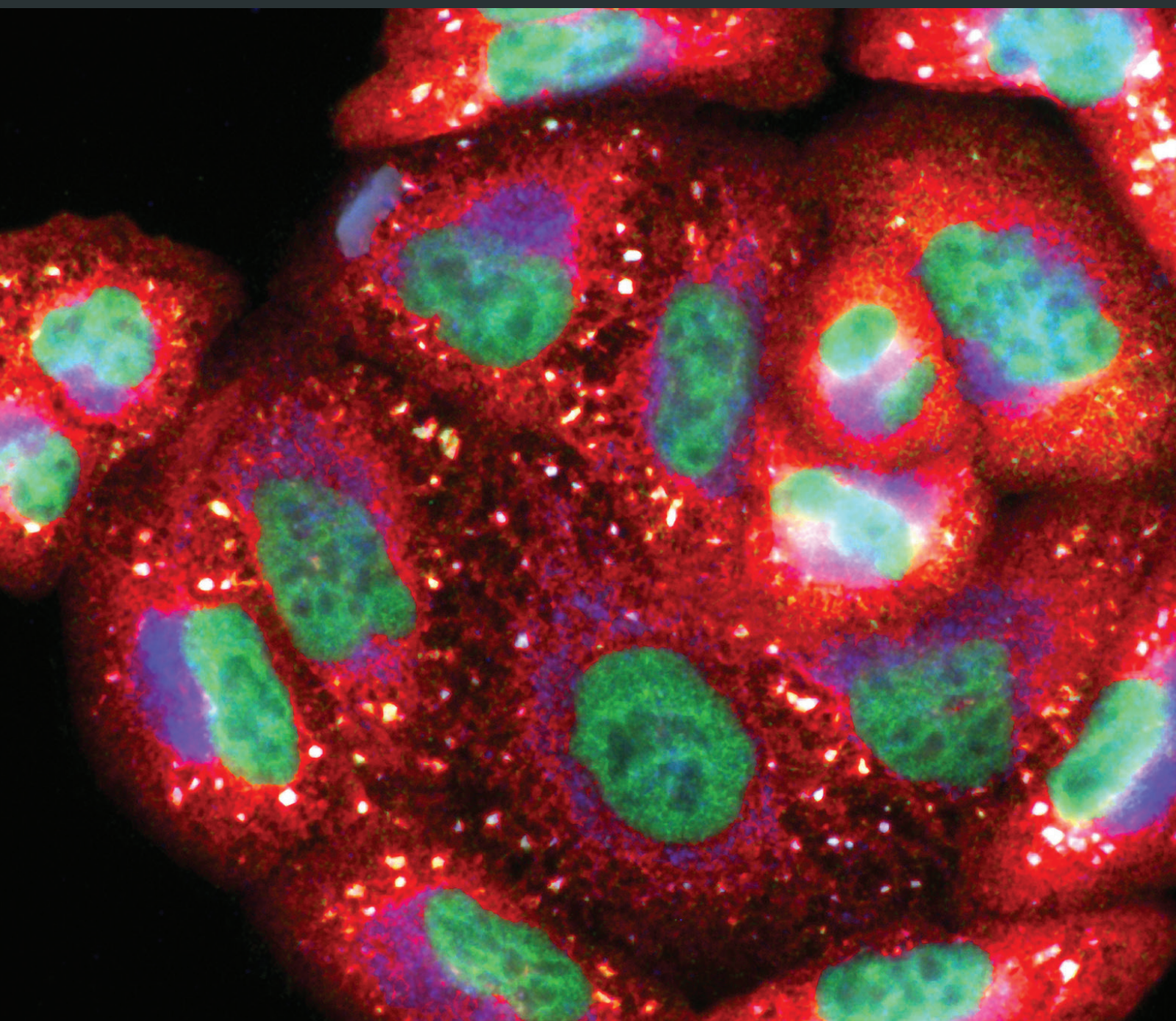

Redox Signaling and Neural Control of Cardiovascular Function

Oxidative Medicine and Cellular Longevity

Redox Signaling and Neural Control of Cardiovascular Function

Guest Editors: Hanjun Wang, Adam J. Case, Wei-Zhong Wang, Patrick J. Mueller, and Scott A. Smith

Editorial Board

Contents

Hindawi Publishing Corporation
Oxidative Medicine and Cellular Longevity
Volume 2016, Article ID 7086018, 2 pages
http://dx.doi.org/10.1155/2016/7086018

Editorial

Redox Signaling and Neural Control of Cardiovascular Function

Hanjun Wang,[1,2] Adam J. Case,[2] Wei-Zhong Wang,[3] Patrick J. Mueller,[4] and Scott A. Smith[5]

[1]*Department of Anesthesiology, University of Nebraska Medical Center, Omaha, NE 68198-4455, USA*
[2]*Department of Cellular and Integrative Physiology, University of Nebraska Medical Center, Omaha, NE 68198-5850, USA*
[3]*Department of Physiology, Second Military Medical University, 800 Xiangyin Road, Shanghai 200433, China*
[4]*Department of Physiology, Wayne State University, 5263 Scott Hall, 540 E. Canfield, Detroit, MI 48201, USA*
[5]*Departments of Health Care Sciences and Internal Medicine, UT Southwestern Medical Center, Dallas, TX 75390, USA*

Correspondence should be addressed to Hanjun Wang; hanjunwang@unmc.edu

Received 21 February 2016; Accepted 22 February 2016

Redox signaling has been widely reported to be involved in modulation of the cardiovascular system in both healthy and disease conditions. Redox imbalance such as oxidative stress contributes to the pathological process of many cardiovascular-related diseases such as diabetes, heart failure, and hypertension while also playing a negative role in the aging process [1–4]. Overactivation of the sympathetic nervous system (SNS) is a key event in each of these conditions. However, it is not fully understood how redox signaling interacts with the SNS in either aging or cardiovascular diseases. In this special issue, a number of contributions have been made to address this issue. An original research article by E. Moya et al. demonstrated that peroxynitrite formation mediates chronic intermittent hypoxia-induced hypertension via carotid body chemosensory potentiation. This study provides an excellent example that redox signaling can activate the SNS via an interaction with peripheral chemosensory afferents. On the other hand, J. P. Collister and colleagues reported that selective overexpression of superoxide dismutase (SOD) in one of the circumventricular organs (organum vasculosum of the lamina terminalis, OVLT) via injection of adenoviral vectors encoding human CuZnSOD (SOD1) significantly decreases blood pressure in an AngII-induced rat model of hypertension. This finding suggests that redox signaling in the central nervous system (e.g., OVLT) might play an important role in the development of AngII-induced hypertension. Finally, J. Hatcher and colleagues used SOD1 transgenic mice to determine the effect of reactive oxygen species (ROS) on arterial baroreflex sensitivity. They demonstrate that global overexpression of SOD1 preserves normal blood pressure (BP) and heart rate (HR) but enhances aortic depressor nerve function in mice. Although the authors did not further address the issue in which part of baroreflex arc was affected by overexpression of SOD1, this study did provide strong evidence that redox signaling might be involved in autonomic regulation.

In addition to identification and description of central mechanisms mediated by redox signaling, understanding how sex differences also contribute to these physiological processes is becoming increasingly important. In this special issue, original research articles by F. Hao et al. and S. Dai et al. highlight that female sex hormones, such as estrogen, are critical to the operation of central neural pathways that modulate cardiovascular function through antioxidant and anti-inflammation mechanisms. The article by F. Hao et al. reports that estrogen replacement reduces oxidative stress in the rostral ventrolateral medulla (RVLM) as well as sympathetic outflow in ovariectomized (OVX) rats. These findings elucidate a potential antioxidant role of estrogen in the central nervous system. The second article by S. Dai et al. suggests that the chronic antihypertensive and anti-inflammatory effects of Compound 21 (a selective angiotensin type 2 receptor (AT2R) agonist) in DOCA/NaCl-induced female hypertensive rats may function through female sex hormones. As evidence, these beneficial effects of Compound 21 could be abolished by OVX.

Several papers in this special issue also described new insights into the antioxidant therapeutic potential of various pharmacological and dietary compounds in spinal cord injury, asthma, and cardiomyopathy. M. Su and colleagues demonstrated a role for histone deacetylase-6 (HDAC6) in the protection of neurons after spinal cord injury and the

resulting hypoxia-ischemia insult. The investigators demonstrate that inhibition of HDAC6 *in vivo* and *in vitro* exacerbates ROS production and neuronal apoptosis, indicating that HDAC6 might serve as a new antioxidant target in neurotrauma. In another report in this issue, Y. Ma and colleagues provided evidence that an active compound found in figs and mulberries, known as morin, abrogated immune cell migration as well as cytokine production and ROS attenuating inflammatory processes in a model of asthma. This study highlights a novel profile of morin as a potent antioxidant and anti-inflammatory agent for asthma. In addition, a paper by M. Zhao et al. investigated the potential redox signaling pathways involved in cardiomyocyte hypertrophy induced by palmitic acid, the most common saturated fatty acid found in animals, plants, and microorganisms. These investigators demonstrated that palmitic acid-induced cardiomyocyte hypertrophy is associated with activation of necroptosis markers such as receptor interacting protein kinases (RIPK) 1 and 3. Moreover, the authors observed crosstalk between ER stress and necroptosis induced by palmitic acid. They suggested that mammalian target of rapamycin (mTOR) signaling was a key factor mediating the palmitic acid-induced activation of necroptosis and cardiac hypertrophy. Finally, the article by T. Dong et al. provided a very interesting observation that renal denervation slowed the development of deep venous thrombosis (DVT). They utilized several different measures to show that the mechanisms related to DVT are related to oxidative stress, as antioxidants such as tempol (small molecule superoxide scavenger) could achieve a protective effect similar to renal denervation. These findings extend our understanding of how neurons may affect the circulation via interactions with redox signaling.

The final topic of this special issue is related to exercise. It is well known that acute exercise can dramatically increase ROS production whereas long-term exercise training (ExT) plays an antioxidant and anti-inflammatory role [5–7]. Two papers in this special issue are focused on the ExT-mediated cardiovascular benefits in hypertension and diabetes, respectively. C. Ren and colleagues examined the effects of ExT on the components of brain renin-angiotensin system in the RVLM of spontaneously hypertensive rats (SHR). The data indicated that ExT for 12 weeks decreased the expression of ACE and AT-1R in the RVLM but increased the expression of ACE-2 and Mas receptors. Therefore, the authors concluded that ExT improves hypertension via resetting the balance of ANG II and ANG 1–7 at the level of the RVLM. N. Sharma and colleagues reported that ExT significantly reduced expression of NADPH oxidase subunits p47 and p67 in hearts of streptozotocin-induced diabetic rats. They also confirm that ExT reduced the elevated levels of collagen type III in diabetic hearts. Taken together, these data suggest that ExT attenuates oxidative stress in the diabetic heart. This new evidence is useful to our understanding of the beneficial effects of ExT on the cardiac extracellular matrix, cardiac function, and cardiac remodeling in diabetes.

In summary, the articles presented in this special issue highlight the current advances in the research fields of redox biology, neural science, and exercise physiology. These articles enrich our understanding of how redox signaling interacts within the nervous system both at rest and during exercise. Moreover, the works highlight the therapeutic potential of antioxidants as effective treatments for various cardiovascular and neural diseases.

Acknowledgments

We would like to thank the reviewers for their expert assistance and all authors for the contribution to this issue. The editors acknowledge their individual funding that aided in the development of this special issue: the American Heart Association (no. 12SDG12040062 to Hanjun Wang; no. 15GRNT25810010 to Patrick J. Mueller) and the National Institutes of Health (NIH 1R01HL121012-A1 to Hanjun Wang; NIH 1R01HL126796-A1 to Hanjun Wang; NIH K99HL123471 to Adam J. Case; NIH R01 HL096787-05 to Patrick J. Mueller; NIH RO1HL088422 to Scott A. Smith), and the National Natural Science Foundation of China (NSFC 81170240, 81370363, and 81570385 to Wei-Zhong Wang).

Hanjun Wang
Adam J. Case
Wei-Zhong Wang
Patrick J. Mueller
Scott A. Smith

References

[1] H. Cai and D. G. Harrison, "Endothelial dysfunction in cardiovascular diseases: the role of oxidant stress," *Circulation Research*, vol. 87, no. 10, pp. 840–844, 2000.

[2] N. R. Madamanchi and M. S. Runge, "Redox signaling in cardiovascular health and disease," *Free Radical Biology and Medicine*, vol. 61, pp. 473–501, 2013.

[3] C. Heymes, J. K. Bendall, P. Ratajczak et al., "Increased myocardial NADPH oxidase activity in human heart failure," *Journal of the American College of Cardiology*, vol. 41, no. 12, pp. 2164–2171, 2003.

[4] E. J. Henriksen, M. K. Diamond-Stanic, and E. M. Marchionne, "Oxidative stress and the etiology of insulin resistance and type 2 diabetes," *Free Radical Biology and Medicine*, vol. 51, no. 5, pp. 993–999, 2011.

[5] S. K. Powers, W. B. Nelson, and M. B. Hudson, "Exercise-induced oxidative stress in humans: cause and consequences," *Free Radical Biology and Medicine*, vol. 51, no. 5, pp. 942–950, 2011.

[6] M.-C. Gomez-Cabrera, E. Domenech, and J. Viña, "Moderate exercise is an antioxidant: upregulation of antioxidant genes by training," *Free Radical Biology and Medicine*, vol. 44, no. 2, pp. 126–131, 2008.

[7] S. A. Phillips, A. M. Mahmoud, M. D. Brown, and J. M. Haus, "Exercise interventions and peripheral arterial function: implications for cardio-metabolic disease," *Progress in Cardiovascular Diseases*, vol. 57, no. 5, pp. 521–534, 2015.

Hindawi Publishing Corporation
Oxidative Medicine and Cellular Longevity
Volume 2016, Article ID 5868913, 11 pages
http://dx.doi.org/10.1155/2016/5868913

Research Article

Exercise Training Attenuates Upregulation of $p47^{phox}$ and $p67^{phox}$ in Hearts of Diabetic Rats

Neeru M. Sharma,[1] Brandon Rabeler,[1] Hong Zheng,[1] Eugenia Raichlin,[2] and Kaushik P. Patel[1]

[1]*Department of Cellular & Integrative Physiology, University of Nebraska Medical Center, Omaha, NE 68198, USA*
[2]*Division of Cardiology, University of Nebraska Medical Center, Omaha, NE 68198, USA*

Correspondence should be addressed to Kaushik P. Patel; kpatel@unmc.edu

Received 14 July 2015; Revised 24 September 2015; Accepted 21 December 2015

Academic Editor: José Luís García-Giménez

Exercise training (ExT) is currently being used as a nonpharmacological strategy to improve cardiac function in diabetic patients. However, the molecular mechanism(s) underlying its beneficial effects remains poorly understood. Oxidative stress is known to play a key role in the pathogenesis of diabetic cardiomyopathy and one of the enzyme systems that produce reactive oxygen species is NADH/NADPH oxidase. The goal of this study was to investigate the effect of streptozotocin- (STZ-) induced diabetes on expression of $p47^{phox}$ and $p67^{phox}$, key regulatory subunits of NADPH oxidase, in cardiac tissues and determine whether ExT can attenuate these changes. Four weeks after STZ treatment, expression of $p47^{phox}$ and $p67^{phox}$ increased 2.3-fold and 1.6-fold, respectively, in left ventricles of diabetic rats and these increases were attenuated with three weeks of ExT, initiated 1 week after onset of diabetes. In atrial tissues, there was increased expression of $p47^{phox}$ (74%), which was decreased by ExT in diabetic rats. Furthermore, increased collagen III levels in diabetic hearts (52%) were significantly reduced by ExT. Taken together, ExT attenuates the increased expression of $p47^{phox}$ and $p67^{phox}$ in the hearts of diabetic rats which could be an underlying mechanism for improving intracardiac matrix and thus cardiac function and prevent cardiac remodeling in diabetic cardiomyopathy.

1. Introduction

Diabetes mellitus (DM) is leading metabolic disease with the highest morbidity and mortality and according to 2014 estimate of International Diabetes Federation the disease now affects more than 387 million people worldwide. DM is associated with an increased risk of cardiovascular complications, including hypertension and coronary artery disease [1]. There is growing recognition of diabetic cardiomyopathy, a primary myocardial disease, defined as either systolic or diastolic left ventricular dysfunction in otherwise healthy diabetic person. This is one of the most serious complications of diabetes; however, the underlying mechanism/s for this dysfunction are not clearly understood [2, 3]. Originally, Rubler et al. in 1972 [4], based on postmortem findings, proposed that diabetic cardiomyopathy is secondary to underlying hyperglycemia resulting in a multitude of adverse downstream effects, including impaired myocyte calcium handling, renin-angiotensin-aldosterone activation, microangiopathy, myocardial fibrosis, and increased oxidative stress [5–7]. Mechanistically, chronic hyperglycemia exerts oxidative stress to cardiomyocytes by the production of reactive oxygen species (ROS) culminating in these pathological abnormalities [8, 9]. Indeed, a number of studies have reported increased ROS formation in cultured cells exposed to high glucose concentrations. Similarly, in animal models of diabetes, ROS are generated as natural byproducts of oxygen metabolism and their moderate levels are thought to function as intracellular signaling molecules; however, high levels of ROS are detrimental to cardiomyocytes and lead to cell death, mitochondrial dysfunction due to mitochondrial fragmentation [10], or impaired insulin signaling [11]. ROS contribute to inducing various cardiovascular complications including cardiac dysfunction accelerated by inflammation, apoptosis, and

fibrosis [12–14]. Furthermore, O_2^- has been shown to impair nitric oxide (NO) dependent vasodilation [15, 16] and thus enhance endothelium-dependent vasoconstriction [17, 18] and precipitate cardiomyocyte hypertrophy [19].

ROS is generated by all cell types within the heart, including cardiomyocytes, endothelial cells, vascular smooth muscle cells (VSMCs), fibroblasts, and infiltrating inflammatory cells [20]. Nicotinamide adenine dinucleotide phosphate (NADPH) oxidases (NOXs) are membrane-associated enzymes which are the primary physiological producers of O_2^- [21] and ROS [20, 22]. NOXs consist of 4 major subunits: a plasma membrane-spanning cytochrome b_{558} composed of a large $gp91^{phox}$ subunit and a smaller $p22^{phox}$ subunit, whereas 2 cytosolic subunits are $p47^{phox}$ and $p67^{phox}$. Endothelial cells (ECs) and myocytes express all four components of NADPH oxidase [23, 24], while VSMCs express all of the subunits with the exception of $p67^{phox}$ subunit [25]. The low molecular weight G protein rac2 (in some cells rac1) participates in the assembly of the active complex, and a second G protein, rap1A, is thought to be involved in the deactivation of NADPH oxidase enzyme activity.

DM is associated with increased levels of Ang II [26–30] and numerous studies have shown that Ang II upsurges production of O_2^- by activating NADPH oxidases [31–34] in VSMCs [35–37], adventitial fibroblasts [32, 38], ECs [33, 39], and cardiomyocytes [34]. Additionally, hyperglycemia, a key clinical manifestation of diabetes, also produces ROS via NADPH oxidase activation by glycation end products [40], while blocking of ROS formation is known to prevent hyperglycemic damage [41]. In rat ventricular myocytes, high glucose conditions induced cardiac contractile dysfunction and cardiomyopathy occurs via Ang II type 1 receptor (AT_1R) mediated activation of NADPH oxidase [27, 28, 30]. High glucose conditions may also increase the activity of NADPH oxidase by increasing the expression of its various subunits resulting in increased production of ROS [8, 42]. Infusion of Ang II has also been shown to increase NADPH oxidase activity and O_2^- production by increasing expression of $p67^{phox}$ and $gp91^{phox}$ in aortic adventitial cells [32]. Exposure of ventricular myocytes to high glucose also increases expression of $p47^{phox}$ and production of ROS and these increases were blocked by AT_1R antagonist, L-158,809 [42]. Additionally, Hink et al. [43] found increased NADPH oxidase activity and a 7-fold increase in $gp91^{phox}$ mRNA in aortic tissue from rats with streptozotocin- (STZ-) induced diabetes.

Aerobic exercise of moderate intensity and frequency is one of a number of cardiac rehabilitation programs prescribed to patients with chronic heart failure [44]. Exercise training (ExT) reduces blood glucose, body fat, and insulin resistance and improves glycemic control, lipid metabolism, and baroreflex sensitivity in diabetes [45–48]. Additionally, ExT lowers plasma Ang II levels [49–51] and reduces renal sympathetic nerve activity and arterial pressure responses to Ang II [50–53]. Previous studies have also shown that ExT increases expression of superoxide dismutase (SOD), catalase, and glutathione in cardiac tissues [49, 54–56]. The ability of these antioxidant enzymes to reduce ROS has also been well documented [57, 58]. However, the impact of ExT on NADPH oxidase activity and expression of its subunits in diabetes is not entirely clear. These findings have led us to investigate whether diabetes-induced cardiac dysfunction may be due in part to increased expression of $p47^{phox}$ and $p67^{phox}$ and further whether ExT could improve/attenuate the increased expression of these subunits induced by diabetes.

2. Materials and Methods

2.1. Induction and Verification of Experimental Diabetes. Animals used for this study were approved by the Animal Care and Use Committee of the University of Nebraska Medical Center and all experiments were conducted according to the APS's *Guiding Principles for Research Involving Animals and Human Beings* and the *National Institutes of Health Guide for the Care and Use of Laboratory Animals*. Male Sprague-Dawley rats weighing between 180 and 190 g were purchased from Sasco Breeding Laboratories (Omaha, NE). After 1 week of acclimatization in housing facilities diabetes was induced by a single intraperitoneal injection (65 mg/kg) of streptozotocin (STZ, Sigma) in a 2% solution of cold 0.1 M citrate buffer (pH 4.5). Onset of diabetes was identified by polydipsia, polyuria, and blood glucose levels >250 mg/dL. Control animals were injected with citrate buffer containing no STZ. Throughout the study, animals were housed in pairs (similar weights to minimize dominance) at 22°C with fixed 12 h light/dark cycles and humidity at 30–40%. Laboratory chow (Harlan, Madison, WI) and tap water were available *ad libitum*. Experiments were performed 4 weeks after the injection of STZ or vehicle.

2.2. Exercise Protocol. After one week, rats in each of control and diabetic groups were randomly divided into two groups. One subgroup of control and one subgroup of diabetic rats remained sedentary, while the other two subgroups were subjected to ExT according to the protocols used by Musch and Terrell [59] with modifications [60] for three weeks after one week after diabetes induction. The resulting four subgroups of animals were referred to as nonexercised controls (Sed-control, $n = 16$), diabetic nonexercise (Sed-Dia, $n = 16$), exercise trained controls (ExT-control, $n = 20$), and exercise trained diabetic (ExT-Dia, $n = 20$). During the training period, rats were exercised between 5 and 15 min/day at an initial treadmill speed of 10 m/min up a 0% grade for 5 days. In order to ensure a significant endurance ExT regimen, the treadmill grade and speed were gradually increased to 10% and 25 m/min, respectively, and the exercise duration was increased to 60 min/day. Animals demonstrating the ability to run steadily on the treadmill with very little or no prompting (with electrical stimulation) were used in the study. The Sed-control and Sed-Dia rats were treated similarly to the ExT-control and ExT-Dia subgroup and handled daily except for the treadmill running.

2.3. Sample Collection. At the end of the *in vivo* protocol, animals in all four subgroups (Sed-control, Sed-Dia, ExT-control, and ExT-Dia) were anesthetized using overdose of pentabarbital (65 mg/kg, i.p.). Chest cavities were opened and hearts were removed, quick-frozen by dropping into liquid

nitrogen, and stored at −80°C. Soleus muscle from hind legs was also removed, quick-frozen, and stored at −80°C.

2.4. Citrate Synthase Assay. The efficacy of ExT was assessed by measuring citrate synthase activity in whole muscle homogenate as previously described [51, 61]. Citrate synthase activities were normalized to total protein content and reported as micromoles per milligram protein per minute.

2.5. Semiquantitative RT-PCR. Relative levels of $p47^{phox}$ and $p67^{phox}$ in left and right ventricles and atria tissues were determined using semiquantitative RT-PCR. One hundred micron (100 μm) thick coronal sections were cut on a cryostat from the left and right ventricles and a 15-gauge needle stub was used to punch atrial samples. Total RNA from left ventricle, right ventricle, and atrial tissue was isolated by TRI Reagent (MRC) method as per the manufacturer's instructions as previously described [62, 63]. Equivalent amounts of total RNA (1 μg) from each of Sed-control, Sed-Dia, ExT-control, and ExT-Dia rats were then reverse-transcribed for 40 min at 37°C in the presence of 1.5 μM of random hexamers and 100 U of MMLV-Reverse transcriptase. Primers for $p47^{phox}$ and $p67^{phox}$ (200 nM) were used in polymerase chain reactions to determine the amount of transcripts in each sample. β-actin was coamplified as an internal control. After 10 min of denaturing at 94°C, the amplification was performed at 94°C for 1 min, at 56°C for 1 min, and at 72°C for 1 min for 33 cycles with the final extension at 72°C for 10 min. At the end of the reaction, 7 μL from each PCR reaction was mixed with Blue/Orange loading dye (Promega) and electrophoresed for 45 min at 100 V using 1% agarose gels containing ethidium bromide. The gels were visualized with gel doc system (Kodak ID gel Imager). Band intensities were then analyzed with the Kodak analysis software and normalized to that of their respective β-actin bands. Oligoprimers for PCR were synthesized in-house at University of Nebraska Medical Center. Sequences of primers used were as follows: $p47^{phox}$: 5′-ACCTGTCGGAGAAGGTGGT (forward), 5′-TAGGTCTGAAGGATGATGGG (reverse); $p67^{phox}$: 5′-AGGACTATCTGGGCAAGGC (forward), 5′-GCTGCGACTGAGGGTGAAT (reverse); β-actin 5′-GGGAAATCGTGCGTGACATT (forward), 5′-CGGATGTCAACGTCACACTT (reverse).

2.6. Western Blotting. Western blot analyses were used to determine $p47^{phox}$ and $p67^{phox}$ in the left ventricle, right ventricle, and atria tissues in the four subgroups of rats. Protein was extracted from the heart after homogenization in RIPA buffer (cat. number BP-115, Boston BioProducts, Worcester, MA, USA) supplemented with 1 mM phenylmethylsulfonyl fluoride and protease inhibitor cocktail. Collagen III levels were measured as an index of myocardial stiffness (diabetic cardiomyopathy) in atrial tissue. 30–40 μg of each protein sample was mixed with an equal volume of 4% SDS sample buffer, fractionated on 7.5% polyacrylamide-sodium dodecyl sulfate gel, and transferred to a PVDF membrane (Millipore). After transfer, the membranes were blocked with 5% nonfat dry milk powder in TBST (20 mM Tris/HCl, pH 7.4, 150 mM NaCl, 0.1% (v/v) Tween 20) at room temperature for 1 h. Subsequently, membranes were probed with a primary anti-$p47^{phox}$ rabbit polyclonal or anti-$p67^{phox}$ rabbit polyclonal or anti-collagen III goat polyclonal antibody from Santa Cruz Biotechnology overnight at 4°C followed by incubation with a corresponding peroxidase-conjugated secondary antibody for one hour. The signals were visualized using an enhanced chemiluminescence (Pierce Chemical, Rockford) and detected by a UVP digital imaging system. ImageJ-NIH program was used to quantify the signal.

Table 1: Characteristics of the Sed-control, Sed-Dia, ExT-control, and ExT-Dia groups. $n = 10$ in each group. Values represent mean ± S.E. $^{*}P < 0.01$ versus Sed-control. $^{\#}P < 0.05$ versus Sed-Dia group.

	Sed-control ($n = 10$)	Sed-Dia ($n = 10$)	ExT-control ($n = 10$)	ExT-Dia ($n = 10$)
Body weight (g)	323 ± 7	209 ± 7*	226 ± 2*	208 ± 12*
Blood glucose (mg/dL)	72 ± 6	362 ± 18*	78 ± 7	315 ± 11#
Citrate synthase (mmol/g/min)	4.58 ± 0.34	4.01 ± 0.42	6.93 ± 0.56*	6.94 ± 0.56*

2.7. Statistical Analysis. Data was presented as mean ± SEM and subjected to Student-Newman-Keuls test. P values < 0.05 were considered to indicate statistical significance.

3. Results

3.1. General Characteristics of Animals. Table 1 summarizes the characteristics of the Sed-control, Sed-Dia, ExT-control, and ExT-Dia animals used in the present study. Mean body weight of all animals at the start of the study was 186 ± 2 g. As shown in Table 1, after 28 days, the mean body weight of Sed-control animals increased to 323 ± 7 g, whereas the mean body weight of ExT-control animals was 226 ± 2 g. Mean body weight of sedentary and exercised trained diabetic animals increased modestly to 209 ± 7 and 208 ± 12 g, respectively. In the animals injected with citrate buffer only, mean blood glucose levels did not change significantly during the study (72.0 ± 6.0 mg/dL at start and 78.0 ± 7.0 mg/dL at the time of sacrifice). Sed-Dia animals had significant high blood glucose levels at the time of sacrifice, 362 ± 18 mg/dL, whereas ExT had significantly lowered blood glucose levels, 315 ± 11 mg/dL. We have used citrate synthase activity as a marker of increased aerobic metabolism in the soleus muscle. The enzyme citrate synthase catalyzes the formation of citrate from acetic acid and oxaloacetic acid in the first step of Krebs cycle. Regular exercise increases the size and number of skeletal muscle mitochondria to increase respiratory capacity of the muscle. Increased mitochondria translate to increased citrate synthase activity, reflecting the increased activity of muscle associated with ExT [51, 61]. Cardiac muscle does not increase respiratory capacity in response to ExT as skeletal

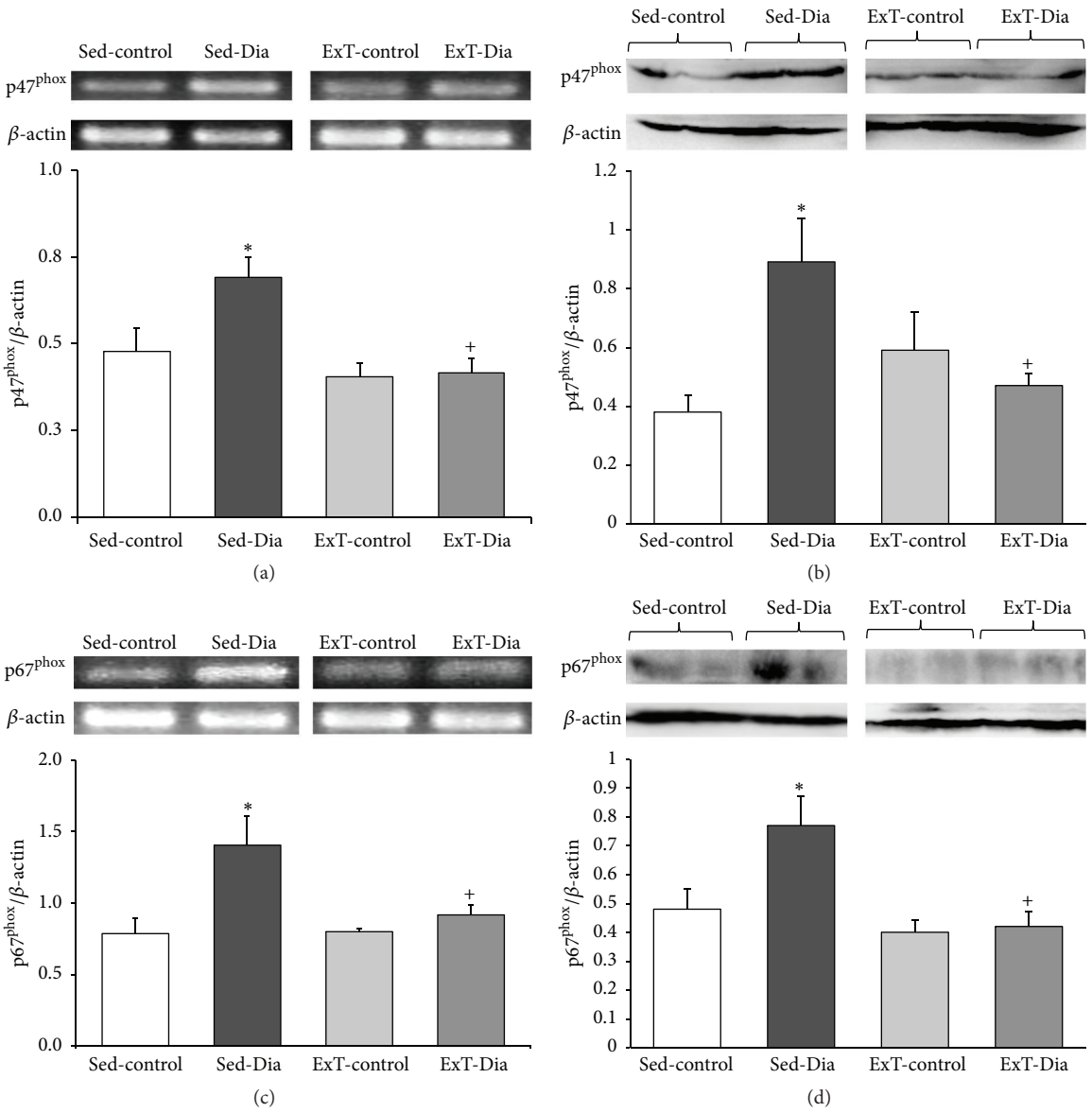

Figure 1: Expression of left ventricle p47^{phox} and p67^{phox} in Sed-control, Sed-Dia, ExT-control, and ExT-Dia animals. (a) RT-PCR of p47^{phox}: top: a representative gel; bottom: quantification of p47^{phox} transcript normalized to β-actin as loading control. $n = 10$ in each group. (b) Western blot analysis of left ventricle p47^{phox} in four groups: top: a representative gel; bottom: bar graph of summary data of densitometry analyses of p47^{phox} protein level normalized to actin for loading variations. $n = 6$–8 in each group. Values represent mean ± S.E. (c) RT-PCR of left ventricle p67^{phox} in Sed-control, Sed-Dia, ExT-control, and ExT-Dia animals: top: a representative gel; bottom: quantification of p67^{phox} transcript normalized to β-actin as loading control. $n = 6$ in each group. (d) Protein expression of p67^{phox} in four groups: top: a representative Western blot; bottom: densitometry analysis of p67^{phox} protein normalized to β-actin as loading control. $n = 3$-4 in each group. Values are represented as mean ± S.E. $^{*}P < 0.05$ versus Sed-control. $^{+}P < 0.05$ versus Sed-Dia group.

muscle does [64]. Therefore measuring the citrate synthase activity in soleus muscle is extensively used as a metabolic marker in assessing oxidative and respiratory capacity. In the current study, Sed-control and diabetic animals had a lower citrate synthase activity (4.58 ± 0.34 μmol/g/min and 4.01 ± 0.42 μmol/g/min, resp.) than ExT animals (6.93 ± 0.56 μmol/g/min for ExT-control and 6.94 ± 0.56 μmol/g/min for ExT-diabetic). These data also indicate that similar level of ExT was performed in the two groups of animals.

3.2. Increased Expression of p47^{phox} and p67^{phox} in Left Ventricle Alleviated with ExT in Diabetic Animals. Expressions of p47^{phox} and p67^{phox} were determined by semiquantitative RT-PCR and Western blot using actin as an internal reference in four groups of rats, namely, Sed-control, Sed-Dia, ExT-control, and ExT-Dia (Figure 1). There were significantly increased transcripts of p47^{phox} I (45.8% increase) and protein (2.3-fold) in the left ventricle of 4-week Sed-Dia versus 4-week Sed-control rats (Figures 1(a) and 1(b)).

Sed-Dia animals also demonstrated increased steady-state levels of mRNA encoding $p67^{phox}$ (increased 78.1% of the 4-week Sed-control) (Figure 1(c)) and protein (1.6-fold) (Figure 1(d)) in the left ventricle. Three weeks of ExT, initiated after 1 week of diabetes, reduced mRNA and protein levels of $p47^{phox}$ and $p67^{phox}$ in the left ventricle of the heart to levels similar to those of the ExT controls (≈40–50% less than Sed-Dia).

3.3. Increased Expression of $p47^{phox}$ and $p67^{phox}$ in Right Ventricle Alleviated with ExT in Diabetic Animals. Similar to the left ventricle, 4 weeks of diabetes also increased $p47^{phox}$ mRNA and protein expression in the right ventricle, albeit not reaching statistical significance compared to Sed-control (Figure 2(a)). Steady-state levels of mRNA encoding $p67^{phox}$ in the right ventricle of the heart increased slightly (17.7%). However, there were no significant differences in $p67^{phox}$ protein expression between the two groups (Figures 2(c) and 2(d)). Three weeks of ExT regimen attenuated the increase in steady-state levels of mRNA encoding $p47^{phox}$ to similar levels in ExT-control and ExT-Dia groups.

3.4. Increased Expression of $p47^{phox}$ and $p67^{phox}$ in the Atria Alleviated with ExT in Diabetic Animals. As shown in Figure 3, steady-state levels of mRNA encoding $p47^{phox}$ and $p67^{phox}$ were increased significantly in atria of the diabetic group. The increase was 30.1% for $p47^{phox}$ and 35.5% for $p67^{phox}$ over sedentary controls (Figures 3(a) and 3(c)). As expected, three weeks of ExT, initiated after 1 week of diabetes, significantly lowered mRNA levels of $p47^{phox}$ and $p67^{phox}$ in the atria of ExT-Dia heart compared to Sed-Dia group. Protein expression of $p47^{phox}$ was increased 74%, while $p67^{phox}$ protein expression increased but did not reach statistical significance (Figures 3(b) and 3(d)). Interestingly, $p47^{phox}$ mRNA and protein expression in ExT-control and ExT-Dia atria was decreased to almost similar levels suggesting that ExT attenuated the increase in steady-state levels of $p47^{phox}$ expression in atria.

3.5. Increased Expression of Arterial Collagen III Is Alleviated with ExT in Diabetic Animals. As shown in Figure 4, expression of the extracellular matrix protein collagen III significantly increased by 53% in 4 weeks Sed-Dia group. This increase in steady-state levels of collagen III suggests increasing ventricular stiffening, a characteristic feature of diabetic cardiomyopathy. Three weeks of ExT initiated after 1 week of STZ-induced diabetes attenuated the increase in collagen III protein expression (38%) in the diabetic group at the same level as control, while three weeks of ExT had no effect on collagen III expression in nondiabetic control animals.

4. Discussion

The principal finding of the present study is that expression of the cytosolic subunits of NADPH oxidase, $p47^{phox}$ and $p67^{phox}$, is upregulated in hearts of STZ-induced diabetic rats and the increased expression was attenuated with ExT. Since ExT was initiated after 1 week of diabetes, it is likely that it is preventing or minimizing rather than reversing the increase in expression induced by diabetes. Previously, we have reported that Sed-Dia animals demonstrated significant reductions in fractional shortening, ejection fraction, stroke volume, and cardiac output compared with Sed-control animals and ExT (for 3 weeks) implemented 4 weeks after the onset of diabetes significantly increased percent ejection fraction, attenuated the increase in left ventricular end-systolic diameter, and improved dP/dt and isoproterenol induced increase in dP/dt in the diabetic group [60]. It is possible that these changes in expression of NADPH oxidase subunits in the heart are associated with improvement in cardiac function in diabetes.

There is increasing information that mitochondria and NADPH oxidase play a fundamental role in ROS production in the diabetic heart [12]. Furthermore, ROS-mediated increase in peroxynitrite formation induces apoptosis in cardiomyocytes *in vitro* and in the myocardium *in vivo* as shown by Levrand et al. [65] suggesting that oxidative stress is a common mediator for apoptosis induced cardiac damage in diabetic rats [13]. Our data suggest that the increased oxidative stress levels observed in diabetic hearts may be in part due to the upregulation of NADPH oxidase subunits and this change can be alleviated by ExT. These results suggest that beneficial effects of ExT may involve improvement in oxidative stress commonly observed in diabetic cardiomyopathy.

Diabetic cardiomyopathy, one of the leading causes of increased morbidity and mortality in the diabetic population, is characterized by the prolongation of action potential duration, delayed cytosolic Ca^{2+} clearance, and impaired systolic and diastolic left ventricular function [42, 60]. Several factors are believed to contribute to the pathogenesis of diabetic cardiomyopathy, including insulin resistance, enhanced renin-angiotensin system activation, hyperglycemia, and damage from ROS [66]. These pathophysiological factors associated with diabetes, including hyperglycemia and elevated Ang II levels, have been shown to increase the expression of NADPH oxidase subunits and the enzyme's activity [32, 43, 67] leading to myocardial oxidative stress. A pivotal role of NADPH oxidase in Ang II-induced cardiac hypertrophy and interstitial fibrosis was demonstrated by using mice with targeted disruption of the NADPH oxidase subunit $gp91^{phox}$ [34]. $p47^{phox}$ subunit of NADPH oxidase has also been demonstrated to play a key role in the enzyme's activation by agonists. Using $p47^{phox}$ knockout mice and $p47^{phox}$ cDNA transfection and antisense techniques, Li et al. [68] demonstrated the necessity of $p47^{phox}$ subunit for the activation of NADPH oxidase when exposed to the agonists Ang II, TNF-α, or phorbol 12-myristate 13-acetate, an activator of protein kinase C. The phosphorylation of $p47^{phox}$ is believed to induce conformational changes that facilitate its binding to the other cytosolic subunits, including $p67^{phox}$, and their subsequent binding to the membrane-bound cytochrome b_{558} to allow optimal O_2^- production [69]. Precise mechanisms underlying agonist-induced nonphagocytic NADPH oxidase activation are not yet understood, but it is clear that both

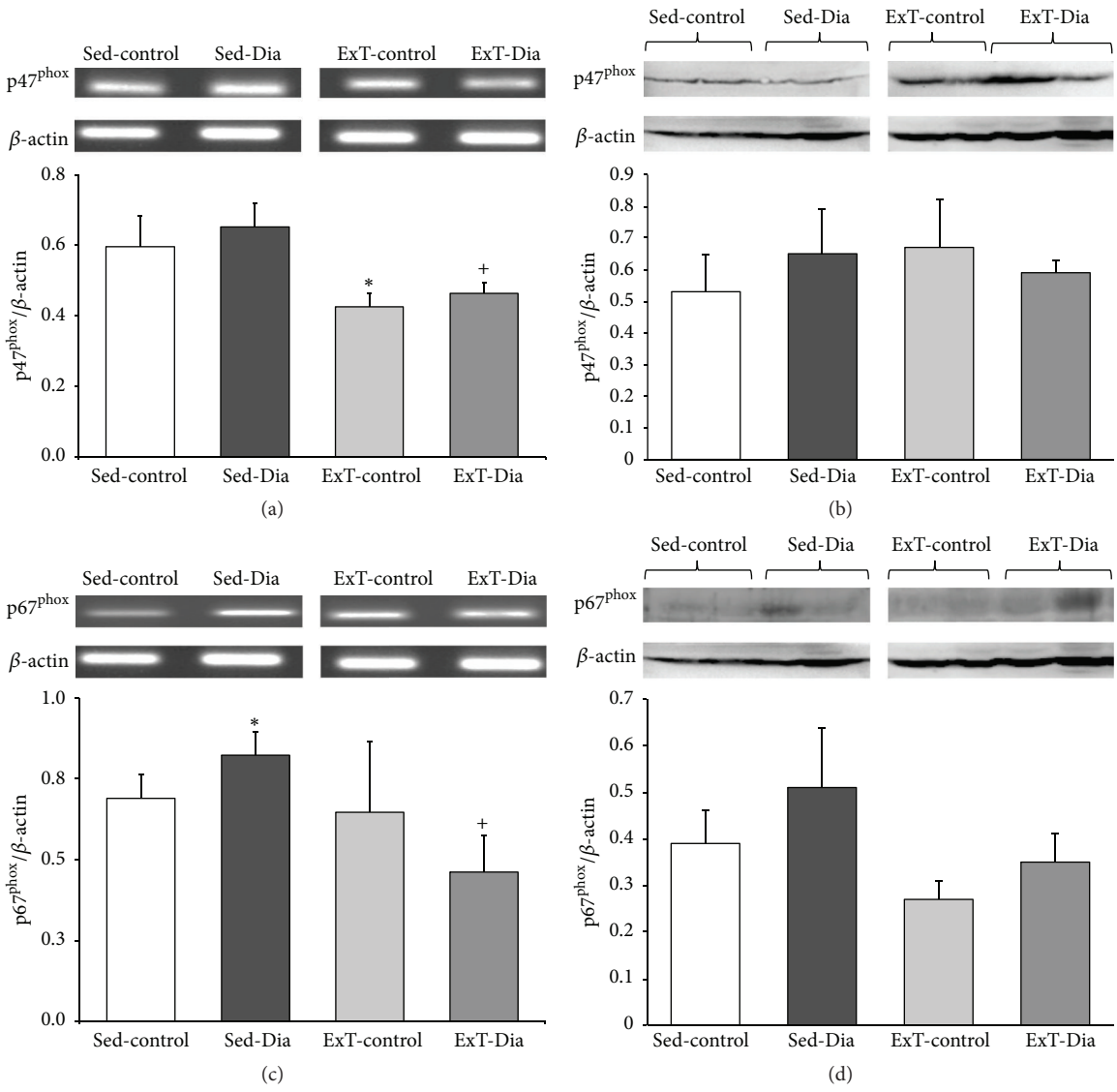

Figure 2: Expression of right ventricle p47^{phox} and p67^{phox} in Sed-control, Sed-Dia, ExT-control, and ExT-Dia animals. (a) RT-PCR of p47^{phox}: top: a representative gel; bottom: bar graph shows quantification of densitometry analysis of p47^{phox} normalized to β-actin. $n = 10$ in each group. Values represent mean ± S.E. (b) Protein expression of p47^{phox} in four groups: top: a representative gel; bottom: densitometry analyses of p47^{phox} protein level normalized to actin. $n = 3$-4 in each group. Values represent mean ± S.E. (c) RT-PCR of right ventricle p67^{phox} in Sed-control, Sed-Dia, ExT-control, and ExT-Dia animals: top: a representative gel; bottom: quantification of p67^{phox} transcript normalized to β-actin as loading control. $n = 6$ in each group. (d) Protein expression of p67^{phox} in four groups: top: a representative Western blot; bottom: densitometry analysis of p67^{phox} protein normalized to β-actin as loading control. $n = 3$-4 in each group. Values are represented as mean ± S.E. $^{*}P < 0.05$ versus Sed-control. $^{+}P < 0.05$ versus Sed-Dia group.

acute protein modification and chronic changes in expression levels may be involved.

Our findings indicate that the cardiac tissue expressions for p47^{phox} and p67^{phox} are upregulated in the diabetic rats. This upregulation was greatest in the left ventricle and atria, while it was slightly elevated in the right ventricle of the diabetic group. These findings are consistent with clinical data showing an association of DM with an increased risk of systolic, diastolic, and any left ventricular dysfunction and the relative sparing of the right ventricle [1, 2]. In ventricular myocytes, it was reported that hyperglycemic conditions increase the production of ROS via an enhanced expression of p47^{phox} protein, which could be blocked by an AT_1R antagonist [42]. Cifuentes et al. [32] have also shown that Ang II infusion, via the AT_1R activation, induces an enhanced expression of p67^{phox} and gp91^{phox} proteins in aortic adventitia. Additionally, an increased NADPH oxidase activity and a 7-fold upregulation of gp91^{phox} mRNA in aortic tissue have been reported in STZ-induced diabetic rats [43]. Furthermore, increased NADPH oxidase activity and collagen 3 were demonstrated in pathogenesis of the heart failure as seen in hearts of Duchenne muscular dystrophy rat model [70]

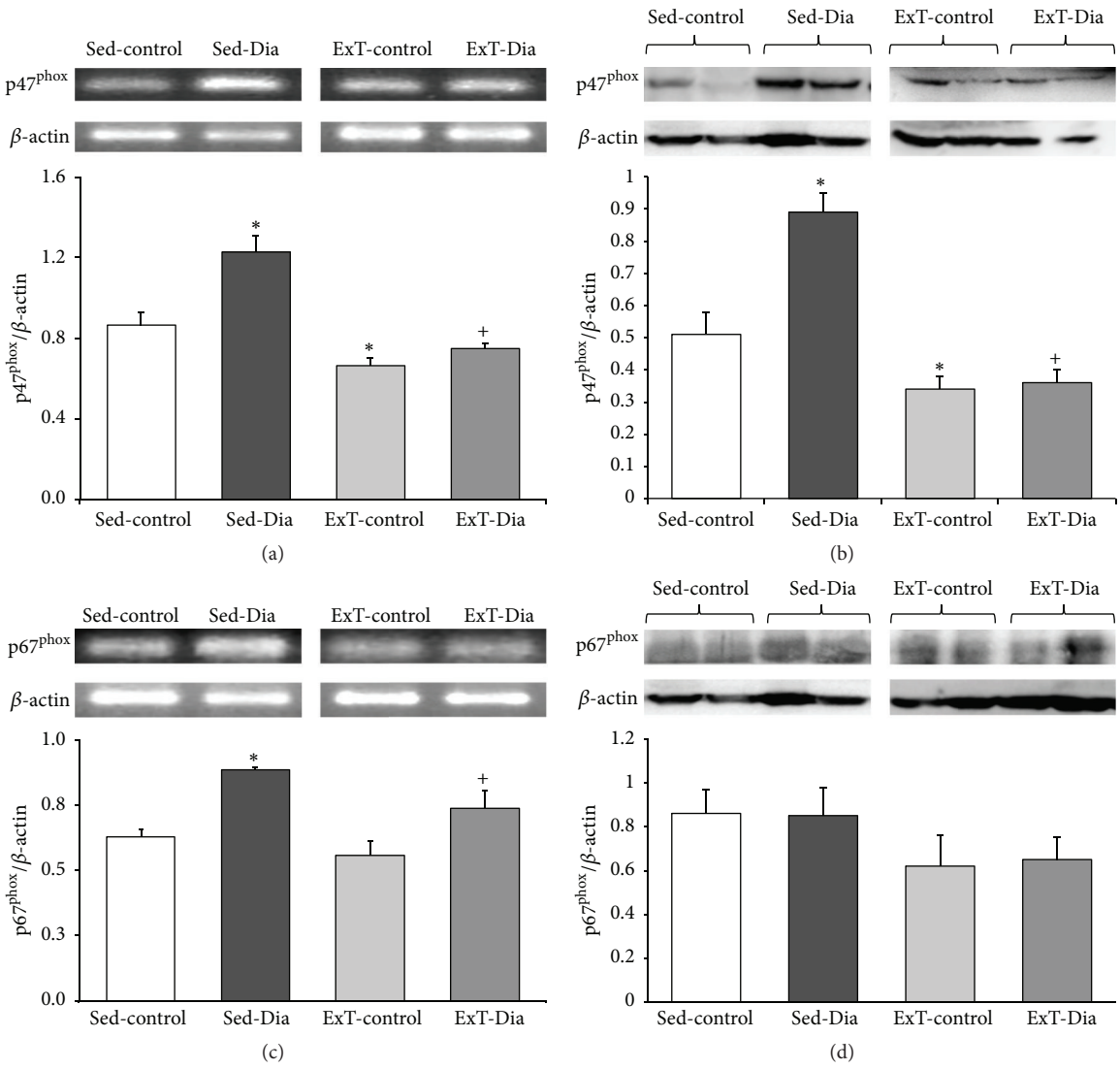

Figure 3: Expression of atrium $p47^{phox}$ and $p67^{phox}$ in Sed-control, Sed-Dia, ExT-control, and ExT-Dia animals. (a) RT-PCR of $p47^{phox}$: top: a representative gel; bottom: bar graph shows quantification of densitometry analysis of $p47^{phox}$ normalized to β-actin. $n = 10$ in each group. Values represent mean ± S.E. (b) Protein expression of $p47^{phox}$ in four groups: top: a representative gel; bottom: densitometry analyses of $p47^{phox}$ protein level normalized to actin. $n = 6$–8 in each group. Values represent mean ± S.E. (c) RT-PCR of atrium $p67^{phox}$ in Sed-control, Sed-Dia, ExT-control, and ExT-Dia animals: top: a representative gel; bottom: quantification of $p67^{phox}$ transcript normalized to β-actin as loading control. $n = 6$ in each group. (d) Protein expression of $p67^{phox}$ in four groups: top: a representative Western blot; bottom: densitometry analysis of $p67^{phox}$ protein normalized to β-actin as loading control. $n = 3$-4 in each group. Values are represented as mean ± S.E. $^{*}P < 0.05$ versus Sed-control. $^{+}P < 0.05$ versus Sed-Dia group.

and also a significant increase in collagen III was found in endomyocardial biopsies obtained from patients with DM [71]. Ang II has also been shown to stimulate collagen I and collagen III in cardiac fibroblast, and apocynin, an inhibitor of NADPH oxidase, prevents this initiation suggesting a critical role for ROS in cardiac remodelling [72]. Although a medical treatment with different antioxidant has been proposed for diabetic cardiomyopathy for decades, unfortunately, such treatments have failed to attenuate cardiac dysfunction or improve outcomes [73]. This may be due to lack of improving the ROS load in an appropriate measure in the myocardium rather than an overall reduction in ROS.

Physical activity is widely accepted as a key element in the prevention of type 2 diabetes [74] and also has beneficial effects in patients with established heart disease [75], although the physiological mechanisms explaining how physical activity promotes health remain to be fully elucidated. ExT maintains cardiac output by blunting diabetes-induced bradycardia and the reduction in force of myocardial contractility [60]. ExT has been shown to elicit a number of beneficial physiological changes in animals and clinical studies. These include (1) a reduction in blood glucose, body fat, and insulin resistance [45, 47], (2) improved glycemic control and lipid metabolism [45, 76], (3) improved baroreflex sensitivity

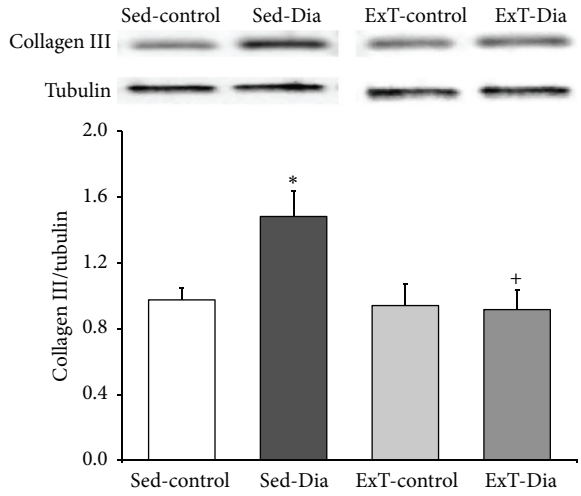

Figure 4: Collagen III expression in atria: top: representative Western blot showing collagen III protein expression in Sed-control, Sed-Dia, ExT-control, and ExT-Dia animals; bottom: densitometry analysis of collagen III expression normalized to β-tubulin as loading control. $n = 6$ in each group. Values represent mean ± S.E. $^{*}P < 0.01$ versus Sed-control group. $^{+}P < 0.05$ versus Sed-Dia group.

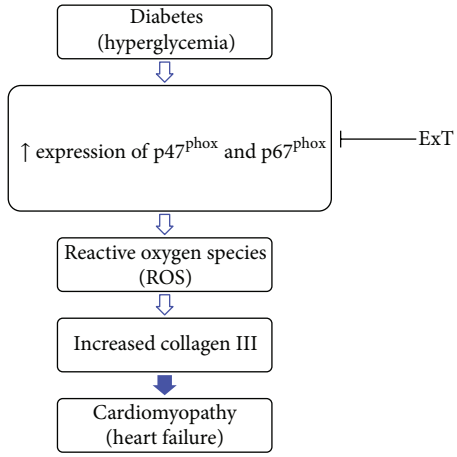

Figure 5: Amelioration of cardiomyopathy by exercise training. Hyperglycemia induces overexpression of cytoplasmic subunits of NADH oxidase ($p47^{phox}$ and $p67^{phox}$) in left ventricle. Overexpression of these subunits exhibits high reactive oxygen species and leads to increased collagen III and hence cardiomyopathy. Exercise training (ExT) mitigates the expression of $p47^{phox}$, and $p67^{phox}$ consequently ameliorates heart dysfunctions.

[46], (4) reduced plasma Ang II levels [49–51, 54], and (5) reduced renal sympathetic nerve activity and arterial pressure responses to Ang II [50, 52, 54, 77]. Additionally, the ability of ExT to upregulate antioxidant enzyme expression and activity in the cardiovascular system has been clearly demonstrated [48, 54, 55, 78, 79]. Previously, our lab showed ExT initiated after the onset of diabetes blunts primarily beta(1)-adrenoceptor expression loss and improves cardiac function in diabetic rats [60].

The current study adds to this literature by demonstrating for the first time that ExT significantly reduces $p47^{phox}$ mRNA expression in the left and right ventricles and atria of diabetic rats. In diabetic rats, ExT significantly reduced $p67^{phox}$ mRNA expression of the left ventricle and attenuated the increased $p67^{phox}$ message in the atria. The increase in NADPH oxidase subunit expression observed in the diabetic condition and its attenuation by ExT may occur via a variety of mechanisms. Hyperglycemia, enhanced renin-angiotensin system activity, and elevated levels of circulating cytokines are all clinical manifestations associated with the diabetic condition, and each is known to promote NADPH-derived O_2^- production. TNF-α, a cytokine that activates transcription factors which induce the expression of genes involved in inflammation and cell growth, has been identified as an agonist for NADPH oxidase [68]. Levels of TNF-α are increased in response to both hyperglycemic conditions and elevated Ang II levels, and the increase is mediated via AT_1R [68, 80]. Hyperglycemia and elevated Ang II levels have been clearly shown to upregulate the expression of NADPH oxidase subunits and increase NADPH oxidase activity and O_2^- production [32, 39, 67, 81]. Based on these findings, it appears that hyperglycemia and elevated Ang II associated with diabetes work via the AT_1 receptor to increase TNF-α levels and NADPH oxidase activity, while ExT suppresses expression of TNF-alpha and thus offers a potential protection against TNF-alpha-induced insulin resistance [82] and increased ROS production [83, 84].

Our study provides evidence that increase in oxidative stress, specifically in left ventricle, may be due to an enhanced transcription as well as translation of $p47^{phox}$ and $p67^{phox}$ subunits of NADPH oxidase. Expression of $p67^{phox}$ was increased at transcription level but not at the protein level in atria of diabetic rats suggesting that increased transcription did not contribute to changes in protein expression in this tissue. Translocation of cytosolic subunits ($p47^{phox}$, $p67^{phox}$, $p40^{phox}$, and rac1) and their association with membrane-bound cytochrome b_{558} (consisting of one $p22^{phox}$ and one $gp91^{phox}$ subunit) follows during acute oxidase activation [85]. In present studies perhaps there was only translocation of $p67^{phox}$ in the atria of diabetic heart rather than overall expression of synthesis, a possibility that remains to be explored.

The numerous physiological benefits of ExT offer several mechanisms via which the expression and activity of NADPH oxidase may be attenuated in diabetes. ExT has been shown to normalize diabetes-related elevations in blood glucose [45–47], plasma Ang II [49, 50, 53], and TNF-α [83, 84]. Normalizing these factors could lower levels of ROS-inducing agonists, thus dampening NADPH oxidase activity. Additionally, ExT has repeatedly been shown to upregulate antioxidant expression and activity, including SOD, catalase, and glutathione, in aortic and cardiac tissues [48, 49, 54, 56, 78, 79]. However, while the literature provides some insight, the specific mechanism by which ExT lowered the mRNA expression of $p47^{phox}$ and $p67^{phox}$ in our current study remains to be elucidated.

5. Conclusions

In summary, our data show that the mRNA expressions of the NADPH oxidase subunits $p47^{phox}$ and $p67^{phox}$ are upregulated in cardiac tissue in the diabetic condition. Furthermore, our data show that ExT attenuates the upregulated expression of these NADPH oxidase subunits and normalizes the increased collagen III levels (Figure 5) and provides support with a potential mechanistic link for exercise training as being an effective nonpharmacological tool in regulating oxidative stress levels in the diabetic heart. Future areas of research will need to focus on understanding some of the mechanisms involved in diabetic cardiomyopathy and the therapeutic strategies such as ExT to halt or slow its progression.

Conflict of Interests

The authors declare that there is no conflict of interests regarding the publication of this paper.

Acknowledgments

Funding from National Institutes of Health, Heart, Lung, and Blood Institute, R56 HL124104, and American Heart Association 14SDG19980007 grant supported the work. The technical assistance of Dr. Xuefei Liu is greatly appreciated.

References

[1] S. Dandamudi, J. Slusser, D. W. Mahoney, M. M. Redfield, R. J. Rodeheffer, and H. H. Chen, "The prevalence of diabetic cardiomyopathy: a population-based study in Olmsted County, Minnesota," *Journal of Cardiac Failure*, vol. 20, no. 5, pp. 304–309, 2014.

[2] R. B. Devereux, M. J. Roman, M. Paranicas et al., "Impact of diabetes on cardiac structure and function: the Strong Heart study," *Circulation*, vol. 101, no. 19, pp. 2271–2276, 2000.

[3] A. Ilercil, R. B. Devereux, M. J. Roman et al., "Relationship of impaired glucose tolerance to left ventricular structure and function: the Strong Heart study," *American Heart Journal*, vol. 141, no. 6, pp. 992–998, 2001.

[4] S. Rubler, J. Dlugash, Y. Z. Yuceoglu, T. Kumral, A. W. Branwood, and A. Grishman, "New type of cardiomyopathy associated with diabetic glomerulosclerosis," *The American Journal of Cardiology*, vol. 30, no. 6, pp. 595–602, 1972.

[5] S. Boudina and E. D. Abel, "Diabetic cardiomyopathy revisited," *Circulation*, vol. 115, no. 25, pp. 3213–3223, 2007.

[6] A. Aneja, W. H. W. Tang, S. Bansilal, M. J. Garcia, and M. E. Farkouh, "Diabetic cardiomyopathy: insights into pathogenesis, diagnostic challenges, and therapeutic options," *American Journal of Medicine*, vol. 121, no. 9, pp. 748–757, 2008.

[7] I. Falcão-Pires and A. F. Leite-Moreira, "Diabetic cardiomyopathy: understanding the molecular and cellular basis to progress in diagnosis and treatment," *Heart Failure Reviews*, vol. 17, no. 3, pp. 325–344, 2012.

[8] J. W. Baynes and S. R. Thorpe, "Role of oxidative stress in diabetic complications: a new perspective on an old paradigm," *Diabetes*, vol. 48, no. 1, pp. 1–9, 1999.

[9] D. Giugliano, A. Ceriello, and G. Paolisso, "Oxidative stress and diabetic vascular complications," *Diabetes Care*, vol. 19, no. 3, pp. 257–267, 1996.

[10] T. Yu, S.-S. Sheu, J. L. Robotham, and Y. Yoon, "Mitochondrial fission mediates high glucose-induced cell death through elevated production of reactive oxygen species," *Cardiovascular Research*, vol. 79, no. 2, pp. 341–351, 2008.

[11] S. Boudina, H. Bugger, S. Sena et al., "Contribution of impaired myocardial insulin signaling to mitochondrial dysfunction and oxidative stress in the heart," *Circulation*, vol. 119, no. 9, pp. 1272–1283, 2009.

[12] Y. Teshima, N. Takahashi, S. Nishio et al., "Production of reactive oxygen species in the diabetic heart: roles of mitochondria and NADPH oxidase," *Circulation Journal*, vol. 78, no. 2, pp. 300–306, 2014.

[13] M. M. Dallak, D. P. Mikhailidis, M. A. Haidara et al., "Oxidative stress as a common mediator for apoptosis induced-cardiac damage in diabetic rats," *Open Cardiovascular Medicine Journal*, vol. 2, no. 1, pp. 70–78, 2008.

[14] N. Takahashi, O. Kume, O. Wakisaka et al., "Novel strategy to prevent atrial fibrosis and fibrillation," *Circulation Journal*, vol. 76, no. 10, pp. 2318–2326, 2012.

[15] R. J. Gryglewski, R. M. J. Palmer, and S. Moncada, "Superoxide anion is involved in the breakdown of endothelium-derived vascular relaxing factor," *Nature*, vol. 320, no. 6061, pp. 454–456, 1986.

[16] A. Mugge, J. H. Elwell, T. E. Peterson, and D. G. Harrison, "Release of intact endothelium-derived relaxing factor depends on endothelial superoxide dismutase activity," *The American Journal of Physiology—Cell Physiology*, vol. 260, no. 2, part 1, pp. C219–C225, 1991.

[17] B. Tesfamariam and R. A. Cohen, "Enhanced adrenergic neurotransmission in diabetic rabbit carotid artery," *Cardiovascular Research*, vol. 29, no. 4, pp. 549–554, 1995.

[18] Z. S. Katusic and P. M. Vanhoutte, "Superoxide anion is an endothelium-derived contracting factor," *The American Journal of Physiology—Heart and Circulatory Physiology*, vol. 257, no. 1, part 2, pp. H33–H37, 1989.

[19] P. H. Sugden and A. Clerk, "Cellular mechanisms of cardiac hypertrophy," *Journal of Molecular Medicine*, vol. 76, no. 11, pp. 725–746, 1998.

[20] A. Akki, M. Zhang, C. Murdoch, A. Brewer, and A. M. Shah, "NADPH oxidase signaling and cardiac myocyte function," *Journal of Molecular and Cellular Cardiology*, vol. 47, no. 1, pp. 15–22, 2009.

[21] K. K. Griendling, D. Sorescu, and M. Ushio-Fukai, "NAD(P)H oxidase: role in cardiovascular biology and disease," *Circulation Research*, vol. 86, no. 5, pp. 494–501, 2000.

[22] H. D. Wang, S. Xu, D. G. Johns et al., "Role of NADPH oxidase in the vascular hypertrophic and oxidative stress response to angiotensin II in mice," *Circulation Research*, vol. 88, no. 9, pp. 947–953, 2001.

[23] J.-M. Li and A. M. Shah, "Differential NADPH- versus NADH-dependent superoxide production by phagocyte-type endothelial cell NADPH oxidase," *Cardiovascular Research*, vol. 52, no. 3, pp. 477–486, 2001.

[24] A. Cave, D. Grieve, S. Johar, M. Zhang, and A. M. Shah, "NADPH oxidase-derived reactive oxygen species in cardiac pathophysiology," *Philosophical Transactions of the Royal Society B: Biological Sciences*, vol. 360, no. 1464, pp. 2327–2334, 2005.

[25] C. Patterson, J. Ruef, N. R. Madamanchi et al., "Stimulation of a vascular smooth muscle cell NAD(P)H oxidase by thrombin: evidence that $p47^{phox}$ may participate in forming this oxidase *in vitro* and *in vivo*," *Journal of Biological Chemistry*, vol. 274, no. 28, pp. 19814–19822, 1999.

[26] K. P. Patel, W. G. Mayhan, K. R. Bidasee, and H. Zheng, "Enhanced angiotensin II-mediated central sympathoexcitation in streptozotocin-induced diabetes: role of superoxide anion," *American Journal of Physiology—Regulatory Integrative and Comparative Physiology*, vol. 300, no. 2, pp. R311–R320, 2011.

[27] H. M. Siragy, "AT(1) and AT(2) receptors in the kidney: role in disease and treatment," *American Journal of Kidney Diseases*, vol. 36, no. 3, supplement 1, pp. S4–S9, 2000.

[28] J. R. Sowers, M. Epstein, and E. D. Frohlich, "Diabetes, hypertension, and cardiovascular disease—an update," *Hypertension*, vol. 37, no. 4, pp. 1053–1059, 2001.

[29] V. Koshkin, O. Lotan, and E. Pick, "The cytosolic component p47(phox) is not a sine qua non participant in the activation of NADPH oxidase but is required for optimal superoxide production," *The Journal of Biological Chemistry*, vol. 271, no. 48, pp. 30326–30329, 1996.

[30] H. M. Siragy, A. Awad, P. Abadir, and R. Webb, "The angiotensin II type 1 receptor mediates renal interstitial content of tumor necrosis factor-alpha in diabetic rats," *Endocrinology*, vol. 144, no. 6, pp. 2229–2233, 2003.

[31] K. K. Griendling, C. A. Minieri, J. D. Ollerenshaw, and R. W. Alexander, "Angiotensin II stimulates NADH and NADPH oxidase activity in cultured vascular smooth muscle cells," *Circulation Research*, vol. 74, no. 6, pp. 1141–1148, 1994.

[32] M. E. Cifuentes, F. E. Rey, O. A. Carretero, and P. J. Pagano, "Upregulation of p67(phox) and gp91(phox) in aortas from angiotensin II-infused mice," *The American Journal of Physiology—Heart and Circulatory Physiology*, vol. 279, no. 5, pp. H2234–H2240, 2000.

[33] D. Lang, S. I. Mosfer, A. Shakesby, F. Donaldson, and M. J. Lewis, "Coronary microvascular endothelial cell redox state in left ventricular hypertrophy: the role of angiotensin II," *Circulation Research*, vol. 86, no. 4, pp. 463–469, 2000.

[34] J. K. Bendall, A. C. Cave, C. Heymes, N. Gall, and A. M. Shah, "Pivotal role of a $gp91^{phox}$-containing NADPH oxidase in angiotensin II-induced cardiac hypertrophy in mice," *Circulation*, vol. 105, no. 3, pp. 293–296, 2002.

[35] K. K. Griendling, T. J. Murphy, and R. W. Alexander, "Molecular biology of the renin-angiotensin system," *Circulation*, vol. 87, no. 6, pp. 1816–1828, 1993.

[36] K. K. Griendling, D. Sorescu, B. Lassègue, and M. Ushio-Fukai, "Modulation of protein kinase activity and gene expression by reactive oxygen species and their role in vascular physiology and pathophysiology," *Arteriosclerosis, Thrombosis, and Vascular Biology*, vol. 20, no. 10, pp. 2175–2183, 2000.

[37] K. K. Griendling and M. Ushio-Fukai, "Reactive oxygen species as mediators of angiotensin II signaling," *Regulatory Peptides*, vol. 91, no. 1–3, pp. 21–27, 2000.

[38] P. J. Pagano, J. K. Clark, M. E. Cifuentes-Pagano, S. M. Clark, G. M. Callis, and M. T. Quinn, "Localization of a constitutively active, phagocyte-like NADPH oxidase in rabbit aortic adventitia: enhancement by angiotensin II," *Proceedings of the National Academy of Sciences of the United States of America*, vol. 94, no. 26, pp. 14483–14488, 1997.

[39] H. Zhang, A. Schmeisser, C. D. Garlichs et al., "Angiotensin II-induced superoxide anion generation in human vascular endothelial cells: role of membrane-bound NADH-/NADPH-oxidases," *Cardiovascular Research*, vol. 44, no. 1, pp. 215–222, 1999.

[40] M. Zhang, A. L. Kho, N. Anilkumar et al., "Glycated proteins stimulate reactive oxygen species production in cardiac myocytes: involvement of Nox2 (gp91phox)-containing NADPH oxidase," *Circulation*, vol. 113, no. 9, pp. 1235–1243, 2006.

[41] S. Nishio, Y. Teshima, N. Takahashi et al., "Activation of CaMKII as a key regulator of reactive oxygen species production in diabetic rat heart," *Journal of Molecular and Cellular Cardiology*, vol. 52, no. 5, pp. 1103–1111, 2012.

[42] J. R. Privratsky, L. E. Wold, J. R. Sowers, M. T. Quinn, and J. Ren, "AT_1 blockade prevents glucose-induced cardiac dysfunction in ventricular myocytes: role of the AT_1 receptor and NADPH oxidase," *Hypertension*, vol. 42, no. 2, pp. 206–212, 2003.

[43] U. Hink, H. Li, H. Mollnau et al., "Mechanisms underlying endothelial dysfunction in diabetes mellitus," *Circulation Research*, vol. 88, no. 2, pp. E14–E22, 2001.

[44] D. H. J. Thijssen, A. J. Maiorana, G. O'Driscoll, N. T. Cable, M. T. E. Hopman, and D. J. Green, "Impact of inactivity and exercise on the vasculature in humans," *European Journal of Applied Physiology*, vol. 108, no. 5, pp. 845–875, 2010.

[45] S. Li, B. Culver, and J. Ren, "Benefit and risk of exercise on myocardial function in diabetes," *Pharmacological Research*, vol. 48, no. 2, pp. 127–132, 2003.

[46] A. Loimaala, H. V. Huikuri, T. Kööbi, M. Rinne, A. Nenonen, and I. Vuori, "Exercise training improves baroreflex sensitivity in type 2 diabetes," *Diabetes*, vol. 52, no. 7, pp. 1837–1842, 2003.

[47] S. Rousseau-Migneron, L. Turcotte, G. Tancrede, and A. Nadeau, "Transient increase in basal insulin levels in severely diabetic rats submitted to physical training," *Diabetes Research*, vol. 9, no. 2, pp. 97–100, 1988.

[48] M. E. Davis, H. Cai, L. McCann, T. Fukai, and D. G. Harrison, "Role of c-Src in regulation of endothelial nitric oxide synthase expression during exercise training," *The American Journal of Physiology—Heart and Circulatory Physiology*, vol. 284, no. 4, pp. H1449–H1453, 2003.

[49] H. Kohno, S. Furukawa, H. Naito, K. Minamitani, D. Ohmori, and F. Yamakura, "Contribution of nitric oxide, angiotensin II and superoxide dismutase to exercise-induced attenuation of blood pressure elevation in spontaneously hypertensive rats," *Japanese Heart Journal*, vol. 43, no. 1, pp. 25–34, 2002.

[50] R. W. Braith and D. G. Edwards, "Neurohormonal abnormalities in heart failure: impact of exercise training," *Congestive Heart Failure*, vol. 9, no. 2, pp. 70–76, 2003.

[51] T. L. Llewellyn, N. M. Sharma, H. Zheng, and K. P. Patel, "Effects of exercise training on SFO-mediated sympathoexcitation during chronic heart failure," *The American Journal of Physiology—Heart and Circulatory Physiology*, vol. 306, no. 1, pp. H121–H131, 2014.

[52] C. E. Negrao, M. C. Irigoyen, E. D. Moreira, P. C. Brum, P. M. Freire, and E. M. Krieger, "Effect of exercise training on RSNA, baroreflex control, and blood pressure responsiveness," *The American Journal of Physiology*, vol. 265, no. 2, part 2, pp. R365–R370, 1993.

[53] I. H. Zucker and R. U. Pliquett, "Novel mechanisms of sympatho-excitation in chronic heart failure," *Heart Failure Monitor*, vol. 3, no. 1, pp. 2–7, 2002.

[54] K. Husain, "Interaction of physical training and chronic nitroglycerin treatment on blood pressure, nitric oxide, and oxidants/antioxidants in the rat heart," *Pharmacological Research*, vol. 48, no. 3, pp. 253–261, 2003.

[55] T. Fukai, M. R. Siegfried, M. Ushio-Fukai, Y. Cheng, G. Kojda, and D. G. Harrison, "Regulation of the vascular extracellular superoxide dismutase by nitric oxide and exercise training," *Journal of Clinical Investigation*, vol. 105, no. 11, pp. 1631–1639, 2000.

[56] S. K. Powers, S. L. Lennon, J. Quindry, and J. L. Mehta, "Exercise and cardioprotection," *Current Opinion in Cardiology*, vol. 17, no. 5, pp. 495–502, 2002.

[57] I. Fridovich, "The biology of oxygen radicals," *Science*, vol. 201, no. 4359, pp. 875–880, 1978.

[58] R. Balzan, D. R. Agius, and W. H. Bannister, "Cloned prokaryotic iron superoxide dismutase protects yeast cells against oxidative stress depending on mitochondrial location," *Biochemical and Biophysical Research Communications*, vol. 256, no. 1, pp. 63–67, 1999.

[59] T. I. Musch and J. A. Terrell, "Skeletal muscle blood flow abnormalities in rats with a chronic myocardial infarction: rest and exercise," *The American Journal of Physiology—Heart and Circulatory Physiology*, vol. 262, no. 2, pp. H411–H419, 1992.

[60] K. R. Bidasee, H. Zheng, C.-H. Shao, S. K. Parbhu, G. J. Rozanski, and K. P. Patel, "Exercise training initiated after the onset of diabetes preserves myocardial function: effects on expression of beta-adrenoceptors," *Journal of Applied Physiology*, vol. 105, no. 3, pp. 907–914, 2008.

[61] P. A. Srere, "[1] Citrate synthase: [EC 4.1.3.7. Citrate oxaloacetate-lyase (CoA-acetylating)]," *Methods in Enzymology*, vol. 13, pp. 3–11, 1969.

[62] N. M. Sharma, H. Zheng, P. P. Mehta, Y.-F. Li, and K. P. Patel, "Decreased nNOS in the PVN leads to increased sympathoexcitation in chronic heart failure: role for CAPON and Ang II," *Cardiovascular Research*, vol. 92, no. 2, pp. 348–357, 2011.

[63] N. M. Sharma, H. Zheng, Y.-F. Li, and K. P. Patel, "Nitric oxide inhibits the expression of AT_1 receptors in neurons," *American Journal of Physiology: Cell Physiology*, vol. 302, no. 8, pp. C1162–C1173, 2012.

[64] P. M. Siu, D. A. Donley, R. W. Bryner, and S. E. Alway, "Citrate synthase expression and enzyme activity after endurance training in cardiac and skeletal muscles," *Journal of Applied Physiology*, vol. 94, no. 2, pp. 555–560, 2003.

[65] S. Levrand, C. Vannay-Bouchiche, B. Pesse et al., "Peroxynitrite is a major trigger of cardiomyocyte apoptosis in vitro and in vivo," *Free Radical Biology and Medicine*, vol. 41, no. 6, pp. 886–895, 2006.

[66] V. J. Dzau, "Tissue angiotensin and pathobiology of vascular disease: a unifying hypothesis," *Hypertension*, vol. 37, no. 4, pp. 1047–1052, 2001.

[67] T. Fukui, N. Ishizaka, S. Rajagopalan et al., "p22phox mRNA expression and NADPH oxidase activity are increased in aortas from hypertensive rats," *Circulation Research*, vol. 80, no. 1, pp. 45–51, 1997.

[68] J.-M. Li, A. M. Mullen, S. Yun et al., "Essential role of the NADPH oxidase subunit $p47^{phox}$ in endothelial cell superoxide production in response to phorbol ester and tumor necrosis factor-α," *Circulation Research*, vol. 90, no. 2, pp. 143–150, 2002.

[69] B. M. Babior, "NADPH oxidase: an update," *Blood*, vol. 93, no. 5, pp. 1464–1476, 1999.

[70] I. A. Williams and D. G. Allen, "The role of reactive oxygen species in the hearts of dystrophin-deficient mdx mice," *The American Journal of Physiology—Heart and Circulatory Physiology*, vol. 293, no. 3, pp. H1969–H1977, 2007.

[71] M. Shimizu, K. Umeda, N. Sugihara et al., "Collagen remodelling in myocardia of patients with diabetes," *Journal of Clinical Pathology*, vol. 46, no. 1, pp. 32–36, 1993.

[72] P. J. Lijnen, J. F. van Pelt, and R. H. Fagard, "Stimulation of reactive oxygen species and collagen synthesis by angiotensin II in cardiac fibroblasts," *Cardiovascular Therapeutics*, vol. 30, no. 1, pp. e1–e8, 2012.

[73] J. Kasznicki and J. Drzewoski, "Heart failure in the diabetic population—pathophysiology, diagnosis and management," *Archives of Medical Science*, vol. 10, no. 3, pp. 546–556, 2014.

[74] P. De Feo and P. Schwarz, "Is physical exercise a core therapeutical element for most patients with type 2 diabetes?" *Diabetes Care*, vol. 36, supplement 2, pp. S149–S154, 2013.

[75] J. Myers, M. Prakash, V. Froelicher, D. Do, S. Partington, and J. Edwin Atwood, "Exercise capacity and mortality among men referred for exercise testing," *The New England Journal of Medicine*, vol. 346, no. 11, pp. 793–801, 2002.

[76] J. M. Goguen and L. A. Leiter, "Lipids and diabetes mellitus: a review of therapeutic options," *Current Medical Research and Opinion*, vol. 18, supplement 1, pp. s58–s74, 2002.

[77] H. Zheng, N. M. Sharma, X. Liu, and K. P. Patel, "Exercise training normalizes enhanced sympathetic activation from the paraventricular nucleus in chronic heart failure: role of angiotensin II," *American Journal of Physiology: Regulatory Integrative and Comparative Physiology*, vol. 303, no. 4, pp. R387–R394, 2012.

[78] J. W. E. Rush, J. R. Turk, and M. H. Laughlin, "Exercise training regulates SOD-1 and oxidative stress in porcine aortic endothelium," *The American Journal of Physiology—Heart and Circulatory Physiology*, vol. 284, no. 4, pp. H1378–H1387, 2003.

[79] K. Husain and S. R. Hazelrigg, "Oxidative injury due to chronic nitric oxide synthase inhibition in rat: effect of regular exercise on the heart," *Biochimica et Biophysica Acta (BBA)—Molecular Basis of Disease*, vol. 1587, no. 1, pp. 75–82, 2002.

[80] N. Shanmugam, M. A. Reddy, M. Guha, and R. Natarajan, "High glucose-induced expression of proinflammatory cytokine and chemokine genes in monocytic cells," *Diabetes*, vol. 52, no. 5, pp. 1256–1264, 2003.

[81] S. Rajagopalan, S. Kurz, T. Münzel et al., "Angiotensin II-mediated hypertension in the rat increases vascular superoxide production via membrane NADH/NADPH oxidase activation. Contribution to alterations of vasomotor tone," *The Journal of Clinical Investigation*, vol. 97, no. 8, pp. 1916–1923, 1996.

[82] A. M. W. Petersen and B. K. Pedersen, "The anti-inflammatory effect of exercise," *Journal of Applied Physiology*, vol. 98, no. 4, pp. 1154–1162, 2005.

[83] W. Aldhahi and O. Hamdy, "Adipokines, inflammation, and the endothelium in diabetes," *Current Diabetes Reports*, vol. 3, no. 4, pp. 293–298, 2003.

[84] M. Straczkowski, I. Kowalska, S. Dzienis-Straczkowska et al., "Changes in tumor necrosis factor-alpha system and insulin sensitivity during an exercise training program in obese women with normal and impaired glucose tolerance," *European Journal of Endocrinology*, vol. 145, no. 3, pp. 273–280, 2001.

[85] Z. Guo, Z. Xia, J. Jiang, and J. H. McNeill, "Downregulation of NADPH oxidase, antioxidant enzymes, and inflammatory markers in the heart of streptozotocin-induced diabetic rats by *N*-acetyl-L-cysteine," *American Journal of Physiology: Heart and Circulatory Physiology*, vol. 292, no. 4, pp. H1728–H1736, 2007.

Hindawi Publishing Corporation
Oxidative Medicine and Cellular Longevity
Volume 2016, Article ID 3959087, 9 pages
http://dx.doi.org/10.1155/2016/3959087

Research Article

Angiotensin II-Induced Hypertension Is Attenuated by Overexpressing Copper/Zinc Superoxide Dismutase in the Brain Organum Vasculosum of the Lamina Terminalis

John P. Collister,[1] Heather Taylor-Smith,[1] Donna Drebes,[1] David Nahey,[1] Jun Tian,[2] and Matthew C. Zimmerman[2]

[1]*Department of Veterinary and Biomedical Sciences, College of Veterinary Medicine, University of Minnesota, St. Paul, MN 55108, USA*
[2]*Department of Cellular and Integrative Physiology, University of Nebraska Medical Center, Omaha, NE 68198, USA*

Correspondence should be addressed to John P. Collister; colli066@umn.edu

Received 14 September 2015; Accepted 30 November 2015

Academic Editor: Wei-Zhong Wang

Angiotensin II (AngII) can access the brain via circumventricular organs (CVOs), including the subfornical organ (SFO) and organum vasculosum of the lamina terminalis (OVLT), to modulate blood pressure. Previous studies have demonstrated a role for both the SFO and OVLT in the hypertensive response to chronic AngII, yet it is unclear which intracellular signaling pathways are involved in this response. Overexpression of copper/zinc superoxide dismutase (CuZnSOD) in the SFO has been shown to attenuate the chronic hypertensive effects of AngII. Presently, we tested the hypothesis that elevated levels of superoxide ($O_2^{\bullet-}$) in the OVLT contribute to the hypertensive effects of AngII. To facilitate overexpression of superoxide dismutase, adenoviral vectors encoding human CuZnSOD or control adenovirus (AdEmpty) were injected directly into the OVLT of rats. Following 3 days of control saline infusion, rats were intravenously infused with AngII (10 ng/kg/min) for ten days. Blood pressure increased 33 ± 8 mmHg in AdEmpty rats ($n = 6$), while rats overexpressing CuZnSOD ($n = 8$) in the OVLT demonstrated a blood pressure increase of only 18 ± 5 mmHg after 10 days of AngII infusion. These results support the hypothesis that overproduction of $O_2^{\bullet-}$ in the OVLT plays an important role in the development of chronic AngII-dependent hypertension.

1. Introduction

Many years ago the anterior ventral portion of the hypothalamus lining the third ventricle (AV3V) was implicated in playing a role in almost every form of experimental hypertension [1, 2]. This hypothalamic region is comprised primarily of the organum vasculosum of the lamina terminalis (OVLT), median preoptic nucleus (MnPO), and efferent fibers of the subfornical organ (SFO) [3]. Both the SFO and OVLT are known circumventricular organs (CVOs) devoid of the normal blood brain barrier and have been shown to be directly responsive to actions of angiotensin II (AngII) [4, 5]. While not a CVO, the MnPO of the lamina terminalis has both anatomical and functional connections to/from the SFO and OVLT [6–11], and its lesion or disruption from these other brain nuclei has been shown to inhibit the AngII-induced drinking response, elevation in blood pressure, and vasopressin secretion [12–16].

In recent years, our laboratory has been dissecting the individual components of this AV3V region and their role in chronic AngII-induced hypertension in order to better understand the exact involvement of these specific central nuclei. Indeed, through lesions of individual components of the AV3V, we have shown a role for each of these areas in the chronic hypertensive response to AngII. In response to a 10-day infusion of AngII, we have previously shown that rats with specific lesions of each of the SFO, MnPO, and OVLT have demonstrated an attenuated hypertensive response, implicating each of these sites as having a specific role in the chronic actions of AngII [17–22].

More recently, in an attempt to investigate the underlying signaling mechanisms in the central hypertensive response to peripherally administered AngII, we investigated the role of central superoxide ($O_2^{\bullet-}$) production during AngII-induced hypertension. Previously, it has been reported that overexpression of copper/zinc superoxide dismutase (CuZnSOD), an antioxidant enzyme that specifically scavenges $O_2^{\bullet-}$, in the SFO markedly attenuates the gradual and chronic hypertension produced by peripheral administration of AngII [23]. These results were very similar to those in which we reported an attenuation of AngII-induced hypertension in rats with lesions of the SFO [17, 18]. More recently, we tested the hypothesis that elevated $O_2^{\bullet-}$ levels in the MnPO additionally play a role in the chronic hypertensive response to AngII. Utilizing direct central injections of adenovirus encoding CuZnSOD into the MnPO, we demonstrated an attenuated hypertensive response to chronic intravenously administered AngII [24]. Collectively, these previous studies have (1) demonstrated a role for each of the SFO, MnPO, and the OVLT in the chronic hypertensive response to AngII [17–22] and (2) demonstrated a role for $O_2^{\bullet-}$-dependent signaling in mediating these effects, thus far, in the SFO and MnPO [23, 24].

In the present study, we hypothesized that elevated levels of $O_2^{\bullet-}$ in the OVLT contribute to the AngII-induced increase in blood pressure observed during peripheral infusion of AngII. To test this hypothesis, we overexpressed CuZnSOD specifically in the OVLT of rats by utilizing direct injections of adenoviral vectors encoding CuZnSOD into the OVLT. Rats were instrumented with telemetric blood pressure measuring transducers and peripherally infused with AngII for 10 days, as we have previously described [17, 19]. Our results demonstrate that the chronic hypertensive effects of AngII are reduced in rats with overexpression of CuZnSOD in the OVLT.

2. Materials and Methods

All experiments were approved by the University of Minnesota Institutional Animal Care and Use Committee (IACUC) and conducted according to guidelines of the National Institutes of Health. Adult male Sprague Dawley (Charles River Laboratory, Wilmington, MA, USA) rats (250–275 g) were used in all experiments. Animals were housed in an IACUC approved and monitored facility with a 12-hour day/night light cycle (lights on 7:00 AM).

2.1. Surgical Procedures. Rats were anesthetized with an intraperitoneal injection of ketamine (75 mg/kg) and xylazine (10 mg/kg). Rats were then placed in a stereotaxic apparatus with the head level and fixed. A dorsal midline skull incision was made and a 2 mm hole was drilled in the skull just caudal to bregma. Replication-deficient adenoviral vectors encoding human CuZnSOD (AdCuZnSOD) or control adenovirus (AdEmpty) (Viraquest Inc., North Liberty, IA) were pair matched at titers of 10^9 pfu/mL. Using a Hamilton syringe, 50 nL of either virus was directly injected into the dorsal OVLT of rats ($n = 8$ AdCuZnSOD; $n = 6$ AdEmpty). The coordinates used for injection caudal and ventral to bregma, respectively, were as follows in mm: (+0.65, −7.95). The hole in the skull was repaired with bone wax and the skin was closed with 3-0 silk suture. After completion of surgery, all rats were given antibiotic and analgesic injections (gentamicin; 2.5 mg, I.M. and butorphanol tartrate; 0.075 mg, S.C., resp.).

After one week of recovery, all rats were instrumented with blood pressure monitoring radiotelemeter devices (model number TA11PA-C40, Data Sciences International, St. Paul, MN) and femoral venous catheters, as we previously described [17, 20]. Rats were anesthetized as described above and an abdominal incision was made to expose and clamp the abdominal aorta proximally. The distal aorta was punctured with a 19-gauge needle and the tip of the transducer catheter was introduced into the aorta and secured in place with tissue adhesive. The body of the transducer was secured to the abdominal wall and the incision was closed. All rats were given antibiotics and analgesics as described above and individually placed in metabolic cages upon recovery. Rats were started on a continuous IV isotonic saline infusion of 7 mL/24 hr and given a 0.4% NaCl diet and water *ad libitum*.

2.2. Experimental Protocol. Following another week of recovery, all rats entered the experimental protocol. The first three days of the protocol served as a control period during which time a continuous intravenous infusion of 0.9% sterile saline (7 mL/24 hr) was maintained. This was followed by a 10-day infusion of AngII (10 ng/kg/min) which was dissolved in 0.9% sterile saline and intravenously infused at a rate of 7 mL/24 hr. Finally, a 3-day recovery period identical to the control period (i.e., saline infusion) completed the protocol.

Measurements of food intake, water intake, and urine output were made daily. Twenty-four-hour sodium intake was calculated as dietary sodium intake (product of food intake and sodium content of the food (0.4% NaCl, 0.07 mmol/g) plus infused sodium (1 mmol/day)). Urinary sodium was measured using a NOVA-5+ ion specific electrode (Biomedical, Waltham, MA, USA). Daily urinary sodium excretion was calculated as the product of urinary sodium content and daily urine volume. Total water intake was calculated as water ingested plus 7 mL from the daily IV infusion. Balance measurements were calculated as the difference between total input and excretion.

2.3. Immunofluorescent Detection of CuZnSOD. Following the measurement of hemodynamic parameters, rats were euthanized and perfused with 4.0% paraformaldehyde, and brains were removed. Coronal brain sections were processed for CuZnSOD protein immunoreactivity, as previously described [23]. Briefly, brain sections were incubated overnight at 4°C with human CuZnSOD antibody (1 : 500; sheep anti-human CuZnSOD; The Binding Site, Birmingham, UK) in 2% normal horse serum and 0.3% Triton followed by incubation with donkey anti-sheep AlexaFluor 488 secondary antibody (1 : 200; Invitrogen, Molecular Probes, Carlsbad, CA). CuZnSOD immunofluorescence in the OVLT was imaged with confocal microscopy (Zeiss 510 Meta Confocal Microscope, Carl Zeiss Microscopy GmbH, Jena,

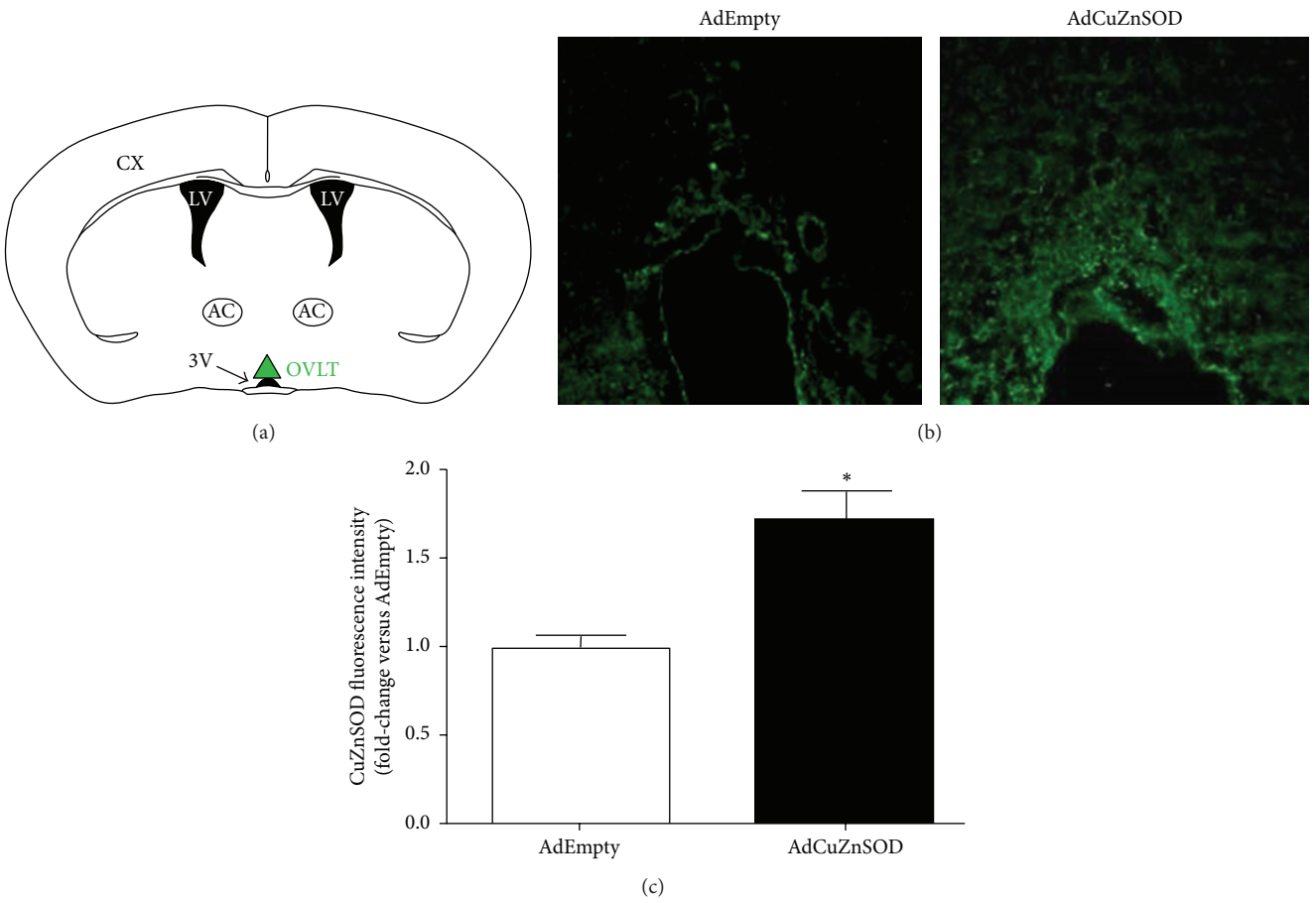

Figure 1: Schematic of coronal brain section showing location of OVLT (a). Representative confocal microscopy immunofluorescence images demonstrating CuZnSOD expression (green fluorescence) in the OVLT from an AdEmpty- or AdCuZnSOD-injected rat (b). Fluorescence intensity in the OVLT was quantified with Image J analysis software and is reported as fold-change in AdCuZnSOD rats ($n = 8$) versus AdEmpty rats ($n = 6$) (c). $^{*}P < 0.05$ versus AdEmpty-injected rats.

Germany). Image J analysis software was used to quantify fluorescence intensity in OVLT brain sections from rats injected with AdEmpty or AdCuZnSOD. Fluorescence intensity in brain sections from AdCuZnSOD-injected is reported as fold-change versus intensity in sections from AdEmpty-injected rats.

2.4. Statistical Analysis. Data are reported as mean ± SE. Student's t-test was used to compare two groups while one- or two-way ANOVA was used for multiple comparisons combined with a Student-Newman-Keuls post hoc analysis. Differences were considered significant at $P < 0.05$.

3. Results

3.1. Adenovirus-Mediated Overexpression of CuZnSOD in the OVLT. Immunofluorescence confocal microscopy was used to confirm overexpression of CuZnSOD in the OVLT in brain sections from rats that received an injection of AdCuZnSOD directly into the OVLT. Approximately 5 weeks after direct injection of either AdCuZnSOD or AdEmpty, levels of CuZnSOD were significantly elevated (1.7-fold increase, $P < 0.05$; Figure 1(c)) in the OVLT of rats receiving the AdCuZnSOD injection compared to those of rats receiving direct injection of AdEmpty. Representative confocal microscopy images showing CuZnSOD immunoreactivity are presented in Figure 1(b). It should be noted regarding the study population that all AdCuZnSOD-injected rats included in the final hemodynamic analyses (described below) were confirmed to have robust CuZnSOD expression in and confined to the OVLT relative to the low fluorescence detected in the OVLT of AdEmpty-treated rats.

3.2. CuZnSOD Overexpression in the OVLT Attenuates AngII-Induced Hypertension. Average baseline mean arterial pressure (MAP) was not different between AdCuZnSOD- (105 ± 2 mmHg) and AdEmpty-injected (106 ± 3 mmHg) rats during the control saline infusion period (Figure 2(a)). However, during the 10-day AngII infusion period, MAP was significantly reduced (on days 6–10 of AngII and on days 1 and 2 of the recovery period) in AdCuZnSOD-treated rats compared to MAP of AdEmpty-injected rats (Figure 2(a)). Specifically, MAP reached 121 ± 6 mmHg in AdCuZnSOD rats by day 10 of AngII infusion but increased to 140 ± 8 mmHg in

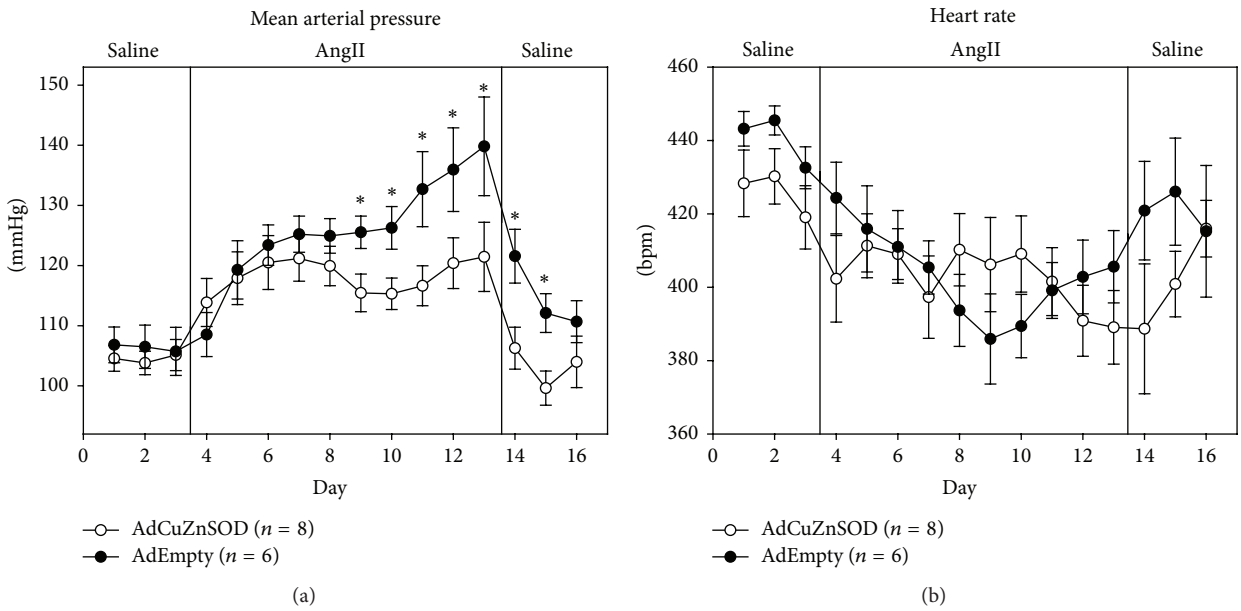

Figure 2: Summary data showing average 24-hour mean arterial pressure (a) and heart rate (b) recorded during saline infusion (3 days), AngII infusion (10 ng/kg/min) for 10 days, and recovery saline infusion (3 days) in rats that were OVLT injected with AdCuZnSOD (n = 8) or AdEmpty (n = 6). $^*P < 0.05$ versus AdCuZnSOD-injected rats.

AdEmpty rats. Average heart rate (HR) (Figure 2(b)) was not significantly different between the two groups during the control saline infusion period (AdCuZnSOD: 424 ± 9, AdEmpty: 440 ± 4 beats/min). In addition, while all rats were observed to have generally lower HR during AngII infusion, there was no statistical significance between the two groups.

3.3. CuZnSOD Overexpression in the OVLT Does Not Affect Sodium and Water Balance in AngII-Infused Hypertensive Rats. To determine if overexpression of CuZnSOD in the OVLT affects body fluid homeostasis during AngII-induced hypertension, sodium intake, sodium excretion, and sodium balance (Figure 3), as well as water intake, urine output, and water balance (Figure 4), were measured throughout the protocol. Regarding sodium intake, sodium excretion, and sodium balance, no differences were observed between groups throughout the protocol. Regarding water intake, AdCuZnSOD-treated rats showed a significant increase on days 2 and 3 of saline infusion, day 1 of AngII treatment, and the last 2 recovery days (Figure 4(a)) and tended to have increased water intake during the protocol. However, this was offset by a slightly increased urine output throughout the protocol (Figure 4(b)). Thus, no change in overall water balance (Figure 4(c)) was observed between the groups. Collectively, overexpression of CuZnSOD in the OVLT did not alter sodium and water balance during the protocol compared to AdEmpty-injected control rats.

4. Discussion

Much research has been conducted examining the AngII model of hypertension and its neurogenic component(s) [25, 26]. However, we still do not have a complete understanding of the integrative pathways and central nuclei involved in the hypertensive response to peripherally administered AngII. Our laboratory has characterized and extensively used a modest dose of AngII and normal salt diet in rats to produce a reproducible and chronic hypertension model that is gradual and progressive in onset similar to human hypertension [17, 19, 20]. It does not appear to be associated with or dependent on the angiotensin converting enzyme 2 (ACE2) and angiotensin (1–7) (Ang(1–7)) axis [27], and despite known renal actions of AngII given at higher doses, we have repeatedly reported no chronic changes in sodium or water balance using this model of hypertension [17, 19, 21]. Rather, it appears that there is a significant central nervous system signaling component via CVOs associated with the chronic hypertension in this model [17–22]. By utilizing lesion studies, our laboratory has previously demonstrated that both the SFO and OVLT, as well as one of their downstream integration sites, the MnPO, are each independently necessary for the full hypertensive response to elevated AngII [17–22].

More recently, attention has also been directed toward fully understanding the intracellular signaling pathways involved in the chronic hypertensive response to AngII. In the current study, we report that overexpression of CuZnSOD, an intracellular superoxide scavenging enzyme, in the OVLT significantly attenuates the increase in MAP induced by chronic, peripheral infusion of AngII. Control rats that received an injection of an empty adenovirus into the OVLT responded to AngII with a 33 ± 8 mmHg rise in arterial pressure after 10 days of exogenous AngII, while rats overexpressing CuZnSOD in the OVLT showed a markedly attenuated response of only 18 ± 5 mmHg over the same 10 days of AngII treatment. These results support the hypothesis that

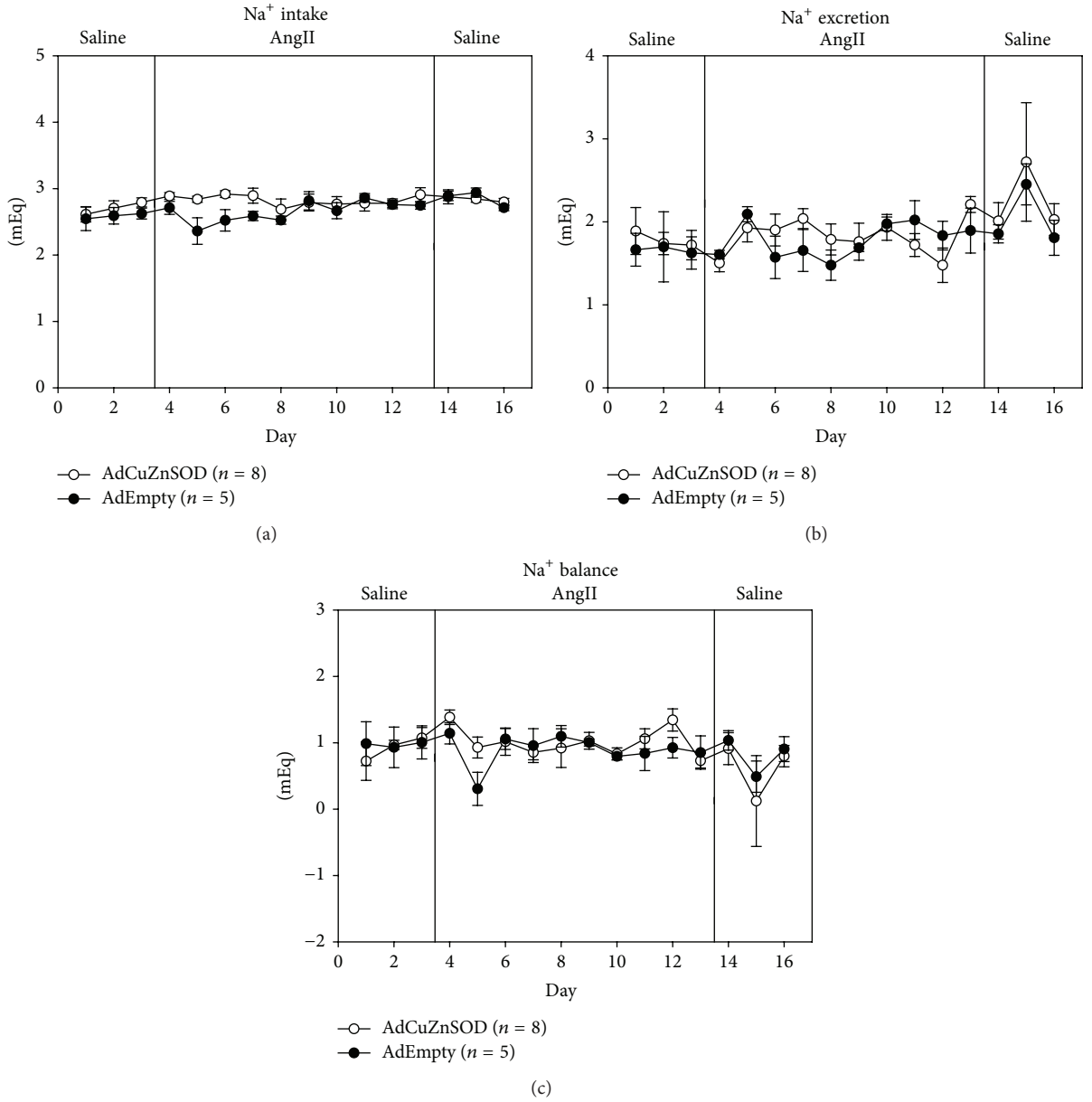

Figure 3: Summary data showing average 24-hour sodium intake (a), sodium output (b), and sodium balance (c) during control saline infusion and subsequent AngII infusion (10 ng/kg/min) for 10 days in rats that were OVLT injected with AdCuZnSOD ($n = 8$) or AdEmpty ($n = 5$).

overproduction of $O_2^{\bullet-}$ in the OVLT significantly contributes to the full hypertensive response to AngII.

The SFO has been one of the more extensively studied CVOs and has been widely reported as having an important role in the dipsogenic and hypertensive effects of circulating AngII [28–32]. We have previously demonstrated that the SFO is necessary to achieve the full hypertensive response to chronic peripheral AngII infusion in studies utilizing electrolytic lesion of this CVO [17, 18]. Furthermore, it has been shown that this effect is mediated, at least in part, through increased $O_2^{\bullet-}$ signaling in the SFO [23]. Thus, the SFO has clearly been given much deserved attention as having a major role in the chronic AngII-induced hypertension model. In addition to the SFO, the OVLT is a hypothalamic sensory CVO of significance and part of the originally described anterior ventral 3rd ventricle (AV3V). Along with the OVLT, this area contains the ventral part of the MnPO and the periventricular tissue surrounding the 3rd ventricle [3] and was originally characterized for its role in the mechanisms of hypertension, as lesion of this area prevents many forms of experimental hypertension including the AngII-dependent model [1, 2]. Therefore, we recently attempted to dissect the individual role of the OVLT itself in chronic AngII-dependent hypertension by discrete

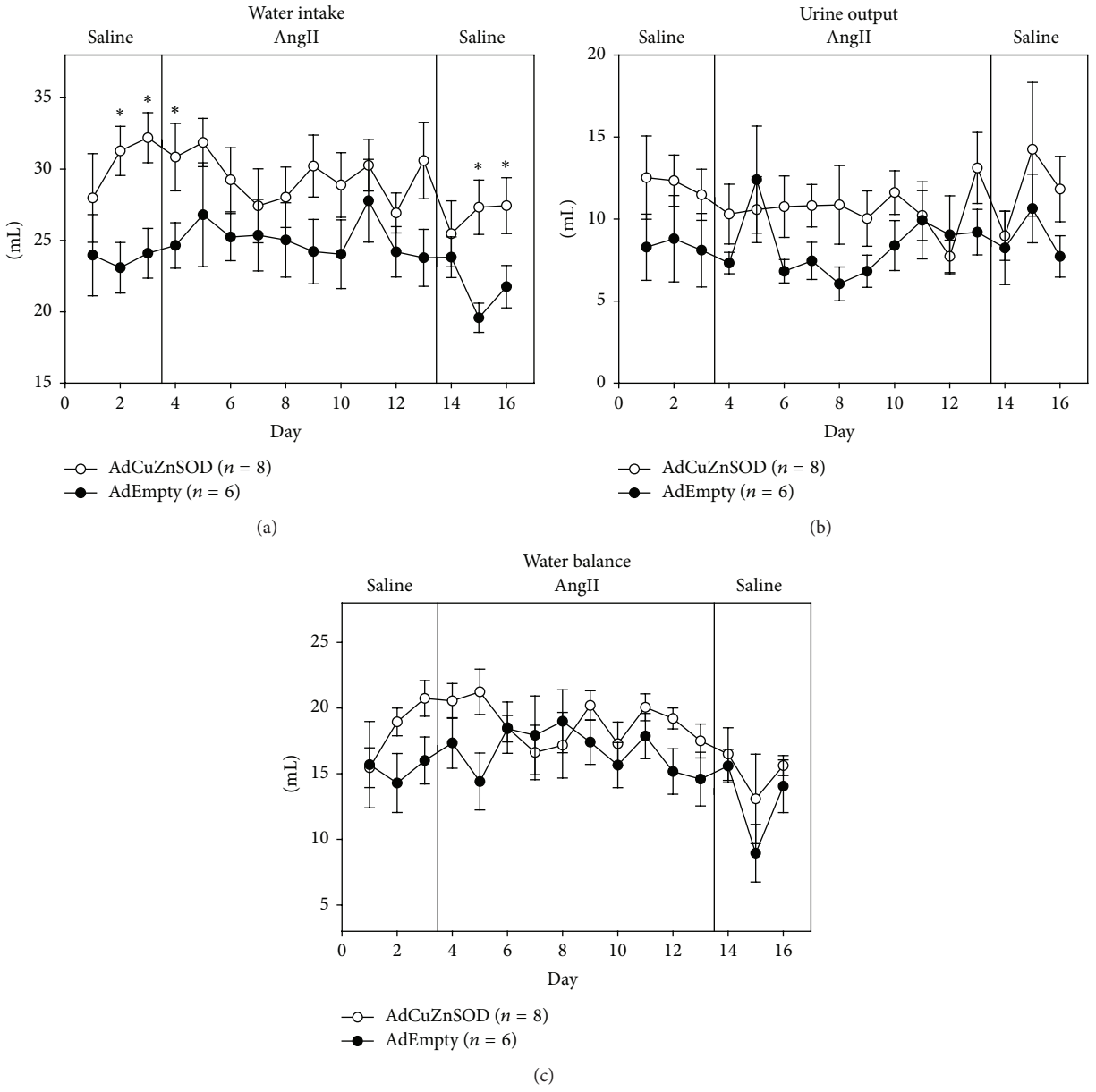

Figure 4: Summary data showing average 24-hour water intake (a), urine output (b), and water balance (c) during control saline infusion followed by AngII infusion (10 days; 10 ng/kg/min) and recovery saline infusion (3 days) in rats that were OVLT injected with AdCuZnSOD (n = 8) or AdEmpty (n = 6). $^{*}P < 0.05$ versus AdEmpty-injected rats.

lesion of the OVLT followed by administration of AngII. In those studies, we observed that specific lesion of the OVLT markedly attenuated the effects of a 10-day infusion of AngII in rats [21]. In the current study, similar to what has been studied in the SFO, we aimed to further elucidate the mechanisms of this response by testing the hypothesis that increased levels of $O_2^{\bullet-}$ contribute to the long-term hypertensive effects of AngII. To do this, an adenovirus encoding CuZnSOD was injected directly into the OVLT to selectively overexpress this $O_2^{\bullet-}$ scavenging enzyme in this brain region involved in cardiovascular control. The results of the study demonstrate a strikingly similar inhibition of the rise in arterial pressure during 10 days of intravenous AngII infusion to what we have previously reported in SFO or OVLT lesioned rats [17, 21]. Furthermore, these results suggest that not only is $O_2^{\bullet-}$ playing a role in the signaling mechanism at the SFO during AngII-induced hypertension [23], but also it has at least an equally important role in the OVLT in this model of hypertension.

The present study suggests a definitive role of $O_2^{\bullet-}$ in the OVLT as an intracellular signaling mechanism in chronic AngII-induced hypertension. While these results are similar to the attenuation of the hypertensive effects of AngII that was previously reported in mice with overexpression of CuZnSOD in the SFO [23], there are some notable differences. The above-mentioned study conducted by Zimmerman et al. used a mouse model in which AdCuZnSOD was injected intracerebroventricularly (ICV), and AngII was

delivered subcutaneously via osmotic minipump at a dose of 600 ng/kg/min over a period of 16 days [23]. In the current study, we used direct injection of AdCuZnSOD into the OVLT and a continuous IV infusion of AngII (10 ng/kg/min) for 10 days. In both studies, MAP gradually increased in control animals, an effect that was significantly attenuated in AdCuZnSOD-treated animals throughout the course of AngII treatment. In the above-mentioned AdCuZnSOD SFO mouse study, MAP rose to approximately 150–160 mmHg, and this effect was attenuated after 11 days of AngII infusion in mice overexpressing SOD in the SFO [23] compared to the present study, in which we report a peak MAP of 140 mmHg in control animals after 10 days of AngII treatment that was attenuated after 6 days of AngII at a level of approximately 120 mmHg in AdCuZnSOD rats. These differences are probably attributable to a number of factors including the choice of animal model, as well as the dose and route of AngII administration. Nevertheless, both studies demonstrate a chronic hypertension during AngII treatment that was significantly attenuated only after several days in animals treated with central AdCuZnSOD, equally implicating $O_2^{\bullet-}$ signaling in the OVLT as well as in the SFO as a mechanism mediating chronic AngII-induced hypertension. Another difference between previous studies and the current study is that AdCuZnSOD was directly injected into the OVLT in the present study. In contrast, Zimmerman et al. performed ICV injections of adenovirus and thus targeted the SFO nonspecifically. Nonetheless, they observed CuZnSOD overexpression predominantly in the SFO and thus concluded that increased scavenging of $O_2^{\bullet-}$ in the SFO attenuated AngII-induced hypertension [23]. Through lesion studies, our laboratory has much previous experience with specifically targeting the OVLT [21, 22] and was therefore able to utilize direct injections into the OVLT in the present study in order to specifically target this important cardiovascular control nucleus.

Downstream of the OVLT, following activation by AngII, the MnPO receives reciprocal inputs from not only the OVLT but also the SFO and is therefore believed to form part of the sympathoexcitatory pathway [10, 11, 33, 34]. In an attempt to further clarify the role of the MnPO in the development of AngII-induced hypertension, our laboratory reported similar decreases in the long-term hypertensive response to AngII in rats with either total electrolytic or chemical ablation of the MnPO [19, 20]. Building from these previous observations, we sought to shed further light on the role of $O_2^{\bullet-}$ as an intracellular signaling molecule in, specifically, the MnPO, using the same model of AngII-induced hypertension [24]. The results from that study again demonstrated a very similar attenuation of the typical development of hypertension during 10 days of exogenous AngII to what has been reported in the SFO [23] and to our current OVLT data presented herein. Collectively, these studies indicate that $O_2^{\bullet-}$-dependent signaling in the SFO, MnPO, and OVLT mediates, at least in part, the hypertensive response to elevated levels of circulating AngII.

While the observations in the MAP response were similar in the present OVLT study to those in the study using overexpression of CuZnSOD in the MnPO [24], there are some apparent differences. Overexpression of CuZnSOD in the MnPO caused an attenuated MAP response to AngII that began after only 2 days of AngII infusion and lasted throughout day 10, whereas the attenuated response to elevated AngII in rats receiving injections into the OVLT in the present study began on day 6 of AngII treatment. Furthermore, the maximal attenuation of MAP was greater in rats with overexpression of CuZnSOD in the MnPO, as MAP in those rats only increased 6 mmHg [24]. These differences are perhaps not surprising considering that if the MnPO is indeed receiving AngII-mediated signaling inputs from both the SFO and OVLT, one would expect a more dramatic attenuation in the MAP response to AngII when the signaling pathway in this integration site for more than one CVO is disrupted compared to blocking signaling mechanisms in either CVO alone. Lastly, of notable interest is that the attenuation of the MAP response in OVLT lesioned animals treated with 10 days of AngII was also much greater than the attenuated response of rats with overexpression of CuZnSOD in the OVLT. We previously reported that rats with lesions of the OVLT responded with a maximal attenuated response of only approximately 25% the rise in MAP compared to sham lesioned rats during a 10-day infusion of AngII [21]. This suggests that while $O_2^{\bullet-}$ in the OVLT is playing an important role in the intracellular signaling cascade mediating the rise in blood pressure during AngII infusion, it is not the only mechanism functioning during this model of hypertension.

In conclusion, our current results support a notable role of elevated $O_2^{\bullet-}$ in the OVLT in mediating the chronic hypertensive effects of AngII. Furthermore, we have now clearly established that $O_2^{\bullet-}$ signaling in both the SFO and OVLT, as well as the downstream MnPO, is all independently important in mediating the chronic hypertensive response to AngII. Some arguable questions remaining are as follows: which CVO is the primary site driving this response, or are they equally important, and if so are they redundant or even compensatory in their function? For example, when this pathway is blocked in one CVO, is it possible that we are not observing the maximal response due to some compensatory function or redundancy in CVO signaling, and therefore we have possibly observed the maximal attenuated response to AngII in our studies involving the MnPO? Taken together, our current and previous data support further investigations into new therapies and technologies for delivering antioxidant treatments to these definitive central nuclei in the treatment of hypertension, specifically targeting reductions in or prevention of increased $O_2^{\bullet-}$ levels.

Conflict of Interests

The authors declare that there is no conflict of interests regarding the publication of this paper.

Acknowledgments

This study was supported by both the University of Minnesota College of Veterinary Medicine Signature Program in Comparative Medicine and the National Heart, Lung, and Blood

Institute at the National Institutes of Health (R01HL103942 to Matthew C. Zimmerman). The authors thank Janice A. Taylor and James R. Talaska at the University of Nebraska Medical Center Confocal Laser Scanning Microscopy Core for providing assistance with confocal microscopy. Notably, the Eppley Cancer Center at the University of Nebraska Medical Center and the Nebraska Research Initiative provide support for this Core Facility.

References

[1] M. J. Brody, G. D. Fink, and J. Buggy, "The role of the anteroventral third ventricle (AV3V) region in experimental hypertension," *Circulation Research*, vol. 43, no. 1, pp. 1–13, 1978.

[2] M. J. Brody and A. K. Johnson, "Role of the anteroventral third ventricle region in fluid and electrolyte balance, arterial pressure regulation and hypertension," in *Frontiers in Neuroendocrinology*, L. Martini and W. F. Ganong, Eds., vol. 6, pp. 249–292, Raven Press, New York, NY, USA, 1980.

[3] M. J. Brody, J. E. Faber, M. L. Mangiapane et al., "The central nervous system and prevention of hypertension," in *Handbook of Hypertension: Experimental and Genetic Models of Hypertension*, W. de Jong, Ed., pp. 474–494, Elsevier, New York, NY, USA, 1984.

[4] M. J. McKinley, A. M. Allen, P. Burns, L. M. Colvill, and B. J. Oldfield, "Interaction of circulating hormones with the brain: the roles of the subfornical organ and the organum vasculosum of the lamina terminalis," *Clinical and Experimental Pharmacology and Physiology*, vol. 25, supplement s1, pp. S61–S67, 1998.

[5] M. J. McKinley, E. Badoer, and B. J. Oldfield, "Intravenous angiotensin II induces Fos-immunoreactivity in circumventricular organs of the lamina terminalis," *Brain Research*, vol. 594, no. 2, pp. 295–300, 1992.

[6] J. Ciriello and M. B. Gutman, "Functional identification of central pressor pathways originating in the subfornical organ," *Canadian Journal of Physiology and Pharmacology*, vol. 69, no. 7, pp. 1035–1045, 1991.

[7] M. B. Gutman, J. Ciriello, and G. J. Mogenson, "Electrophysiological identification of forebrain connections of the subfornical organ," *Brain Research*, vol. 382, no. 1, pp. 119–128, 1986.

[8] R. W. Lind, G. W. Van Hoesen, and A. K. Johnson, "An HRP study of the connections of the subfornical organ of the rat," *Journal of Comparative Neurology*, vol. 210, no. 3, pp. 265–277, 1982.

[9] R. R. Miselis, "The subfornical organ's neural connections and their role in water balance," *Peptides*, vol. 3, no. 3, pp. 501–502, 1982.

[10] C. B. Saper and D. Levisohn, "Afferent connections of the median preoptic nucleus in the rat: anatomical evidence for a cardiovascular integrative mechanism in the anteroventral third ventricular (AV3V) region," *Brain Research*, vol. 288, no. 1-2, pp. 21–31, 1983.

[11] R. R. Miselis, "The efferent projections of the subfornical organ of the rat: a circumventricular organ within a neural network subserving water balance," *Brain Research*, vol. 230, no. 1-2, pp. 1–23, 1981.

[12] J. T. Cunningham, T. Beltz, R. F. Johnson, and A. K. Johnson, "The effects of ibotenate lesions of the median preoptic nucleus on experimentally-induced and circadian drinking behavior in rats," *Brain Research*, vol. 580, no. 1-2, pp. 325–330, 1992.

[13] M. B. Gutman, D. L. Jones, and J. Ciriello, "Contribution of nucleus medianus to the drinking and pressor responses to angiotensin II acting at subfornical organ," *Brain Research*, vol. 488, no. 1-2, pp. 49–56, 1989.

[14] D. L. Jones, "Kainic acid lesions of the median preoptic nucleus: effects on angiotensin II induced drinking and pressor responses in the conscious rat," *Canadian Journal of Physiology and Pharmacology*, vol. 66, no. 8, pp. 1082–1086, 1988.

[15] R. W. Lind and A. K. Johnson, "Subfornical organ-median preoptic connections and drinking and pressor responses to angiotensin II," *Journal of Neuroscience*, vol. 2, no. 8, pp. 1043–1051, 1982.

[16] M. L. Mangiapane, T. N. Thrasher, L. C. Keil, J. B. Simpson, and W. F. Ganong, "Deficits in drinking and vasopressin secretion after lesions of the nucleus medianus," *Neuroendocrinology*, vol. 37, no. 1, pp. 73–77, 1983.

[17] M. D. Hendel and J. P. Collister, "Contribution of the subfornical organ to angiotensin II-induced hypertension," *The American Journal of Physiology—Heart and Circulatory Physiology*, vol. 288, no. 2, pp. H680–H685, 2005.

[18] J. W. Osborn, M. D. Hendel, J. P. Collister, P. A. Ariza-Guzman, and G. D. Fink, "The role of the subfornical organ in angiotensin II-salt hypertension in the rat," *Experimental Physiology*, vol. 97, no. 1, pp. 80–88, 2012.

[19] T. Ployngam and J. P. Collister, "An intact median preoptic nucleus is necessary for chronic angiotensin II-induced hypertension," *Brain Research*, vol. 1162, pp. 69–75, 2007.

[20] T. Ployngam and J. P. Collister, "Role of the median preoptic nucleus in chronic angiotensin II-induced hypertension," *Brain Research*, vol. 1238, pp. 75–84, 2008.

[21] A. A. Vieira, D. B. Nahey, and J. P. Collister, "Role of the organum vasculosum of the lamina terminalis for the chronic cardiovascular effects produced by endogenous and exogenous ANG II in conscious rats," *American Journal of Physiology—Regulatory Integrative and Comparative Physiology*, vol. 299, no. 6, pp. R1564–R1571, 2010.

[22] J. P. Collister, M. K. Olson, D. B. Nahey, A. A. Vieira, and J. W. Osborn, "OVLT lesion decreases basal arterial pressure and the chronic hypertensive response to AngII in rats on a high-salt diet," *Physiological Reports*, vol. 1, no. 5, Article ID e00128, pp. 1–9, 2013.

[23] M. C. Zimmerman, E. Lazartigues, R. V. Sharma, and R. L. Davisson, "Hypertension caused by angiotensin II infusion involves increased superoxide production in the central nervous system," *Circulation Research*, vol. 95, no. 2, pp. 210–216, 2004.

[24] J. P. Collister, M. Bellrichard, D. Drebes, D. Nahey, J. Tian, and M. C. Zimmerman, "Overexpression of copper/zinc superoxide dismutase in the median preoptic nucleus attenuates chronic angiotensin II-induced hypertension in the rat," *International Journal of Molecular Sciences*, vol. 15, no. 12, pp. 22203–22213, 2014.

[25] J. W. Osborn, G. D. Fink, and M. T. Kuroki, "Neural mechanisms of angiotensin II-salt hypertension: implications for therapies targeting neural control of the splanchnic circulation," *Current Hypertension Reports*, vol. 13, no. 3, pp. 221–228, 2011.

[26] J. W. Osborn, G. D. Fink, A. F. Sved, G. M. Toney, and M. K. Raizada, "Circulating angiotensin II and dietary salt: converging signals for neurogenic hypertension," *Current Hypertension Reports*, vol. 9, no. 3, pp. 228–235, 2007.

[27] J. P. Collister and M. D. Hendel, "The role of Ang (1-7) in mediating the chronic hypotensive effects of losartan in normal

rats," *Journal of the Renin-Angiotensin-Aldosterone System*, vol. 4, no. 3, pp. 176–179, 2003.

[28] A. V. Ferguson and J. S. Bains, "Actions of angiotensin in the subfornical organ and area postrema: implications for long term control of autonomic output," *Clinical and Experimental Pharmacology and Physiology*, vol. 24, no. 1, pp. 96–101, 1997.

[29] A. V. Ferguson and K. M. Wall, "Central actions of angiotensin in cardiovascular control: multiple roles for a single peptide," *Canadian Journal of Physiology and Pharmacology*, vol. 70, no. 5, pp. 779–785, 1992.

[30] J. B. Simpson, "The circumventricular organs and the central actions of angiotensin," *Neuroendocrinology*, vol. 32, no. 4, pp. 248–256, 1981.

[31] M. L. Mangiapane and J. B. Simpson, "Subfornical organ lesions reduce the pressor effect of systmic angiotensin II," *Neuroendocrinology*, vol. 31, no. 6, pp. 380–384, 1980.

[32] M. L. Mangiapane and J. B. Simpson, "Subfornical organ: forebrain site of pressor and dipsogenic action of angiotensin II," *The American Journal of Physiology*, vol. 239, no. 5, pp. R382–R389, 1980.

[33] P. E. Sawchenko and L. W. Swanson, "The organization of forebrain afferents to the paraventricular and supraoptic nuclei of the rat," *Journal of Comparative Neurology*, vol. 218, no. 2, pp. 121–144, 1983.

[34] A. M. Zardetto-Smith, R. L. Thunhorst, M. Z. Cicha, and A. K. Johnson, "Afferent signaling and forebrain mechanisms in the behavioral control of extracellular fluid volume," *Annals of the New York Academy of Sciences*, vol. 689, pp. 161–176, 1993.

Hindawi Publishing Corporation
Oxidative Medicine and Cellular Longevity
Volume 2016, Article ID 7413963, 11 pages
http://dx.doi.org/10.1155/2016/7413963

Research Article

Exercise Training Improves the Altered Renin-Angiotensin System in the Rostral Ventrolateral Medulla of Hypertensive Rats

Chang-zhen Ren, Ya-Hong Yang, Jia-cen Sun, Zhao-Tang Wu, Ru-Wen Zhang, Du Shen, and Yang-Kai Wang

Department of Physiology, Second Military Medical University, Shanghai 200433, China

Correspondence should be addressed to Yang-Kai Wang; wyangkai2005@163.com

Received 6 September 2015; Revised 10 November 2015; Accepted 17 November 2015

Academic Editor: Hanjun Wang

The imbalance between angiotensin II (Ang II) and angiotensin 1–7 (Ang 1–7) in the brain has been reported to contribute to cardiovascular dysfunction in hypertension. Exercise training (ExT) is beneficial to hypertension and the mechanism is unclear. This study was aimed to determine if ExT improves hypertension via adjusting renin angiotensin system in cardiovascular centers including the rostral ventrolateral medulla (RVLM). Spontaneously hypertensive rats (SHR, 8 weeks old) were subjected to low-intensity ExT or kept sedentary (Sed) for 12 weeks. Blood pressure elevation coupled with increase in age was significantly decreased in SHR received ExT compared with Sed. The results in vivo showed that ExT significantly reduced or increased the cardiovascular responses to central application of sarthran (antagonist of Ang II) or A779 (antagonist of Ang 1–7), respectively. The protein expression of the Ang II acting receptor AT1R and the Ang 1–7 acting receptor Mas in the RVLM was significantly reduced and elevated in SHR following ExT, respectively. Moreover, production of reactive oxygen species in the RVLM was significantly decreased in SHR following ExT. The current data suggest that ExT improves hypertension via improving the balance of Ang II and Ang 1–7 and antioxidative stress at the level of RVLM.

1. Introduction

Hypertension is characterized by elevated levels of blood pressure (BP) and sympathetic tone, which are associated with the development and prognosis of this disease [1, 2]. It is well known that the rostral ventrolateral medulla (RVLM) is a key region for central control of sympathetic outflow and plays a vital role in maintaining resting BP and sympathetic tone [3]. It has been suggested that abnormalities in structure and function of the RVLM contribute to the pathogenesis of the neurogenic hypertension [4, 5].

It is also well known that the renin-angiotensin system (RAS) has widely cardiovascular regulatory effects and its abnormality participates the generation and development of hypertension [6, 7]. Besides the peripheral RAS as we know well, there is another independent RAS in the central nervous system, which also has been implicated in the pathogenesis of hypertension [8]. All of the components of the RAS (precursor, enzymes, peptides, and receptors) are presented in brain areas (e.g., RVLM, NTS, and PVN) involved in cardiovascular control [9]. In a classical RAS, angiotensin (Ang) II produced from Ang I by an angiotensin-converting enzyme (ACE) is a strong bioactive substance and its activation contributes to the development of the hypertension [10]. Besides the ACE-Ang II-AT_1R axis, recent studies have established a new regulatory axis in the RAS [11]. In this axis, angiotensin (Ang) (1–7) is finally produced from Ang I or Ang II by the catalytic activity of angiotensin-converting enzyme 2 (ACE2). Ang (1–7) shows actions different from those of AT_1R stimulation, such as vasodilatation, natriuresis, and antiproliferation [12]. It has been found that the microinjection of Ang II into the RVLM can cause the higher elevated amplitude of BP, and the expression of AT_1R in the spontaneously hypertensive rats (SHR) was higher than in the normotensive rats [13–16].

In contrast, the evidence showed that the central effect of Ang 1–7 had been downregulated in SHR [17, 18].

Previous studies [19–23] have shown that low-intensity exercise training (ExT) is an efficient strategy for patient with hypertension by reducing BP and cardiovascular risk. However, the mechanisms by which ExT improves cardiovascular dysfunction in hypertension have been still unclear. Previous studies often focused on the peripheral mechanism which ExT may act on, such as predominance of endothelium relaxing over contractile factors [24]. Recent evidence suggested that neural plasticity in the central cardiovascular networks can be more important for the beneficial effects of ExT on cardiovascular dysfunctions [25, 26]. It has been known that antihypertension can be caused by blockade of central/peripheral RAS [27]. A previous study further showed that ExT can affect the central RAS via anti-inflammatory cytokines [28]. However, it is still not known whether the ExT-induced benefit on hypertension is dependent or not on balance of the expression/activity of central Ang II and Ang 1–7. Therefore, this study was designed to determine the effect of ExT on the imbalance of the central Ang II and Ang 1–7 in SHR.

2. Methods

2.1. Animals and General Procedures. Experiments were carried out in eight-week-old male SHR and age-matched normotensive Wistar-Kyoto (WKY) rats purchased from Sino-British SIPPR/BK Laboratory Animal Ltd. (Shanghai, China). All of the procedures in this study were approved by the Second Military Medical University Institutional Animal Care and Use Committee and were performed as per the institutional animal care guidelines.

2.2. ExT Protocol and Experimental Design. Male WKY and SHR (eight-week-old) were preselected from their ability to walk on a treadmill (FT-200, Taimen Co., China), and only active rats (≈80%) were used in this study. These selected rats were randomly assigned to the sedentary group (WKY-Sed; SHR-Sed) or the ExT group (WKY-ExT; SHR-ExT). Briefly, the ExT rats ran on a motor-driven treadmill continuously for a period of 12 weeks (5 days per week; 60 min per day at 15–20 m/min), as described in our and other previous studies [29–31]. The training intensity was based on 50–60% of each animal's maximal running speed, which was measured by maximal exercise tests on weeks 0, 6, and 12 (Table 1). Based on a previous study [32], maximal running speed of each group was estimated from graded exercise on treadmill. The test was started at 7.5 m/min with increments of 1.5 m/min every 2 min up to exhaustion. Maximal running speed achieved was considered as the maximal exercise capacity. Training intensity was at 50–60% of each animal's maximal running speed. The sedentary groups were handled at least 3 times every week to become accustomed to the experimental procedures. A noninvasive computerized tail-cuff system (ALC-NIBP, Shanghai Alcott Biotech, Inc., China), as described previously [28], was used to measure BP and HR under conscious condition. The mean arterial BP and heart rate (HR) were measured with volume pressure recording sensor technology, which measures four parameters simultaneously: systolic blood pressure, diastolic blood pressure, mean arterial pressure, and heart pulse rate. BP was measured on three consecutive days, and values were averaged from at least six consecutive cycles. BP was measured at baseline (8 weeks of age) and then every 4 weeks until the end of the training protocol and sedentary period.

Table 1: Maximal running speeds in ExT groups.

		Maximal speeds (km/h)		
	n	Week 0	Week 6	Week 12
WKY-ExT	15	1.33 ± 0.07	$1.76 \pm 0.05^{*}$	$2.21 \pm 0.06^{*}$
SHR-ExT	15	$1.87 \pm 0.06^{\dagger}$	$2.04 \pm 0.08^{*\dagger}$	$2.43 \pm 0.07^{*\dagger}$

Data are mean ± SE. $^{*}P < 0.05$ versus week 0. $^{\dagger}P < 0.05$ versus WKY-ExT.

After the last exercise session at the age of 20 weeks, animals were allowed at least 24 hr to recover from exercise to minimize alterations in cardiovascular control and further subjected to the following in vivo or in vitro experiments.

2.3. Measurement of Citrate Synthase Concentration. Citrate synthase (CS) activity is a validated biomarker for mitochondrial density in skeletal muscle and used as a biochemical marker which undergoes adaptive increase in skeletal muscle with ExT [33]. Soleus muscles from the right leg of the animals were collected, weighted, and stored at −80°C for measurement of citrate synthase. Rat Citrate Synthase ELISA kit (E03876; Shanghai Yunyan Biological Technology Co, China) was used to measure citrate synthase concentration in the whole muscle. Briefly, muscle tissue was homogenized in an extraction buffer and centrifuged at 4°C and an aliquot of supernatants was collected for measuring the enzyme concentration. Reaction was terminated by an addition of a sulfuric acid solution, and the color change was measured spectrophotometrically at a wavelength of 450 nm. The concentration (pg/mg) of citrate synthase in the samples was then determined by comparing the OD of the samples to the standard curve.

2.4. General Surgical Procedures and Intracerebroventricular (ICV) Injections. The surgical procedures were carried out as our study described previously [34]. Briefly, rats were anesthetized with urethane (800 mg/kg ip) and α-chloralose (40 mg/kg ip), and the trachea was cannulated to facilitate mechanical respiration. The right common carotid artery was catheterized for BP measurement by PowerLab (8SP, AD Instruments). The mean arterial pressure (MAP) and heart rate (HR) were derived from the BP pulse. The vein was cannulated for supplemental anesthesia and drugs. The rat was placed in a stereotaxic frame. A hole in skull surface was drilled for lateral ventricle injections, or the dorsal surface of the medulla was surgically exposed for RVLM microinjections. Body temperature was kept at 37°C by a temperature controller.

The rats were implanted with unilateral guide cannula (21 gauges) for ICV injections of drugs, which was described

previously [35, 36]. Coordinates for lateral ventricle injections (−1.0 mm to Bregma; 1.5 mm lateral to midline; and −4.5 mm to the surface of the skull) were based on the rat atlas of Paxinos and Watson [37]. The guide cannula was fixed to the skull with dental acrylic resin. The needle used for injection into the LV was connected by a PE-10 tubing to a 10 μL Hamilton syringe. The needle was carefully inserted into the guide cannula and slow injections were performed. The volume of LV injection each time was 1 μL.

2.5. RVLM Microinjection. The procedures for RVLM microinjection were described previously [38]. In brief, microinjections were made from a multibarrel micropipette (20–50 μm diameter) and the coordinates for the RVLM (2.0–2.5 mm rostral and 1.8–2.1 mm lateral to Obex and 2.8–3.2 mm ventral to the dorsal surface of the medulla) were based on the rat atlas [37]. Three-barrel micropipette was connected by a pneumatic picopump (PV820, WPI). The three-barrel micropipette was filled with L-glutamate, tempol, and artificial cerebrospinal fluid (aCSF). The injection volume each time was 100 nL and made over a period of 5–10 s. The aCSF served as vehicle control. The RVLM was chemically identified by a pressor response to L-glutamate (1 nmol) microinjection. The levels of BP and HR were monitored before and after RVLM injection of tempol (1 nmol). At the end of experiments, 2% pontamine sky blue solution was injected into the same site for marking the injection distribution.

2.6. Western Blot Analysis. After rats were euthanized with an overdose of pentobarbital sodium (200 mg/kg, ip), the brain tissues including the RVLM, the nucleus of solitary tract (NTS) were punched and collected on coronal sections of brainstem according to the rat atlas [37]. The fixed frozen brainstem was cut into 20 μm thick coronal sections of brainstem by the cryoultramicrotome and punched with a 1 mm internal diameter needle according to the coordinates. As described previously [38], western blot was performed for determining protein levels of ACE, AT_1R, ACE2, and MasR in the RVLM and NTS. The membrane was probed with anti-ACE (sc-20791, Santa Cruz), anti-AT_1R (sc-31181, Santa Cruz), anti-ACE2 (sc-20998, Santa Cruz), and anti-MasR (sc-54848, Santa Cruz). The protein bands were visually detected and analyzed. The levels of target proteins were normalized to α-tubulin (number T6074, Sigma), which served as a loading control.

2.7. High-Performance Liquid Chromatography (HPLC). As described previously [31], HPLC (model 582 pump, ESA, USA) with electrochemical detection (Model 5300, ESA, USA) was performed to detect 24 h urinary excretion of norepinephrine (NE). Briefly, urinary samples (24 h) were collected and acidified with glacial acetic acid. Dihydroxybenzylamine (Sigma) was used as the internal standard. NE was absorbed onto acid-washed alumina with 3 mol/L tris(hydroxymethyl)aminomethane buffer. After shaking and settlement, NE was extracted with 0.2 M glacial acetic acid (400 μL). Supernatant (40 μL) was injected into HPLC column (reverse phase, ESA 150 × 3.2 mm, 3 μm C18 (P/N 70-0636)), and NE was eluted with mobile phase. The flow rate was set at 0.5 mL/min.

2.8. Measurement of Reactive Oxygen Species (ROS) in the RVLM. The level of ROS in the RVLM was evaluated by the oxidative fluorescence dye dihydroethidium (DHE), as described previously [39]. In brief, unfixed frozen brains were cut into 30 μm thick coronal sections of brainstem according to the standard atlas of rat [37]. Brain sections were placed on glass slides. We added the DHE (10 μmol/L) on the brain section directly and did not cover the glass slides with the cover-slips, and then put the glass slides in a light-protected humidified chamber at 37°C for 30 min. The oxidative fluorescence intensity was detected at 585 nm wave length by a laser scanning confocal imaging system (Leica SP5). The average fluorescent intensities were evaluated by Leica software and used for image quantification. This software was designed with the auto model to calculate the fluorescence intensity in the chosen areas.

2.9. Statistical Analysis. All data were presented as mean ± SEM. Two-way ANOVA with repeated measures was used to assess the efficacy of ExT during the ExT. Student's t-test or two-way ANOVA followed by Newman-Keuls post hoc test was used to assess the differences between groups (WKY and SHR) and conditions (Sed and ExT). Differences with a $P < 0.05$ were considered significant.

3. Results

3.1. Assessment of ExT Efficacy. At the beginning of ExT (rats at age of 8 weeks), MAP of SHR-Sed (157 ± 5.1 mmHg) in conscious condition was significantly higher ($P < 0.05$, $n = 15$) than WKY-Sed (118 ± 6.2 mmHg) and remained the higher levels for the time of the study. After 12 wk period of ExT, MAP was significantly lower ($P < 0.05$, $n = 15$) in SHR-ExT (183 ± 6.2 mmHg) than in SHR-Sed (198 ± 3.2 mmHg). However, WKY rats showed no change of BP following ExT treatment (Figure 1). As shown in Table 2, several values were measured for effects of ExT at the end of Sed or ExT protocol (at age of 20 weeks). Body weight in ExT groups was significantly reduced compared with Sed groups. Soleus muscle weight was significantly increased in ExT groups compared to Sed groups. Twenty-four-hour urinary excretion of NE level was higher in SHR-Sed than in WKY-Sed, whereas it was significantly reduced following ExT protocol. In additional, we confirmed that the concentration of citrate synthase, a marker of ExT efficacy, in soleus muscle was significantly higher in ExT than in Sed rats.

3.2. ExT Modulates RAS Components in the RVLM of SHR. To determine whether ExT modulates the components of RAS, we examined the protein levels of ACE, AT_1R, ACE2, and MasR in the RVLM and the NTS. As shown in Figure 2, the protein expressions of ACE and AT_1R in the RVLM

Table 2: Measurements of parameters for determining efficacy of ExT.

Parameters	n	WKY-Sed	WKY-ExT	SHR-Sed	SHR-ExT
Body weight (BW, g)	15	320 ± 5	292 ± 4*	305 ± 5	280 ± 4†
SMW (mg)	15	110 ± 3	136 ± 4*	105 ± 5	137 ± 4†
SMW/BW (mg/g)	15	0.34 ± 0.01	0.47 ± 0.01*	0.34 ± 0.01	0.49 ± 0.01†
CS in SMW (pg/mg)	15	672 ± 25	790 ± 35*	685 ± 25	778 ± 30†
MAP (mmHg)	10	122 ± 3	116 ± 6	175 ± 5*	150 ± 5*†
HR (beats/min)	10	397 ± 8	352 ± 9*	453 ± 8*	392 ± 7†
NE in 24 h urine (μg)	10	0.41 ± 0.03	0.39 ± 0.05	0.71 ± 0.05*	0.55 ± 0.04*†

n: number of animals; MAP: mean arterial pressure; SMW: soleus muscle wet weight; CS: citrate synthase; MAP: mean arterial pressure; NE: norepinephrine; WKY-Sed: Wistar-Kyoto-sedentary; SHR-Sed: spontaneously hypertensive rat-sedentary; WKY-ExT: Wistar-Kyoto-exercise training; SHR-ExT: spontaneously hypertensive rat-exercise training. Data are mean ± SE. Values for MAP and HR were obtained in anaesthetized rats. MAP was measured by catheterizing femoral artery. *$P < 0.05$ versus WKY-Sed. †$P < 0.05$ versus SHR-Sed.

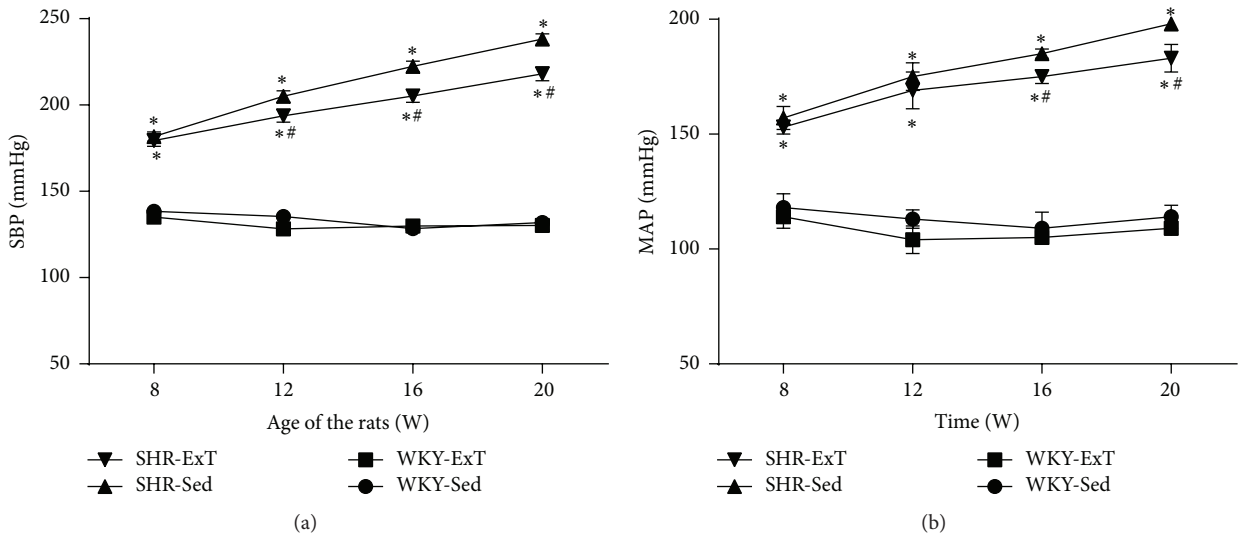

Figure 1: Time course of systolic blood pressure (a) and mean arterial pressure (b) in sedentary or exercised WKY and SHR groups. The values for blood pressure in conscious rats were measured by tail-cuff method. Blood pressure has already lowered in SHR-ExT compared with SHR-Sed rats from 8th week of ExT (at 16 weeks of age). $n = 15$ in each group. *$P < 0.05$ versus WKY-Sed; #$P < 0.05$ versus SHR-Sed. P value for groups was <0.001, P value for time was <0.001, and group x time interaction was <0.001.

were significantly higher in SHR-Sed compared with WKY-Sed, which were downregulated following ExT treatment. However, these two proteins showed no differences in the NTS of rats with or without ExT. In additional, the protein expressions of ACE2 and MasR levels in the RVLM and NTS were significantly reduced in SHR-Sed compared with WKY-Sed (Figure 3). ExT significantly increased ACE2 and MasR expression in the RVLM of SHR. In the NTS, interestingly, only MasR expression was significantly increased in SHR with ExT.

3.3. ExT Improves Central Functionality of ACE-Ang II-AT$_1$R Axis and ACE2-Ang-1–7-MasR Axis in SHR. To investigate the influence of ExT on central functionality of RAS in SHR, we examined the cardiovascular response to acute ICV injection of the Ang II antagonist sarthran and the Ang 1–7 antagonist A779. As shown in Figure 4, the depressor response evoked by ICV injection of sarthran (15 nmol) was significantly attenuated (−40 ± 3.4 versus −28 ± 3.8 mmHg) in SHR with ExT treatment. It was interesting that the depressor effect (−10 ± 3.5 mmHg) of ICV injection of A779 (500 pmol) was reversed to a pressor response (13.2 ± 2.5 mmHg) in SHR following ExT treatment. However, there was no difference in HR between SHR-Sed and SHR-ExT.

3.4. ExT Attenuated ROS Production in the RVLM of SHR. As shown in Figure 5, microinjection of the SOD mimic tempol (1 nmol) into the RVLM produced a greater depressor response in SHR-Sed, which was significantly attenuated in SHR with ExT treatment. DHE staining showed that the production of ROS in the RVLM was significantly higher in SHR-Sed than in WKY-Sed, which was significantly decreased in SHR-ExT (Figure 6).

4. Discussion

The major observations of this study are that (1) ExT significantly reduces BP and sympathetic activity in SHR; (2)

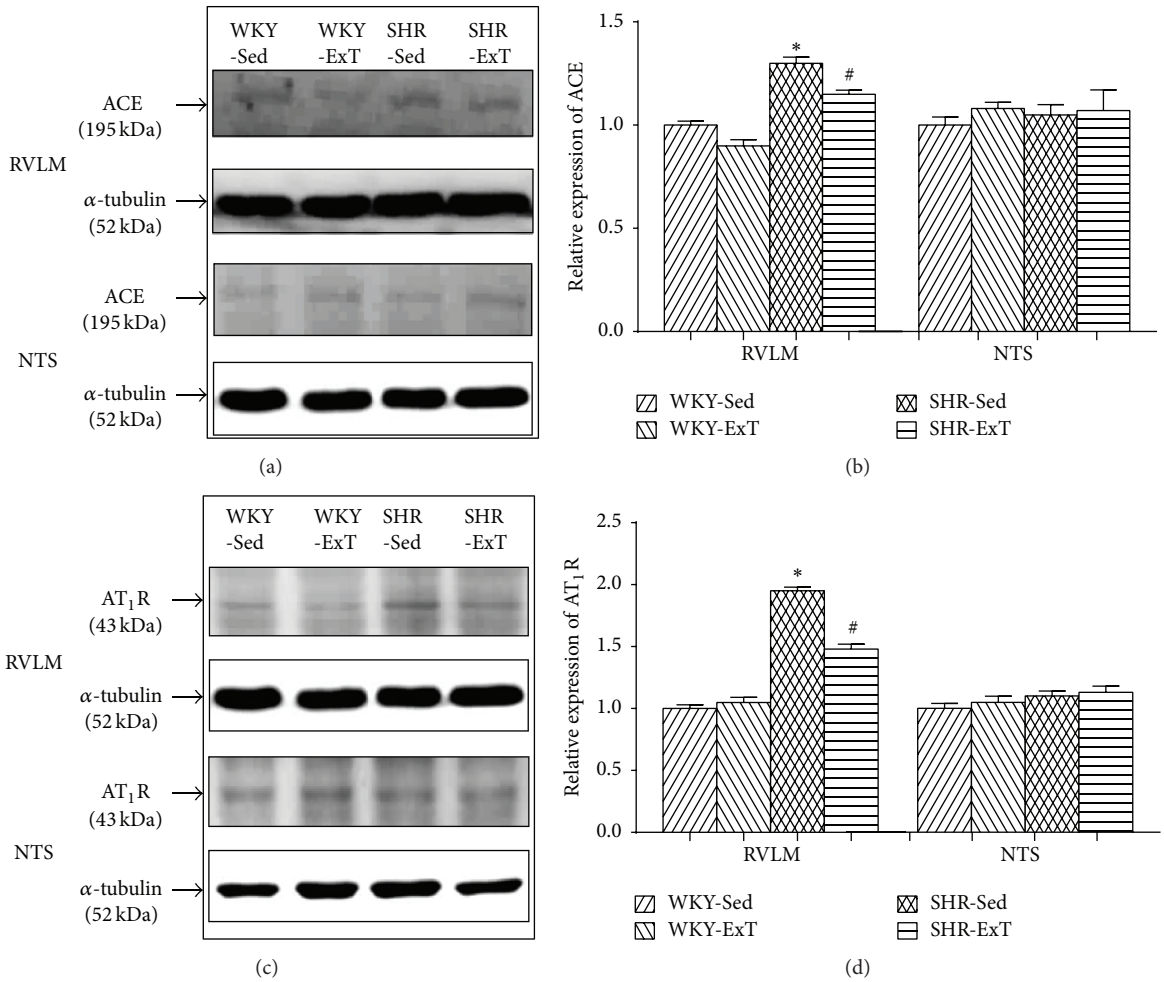

Figure 2: Representative western blot (a, c) and densitometric analysis (b, d) of ACE and AT_1R in the RVLM and NTS of sedentary or exercised WKY and SHR groups. $n = 5$ in each group. $^*P < 0.05$ versus WKY-Sed; $^\#P < 0.05$ versus SHR-Sed. As to AT_1R in the RVLM, P value for WKY-SHR was 0.0006, P value for Sed-ExT was 0.0616, and P value for cross interactions was 0.0177; as to ACE in the RVLM, P value for WKY-SHR was <0.0001, P value for Sed-ExT was 0.0045, and P value for cross interactions was 0.1937; as to AT_1R in the NTS, P value for WKY-SHR was 0.3501, P value for Sed-ExT was 0.7997, and P value for cross interactions was 0.8495; as to ACE in the NTS, P value for WKY-SHR was 0.5408, P value for Sed-ExT was 0.4906, and P value for cross interactions was 0.9744.

ExT treatment improves the functionality of central ACE-Ang II-AT_1R and ACE2-Ang-1–7-MasR in SHR; and (3) ExT significantly reduced the level of ROS in the RVLM of SHR. On basis of these results, we conclude that ExT improves central RAS and decreases oxidative stress in the RVLM of SHR.

ExT, a part of lifestyle modification, has been recognized as an important strategy for antihypertension [40, 41]. However, the exact mechanism by which ExT improves the cardiovascular dysfunctions in hypertension is still unclear. It has been documented that the low-intensity ExT effectively decreases BP in hypertension [42]. In this work, we tested the maximum ExT capacity (velocity) at the beginning of the protocol and further determined the ExT intensity at weeks 6 and 12, which was controlled at 50–60% of maximal ExT capacity according to previous studies [31]. Our study showed that the maximal running speed of SHR was faster than the WKY rats, which was completely consistent with a previous study [43]. The reason for high exercise capacity in the SHR is not clear. It is possible that the enhanced cardiac output, blood pressure, and sympathetic activity in the SHR are attributed to the higher exercise capacity than WKY rats. We found that soleus muscle weight and citrate synthase concentration were significantly increased in ExT groups compared to Sed groups, whereas body weight was reduced in ExT group compared to Sed groups. We also confirmed that ExT significantly lowers BP in SHR but in WKY, as described previously [44]. It is notable that the data of BP was somewhat higher in conscious animals (measured by tail-cuff method) than in anesthetized rats (measured by arterial cannula). This high level of BP in conscious rats may have resulted from the stress induced by the tail-cuff method. Additionally, urinary excretion of NE was significantly decreased in SHR after treatment of ExT. It may be a limitation that the direct recording of sympathetic nerve activity in rats was not performed, which would be more specific measurement.

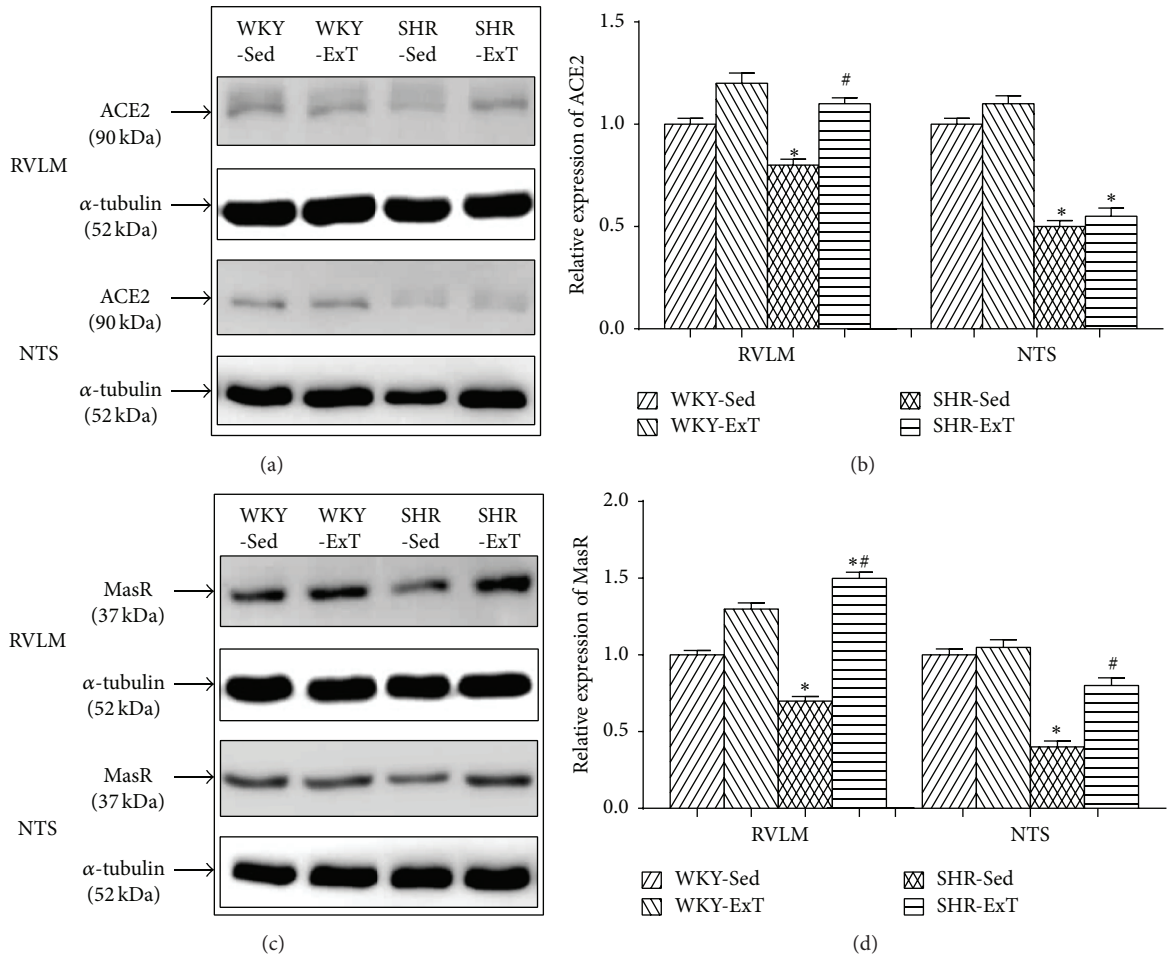

Figure 3: Representative western blot (a, c) and densitometric analysis (b, d) of ACE2 and MasR in the RVLM and NTS of sedentary or exercised WKY and SHR groups. $n = 5$ in each group. $^{*}P < 0.05$ versus WKY-Sed; $^{\#}P < 0.05$ versus SHR-Sed. As to ACE2 in the RVLM, P value for WKY-SHR was <0.0001, P value for Sed-ExT was <0.0001, and P value for cross interactions was 0.0002; as to MasR in the RVLM, P value for WKY-SHR was 0.1891, P value for Sed-ExT was <0.0001, and P value for cross interactions was 0.0003; as to ACE2 in the NTS, P value for WKY-SHR was 0.0002, P value for Sed-ExT was 0.9242, and P value for cross interactions was 0.8496; as to MasR in the NTS, P value for WKY-SHR was 0.0075, P value for Sed-ExT was 0.0231, and P value for cross interactions was 0.0612.

However, elevation of NE can be partly correlated with the enhanced cardiovascular sympathetic activity. Collectively, the current data confirmed the efficacy of ExT to BP and sympathetic activity in SHR.

Previous studies showed that ExT improved the cardiovascular function in hypertension via peripheral and central pathways [24, 26]. For example, ExT can enhance the release of nitric oxide which had been downregulated in hypertension [24]. However, it is also suggested that the central effect of the ExT plays an important role in antihypertensive mechanism [25, 26, 43, 45]. For example, ExT effectively improves abnormalities in the cardiovascular reflex (e.g., baroreflex, chemoreflex). In hypertension, the function of central Ang II is upregulated, whereas central Ang 1–7 is downregulated [16]. Previous study also showed that ExT can change components of RAS via anti-inflammatory cytokines [28]. This study focused on balance between pro- and anti-inflammatory cytokines in the brain of SHR affected by ExT, but the effect of ExT on the functional change of endogenous RAS was still unknown. In order to detect the effect of ExT on RAS involved in cardiovascular regulation in the whole central nervous system, the agents of A779 or sarthran were injected into the lateral ventricles in this study. Because the RVLM is a key region involved in control of resting blood pressure and sympathetic outflow, it was further subjected for detecting the protein levels of ACE, AT_1R, ACE2, and MasR in response to ExT, which is helpful for determining the possible mechanism responsible for the effect of ExT on central cardiovascular regulation. However, BP and HR in WKY groups have not been changed in response to ExT treatment. Moreover, ExT did not change the expression levels of RAS components in the RVLM of WKY groups. Our data suggested that ExT is capable of improving the balance between Ang II and Ang 1–7 in the brain of SHR. The data from in vivo experiments showed that ExT decreased the cardiovascular response to central blockade of Ang II in SHR. The change in BP evoked by acute injection of Ang 1–7 seems to be similar to Ang II, while the response

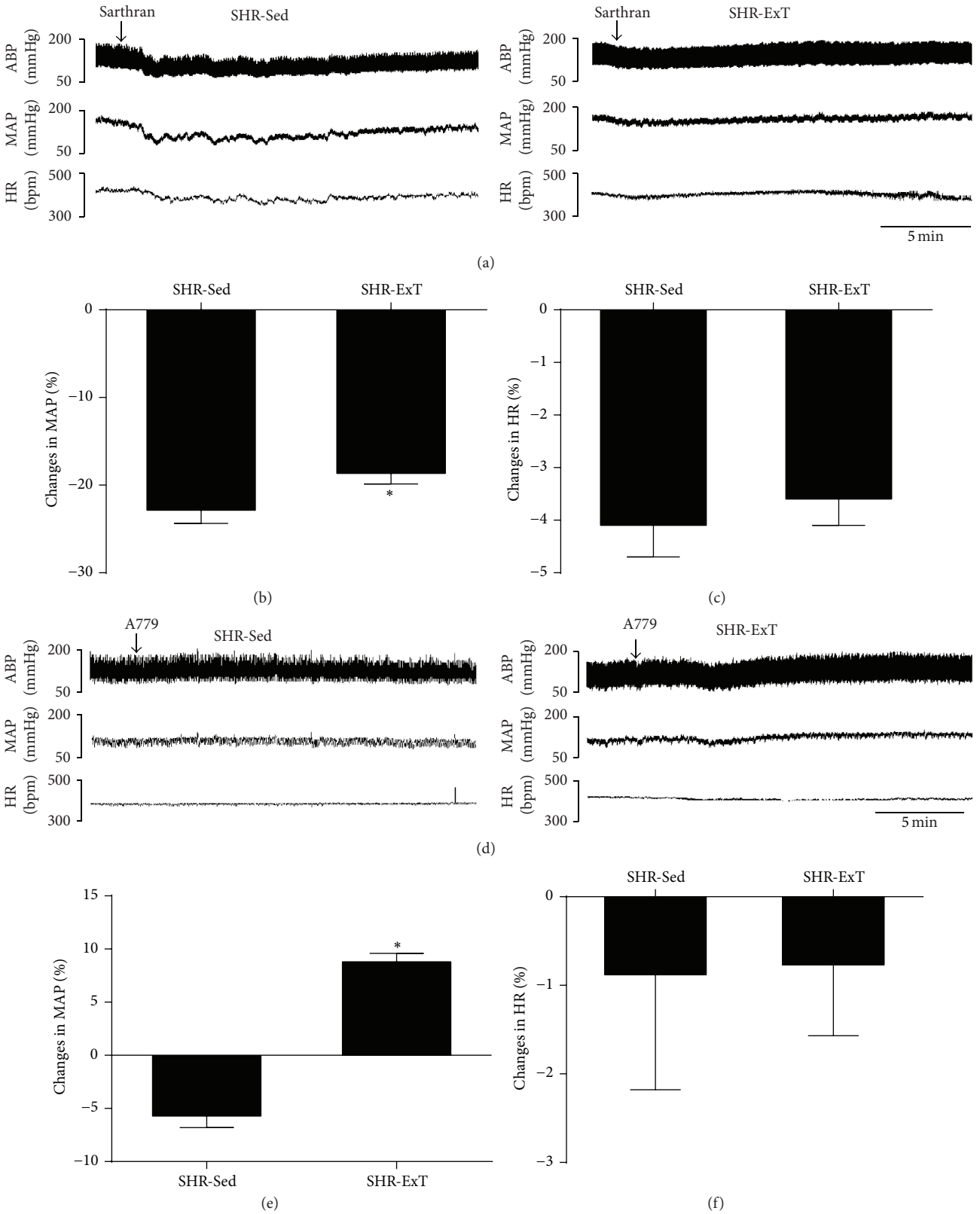

Figure 4: Representative original recordings of effects of ICV infusion of sarthran (15 nmol) or A779 (500 pmol) on cardiovascular activities in sedentary or exercised SHR groups (a, d). ABP: arterial blood pressure; MAP: mean arterial pressure; bpm: beats/min. Percent changes in mean arterial pressure (b, e) and HR (c, f) induced by ICV infusion of sarthran (15 nmol) or A779 (500 pmol) in the two groups. $n = 5$ in each group. $^{*}P < 0.05$ versus SHR-Sed.

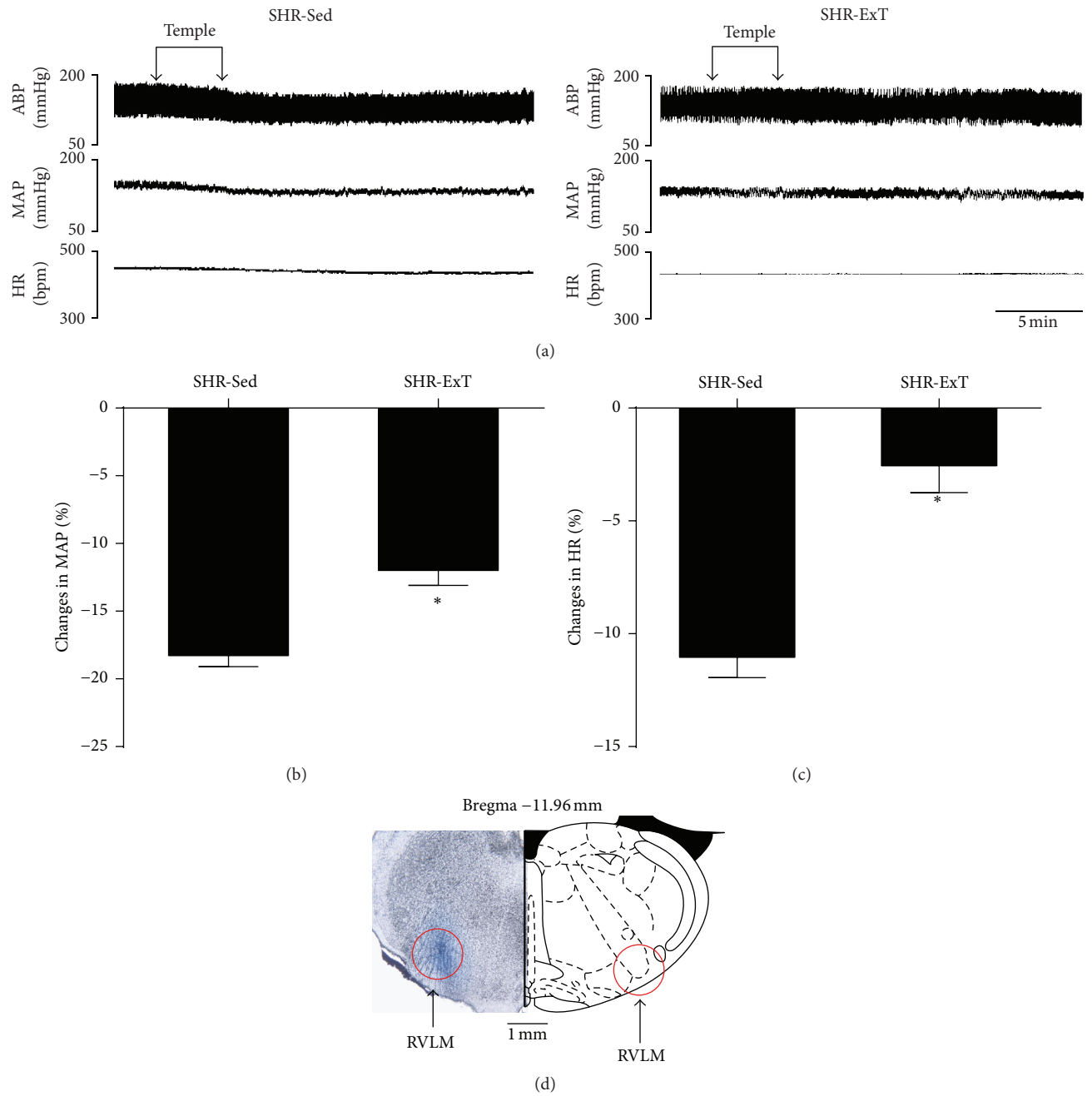

FIGURE 5: (a) Representative original recordings of effects of the SOD mimic tempol (1 nmol) bilaterally injected into the RVLM on BP and HR in sedentary or exercised spontaneously hypertensive rat groups. ABP: arterial blood pressure; MAP: mean arterial pressure; bpm: beats/min. Percent changes in mean arterial pressure (b) and HR (c) induced by bilateral microinjection of tempol into the RVLM. (d) Distribution of the maker sky blue within the brain section. $n = 5$ in each group. $^{*}P < 0.05$ versus SHR-Sed.

sensitivity to central Ang 1–7 is increased in SHR following ExT. This data reveals that ExT increases the MasR-mediated actions in central nervous system. ExT reduces the depressor response to central blockade of AT_1R with sarthran in SHR, suggesting that ExT decreases the endogenous Ang II via downregulating ACE. Additionally, blockade of the MasR with A779 showed that the cardiovascular response to the endogenous Ang 1–7 was more sensitive in SHR with ExT, suggesting that the activity of the MasR is upregulated by ExT treatment. Previous studies show that acute injection of exogenous Ang II and Ang 1–7 produced a similar effect on BP in the RVLM [46] and NTS [47]. Interestingly, increase in endogenous Ang 1–7 by overexpression of ACE2 in the RVLM produced a long-term decrease in BP in hypertensive rats [48]. Acute or chronic increase in Ang 1–7 may present different effect on cardiovascular regulation. So, the significance of Ang 1–7 in the brain area in cardiovascular regulation needs to be further determined. In this study,

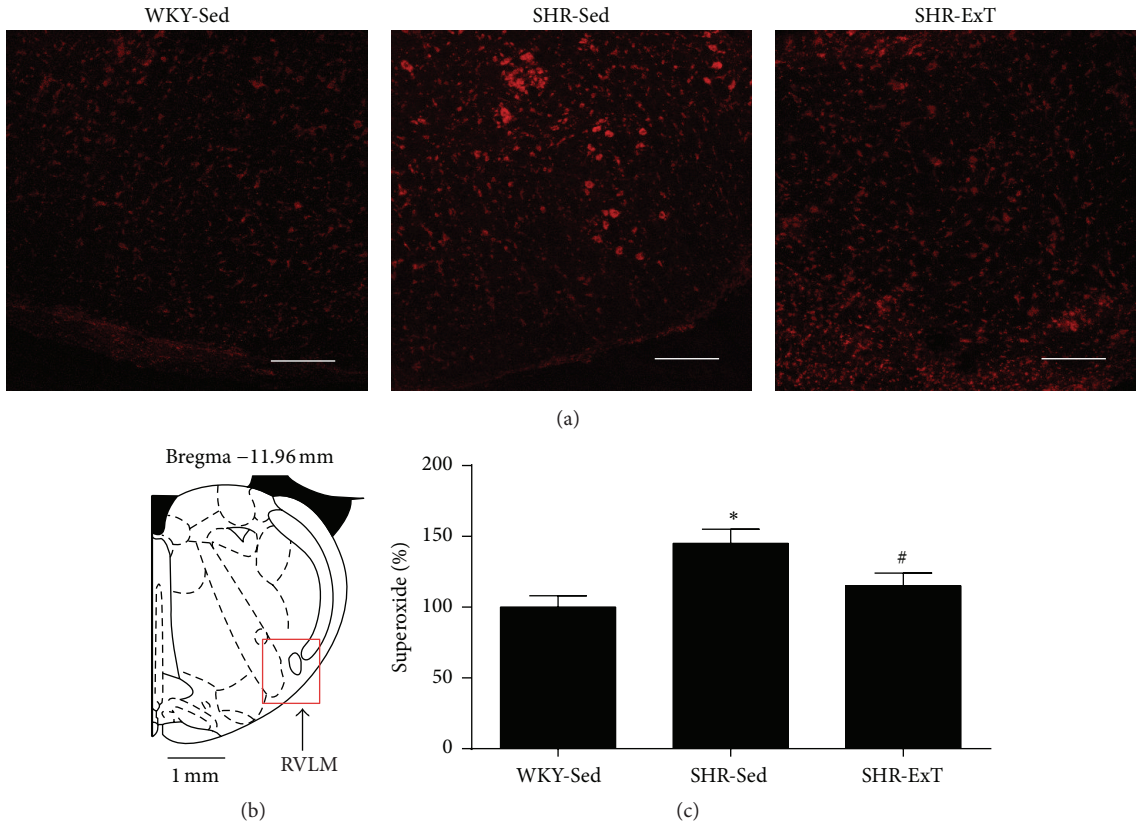

Figure 6: Effects of exercise training on level of ROS in the RVLM from SHR. (a) Representative DHE fluorescence staining images (red color) ROS content in the RVLM of sedentary or exercised SHR and sedentary WKY groups. (b) A red square in a coronary drawing of rat standard atlas of RVLM. (c) Bar graphs show ROS content obtained from DHE fluorescence intensities in the RVLM of SHR. The value of DHE fluorescence intensities in the sedentary WKY was normalized as 100%. $n = 5$ per group. $^{*}P < 0.05$ versus WKY-Sed, $^{\#}P < 0.05$ versus SHR-Sed. Scale bars = 200 μm.

the ExT-induced enhancement in Ang-1–7/MasR axis may have resulted from chronic upregulation of ACE2. Because comparison of central cardiovascular response to RAS components between SHR and WKY has widely been reported, only SHR rats with or without ExT were performed to in vivo functional experiments in the present study. This may be a limitation in this study. However, we had verified the change of RAS in WKY and SHR groups via the western blot showing the change of protein expression of RAS components.

Although ExT adjusts the central RAS-mediated cardiovascular effects, it is not clear which cardiovascular region is involved in the effect of ExT on central RAS in hypertension. In view of the importance of the NTS and RVLM in regulating cardiovascular function [49, 50], they are subjected to further experiments. It is reported that ExT downregulates the expression of angiotensinogen mRNA but has no effect on AT_1R in the NTS [43]. We also confirmed that ExT had no effect on AT_1R expression in the NTS of SHR. In the RVLM, ExT significantly reduced ACE and AT_1R expression and increased ACE2 and MasR expression in the RVLM of SHR. It is worth to concern the specificity of commercially available antibodies for the AT_1R [51]. In this work, however, we confirmed that functional state of central AT_1R by ExT was reduced by observation of BP and HR changes in response to central injection of sarthran. These data indicate that the RVLM may be a main region involved in the effect of ExT on central RAS in hypertension.

In the RVLM, oxidative stress originated from RAS contributes to high levels of BP in hypertension. We first confirm that the decrease in BP evoked by injection of the SOD mimic tempol into the RVLM is attenuated by ExT in SHR, suggesting that ExT effectively reduced the ROS-mediated cardiovascular function in SHR. This is consistent with a previous study [52]. Importantly, we directly detected the level of ROS by DHE probe in the RVLM. We further confirmed that the level of ROS within the RVLM was higher in SHR than in WKY, which was attenuated by ExT. It may be a limitation that the ROS level between WKY-Sed and WKY-ExT was not further compared. The mechanism responsible for the ExT-mediated antioxidative stress in the RVLM of hypertension is not clear. It is reported that activation of the AT_1R-mediated NADPH oxidase plays an important role in ROS production in hypertension [53]. Therefore, it is possible that downregulation of ACE-Ang II- AT_1R axis by ExT is

an important pathway for antioxidative stress in the RVLM. Additionally, upregulation of ACE2-Ang-1–7-MasR axis by ExT is also involved in reducing oxidative stress in the RVLM.

In summary, the chronic ExT improves the cardiovascular function in hypertension. However, the antihypertensive mechanism of ExT is fully not understood. Here we provide new insight into the signaling mechanism by which ExT is capable of improving the balance between Ang II and Ang 1–7 in the RVLM of hypertensive rats.

Conflict of Interests

The authors declared no competing financial interests exist.

Authors' Contribution

Chang-zhen Ren, Ya-Hong Yang, and Jia-cen Sun contribute equally to this work.

Acknowledgments

The authors gratefully acknowledge the statistical assistance of Dr. Jian Lu (from the Department of Statistical Analysis, SMMU). This work was supported by the National Natural Science Foundation of China (81170240, 81370363, 81470534, and 3150070161).

References

[1] G. Grassi, A. Mark, and M. Esler, "The sympathetic nervous system alterations in human hypertension," *Circulation Research*, vol. 116, no. 6, pp. 976–990, 2015.

[2] G. Seravalle, G. Mancia, and G. Grassi, "Role of the sympathetic nervous system in hypertension and hypertension-related cardiovascular disease," *High Blood Pressure and Cardiovascular Prevention*, vol. 21, no. 2, pp. 89–105, 2014.

[3] S. C. Malpas, "Sympathetic nervous system overactivity and its role in the development of cardiovascular disease," *Physiological Reviews*, vol. 90, no. 2, pp. 513–557, 2010.

[4] N. Charkoudian and J. A. Rabbitts, "Sympathetic neural mechanisms in human cardiovascular health and disease," *Mayo Clinic Proceedings*, vol. 84, no. 9, pp. 822–830, 2009.

[5] K. Wustmann, J. P. Kucera, I. Scheffers et al., "Effects of chronic baroreceptor stimulation on the autonomic cardiovascular regulation in patients with drug-resistant arterial hypertension," *Hypertension*, vol. 54, no. 3, pp. 530–536, 2009.

[6] M. Johansson, S. A. Gao, P. Friberg et al., "Baroreflex effectiveness index and baroreflex sensitivity predict all-cause mortality and sudden death in hypertensive patients with chronic renal failure," *Journal of Hypertension*, vol. 25, no. 1, pp. 163–168, 2007.

[7] T. D. Giles, "Renin-angiotensin system modulation for treatment and prevention of cardiovascular diseases: toward an optimal therapeutic strategy," *Reviews in Cardiovascular Medicine*, vol. 8, supplement 2, pp. S14–S21, 2007.

[8] M. I. Phillips and E. M. De Oliveira, "Brain renin angiotensin in disease," *Journal of Molecular Medicine*, vol. 86, no. 6, pp. 715–722, 2008.

[9] O. V. B. Und Halbach and D. Albrecht, "The CNS renin-angiotensin system," *Cell and Tissue Research*, vol. 326, no. 2, pp. 599–616, 2006.

[10] M. Bader and D. Ganten, "Update on tissue renin-angiotensin systems," *Journal of Molecular Medicine*, vol. 86, no. 6, pp. 615–621, 2008.

[11] M. A. Crackower, R. Sarao, G. Y. Oudit et al., "Angiotensin-converting enzyme 2 is an essential regulator of heart function," *Nature*, vol. 417, no. 6891, pp. 822–828, 2002.

[12] R. A. S. Santos, A. C. Simoes e Silva, C. Maric et al., "Angiotensin-(1-7) is an endogenous ligand for the G protein-coupled receptor Mas," *Proceedings of the National Academy of Sciences of the United States of America*, vol. 100, no. 14, pp. 8258–8263, 2003.

[13] R. A. L. Dampney, M. A. P. Fontes, Y. Hirooka, J. Horiuchi, P. D. Potts, and T. Tagawa, "Role of angiotensin II receptors in the regulation of vasomotor neurons in the ventrolateral medulla," *Clinical and Experimental Pharmacology and Physiology*, vol. 29, no. 5-6, pp. 467–472, 2002.

[14] L. Hu, D.-N. Zhu, Z. Yu, J. Q. Wang, Z.-J. Sun, and T. Yao, "Expression of angiotensin II type 1 (AT_1) receptor in the rostral ventrolateral medulla in rats," *Journal of Applied Physiology*, vol. 92, no. 5, pp. 2153–2161, 2002.

[15] H. Muratani, C. M. Ferrario, and D. B. Averill, "Ventrolateral medulla in spontaneously hypertensive rats: role of angiotensin II," *American Journal of Physiology—Regulatory Integrative and Comparative Physiology*, vol. 264, no. 2, part 2, pp. R388–R395, 1993.

[16] M. A. P. Fontes, M. C. M. Pinge, V. Naves et al., "Cardiovascular effects produced by microinjection of angiotensins and angiotensin antagonists into the ventrolateral medulla of freely moving rats," *Brain Research*, vol. 750, no. 1-2, pp. 305–310, 1997.

[17] G. Z. Chaves, S. M. Caligiorne, R. A. S. Santos, M. C. Khosla, and M. J. Campagnole-Santos, "Modulation of the baroreflex control of heart rate by angiotensin-(1-7) at the nucleus tractus solitarii of normotensive and spontaneously hypertensive rats," *Journal of Hypertension*, vol. 18, no. 12, pp. 1841–1848, 2000.

[18] D. R. Oliveira, R. A. S. Santos, G. F. F. Santos, M. C. Khosla, and M. J. Campagnole-Santos, "Changes in the baroreflex control of heart rate produced by central infusion of selective angiotensin antagonists in hypertensive rats," *Hypertension*, vol. 27, no. 6, pp. 1284–1290, 1996.

[19] S. Lamina, C. G. Okoye, and S. M. Hanif, "Effects of interval exercise training programme on the indices of adiposity and biomarker of inflammation in hypertension: a randomised controlled trial," *The Nigerian Postgraduate Medical Journal*, vol. 21, no. 2, pp. 136–143, 2014.

[20] A. S. Ghadieh and B. Saab, "Evidence for exercise training in the management of hypertension in adults," *Canadian Family Physician*, vol. 61, no. 3, pp. 233–239, 2015.

[21] L. H. Kuller, "Weight loss and reduction of blood pressure and hypertension," *Hypertension*, vol. 54, no. 4, pp. 700–701, 2009.

[22] L. P. Svetkey, K. I. Pollak, W. S. Yancy et al., "Hypertension improvement project: randomized trial of quality improvement for physicians and lifestyle modification for patients," *Hypertension*, vol. 54, no. 6, pp. 1226–1233, 2009.

[23] M. Leggio, A. Mazza, G. Cruciani et al., "Effects of exercise training on systo-diastolic ventricular dysfunction in patients with hypertension: an echocardiographic study with tissue velocity and strain imaging evaluation," *Hypertension Research*, vol. 37, no. 7, pp. 649–654, 2014.

[24] Y. Higashi and M. Yoshizumi, "Exercise and endothelial function: role of endothelium-derived nitric oxide and oxidative stress in healthy subjects and hypertensive patients," *Pharmacology and Therapeutics*, vol. 102, no. 1, pp. 87–96, 2004.

[25] M. C. Laterza, L. D. N. J. De Matos, I. C. Trombetta et al., "Exercise training restores baroreflex sensitivity in never-treated hypertensive patients," *Hypertension*, vol. 49, no. 6, pp. 1298–1306, 2007.

[26] C. W. Cotman and N. C. Berchtold, "Exercise: a behavioral intervention to enhance brain health and plasticity," *Trends in Neurosciences*, vol. 25, no. 6, pp. 295–301, 2002.

[27] U. C. Brewster, J. F. Setaro, and M. A. Perazella, "The renin-angiotensin-aldosterone system: cardiorenal effects and implications for renal and cardiovascular disease states," *The American Journal of the Medical Sciences*, vol. 326, no. 1, pp. 15–24, 2003.

[28] D. Agarwal, M. Haque, S. Sriramula, N. Mariappan, R. Pariaut, and J. Francis, "Role of proinflammatory cytokines and redox homeostasis in exercise-induced delayed progression of hypertension in spontaneously hypertensive rats," *Hypertension*, vol. 54, no. 6, pp. 1393–1400, 2009.

[29] K. T. Higa-Taniguchi, F. C. P. Silva, H. M. V. Silva, L. C. Michelini, and J. E. Stern, "Exercise training-induced remodeling of paraventricular nucleus (nor)adrenergic innervation in normotensive and hypertensive rats," *American Journal of Physiology—Regulatory Integrative and Comparative Physiology*, vol. 292, no. 4, pp. R1717–R1727, 2007.

[30] J. S. Gilbert, C. T. Banek, A. J. Bauer, A. Gingery, and K. Needham, "Exercise training attenuates placental ischemia-induced hypertension and angiogenic imbalance in the rat," *Hypertension*, vol. 60, no. 6, pp. 1545–1551, 2012.

[31] Y.-P. Zha, Y.-K. Wang, Y. Deng et al., "Exercise training lowers the enhanced tonically active glutamatergic input to the rostral ventrolateral medulla in hypertensive rats," *CNS Neuroscience and Therapeutics*, vol. 19, no. 4, pp. 244–251, 2013.

[32] R. M. Melo, E. Martinho Jr., and L. C. Michelini, "Training-induced, pressure-lowering effect in SHR: wide effects on circulatory profile of exercised and nonexercised muscles," *Hypertension*, vol. 42, no. 4, pp. 851–857, 2003.

[33] H. Kainulainen, E. Ahomaki, and V. Vihko, "Selected enzyme activities in mouse cardiac muscle during training and terminated training," *Basic Research in Cardiology*, vol. 79, no. 1, pp. 110–123, 1984.

[34] J. Peng, Y.-K. Wang, L.-G. Wang et al., "Sympathoinhibitory mechanism of moxonidine: role of the inducible nitric oxide synthase in the rostral ventrolateral medulla," *Cardiovascular Research*, vol. 84, no. 2, pp. 283–291, 2009.

[35] I. M. Ribeiro, H. C. Ferreira-Neto, and V. R. Antunes, "Subdiaphragmatic vagus nerve activity and hepatic venous glucose are differentially regulated by the central actions of insulin in Wistar and SHR," *Physiological Reports*, vol. 3, no. 5, Article ID e12381, 2015.

[36] G. C. Vaz, A. P. C. O. Bahia, F. C. De Figueiredo Müller-Ribeiro et al., "Cardiovascular and behavioral effects produced by administration of liposome-entrapped GABA into the rat central nervous system," *Neuroscience*, vol. 285, pp. 60–69, 2015.

[37] P. G. Wc, *The Rat Brain in Stereotaxic Coordinates*, Elsevier, 1998.

[38] J.-F. Peng, Z.-T. Wu, Y.-K. Wang et al., "GABAergic mechanism in the rostral ventrolateral medulla contributes to the hypotension of moxonidine," *Cardiovascular Research*, vol. 89, no. 2, pp. 473–481, 2011.

[39] H. V. Robles, E. Romo, A. Sanchez-Mendoza et al., "Lead exposure effect on angiotensin II renal vasoconstriction," *Human and Experimental Toxicology*, vol. 26, no. 6, pp. 499–507, 2007.

[40] F. Manfredini, A. M. Malagoni, S. Mandini et al., "Sport therapy for hypertension: why, how, and how much?" *Angiology*, vol. 60, no. 2, pp. 207–216, 2009.

[41] M. J. Joyner and D. J. Green, "Exercise protects the cardiovascular system: effects beyond traditional risk factors," *Journal of Physiology*, vol. 587, no. 23, pp. 5551–5558, 2009.

[42] L. S. Pescatello, B. A. Franklin, R. Fagard, W. B. Farquhar, G. A. Kelley, and C. A. Ray, "American College of Sports Medicine position stand. Exercise and hypertension," *Medicine & Science in Sports & Exercise*, vol. 36, no. 3, pp. 533–553, 2004.

[43] J. V. C. Felix and L. C. Michelini, "Training-induced pressure fall in spontaneously hypertensive rats is associated with reduced angiotensinogen mRNA expression within the nucleus tractus solitarii," *Hypertension*, vol. 50, no. 4, pp. 780–785, 2007.

[44] P. C. Brum, G. J. Justo Da Silva, E. D. Moreira, F. Ida, C. E. Negrão, and E. M. Krieger, "Exercise training increases baroreceptor gain sensitivity in normal and hypertensive rats," *Hypertension*, vol. 36, no. 6, pp. 1018–1022, 2000.

[45] L. C. Michelini, "Differential effects of vasopressinergic and oxytocinergic pre-autonomic neurons on circulatory control: reflex mechanisms and changes during exercise," *Clinical and Experimental Pharmacology and Physiology*, vol. 34, no. 4, pp. 369–376, 2007.

[46] L.-M. Zhou, Z. Shi, J. Gao et al., "Angiotensin-(1–7) and angiotension II in the rostral ventrolateral medulla modulate the cardiac sympathetic afferent reflex and sympathetic activity in rats," *Pflügers Archiv—European Journal of Physiology*, vol. 459, no. 5, pp. 681–688, 2010.

[47] A. Sakima, D. B. Averill, S. O. Kasper et al., "Baroreceptor reflex regulation in anesthetized transgenic rats with low glia-derived angiotensinogen," *American Journal of Physiology—Heart and Circulatory Physiology*, vol. 292, no. 3, pp. H1412–H1419, 2007.

[48] Y.-K. Wang, D. Shen, Q. Hao et al., "Overexpression of angiotensin-converting enzyme 2 attenuates tonically active glutamatergic input to the rostral ventrolateral medulla in hypertensive rats," *The American Journal of Physiology—Heart and Circulatory Physiology*, vol. 307, no. 2, pp. H182–H190, 2014.

[49] R. A. L. Dampney, "Functional organization of central pathways regulating the cardiovascular system," *Physiological Reviews*, vol. 74, no. 2, pp. 323–364, 1994.

[50] A. J. Lawrence and B. Jarrott, "Neurochemical modulation of cardiovascular control in the nucleus tractus solitarius," *Progress in Neurobiology*, vol. 48, no. 1, pp. 21–53, 1996.

[51] M. Herrera, M. A. Sparks, A. R. Alfonso-Pecchio, L. M. Harrison-Bernard, and T. M. Coffman, "Lack of specificity of commercial antibodies leads to misidentification of angiotensin type 1 receptor protein," *Hypertension*, vol. 61, no. 1, pp. 253–258, 2013.

[52] T. Kishi, Y. Hirooka, M. Katsuki et al., "Exercise training causes sympathoinhibition through antioxidant effect in the rostral ventrolateral medulla of hypertensive rats," *Clinical and Experimental Hypertension*, vol. 34, no. 4, pp. 278–283, 2012.

[53] L. Gao, W. Wang, Y.-L. Li et al., "Superoxide mediates sympathoexcitation in heart failure: roles of angiotensin II and NAD(P)H oxidase," *Circulation Research*, vol. 95, no. 9, pp. 937–944, 2004.

Hindawi Publishing Corporation
Oxidative Medicine and Cellular Longevity
Volume 2016, Article ID 1451676, 13 pages
http://dx.doi.org/10.1155/2016/1451676

Research Article

Inhibition of Receptor Interacting Protein Kinases Attenuates Cardiomyocyte Hypertrophy Induced by Palmitic Acid

Mingyue Zhao,[1] Lihui Lu,[1] Song Lei,[2] Hua Chai,[1] Siyuan Wu,[1] Xiaoju Tang,[1] Qinxue Bao,[1] Li Chen,[1] Wenchao Wu,[1] and Xiaojing Liu[1]

[1]*Laboratory of Cardiovascular Diseases, Regenerative Medicine Research Center, West China Hospital, Sichuan University, Chengdu 610041, China*
[2]*Department of Pathology, West China Hospital, Sichuan University, Chengdu 610041, China*

Correspondence should be addressed to Xiaojing Liu; liuxq@scu.edu.cn

Received 18 August 2015; Revised 12 October 2015; Accepted 13 October 2015

Academic Editor: Hanjun Wang

Palmitic acid (PA) is known to cause cardiomyocyte dysfunction. Cardiac hypertrophy is one of the important pathological features of PA-induced lipotoxicity, but the mechanism by which PA induces cardiomyocyte hypertrophy is still unclear. Therefore, our study was to test whether necroptosis, a receptor interacting protein kinase 1 and 3 (RIPK1 and RIPK3-) dependent programmed necrosis, was involved in the PA-induced cardiomyocyte hypertrophy. We used the PA-treated primary neonatal rat cardiac myocytes (NCMs) or H9c2 cells to study lipotoxicity. Our results demonstrated that cardiomyocyte hypertrophy was induced by PA treatment, determined by upregulation of hypertrophic marker genes and cell surface area enlargement. Upon PA treatment, the expression of RIPK1 and RIPK3 was increased. Pretreatment with the RIPK1 inhibitor necrostatin-1 (Nec-1), the PA-induced cardiomyocyte hypertrophy, was attenuated. Knockdown of RIPK1 or RIPK3 by siRNA suppressed the PA-induced myocardial hypertrophy. Moreover, a crosstalk between necroptosis and endoplasmic reticulum (ER) stress was observed in PA-treated cardiomyocytes. Inhibition of RIPK1 with Nec-1, phosphorylation level of AKT (Ser473), and mTOR (Ser2481) was significantly reduced in PA-treated cardiomyocytes. In conclusion, RIPKs-dependent necroptosis might be crucial in PA-induced myocardial hypertrophy. Activation of mTOR may mediate the effect of necroptosis in cardiomyocyte hypertrophy induced by PA.

1. Introduction

It is well recognized that excessive intake of dietary saturated fatty acids contributes to heart failure [1]. Considering the elevated plasma concentration of free fatty acids (FFAs), this phenomenon is partly explained by the development of obesity, coronary atherosclerosis, and myocardial ischemia [1]. However, dysfunction of cardiomyocytes caused by excessive intracellular lipids accumulation could be a significant other side of this phenomenon. Overload of lipids in nonadipose tissues that affects cellular functions, namely, lipotoxicity, could also induce cell hypertrophy or even cell death [2]. Evidence suggests that accumulation of PA, the major saturated fatty acids in blood, may give rise to lipotoxicity in cardiomyocytes by induction of oxidative stress [3] and persistent ER stress [4].

ER performs a pivotal role in various cell processes, including synthesizing, assembling, modifying and trafficking of proteins, and maintaining intracellular Ca^{2+} homeostasis [5]. Upon ER stress, accumulation of unfolded proteins leads to activation of sensors (PERK, ATF6, and IRE1) via dissociating GRP78 from them and triggers unfolded protein response (UPR). A short-term UPR functions as a prosurvival response via reducing accumulation of unfolded proteins and restoring ER function. If UPR prolongs, its downstream signaling initiates complicated response to strengthen ER stress, activates proapoptosis pathways, and eventually induces cell death [6]. According to previous studies, myocardial hypertrophy and apoptosis induced by PA are accompanied with increased expression of ER stress markers [7].

Moreover, mammalian target of rapamycin (mTOR), which is also essential for cardiomyocyte development, growth, and functions, regulates mitochondrial fatty acid utilization in the heart [8]. The AKT/mTOR signaling pathway has emerged as an important regulator in the pathogenesis of myocardial hypertrophy [9]. In cardiomyocytes, PI3K/mTOR/p70 (S6K) plays a critical role in the leptin-induced hypertrophy [10]. In islet beta-cells, PA activates mRNA translation and increases ER protein load via activation of the mTOR pathway [11]. In adipocytes, inhibition of AKT or mTOR signals by rapamycin attenuates the PA-induced ER stress [10]. However, whether PA evokes ER stress by activating mTOR signaling in cardiomyocytes is unclear, and the underlying mechanism of the PA-induced cardiomyocyte lipotoxicity, more specifically, in the PA-induced cardiomyocyte hypertrophy still remains elusive.

Recent studies have indicated a previously unknown form of programmed necrosis called necroptosis, which is regulated by the RIPK1 and RIPK3. In particular, a kinase complex consisted of the RIPK1 and RIPK3 is a central step in the programmed necrotic cell death [12]. Necroptosis represents a newly identified mechanism of cell death sharing features of both apoptosis and necrosis. Although RIPKs-dependent necroptosis has been implicated in the development of several cardiovascular diseases, such as atherosclerosis [13], myocardial infarction [14], and ischemia-reperfusion injury [15], the potential role of RIPKs-dependent necroptosis in the PA-induced myocardial hypertrophy is still unknown. Therefore, in the perspective of its critical role in inflammation and cell death in cardiovascular diseases, we hypothesized that necroptosis might participate in the pathophysiological process of cardiomyocyte hypertrophy induced by PA.

In order to verify our hypothesis, we sought to examine the influence of PA on the expression of RIPK1 and RIPK3 in NCMs and in H9c2 cells in this study. It has been reported that blockade of mTOR with its specific inhibitor CCI-779 stimulates autophagy and eliminates the activation of RIPKs in RCC4 cells [16]. Accordingly, the crosstalk between necroptosis, ER stress, and AKT/mTOR signaling pathway in cardiomyocytes with PA treatment was also investigated.

2. Materials and Methods

2.1. Cell Culture and Pharmaceutical Treatments. The NCMs were obtained from decapitated 0 to 3-day-old Sprague-Dawley rats by collagenase II (0.05%) (Gibco) and trypsin (0.05%) digestion according to the methodology of previous studies [17]. The culture medium consisted of DMEM (high glucose) (Gibco) and 10% (v/v) fetal bovine serum (FBS, Hyclone, USA). All cells were maintained in a humidified 5% CO_2/95% air incubator at 37°C. H9c2, rat embryonic cardiac myoblasts from American Type Culture Collection (ATCC), were grown in DMEM with 10% FBS at 37°C and 5% CO_2. When cells reached 70–80% confluence, they were incubated with 1% BSA-DMEM with or without PA (200 μM, Sigma) for 24 h. Thapsigargin (100 nM, Sigma) and pravastatin (10 μM, Squibb) were used as the agonist and antagonist for ER stress [18]. Nec-1 (10 nM, Selleck) was a known specific inhibitor for RIPK1, and rapamycin (1 μM, Sigma) was used to block the mTOR signaling activation. All these treatments were pretreated with the NCMs or H9c2 cells for 2 h before the PA stimulation.

2.2. siRNA Transfection. Transient transfection was performed by use of the cationic lipid Lipofectamine 3000 (Invitrogen, USA) according to the manufacturer's instruction. The H9c2 cells were transfected for 24 h with 50 nM siRNA specific for RIPK1/RIPK3 or negative control siRNA before exposure to PA (200 μM) for another 24 h. The sequences of siRNAs used were as follows:

Negative control siRNA (siNC): 5′-GUG CGU-UGCUAGUACCAAC dUdU-3′.

RIPK1-siRNA (siRIPK1/siR1): 5′-GCG GGCAUG-CACUACUUACAUG dUdU-3′.

RIPK3-siRNA (siRIPK3/siR3): 5′-GCG GGGUCA-GGAUCGAGAGAUU dUdU-3′.

2.3. Real-Time PCR. Gene expression was measured by quantitative RT-PCR (Q-PCR) as our previous report [19]. Total RNA was extracted from cells with TRIzol (Invitrogen, USA), and cDNA was synthesized using a reverse transcription (RT) kit (Toyobo, Japan). Q-PCR was carried out on CFX96 Real-Time PCR Detection System (BIO-RAD, USA) with fluorescence dye SYBR Green (SYBR Green Super mix kit, Bio-Rad, USA). Primer sequences were shown in Table 1. Normalization of gene expression was achieved by comparing the expression of β-actin for the corresponding samples. Relative fold expression values were determined applying the $\Delta\Delta$CT threshold (Ct) method.

2.4. Western Blot Analysis. Total proteins were extracted from cells with radio-immunoprecipitation assay (RIPA) lysis buffer. Protein from cell extracts was quantified by Varioskan (Thermo, USA) using a BCA protein assay kit (Pierce, USA). Equivalent amount of cells lysates (25 μg) was separated by denaturing 10% SDS-PAGE and then transferred to 0.45 μm polyvinylidene difluoride (PVDF) membrane (Millipore, USA) using a MiniProtein III system (Bio-Rad, USA). Membranes were subsequently blocked with 5% skim milk in Tris-buffered saline and Tween 20 (TBST) solution for 2 h and were incubated with primary antibodies at 4°C overnight: RIPK3 (Cell Signaling, number 14401), RIPK1 (Cell Signaling, number 3493), GRP78 (Cell Signaling, number 3183), Phospho-mTOR (Ser2481) (Cell Signaling, number 2974), mTOR (Cell Signaling, number 2983), Calreticulin (Cell Signaling, number 12238), AKT (Cell Signaling, number 4685), and Phospho-AKT (Ser473) (Cell Signaling, number 4058). The antigen-antibody complexes were detected by enhanced chemiluminescence (ECL) substrate kit (Thermo, USA). Specific bands were scanned and quantified by the Quantity One analysis software (Bio-Rad, USA).

2.5. Detection of Cell Surface Area by F-Actin Staining. Cardiomyocytes surface area was detected by F-actin staining as previously reported [20]. After treatment, H9c2 cells

Table 1: Primer sequences and amplicon sizes for real-time RT-PCR.

Genes	GenBank ID	Primer sequence (5′-3′)	Amplicon (bp)
ANP	NM_012612.2	F: 5′ ACCAAGGGCTTCTTCCTCT 3′ R: 5′ TTCTACCGGCATCTTCTCC 3′	141
BNP	NM_031545.1	F: 5′ GCTCTTCTTTCCCCAGCTCT 3′ R: 5′ ACTGTGGCAAGTTTGTGCTG 3′	130
GRP78	NM_013083.2	F:5′ CCCCAGATTGAAGTCACCTTTGAG 3′ R: 5′ CAGGCGGTTTTGGTCATTG 3′	117
CHOP	NM_001109986.1	F: 5′ AGCAGAGGTCACAAGCACCT 3′ R: 5′ CTCCTTCATGCGCTGTTTCC 3′	157
ATF6	NM_001107196.1	F: 5′ GCAGGTGTATTACGCTTCGC 3′ R: 5′ TGTGGTCTTGTTATGGGTGG 3′	136
α-MHC	NM_017239.2	F: 5′ ATACCTCCGCAAGTCAGAGAA 3′ R: 5′ ACGATCTTGGCCTTGACATAC 3′	114
β-actin	NM_001099771	F: 5′ ACTATCGGCAATGAGCGGTTC 3′ R: 5′ ATGCCACAGGATTCCATACCC 3′	77
β-MHC	NM_017239.2	F: 5′ GTGCCAAGGGCCTGAATGAG 3′ R: 5′ GCAAAGGCTCCAGGTCTGA 3′	353
RIPK1	NM_001107350.1	F: 5′ CTTAAGCCCAAGTGCAGTCA 3′ R: 5′ ATAGCCCAACAAGGAGGATG 3′	166
RIPK3	NM_139342.1	F: 5′ CAGTGTTGGCTGGAAGAGAA 3′ R: 5′ AGGCTCAGAACTCCAGCAAT 3′	173

were washed and fixed by 4% paraformaldehyde for 30 min at room temperature. Then the cells were incubated with 0.1% TritonX-100 in PBS for 3 to 5 min and stained with Rhodamine Phalloidin (100 nM, Cytoskeleton) for 20 min. Rinse cells with PBS and incubate them with diluted DAPI for 10 mins, away from light. Images were captured by Eclipse TE2000-U fluorescent microscope system (Nikon, Japan) and semiquantitatively analyzed for cell surface area with ImageJ software (NIH, USA).

2.6. Cells Ultrastructure Observation by Transmission Electron Microscopy [21]. After treatment, H9c2 cells were collected and fixed with 3% glutaraldehyde in 100 mM cacodylate buffer, postfixed in 1% cacodylate-buffer osmium tetroxide for 2 h at room temperature, and dehydrated in a graded series of ethanol. Then the cells were embedded in Epon-Aradite. Ultrathin sections were cut with a diamond knife on a Leica EM UC6rt (Leica, German) and double-stained with uranyl acetate and lead citrate. Ultrastructure of H9c2 cells was observed with a Hitachi H7650 transmission electron microscope (TEM, Hitachi, Japan) at 80 kV.

2.7. Immunofluorescence Staining. H9c2 cells were plated onto coverslips in 6-well plated. When reaching 60–70% confluent, the cells were treated with PA and Nec-1 or with PA alone. Coverslips were then fixed and blocked as described before [22], followed by exposure to the primary antibodies (anti-RIPK1 1 : 100 or anti-RIPK3 1 : 100, Cell Signaling, USA) at 4°C overnight. After washing with PBS, incubate the cells with fluorescent-conjugated secondary antibodies for 2 h at room temperature, away from light. The second antibody used was Alexa Fluor 488 Goat Anti-Rabbit IgG (1 : 400, green fluorescence, Invitrogen, USA) or Alexa Fluor 594 Goat Anti-Rabbit IgG (1 : 400, red fluorescence, Invitrogen, USA). Rinse cells and incubate them with diluted DAPI for 10 min, away from light. Images were collected using an Eclipse TE2000-U fluorescence microscope system (Nikon, Japan) and analyzed with ImageJ software (NIH, USA) to semiquantitatively determine the expression of RIPK1 and RIPK3.

2.8. Oil Red O Staining. To measure intracellular lipid accumulation, H9c2 cells were stained by Oil Red O dye (Sigma-Aldrich, catalog number 398039) according to the methodology of previous study [23]. After treatment, cells were washed and fixed by 4% (v/v) paraformaldehyde. Then the cells were incubated with the Oil Red O working solution for 30 min at room temperature. Subsequently, the cells were washed twice with 60% isopropanol and then counterstained with hematoxylin (Dako, USA) for 30 s. Excess hematoxylin was washed in water. Cells were then observed under the microscope and images were collected using an ECLIPSE 50i system (Nikon, Japan). Oil Red O-staining positive cell counts were determined over five viewing fields and averaged. Totally more than 150 cells in each group were chosen randomly for statistical analysis.

2.9. Statistical Analysis. All results were expressed as mean ± SD. We performed statistical analysis using one- or two-way *ANOVA* and Student-Newman-Keuls *post hoc* tests or *t*-tests. A p value of <0.05 was considered as significant.

3. Results

3.1. Cardiomyocyte Hypertrophy Is Induced by Palmitic Acid Stimulation. In order to observe the lipotoxicity induced by PA administration in cardiomyocytes, we used Oil Red O, an agent that detects neutral lipids, to assess intracellular lipid accumulation in H9c2 cells under different treatments: (1) control (without any treatment); (2) stimulation with PA (200 μM); and (3) pretreatment with Nec-1 (10 nM) and then exposure to PA. As shown in the representative images (Figure 1(a)), PA treatment induced lipids accumulation in H9c2 cells, and the PA-induced intracellular accumulation of neutral lipids in H9c2 cells could be inhibited by Nec-1 (Figure 1(a)).

Cardiomyocyte hypertrophy is one of consequences of lipotoxicity induced by PA treatment. We subsequently detected the changes in expression of hypertrophic marker genes after excessive PA supply in cardiomyocytes. Oleic acid (OA), the major unsaturated fatty acid in plasma which plays different pathophysiological roles [24], was set as another treatment measure for comparison. Thus, we treated H9c2 cells with PA (200 μM) or OA (250 μM) for 24 h. The results exhibited that gene expression of hypertrophic markers, atrial natriuretic peptide (ANP), brain natriuretic peptide (BNP), myocardial α-myosin heavy chain (α-MHC), and β-myosin heavy chain (β-MHC), was upregulated only in the PA stimulation group when compared with controls (without any treatment and with OA treatment) (Figure 1(b)). To confirm the prohypertrophy effect of PA, the primary rat NCMs were treated with PA (200 μM) for 24 h and the gene expression levels of ANP and BNP were nearly 2-fold higher than those in the control (without any treatment) (Figure 1(c)).

We further measured the change of cell surface area by F-actin staining. The results illustrated that a cell surface area enlargement was observed in H9c2 cells treated with PA for 24 h (Figure 1(d)). The above data suggested that it is PA but not OA that could induce cardiomyocyte hypertrophy.

3.2. Necroptosis Is Induced in Cardiomyocytes with PA Stimulation and Is Involved in PA-Induced Cardiomyocyte Hypertrophy. We investigated whether PA could induce necroptosis in cardiomyocytes. For this purpose, we first detected the gene expression of RIPK1 and RIPK3. After treatment with PA or OA for 24 h, the gene expression of both RIPK1 and RIPK3 in primary rat NCMs was upregulated only in the PA stimulation group compared with controls (without any treatment and with OA treatment), while Nec-1, a specific inhibitor of RIPK1, significantly decreased the PA-induced gene expression of RIPK1 and RIPK3 (Figure 2(a)).

Under the normal growth condition, the growth-arrested NCMs showed the low levels of RIPK1/RIPK3 protein expression. Western blot results showed that total cellular RIPK1/RIPK3 protein level was increased markedly after treatment with PA for 24 h and downregulated by Nec-1 (Figure 2(b)). The expression of RIPK1/RIPK3 protein obtained by immunofluorescence staining also indicated that growth-arrested H9c2 cells presented a slight RIPK1 and RIPK3 staining, while treatment with PA for 24 h significantly increased cytoplasmic RIPK1/RIPK3 staining (Figures 2(c) and 2(d)). We further found that expression of both RIPK1 and RIPK3 was repressed by Nec-1 pretreatment.

There are also ultrastructural features of necroptosis [25]. TEM analysis provided evidence for PA-induced lipid accumulation and alterations of ultrastructural features of necrosis, including swollen mitochondria, cytoplasmic clearing, cell membrane damage, and characteristic nuclear changes. Inhibition of RIPK1 with Nec-1 ameliorated necrotic characters of cardiomyocytes (reduction of cells fracture, etc.) (Figure 2(e)). The results displayed that PA stimulation could trigger necroptosis in cardiomyocytes.

Furthermore, we tested the hypothesis that RIPK1/RIPK3-mediated necroptosis may be actively involved in PA-induced cardiomyocyte hypertrophy. We observed that pretreatment with Nec-1 significantly decreased the mRNA expression of hypertrophy markers (including ANP, BNP, α-MHC, and β-MHC) (Figure 2(f)). Moreover, the result of F-actin staining illustrated that Nec-1 significantly decreased the augment of cell surface area induced by PA, as shown in Figure 1(d). Red Oil O staining also demonstrated that lipid accumulation in H9c2 cells induced by PA was attenuated by Nec-1 pretreatment, as shown in Figure 1(a).

To further investigate the role of necroptosis in PA-induced cardiomyocyte hypertrophy, we also used a gene silencing approach to specifically knockdown RIPK1 and RIPK3 expression. In order to confirm the inhibition effect of RIPK1/RIPK3-siRNA, we measured both the gene expression (Figure 2(g)) and the protein level (Figure 2(h)) of RIPK1 and RIPK3 in H9c2 cells after transfection. Subsequent to transfection of RIPK1-siRNA or RIPK3-siRNA into H9c2 cells, the PA-induced expression of RIPK1 or RIPK3 mRNA and protein were significantly suppressed. The knockdown of either RIPK1 or RIPK3 significantly reduced both basal and PA-induced ANP and BNP gene expression in H9c2 cells. As a negative control, the scrambled siRNA had no effect on ANP or BNP expression in H9c2 cells (Figure 2(i)). Altogether, cardiomyocyte hypertrophy induced by PA could be suppressed via specifically blocking RIPKs-dependent necroptosis.

3.3. The Endoplasmic Reticulum Stress Is Involved in the Palmitic Acid-Induced Necroptosis. We investigated whether there was a crosstalk between ER stress and necroptosis evoked by PA. In our experiments, we first treated the NCMs with PA (200 μM) or OA (250 μM) for 24 h. The gene expression of GRP78, ATF6, and CHOP, the markers of ER stress, was upregulated only in the PA stimulation group compared to OA treatment group (Figure 3(a)).

Then we pretreated H9c2 cells with pravastatin (10 μM), which has been recognized as an inhibitor to ER stress. We also pretreated H9c2 cells with thapsigargin (100 nM), a known ER stress agonist. When the ER stress in H9c2 cells was suppressed, we observed that the ER stress markers were downregulated (Figure 3(b)) and the gene expression of RIPK1 and RIPK3 was also decreased compared to PA stimulation group (Figure 3(c)). Interestingly, when necroptosis was inhibited by Nec-1 in primary NCMs, the protein levels

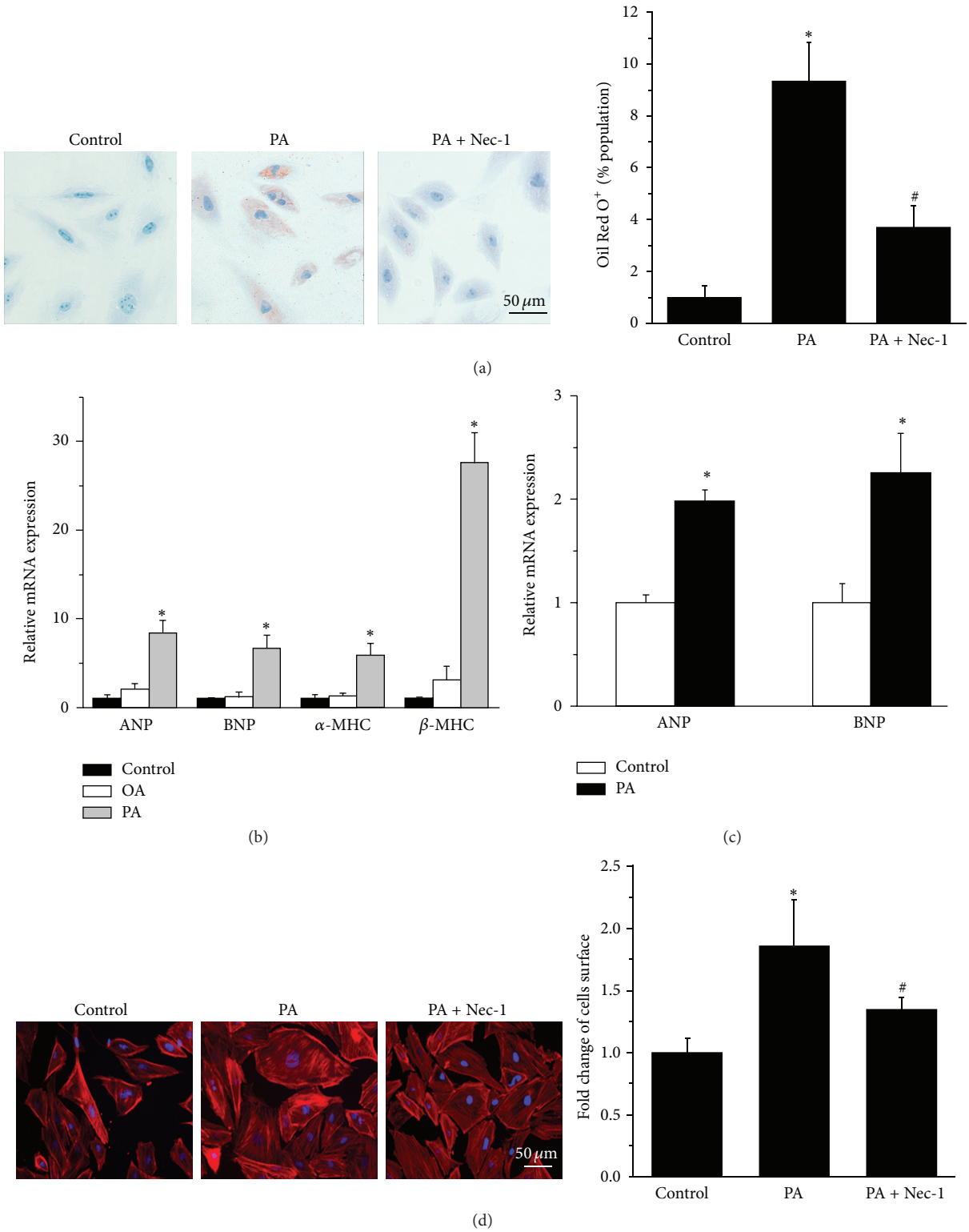

Figure 1: PA-induced hypertrophy in cardiomyocytes. (a) H9c2 cells were stained by Oil Red O dye. (1) Control (without any treatment). (2) Stimulation with PA (200 μM). (3) Pretreatment with Nec-1 (10 nM), $n = 3$. The result of Oil Red O^+ (%population) indicated that lipid accumulation was induced in PA stimulation group in H9c2 cells, and the PA-induced intracellular accumulation of neutral lipids in H9c2 cells decreased in PA + Nec-1 group. (b) Gene expression of ANP, BNP, α-MHC, and β-MHC in H9c2 cells was induced by PA, but not OA, $n = 3$. (c) Gene expression of ANP and BNP was upregulated in NCMs, $n = 4$. (d) Fluorescence microscopy observed the increased H9c2 cells surface area of F-actin staining in PA group, which was suppressed by Nec-1 (10 nM), according to the semiquantitative results by ImageJ software, $n = 3$. The red fluorescence indicated cytoskeleton stained by rhodamine phalloidin and the blue fluorescence indicated the cell nucleus stained by DAPI. Data in (a), (b), (c), and (d) are expressed as mean ± SD, $*$ indicates $p < 0.05$ compared to control treatment, and # indicates $p < 0.05$ compared to PA treatment.

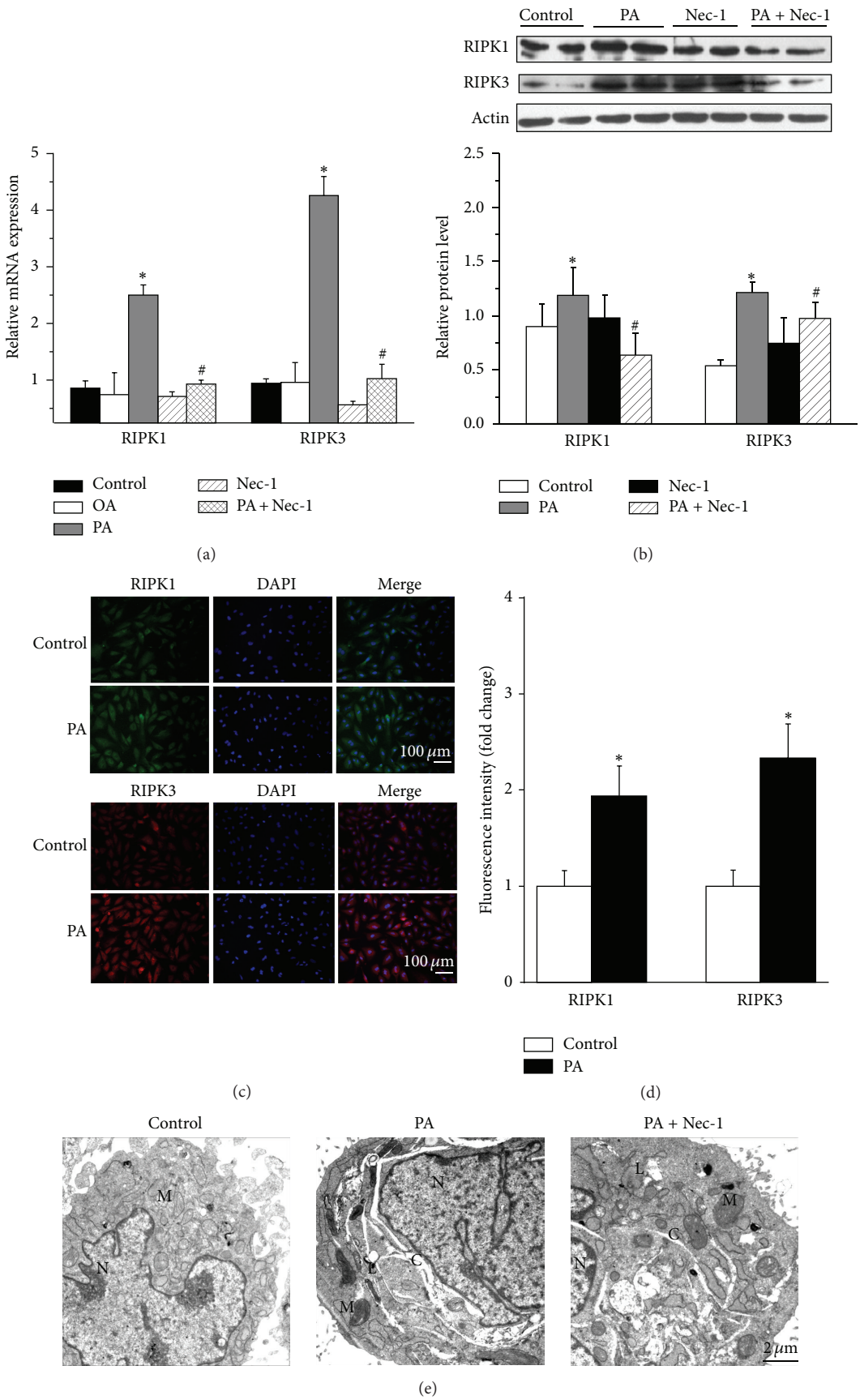

Figure 2: Continued.

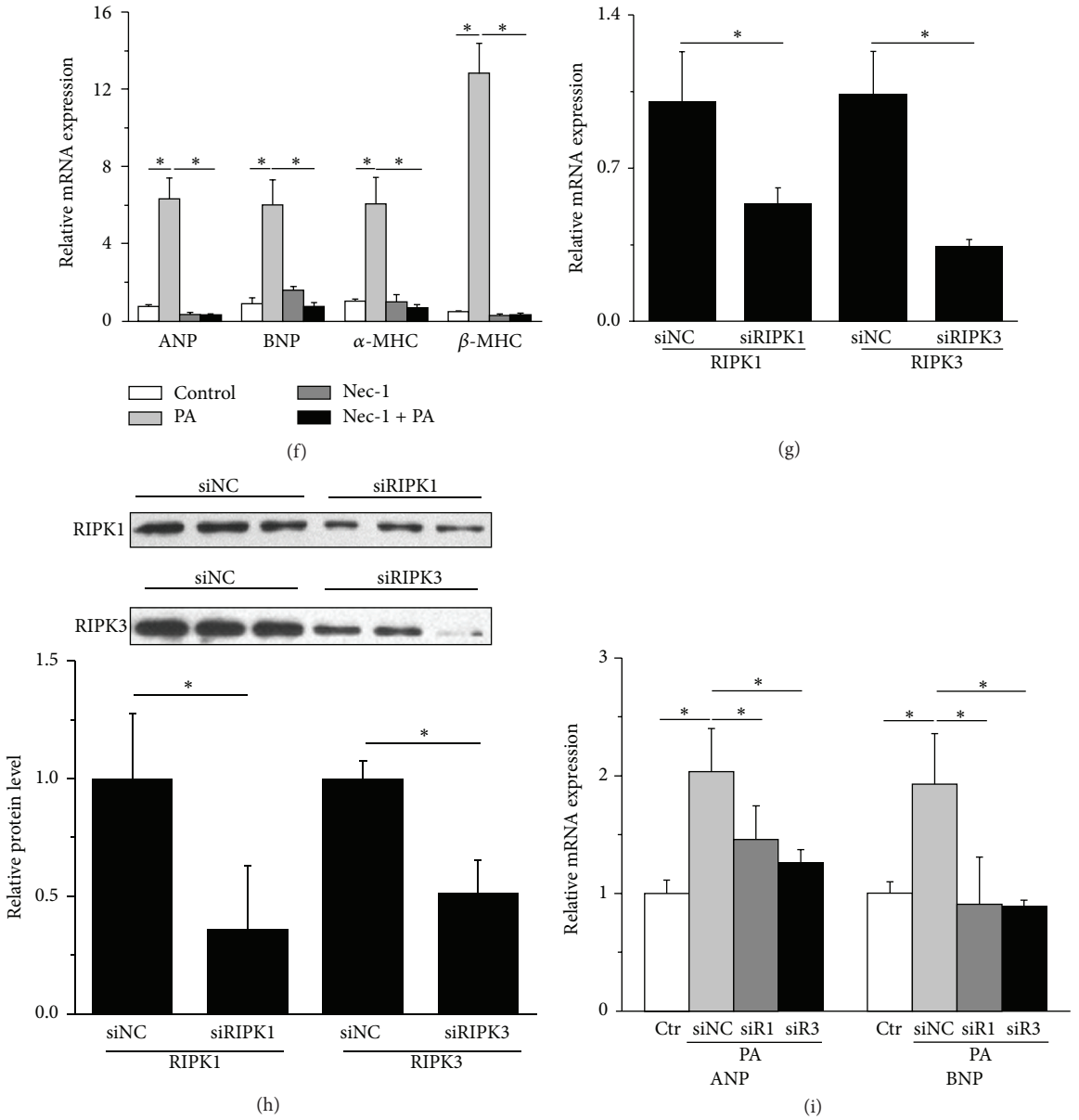

Figure 2: RIPK1/RIPK3 expressions are significantly increased in cardiomyocytes with PA stimulation. (a) The increased gene expression of RIPK1/RIPK3 was inhibited by Nec-1 (10 nM) in NCMs ($n = 3$). (b) The increased protein level of RIPK1/RIPK3 in NCMs was downregulated by Nec-1 (10 nM) ($n = 4$). (c) Immunofluorescence for RIPK1 and RIPK3 in H9c2 cells. Note the higher immunoreactivity for RIPK1/RIPK3 in H9c2 cells (200x) with PA stimulation. The green fluorescence indicated RIPK1 staining, the red fluorescence indicated RIPK3 staining, and the blue fluorescence indicated the cell nucleus stained by DAPI. (d) Quantitative analysis of fluorescent microscopy images (c) ($n = 3$). (e) Transmission electron microscopy images of H9c2 cells treated with PA for 24 h showed lipid deposition within the cells. Necrotic morphology was observed including swollen mitochondria, cytoplasmic clearing, and membrane damage (M: mitochondrion; N: nucleus; L: lipid droplet; C: cytoplasmic clearing. Scale bars: 2 μm). (f) Treating the H9c2 cells with Nec-1 (10 nM), a specific necroptosis inhibitor, the increased gene levels of ANP, BNP, α-MHC, and β-MHC were downregulated via real-time PCR ($n = 3$). (g) After transfection with siRIPK1 or siRIPK3 (50 nM) in H9c2 cells, the PA-induced mRNA expression of RIPK1 or RIPK3 was significantly suppressed ($n = 4$ in each group). (h) After transfection with siRIPK1 or siRIPK3 (50 nM) in H9c2 cells, the PA-induced protein expression of RIPK1 or RIPK3 was significantly suppressed ($n = 3$). (i) Accordingly, silenced RIPK1 with siRIPK1 (siR1) or silenced RIPK3 (siR3) with siRIPK3 significantly inhibited both basal and PA-induced ANP and BNP gene expression in H9c2 cells ($n = 3$), as evaluated by quantitative RT-PCR. Data in (a), (b), (d), (f), (g), (h), and (i) are expressed as mean ± SD; $*$ indicates $p < 0.05$.

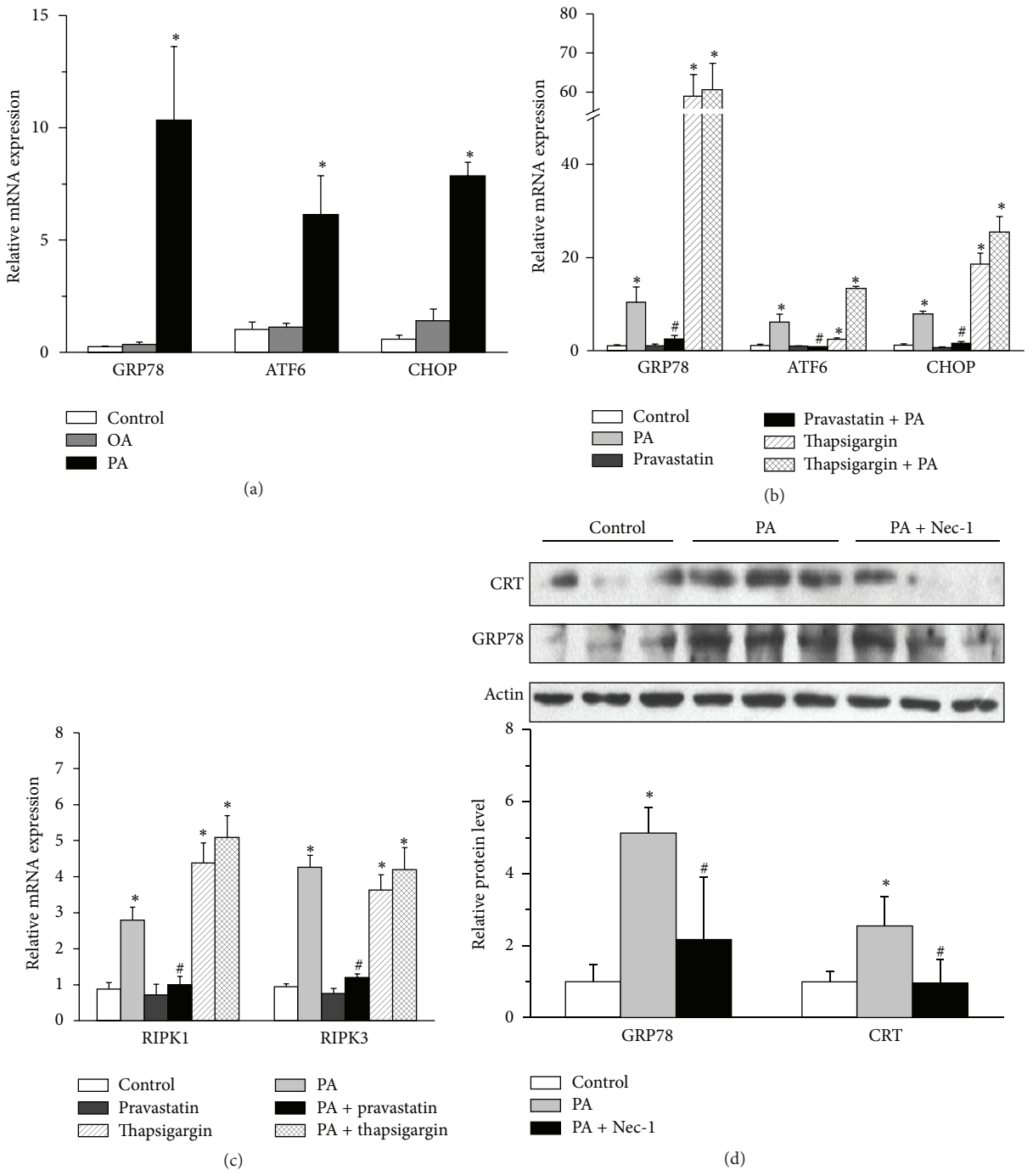

Figure 3: There is a crosstalk between ER stress and necroptosis in PA-induced cardiomyocyte hypertrophy. (a) Treating the NCMs with PA (200 μM) and OA (250 μM), the mRNA expressions of GRP78, ATF6, and CHOP were increased in PA group, not OA group, $n = 4$. (b) Pretreating the H9c2 cells with pravastatin (10 μM) and effectively blocking the upregulated mRNA expression of GRP78, ATF6, and CHOP (ER stress markers) induced by PA and thapsigargin (100 nM) (an ER stress agonists) via real-time PCR, $n = 3$. (c) Pretreating the H9c2 cells with pravastatin (10 μM) and also effectively blocking the upregulated mRNA expression of RIPK1/RIPK3 induced by PA and thapsigargin via real-time PCR, $n = 3$. (d) The increased protein level of GRP78 and CRT in NCMs was downregulated by pravastatin (10 μM) (western blot), $n = 3$. Data in (a), (b), (c), and (d) are expressed as mean ± SD, $*$ indicates $p < 0.05$ compared to control treatment, and # indicates $p < 0.05$ compared to PA treatment.

of the ER stress markers calreticulin (CRT) and GRP78 were also downregulated (Figure 3(d)).

3.4. mTOR Mediates the Necroptosis Induced Cardiomyocyte Hypertrophy. It is recently reported that mTOR is involved in high-fat diet-Induced cardiac hypertrophy in mice [9], and AKT/mTOR mediates programmed necrosis in neurons [26]. Thus, we hypothesized that mTOR signaling participated in PA-induced necroptosis. Firstly, we observed the effect of rapamycin on cardiomyocyte hypertrophy with PA stimulation. Pretreating the NCMs with rapamycin could significantly decrease the mRNA level of ANP and BNP (Figure 4(a)), indicating that mTOR was involved in the PA-induced cardiac hypertrophy. To observe whether a crosstalk between necroptosis and AKT/mTOR signaling pathway exists, we pretreated NCMs with Nec-1 (10 nM) and rapamycin (1 μM). After specifically blocking RIPK1 by Nec-1, the increased phosphorylation of AKT (Ser473) and mTOR (Ser2481) induced by PA stimulation was inhibited (Figures 4(b) and 4(c)), suggesting that activation of AKT/mTOR in response to PA in NCMs is RIPK1-dependent. However, pretreatment with rapamycin had no effect on the protein expression of RIPK1 (Figure 4(d)).

4. Discussion

In the present study, the potential link between PA-induced hypertrophy and necroptosis has been investigated. The major findings are that (1) necroptosis is involved in PA-induced cardiomyocyte hypertrophy; (2) there is a crosstalk between ER stress and necroptosis in PA stimulated hypertrophic cardiomyocytes; and (3) mTOR is identified as one of the molecular bases underlying PA-induced hypertrophy, which might be a downstream signaling molecule of RIPK1.

PA is the major saturated free fatty acid in plasma and is known to induce cellular dysfunction and cell death in a number of cell types, including cardiomyocytes [27]. Inflammation, hypertrophy, and cell death are major pathological events of the PA-induced cardiomyocyte lipotoxicity. The PA-induced inflammation and cell death including apoptosis and autophagy have been widely investigated in different cell types [24]. In the present study, therefore, we focus on the mechanism of the PA-induced cardiomyocyte hypertrophy. Several signaling pathways (e.g., LKB1/AMPK pathway) mediate the development of the PA-induced cardiac hypertrophy [28]. Consistent with previous reports, our data shows that exposure of primary rat NCMs or H9c2 cells to PA but not OA leads to an increase in expression of hypertrophy markers and a cell surface area enlargement. To further elucidate the underlying mechanism, we examined whether PA-induced cardiomyocyte hypertrophy was regulated by necroptosis, a novel cell death manner different from necrosis and apoptosis. It is negatively regulated by caspase and is dependent on the kinase activity of RIPK1 and RIPK3. We have detected an increased expression of RIPK1 and RIPK3 in PA-treated cardiomyocytes, implying activation of necroptosis [15, 22, 29, 30]. By using Nec-1 and specific siRNA for RIPK1 or RIPK3, our results demonstrate that inhibition of RIPK1 or knockdown of RIPK1/RIPK3 expression prevents the expression of hypertrophic marker genes effectively, indicating that necroptosis performs an important role in mediating cardiomyocyte hypertrophy in response to PA.

Necroptosis is regarded as a kind of cell death that is the caspase-independent programmed necrosis. It is involved in myocardial infarction and myocardial ischemia-reperfusion injury, whereas inhibition of both necroptosis and apoptosis could improve the cardioprotective effects [31]. In endothelial cells, the PA-induced necroptosis is carboxyl-terminal hydrolase- (CYLD-) dependent, but RIPK1- independent [32]. Nevertheless, we observed that the PA-induced cardiomyocyte hypertrophy is RIPKs-dependent. Nec-1 could inhibit RIPK1 expression, endogenous RIPK1 autophosphorylation, and even the formation of RIPK1-RIPK3 complex [22, 30, 33]. It has been used in many studies to test the contributions of RIPK1 and RIPK1-RIPK3 complex in cell death and inflammation [29, 33]. In our study, we observed that Nec-1 significantly reduced the intracellular lipid accumulation in PA-treated cardiomyocytes, suggesting that Nec-1 might protect cardiomyocyte from PA stimulation by repairing the cellular membrane damage. Moreover, Nec-1 pretreatment suppressed expression of both RIPK1 and RIPK3, demonstrating that the kinase complex which consisted of RIPK1 and RIPK3 might be essential in PA-induced cardiomyocyte necroptosis. Taken together, we have indicated that necroptosis is one of the main causes of the PA-induced cardiomyocyte hypertrophy.

It is interesting that by which approach the PA-induction of RIPKs-dependent necroptosis leads to cardiomyocyte hypertrophy. Some studies have shown that necroptosis mediates and even promotes the pathological processes of inflammation and cell death, and inhibition of this pathway can limit extensive tissue damage [13]. Elevated level of inflammation and apoptosis accounts mainly for the PA-induced lipotoxicity in cardiomyocytes [27, 34], consequently the inhibition of necroptosis attenuated cardiac hypertrophy. It is suggested that hypertrophy is accompanied by inflammation and apoptosis [35]. This might be the direct role of RIPK inhibition in mediating cardiac hypertrophy induced by PA.

In addition to the direct role, increased RIPKs expression may interact with other signals involved in cardiac hypertrophy. Several intracellular signals elicited by PA are responsible to cardiac hypertrophy, including ER stress and mTOR pathway. Previous studies have verified that ER stress is a pathological characteristic of cardiac hypertrophy, and the expression of related molecules such as GRP78, ATF6, CRT, and CHOP is increased significantly during cardiac hypertrophy [36]. An induction of the prolonged ER stress has also been proposed as a molecular mechanism of the PA-induced cardiomyocyte lipotoxicity [23]. Recently, it is reported that ER stress is able to induce necroptosis in L929 cells in a tumor necrosis factor receptor 1- (TNFR1-) dependent manner, but independent of autocrine TNF or lymphotoxin α production [37]. Therefore, we have investigated a possible crosstalk between ER stress and necroptosis in the PA-induced hypertrophic cardiomyocytes. Our study reveals that inhibiting of ER stress attenuated RIPKs expression induced by PA. On the other hand, blocking necroptosis decreased

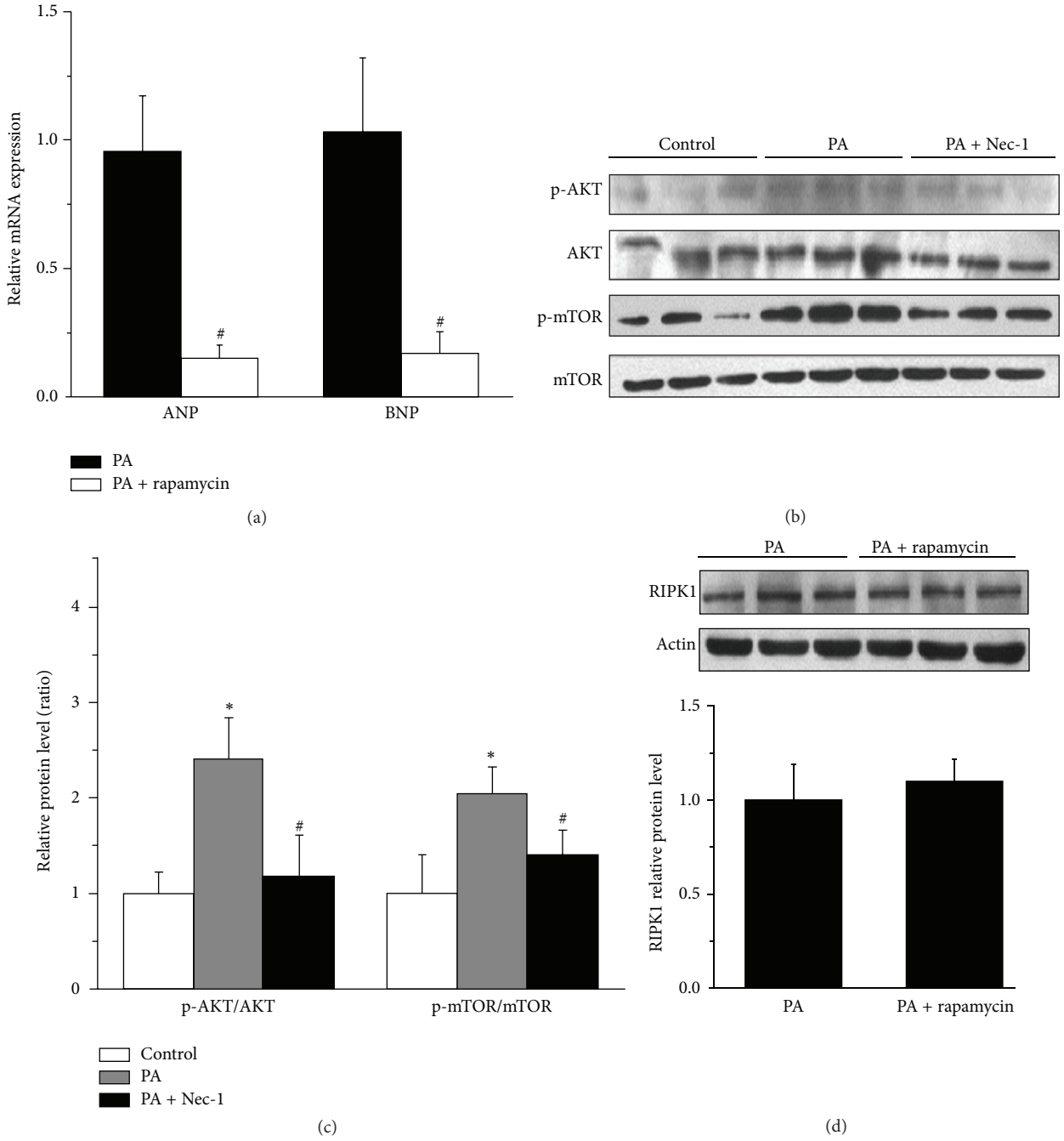

Figure 4: AKT/mTOR mediates necroptosis in the PA-induced cardiomyocyte hypertrophy. (a) Pretreating the NCMs with rapamycin (1 μM), the mRNA level of ANP and BNP was decreased, $n = 4$. (b) Pretreating the NCMs with Nec-1 (10 nM), the upregulated Ser473 of AKT and Ser2481 of mTOR phosphorylation by PA stimulation (western blot) was inhibited. (c) Quantitative analysis of western blots (b), $n = 3$. (d) Pretreating the NCMs with rapamycin (1 μM) had no effect on the upregulated RIPK1 by PA stimulation via western blot, $n = 6$. Data in (a), (c), and (d) are expressed as mean ± SD, $*$ indicates $p < 0.05$ compared to control treatment, and # indicates $p < 0.05$ compared to PA treatment.

the expression of ER stress markers in cardiomyocytes. The effects of PA on ER stress may be different, depending on cell type and the duration of treatment. According to the present study, it is not sufficient to draw a conclusion that ER stress could evoke necroptosis in the PA-induced cardiomyocyte hypertrophy. However, there is a crosstalk between ER stress and necroptosis in mediating cardiomyocyte hypertrophy induced by PA, suggesting that necroptosis might play its role in the PA-induced cardiomyocyte hypertrophy via interaction with ER stress.

Then we pay attention to AKT/mTOR pathway, which is activated in both physiological and pathological cardiac

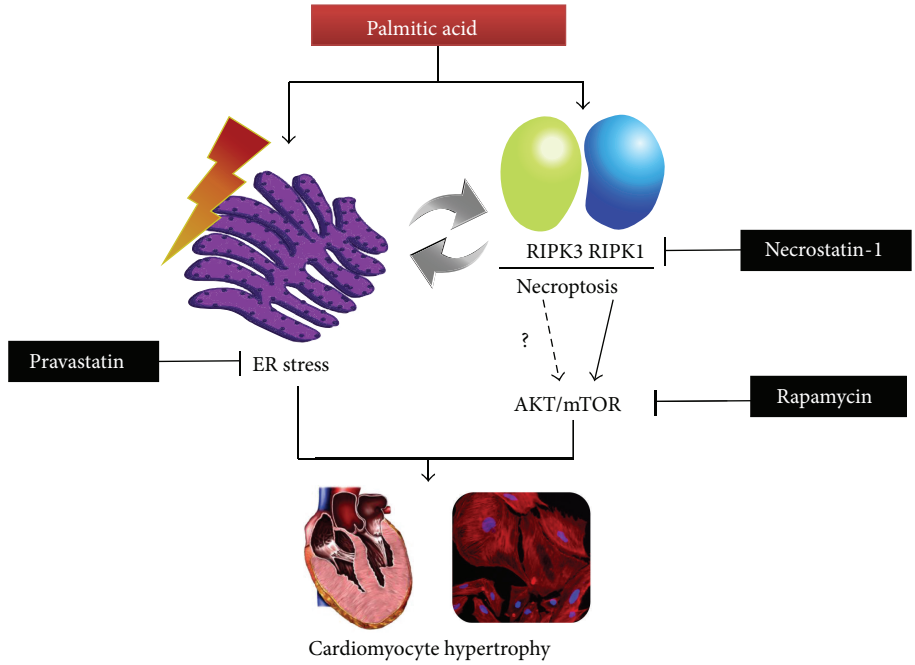

Figure 5: Schematic illustration of the signaling pathways of palmitic acid-induced cardiomyocyte hypertrophy.

hypertrophy. Dysregulation of the mTOR pathway has been implicated in a number of human diseases such as obesity, diabetes mellitus, and cardiovascular diseases [38]. It has been reported that mTOR mediates RhoA-dependent [10] and hormone-induced cardiomyocyte hypertrophy [39], and previous report has shown that dual inhibition of AKT and mTOR reduced acute cell death [40]. AKT/mTOR mediates programmed necrosis in some types of cells such as RCC4 cells and neurons [26]. Recent study has shown that AKT is activated in a RIPK1-dependent way in L929 cells during necroptosis, and AKT regulates necroptosis via its downstream signaling complex mTORC1 [41]. These findings raise the possibility that mTOR mediates necroptosis in the PA-treated cardiomyocytes. We have observed that inhibition of necroptosis by Nec-1 attenuates the phosphorylation of AKT and mTOR induced by PA. However the mTOR inhibitor rapamycin has no influence on the expression of RIPK1, indicating that RIPK1 might be an upstream signal molecule of PA-induced AKT/mTOR activation. But, how about the effect of rapamycin on the activity of RIPK1 in PA-treated cardiomyocytes? To address this question, the phosphorylation of PIPK1 induced by PA may be needed to determine after rapamycin pretreatment in further study [42]. Here the current evidence suggests that necroptosis is involved in the PA-induced cardiac hypertrophy via activation of AKT/mTOR pathway. These phenomena summarized in Figure 5 indicate the processing of PA-induced cardiomyocyte hypertrophy.

In conclusion, necroptosis is involved in PA-induced cardiomyocyte hypertrophy and contributes to the pathogenesis of PA-induced lipotoxicity in the heart. Our work provides a novel insight into the mechanism of cardiac lipotoxicity and suggests a therapeutic potential of blocking necroptosis in the management of cardiac hypertrophy associated with elevated plasma concentration of FFAs.

Conflict of Interests

The authors declare that there is no conflict of interests regarding the publication of this paper.

Acknowledgments

This work was supported by grants from the Natural Science Foundation of China (NSFC nos. 11372204 and 11072163) and the Specialized Research Fund for the Doctoral Program of Higher Education (supported by the doctoral category) of the year 2012 (no. 20120181110012).

References

[1] K. Drosatos and P. C. Schulze, "Savings precede spending: fatty acid utilization relies on triglyceride formation for cardiac energetics," *Circulation*, vol. 130, no. 20, pp. 1775–1777, 2014.

[2] E.-J. Park, A. Y. Lee, S. Park, J.-H. Kim, and M.-H. Cho, "Multiple pathways are involved in palmitic acid-induced toxicity," *Food and Chemical Toxicology*, vol. 67, pp. 26–34, 2014.

[3] Q. Xu, S. Y. Chen, L. D. Deng, L. P. Feng, L. Z. Huang, and R. R. Yu, "Antioxidant effect of mogrosides against oxidative stress induced by palmitic acid in mouse insulinoma NIT-1 cells," *Brazilian Journal of Medical and Biological Research*, vol. 46, no. 11, pp. 949–955, 2013.

[4] F. Rizzi, V. Naponelli, A. Silva et al., "Polyphenon E, a standardized green tea extract, induces endoplasmic reticulum stress, leading to death of immortalized PNT1a cells by anoikis and

tumorigenic PC_3 by necroptosis," *Carcinogenesis*, vol. 35, no. 4, pp. 828–839, 2014.

[5] J. G. Dickhout, R. E. Carlisle, and R. C. Austin, "Interrelationship between cardiac hypertrophy, heart failure, and chronic kidney disease: endoplasmic reticulum stress as a mediator of pathogenesis," *Circulation Research*, vol. 108, no. 5, pp. 629–642, 2011.

[6] V. P. Nakka, P. Prakash-babu, and R. Vemuganti, "Crosstalk between endoplasmic reticulum stress, oxidative stress, and autophagy: potential therapeutic targets for acute CNS injuries," *Molecular Neurobiology*, pp. 1–13, 2014.

[7] N. Bousette, C. Abbasi, R. Chis, and A. O. Gramolini, "Calnexin silencing in mouse neonatal cardiomyocytes induces Ca^{2+} cycling defects, ER stress, and apoptosis," *Journal of Cellular Physiology*, vol. 229, no. 3, pp. 374–383, 2014.

[8] Y. Zhu, J. Soto, B. Anderson et al., "Regulation of fatty acid metabolism by mTOR in adult murine hearts occurs independently of changes in PGC-1α," *The American Journal of Physiology—Heart and Circulatory Physiology*, vol. 305, no. 1, pp. H41–H51, 2013.

[9] J. Liao, Y. Li, F. Zeng, and Y. Wu, "Regulation of mTOR pathway in exercise-induced cardiac hypertrophy," *International Journal of Sports Medicine*, vol. 36, no. 5, pp. 343–350, 2015.

[10] A. Zeidan, J. C. Hunter, S. Javadov, and M. Karmazyn, "mTOR mediates RhoA-dependent leptin-induced cardiomyocyte hypertrophy," *Molecular and Cellular Biochemistry*, vol. 352, no. 1-2, pp. 99–108, 2011.

[11] M. Hatanaka, B. Maier, E. K. Sims et al., "Palmitate induces mRNA translation and increases ER protein load in islet β-cells via activation of the mammalian target of rapamycin pathway," *Diabetes*, vol. 63, no. 10, pp. 3404–3415, 2014.

[12] J. Silke, J. A. Rickard, and M. Gerlic, "The diverse role of RIP kinases in necroptosis and inflammation," *Nature Immunology*, vol. 16, no. 7, pp. 689–697, 2015.

[13] N. Khan, K. E. Lawlor, J. M. Murphy, and J. E. Vince, "More to life than death: molecular determinants of necroptotic and non-necroptotic RIP3 kinase signaling," *Current Opinion in Immunology*, vol. 26, no. 1, pp. 76–89, 2014.

[14] A. Fauster, M. Rebsamen, K. V. Huber et al., "A cellular screen identifies ponatinib and pazopanib as inhibitors of necroptosis," *Cell Death & Disease*, vol. 6, no. 5, article e1767, 2015.

[15] K. Takemoto, E. Hatano, K. Iwaisako et al., "Necrostatin-1 protects against reactive oxygen species (ROS)-induced hepatotoxicity in acetaminophen-induced acute liver failure," *FEBS Open Bio*, vol. 4, pp. 777–787, 2014.

[16] K. Bray, R. Mathew, A. Lau et al., "Autophagy suppresses RIP kinase-dependent necrosis enabling survival to mTOR inhibition," *PLoS ONE*, vol. 7, no. 7, Article ID e41831, 2012.

[17] M. Shen, L. Wang, X. Guo et al., "A novel endoplasmic reticulum stressinduced apoptosis model using tunicamycin in primary cultured neonatal rat cardiomyocytes," *Molecular Medicine Reports*, vol. 12, no. 4, pp. 5149–5154, 2015.

[18] X. Zhang, Y. Yuan, L. Jiang et al., "Endoplasmic reticulum stress induced by tunicamycin and thapsigargin protects against transient ischemic brain injury: involvement of PARK2-dependent mitophagy," *Autophagy*, vol. 10, no. 10, pp. 1801–1813, 2014.

[19] V. N. S. Garikipati, S. Jadhav, L. Pal, P. Prakash, M. Dikshit, and S. Nityanand, "Mesenchymal stem cells from fetal heart attenuate myocardial injury after infarction: an in vivo serial pinhole gated SPECT-CT study in rats," *PLoS ONE*, vol. 9, no. 6, Article ID e100982, 2014.

[20] S. E. Nada, J. Tulsulkar, A. Raghavan, K. Hensley, and Z. A. Shah, "A derivative of the CRMP2 binding compound lanthionine ketimine provides neuroprotection in a mouse model of cerebral ischemia," *Neurochemistry International*, vol. 61, no. 8, pp. 1357–1363, 2012.

[21] A. M. Schrand, J. J. Schlager, L. Dai, and S. M. Hussain, "Preparation of cells for assessing ultrastructural localization of nanoparticles with transmission electron microscopy," *Nature Protocols*, vol. 5, no. 4, pp. 744–757, 2010.

[22] B. Yin, Y. Xu, R. L. Wei, F. He, B. Y. Luo, and J. Y. Wang, "Inhibition of receptor-interacting protein 3 upregulation and nuclear translocation involved in Necrostatin-1 protection against hippocampal neuronal programmed necrosis induced by ischemia/reperfusion injury," *Brain Research*, vol. 1609, pp. 63–71, 2015.

[23] M. Park, A. Sabetski, Y. Kwan Chan, S. Turdi, and G. Sweeney, "Palmitate induces ER stress and autophagy in H9c2 cells: implications for apoptosis and adiponectin resistance," *Journal of Cellular Physiology*, vol. 230, no. 3, pp. 630–639, 2015.

[24] M. Ricchi, M. R. Odoardi, L. Carulli et al., "Differential effect of oleic and palmitic acid on lipid accumulation and apoptosis in cultured hepatocytes," *Journal of Gastroenterology and Hepatology*, vol. 24, no. 5, pp. 830–840, 2009.

[25] J. Karch, O. Kanisicak, M. J. Brody et al., "Necroptosis interfaces with MOMP and the MPTP in mediating cell death," *PLoS ONE*, vol. 10, no. 6, Article ID e0130520, 2015.

[26] Q. Liu, J. Qiu, M. Liang et al., "Akt and mTOR mediate programmed necrosis in neurons," *Cell Death & Disease*, vol. 5, no. 2, Article ID e1084, 2014.

[27] S. Cetrullo, B. Tantini, F. Flamigni et al., "Antiapoptotic and anti-autophagic effects of eicosapentaenoic acid in cardiac myoblasts exposed to palmitic acid," *Nutrients*, vol. 4, no. 2, pp. 78–90, 2012.

[28] H. Chen, G. M. Untiveros, L. A. K. McKee et al., "Micro-RNA-195 and -451 regulate the LKB1/AMPK signaling axis by targeting MO25," *PLoS ONE*, vol. 7, no. 7, Article ID e41574, 2012.

[29] R. Chavez-Valdez, L. J. Martin, D. L. Flock, and F. J. Northington, "Necrostatin-1 attenuates mitochondrial dysfunction in neurons and astrocytes following neonatal hypoxia-ischemia," *Neuroscience*, vol. 219, pp. 192–203, 2012.

[30] M. I. F. J. Oerlemans, J. Liu, F. Arslan et al., "Inhibition of RIP1-dependent necrosis prevents adverse cardiac remodeling after myocardial ischemia-reperfusion in vivo," *Basic Research in Cardiology*, vol. 107, no. 4, article 270, 2012.

[31] S. Koshinuma, M. Miyamae, K. Kaneda, J. Kotani, and V. M. Figueredo, "Combination of necroptosis and apoptosis inhibition enhances cardioprotection against myocardial ischemia-reperfusion injury," *Journal of Anesthesia*, vol. 28, no. 2, pp. 235–241, 2014.

[32] M. J. Khan, M. R. Alam, M. Waldeck-Weiermair et al., "Inhibition of autophagy rescues palmitic acid-induced necroptosis of endothelial cells," *The Journal of Biological Chemistry*, vol. 287, no. 25, pp. 21110–21120, 2012.

[33] Y. S. Cho, S. Challa, D. Moquin et al., "Phosphorylation-driven assembly of the RIP1-RIP3 complex regulates programmed necrosis and virus-induced inflammation," *Cell*, vol. 137, no. 6, pp. 1112–1123, 2009.

[34] Y. Zhao, Y. Tan, S. Xi et al., "A novel mechanism by which SDF-1β protects cardiac cells from palmitate-induced endoplasmic reticulum stress and apoptosis via CXCR7 and AMPK/p38 MAPK-mediated interleukin-6 generation," *Diabetes*, vol. 62, no. 7, pp. 2545–2558, 2013.

[35] A. E. Ghule, A. D. Kandhare, S. S. Jadhav, A. A. Zanwar, and S. L. Bodhankar, "Omega-3-fatty acid adds to the protective effect of flax lignan concentrate in pressure overload-induced myocardial hypertrophy in rats via modulation of oxidative stress and apoptosis," *International Immunopharmacology*, vol. 28, no. 1, pp. 751–763, 2015.

[36] C. S. Park, H. Cha, E. J. Kwon, P. K. Sreenivasaiah, and D. H. Kim, "The chemical chaperone 4-phenylbutyric acid attenuates pressure-overload cardiac hypertrophy by alleviating endoplasmic reticulum stress," *Biochemical and Biophysical Research Communications*, vol. 421, no. 3, pp. 578–584, 2012.

[37] S. Saveljeva, S. L. Mc Laughlin, P. Vandenabeele, A. Samali, and M. J. Bertrand, "Endoplasmic reticulum stress induces ligand-independent TNFR1-mediated necroptosis in L929 cells," *Cell Death & Disease*, vol. 6, no. 1, Article ID e1587, 2015.

[38] T. Aoyagi, J. K. Higa, H. Aoyagi, N. Yorichika, B. K. Shimada, and T. Matsui, "Cardiac mTOR rescues the detrimental effects of diet-induced obesity in the heart after ischemia-reperfusion," *The American Journal of Physiology—Heart and Circulatory Physiology*, vol. 308, no. 12, pp. H1530–H1539, 2015.

[39] G. P. Diniz, M. L. M. Barreto-Chaves, and M. S. Carneiro-Ramos, "Angiotensin type 1 receptor mediates thyroid hormone-induced cardiomyocyte hypertrophy through the Akt/GSK-3β/mTOR signaling pathway," *Basic Research in Cardiology*, vol. 104, no. 6, pp. 653–667, 2009.

[40] X. Liu, R. R. Chhipa, I. Nakano, and B. Dasgupta, "The AMPK inhibitor compound C is a potent AMPK-independent antiglioma agent," *Molecular Cancer Therapeutics*, vol. 13, no. 3, pp. 596–605, 2014.

[41] C. R. McNamara, R. Ahuja, A. D. Osafo-Addo et al., "Akt Regulates TNFalpha synthesis downstream of RIP1 kinase activation during necroptosis," *PLoS ONE*, vol. 8, no. 3, Article ID e56576, 2013.

[42] R. Shindo, H. Kakehashi, K. Okumura, Y. Kumagai, and H. Nakano, "Critical contribution of oxidative stress to TNFα-induced necroptosis downstream of RIPK1 activation," *Biochemical and Biophysical Research Communications*, vol. 436, no. 2, pp. 212–216, 2013.

Hindawi Publishing Corporation
Oxidative Medicine and Cellular Longevity
Volume 2016, Article ID 3686829, 11 pages
http://dx.doi.org/10.1155/2016/3686829

Research Article

SOD1 Overexpression Preserves Baroreflex Control of Heart Rate with an Increase of Aortic Depressor Nerve Function

Jeffrey Hatcher,[1] He Gu,[2] and Zixi (Jack) Cheng[1]

[1]*Biomolecular Science Center, Burnett School of Biomedical Sciences, College of Medicine, University of Central Florida, Orlando, FL 32816, USA*
[2]*Department of Anesthesia, University of Iowa Hospital and Clinics, Iowa City, IA 52242, USA*

Correspondence should be addressed to Zixi (Jack) Cheng; zixi.cheng@ucf.edu

Received 24 July 2015; Accepted 1 October 2015

Academic Editor: Wei-Zhong Wang

Overproduction of reactive oxygen species (ROS), such as the superoxide radical ($O_2^{\bullet-}$), is associated with diseases which compromise cardiac autonomic function. Overexpression of SOD1 may offer protection against ROS damage to the cardiac autonomic nervous system, but reductions of $O_2^{\bullet-}$ may interfere with normal cellular functions. We have selected the C57B6SJL-Tg (SOD1)2 Gur/J mouse as a model to determine whether SOD1 overexpression alters cardiac autonomic function, as measured by baroreflex sensitivity (BRS) and aortic depressor nerve (ADN) recordings, as well as evaluation of baseline heart rate (HR) and mean arterial pressure (MAP). Under isoflurane anesthesia, C57 wild-type and SOD1 mice were catheterized with an arterial pressure transducer and measurements of HR and MAP were taken. After establishing a baseline, hypotension and hypertension were induced by injection of sodium nitroprusside (SNP) and phenylephrine (PE), respectively, and ΔHR versus ΔMAP were recorded as a measure of baroreflex sensitivity (BRS). SNP and PE treatment were administered sequentially after a recovery period to measure arterial baroreceptor activation by recording aortic depressor nerve activity. Our findings show that overexpression of SOD1 in C57B6SJL-Tg (SOD1)2 Gur/J mouse preserved the normal HR, MAP, and BRS but enhanced aortic depressor nerve function.

1. Introduction

Autonomic control of the cardiovascular system is compromised in multiple disease conditions such as diabetes [1–3], hypertension [4], sleep apnea [5], and aging [6–9]. One of the autonomic functions impacted is the baroreflex control of heart rate (HR). Baroreflex sensitivity (BRS) is a measure of the strength of baroreflex control of heart rate in response to changes in arterial pressure, and it is an important index of cardiac autonomic function. Several clinical conditions are strongly associated with an attenuated BRS, including hypertension [10], vasovagal syncope [11], and heart failure [12], and it is considered as an independent risk factor for cardiac failure and sudden death [13–15].

The baroreflex arc is composed of multiple neural components including the aortic and carotid baroreceptors, the nucleus tractus solitarius (NTS), paraventricular nucleus of the hypothalamus (PVN), nucleus ambiguus (NA), caudal ventrolateral medulla (CVLM), and rostral ventrolateral medulla (RVLM) [16–19]. An increase in levels of reactive oxygen species (ROS) in these neural components of the baroreflex arc including the carotid and aortic baroreceptors [20–23], NTS [24–26], PVN [27], and RVLM [28–30] are seen in conditions such as diabetes, sleep apnea, hypertension, and heart failure.

Several lines of research suggest that antioxidant therapy, whether applied locally [20, 21, 31] or systemically [32–34], can restore normal baroreflex function in some of these disease states, ostensibly by decreasing levels of ROS species. However, ROS, including the superoxide radical, play critical roles in regulating the firing properties of neurons [35]. For instance, the ANGII signaling pathway is dependent upon superoxide anions generated by the actions of NADPH oxidase [24, 36]. Indeed, some studies have noted that superoxide scavenging can affect central regulation of heart rate and blood pressure in healthy animals as well as some disease models [31, 32, 37].

Conversely, other investigations have suggested SOD1 overexpression can be detrimental to neuronal tissues. Some studies [38, 39] found evidence of mild axonal degeneration and some death of motor neurons in mice overexpressing hSOD1. In addition, increased lipid peroxidation [40, 41], increased sensitivity to kainic acid excitotoxicity [42], and impaired recovery following nerve injury [43] have been reported in hSOD1 transgenic mice. Though SOD1 overexpression is protective up to a certain level, further increases in expression may contribute to peroxide formation and deleterious sequela for the tissues [44, 45]. SOD1 overexpression has also been investigated as a contributor to the pathology of Down syndrome, a condition in which SOD1 overexpression is well documented [46–48].

All together, the available evidence from the literature has suggested that SOD1 overexpression can have *either* protective *or* detrimental effects on tissues. Therefore, we need to consider if hSOD1 overexpression in animals can affect the neural components of the baroreflex loop in healthy animals. Only then, we can consider any potential benefits of SOD1 overexpression in chronic intermittent hypoxia-, diabetes-, and aging-induced impairment of baroreflex arc as shown in our previous studies [49–57]. In the present study, we have determined the effects of hSOD1 overexpression in transgenic mice on several physiological variables [arterial pressure (AP), heart rate (HR), baroreflex sensitivity (BRS), and aortic depressor nerve function] compared to controls. Our data indicated that hSOD1 overexpression in transgenic mice did not alter the values of AP, HR, and baroreflex sensitivity but enhanced aortic depressor nerve function. This study will provide baseline data on the hSOD1 overexpressing mouse line in order to facilitate future studies on possible baroreflex protective effects of overexpressed SOD1 in murine disease models.

2. Materials and Methods

2.1. Animals. Mice (C57BL/6j 3-4 mo, $n = 16$) were used as controls for the transgenic human Cu/Zn SOD overexpressing mice (C57B6SJL-Tg (SOD1)2 Gur/J, Jackson catalog # 002297, $n = 16$). Procedures were approved by the University of Central Florida Animal Care and Use Committee and followed the guidelines established by the National Institutes of Health. Efforts were made to conduct the experiments humanely and to minimize the numbers of animals used.

2.1.1. Surgical Procedure. The surgical procedure has been described previously in detail [52]. Briefly, mice were anesthetized with 3% isoflurane inhalation and maintained with 1% in a 95% O_2 and 5% CO_2 through a tracheal tube which was connected to a rodent ventilator, as in our previous studies [51–53].

Depth of anesthesia was carefully monitored by eye blink, withdrawal reflexes (toe and tail pinch), and fluctuations of AP. Body temperature was maintained at 37 ± 1°C with a homeostatic plate and a rectal probe (ATC 1000; World Precision Instrument, Sarasota, FL, USA). The tips of plastic catheters (polyethylene-50) were tapered to ~0.3 mm diameter, the right femoral artery and left femoral vein were exposed, and the tapered ends of the two catheters were filled with heparinized saline and inserted into the femoral artery and vein. Measurement of AP was through the artery. Vasoactive drugs sodium nitroprusside (SNP) and phenylephrine (PE) were infused into the femoral vein using a microinfusion pump. These mice were used for AP, HR, baroreflex bradycardia and tachycardia, and aortic depressor nerve (ADN) recordings.

2.1.2. Baroreflex Sensitivity. The blood pressure catheter was connected to a pressure transducer (MIT0699, AD instruments) which was connected to the PowerLab Data Acquisition System (PowerLab/8 SP). Baseline values of mean arterial pressure (MAP) and HR and the MAP and chronotropic responses to sequential SNP/PE applications were measured using Chart 5 software (AD instruments). SNP and PE (Sigma, St. Louis, MO, USA) were freshly prepared, diluted in 0.9% NaCl, and infused by sequential bolus injections. SNP [2.3 ± 0.1 μg (C57) versus 2.2 ± 0.1 μg (SOD1) in 0.1 μg/μL saline, $P > 0.05$] was first injected, and after 10–20 s PE [8.1 ± 0.1 μg (C57) versus 6.9 ± 0.4 μg (SOD1) in 1 μg/μL saline, $P < 0.05$] was then injected. Such doses of sequential bolus injections of SNP/PE could induce a fast and large decrease followed by an increase of the AP. The measurement of decrease and increase in the AP was completed in ~1 min to reduce possible baroreflex resetting. Using these doses, MAP decreases and increases were quite comparable in control and SOD1 mice. Baseline values of MAP and HR were measured from a 30 s interval before SNP injection. After injections, MAP and HR returned to baseline values normally within 10–20 min. HR responses to MAP changes induced by sequential administration of SNP and PE included two phases: tachycardiac and bradycardic responses. During the tachycardiac (SNP) phase, MAP and HR changes were measured in the time window as indicated by a light gray box in Figure 1, that is, the baseline of MAP to the nadir of MAP. During the bradycardic (PE) phase, MAP and HR changes were measured in the time window as indicated by a dark gray box in Figure 1, that is, from the peak of the HR to the nadir of the HR. The MAP and corresponding HR were sampled and averaged every second. We applied linear regression analysis of the ΔHR-ΔMAP relationship for each animal, and the slope of the regression line was used as an indicator for baroreflex sensitivity (BRS) as previously described [52]. Data obtained for SNP and PE injections were averaged separately and reconstructed as separated regression lines for each group.

2.2. Baroreceptor Afferent Function. The aortic depressor nerve (ADN) on the left side was identified in the cervical region using a dissecting microscope. The left ADN was carefully isolated from surrounding connective tissues with fine glass tools to avoid stretching or injury of nerve. After that, the left ADN was placed on miniaturized bipolar platinum electrodes (outer diameter: 0.12-mm). The nerve and electrodes were soaked in mineral oil. Aortic depressor nerve activity (ADNA) was amplified (×10,000) with the band-pass filters set between 300 and 1000 Hz by an AC Amplifier (Model 1800, A-M Systems, Sequim, WA, USA). The ADNA, integrated ADNA, phasic arterial pressure (PAP), HR, ECG,

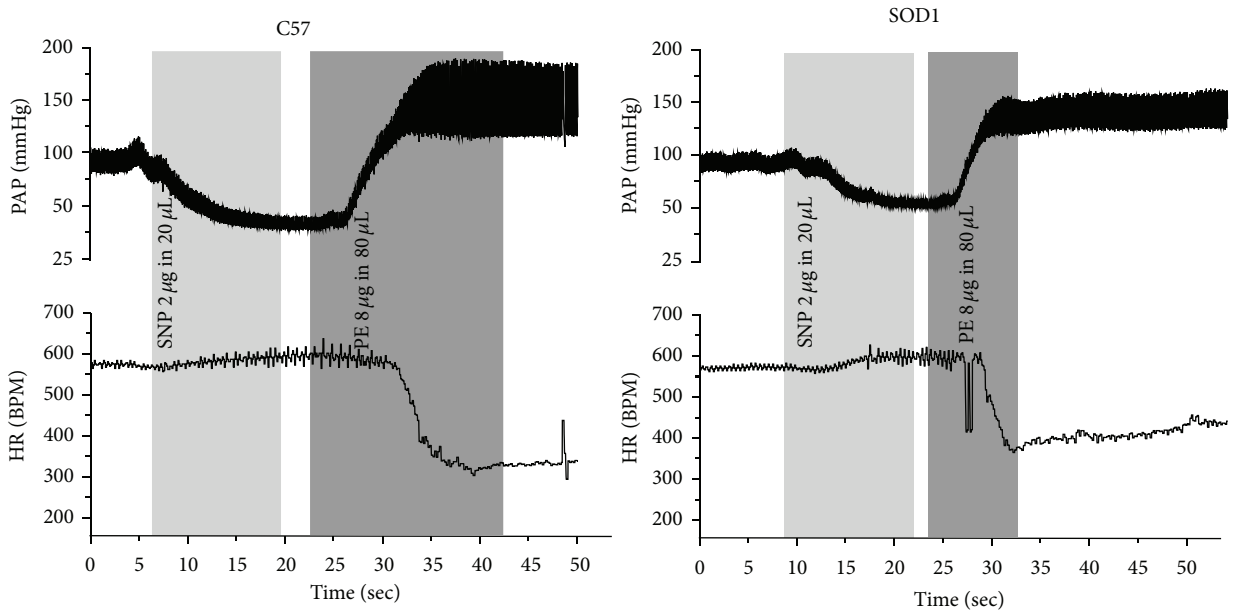

Figure 1: Original recordings of heart rate responses to pulse arterial pressure changes (PAP) induced by the sequential administration of SNP/PE in representative C57 and SOD1 animals. A tachycardiac phase was induced by a baroreflex-mediated increase in heart rate in response to decreased blood pressure due to SNP infusion. A bradycardic phase was induced by a baroreflex-mediated decrease in heart rate in response to increased blood pressure caused by injection of PE. During SNP application, MAP and HR changes from the baseline of MAP to the nadir of MAP were measured as shown in the light gray box. During PE application, MAP and HR changes were measured from the peak of the HR to the nadir of the HR as shown in the dark gray box.

and body temperature were all recorded and simultaneously displayed on different channels of the PowerLab System. Chart 5.2 software and Sigma Plot 9.0 were used for data acquisition, analysis, and presentation. All ADNA for analysis had a signal-to-noise ratio > 10 : 1.

The ADNA signal occurred as rhythmic bursts that exhibited cardiac cycles and were synchronized with PAP (Figure 3). ADNA signal was integrated using a 10 ms time constant to obtain the integrated ADNA (Int. ADNA). The "ADNA silent" or the "noise level" between the ADNA bursts was averaged from 30 "ADNA silent" intervals and was used to determine the noise level for Int. ADNA as shown in Figure 3. This averaged noise level was subtracted from original Int. ADNA signal to obtain the corrected Int. ADNA with the averaged noise level of 0 μV· s. The corrected Int. ADNA and MAP were used to construct baroreceptor afferent function curves using logistic sigmodal function. For simplicity, we used Int. ADNA for corrected Int. ADNA in the text below. The baroreceptor function curve was calculated at the rising phase of PE-induced AP increase starting from the nadir of the SNP-induced fall in AP to the maximum of the AP increase. R waves of ECG signal were used to automatically define cardiac cycles by the Chart 5.2 Macro function (arrows in Figure 3). The baroreceptor function curve was fitted by plotting the percent (%) of change of the mean Int. ADNA per cardiac cycle relative to the Int. ADNA baseline value before drug administration against MAP using a sigmoid logistic function [58]. The logistic function for Int. ADNA used the mathematical expression: $Y = -P_1/\{1 + \exp[P_2(X - P_3)]\} + P_4$, where X = MAP, Y = Int. ADNA (% baseline), P_1 = maximum − minimum (range), Int. ADNA (range), P_2 = slope coefficient, P_3 = MAP at 50% of the Int. ADNA range (P_{mid}), and P_4 = maximum Int. ADNA.

The P_{th} and P_{sat} were calculated from the 3rd derivative of the logistic function, and they were expressed as $P_{th} = P_3 - (1.317/P_2)$ and $P_{sat} = P_3 + (1.317/P_2)$. The maximum slope or gain (G_{max}) was calculated at P_{mid} from the 1st derivative of the logistic function: $G_{max} = P_1 \times P_2/4$. Approximately 200–500 data points measured over 30–50 s were used to construct a baroreceptor function curve using Sigma Plot software. The squared correlation coefficient R^2 was used to determine the goodness of curve fitting.

2.3. Statistical Analysis. Data were presented as means ± S.E. Student's t-test was used to compare the difference of HR, MAP, slopes of the regression lines, and parameters of the baroreceptor function curves between groups. Differences were considered significant at $P < 0.05$.

3. Results

3.1. MAP, HR, and SNP/PE-Induced MAP Changes. hSOD1 overexpression did not alter baseline MAP and HR, and SNP-induced minimums and PE-induced maximums for MAP changes in C57 and SOD1 mice were comparable (Table 1), which allowed us to investigate baroreflex control of HR over a similar range of blood pressure changes (see the following).

Table 1: There were no significant differences in baseline heart rate (HR) and mean arterial pressure (MAP) between C57 and SOD1 mice. Depression in arterial pressure following exposure to SNP, or increase in arterial pressure after PE infusion, was also similar between the two groups of animals.

Animal group	Average HR (BPM)	MAP (mmHg)	SNP MAP (mmHg)	PE MAP (mmHg)
C57 ($n = 8$)	558 ± 8	88.8 ± 2.9	38.7 ± 1.4	135.8 ± 3.1
SOD1 ($n = 8$)	553 ± 13	85.8 ± 2.1	39.5 ± 1.3	136.6 ± 3.5

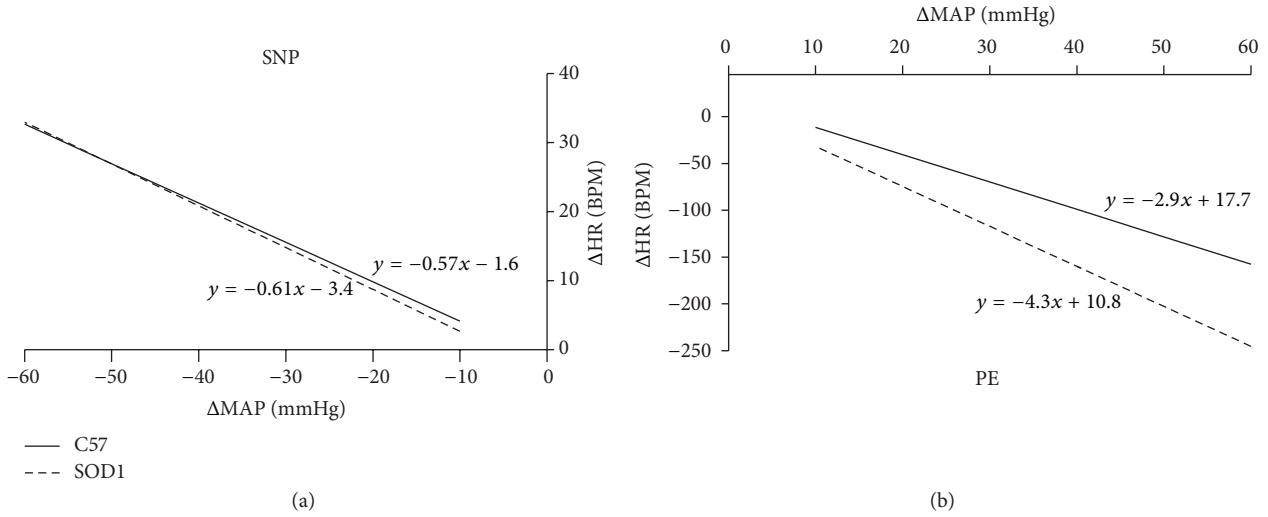

Figure 2: Baroreflex sensitivity. (a) The averaged regression lines for ΔHR/ΔMAP for the SNP-induced tachycardiac baroreflex for C57 ($n = 8$) and SOD1 ($n = 8$). Regression lines for tachycardiac baroreflex response are similar between the two groups. (b) The averaged regression lines for ΔHR/ΔMAP for the PE-induced bradycardic baroreflex for C57 ($n = 8$) and SOD1 ($n = 8$). Though visibly distinct, the slope of the regression line for SOD mice was not significantly different than that of C57 ($P > 0.5$).

3.2. Baroreflex Sensitivity. The original recordings of HR changes (ΔHR) in response to sequential injections of SNP and PE were shown in Figure 1. SNP infusion (light gray box) decreased AP which induced a HR increase (tachycardiac phase). PE infusion (dark gray box) resulted in an increase in AP that drove a baroreflex-mediated reduction in heart rate (bradycardic phase). Tachycardiac and bradycardic responses (ΔHR) against ΔMAP were fitted using separate regression lines for both C57 and SOD1 animals ($n = 8$/group), respectively. The slopes of the regression lines represent the baroreflex sensitivity (BRS) and they were similar (Figures 2(a) and 2(b)) for the tachycardiac phase [C57: −0.57 ± 0.06 bpm/mmHg, SOD1: −0.61 ± 0.08; $P > 0.05$] as well as the bradycardic phase [C57: −2.9 ± 0.57 bpm/mmHg, SOD1: −4.3 ± 0.84 bpm/mmHg; $P > 0.05$]. Even though there was a trend of increased BRS for SOD1 animals during the bradycardic phase, the slopes of the regression lines were not significantly different. Therefore, overexpression of hSOD1 did not significantly change baroreflex-mediated tachycardia and bradycardia.

3.3. Aortic Depressor Nerve Function. Aortic depressor nerve function was measured as the aortic depressor nerve activity (ADNA) decreases in response to SNP/PE-induced AP elevation. Figure 3 shows the original recordings of typical burst ADNA in synchrony with PAP. Figures 4(a) and 4(b) show the original recordings of ADNA in response to changes in blood pressure in representative C57 and SOD1 mice. SNP injection decreased and PE injection increased ADNA. Int. ADNA and MAP relationship curves were fitted using the logistic sigmodal function in these two mice as shown in Figures 4(a′) and 4(b′). The averaged parameters of the logistic function curves (Table 2) show that the SOD1 animals had a significantly larger maximal Int. ADNA response (P_4) compared to C57 ($P < 0.05$). The maximal gain of the ADNA response (G_{max}) was also significantly greater in SOD1 than C57 ($P < 0.01$), indicating that hSOD1 overexpression resulted in more sensitive responses than the control, thus increasing the aortic baroreceptor depressor nerve function. The plots of the sigmoid logistic function curves of the averaged Int. ADNA-MAP relationship for C57 and SOD1 mice were shown in Figure 5.

4. Discussion

In this study, we demonstrated that the overexpression of human SOD1 in mice does not have significant effect on AP, HR, or SNP/PE-induced changes of MAP and BRS as compared to controls. However, SOD1 overexpression enhanced baroreceptor depressor nerve function in response to AP elevation. While we could not fully interpret the mechanism, Li et al. [31] measured a similar increase in baroreceptor sensitivity after application of SOD1 and catalase to the

Table 2: Parameters defining the baroreceptor afferent function curve (ADNA% baseline) in C57 and SOD1 mice.

	R^2	P_1 (%)	P_2	P_3 (mmHg)	P_4 (%)	G_{max} (%/mmHg)	P_{th} (mmHg)	P_{sat} (mmHg)
C57 ($n = 8$)	0.95 ± 0.01	−307 ± 19	0.07 ± 0.006	94 ± 3	314 ± 18	5.4 ± 0.3	74 ± 3	114 ± 4
SOD1 ($n = 8$)	0.95 ± 0.01	−434 ± 44	0.07 ± 0.004	94 ± 3	436 ± 37	7.4 ± 0.5	73 ± 2	114 ± 4
P value	N.S	$P < 0.02$	N.S	N.S	$P < 0.02$	$P < 0.01$	N.S	N.S

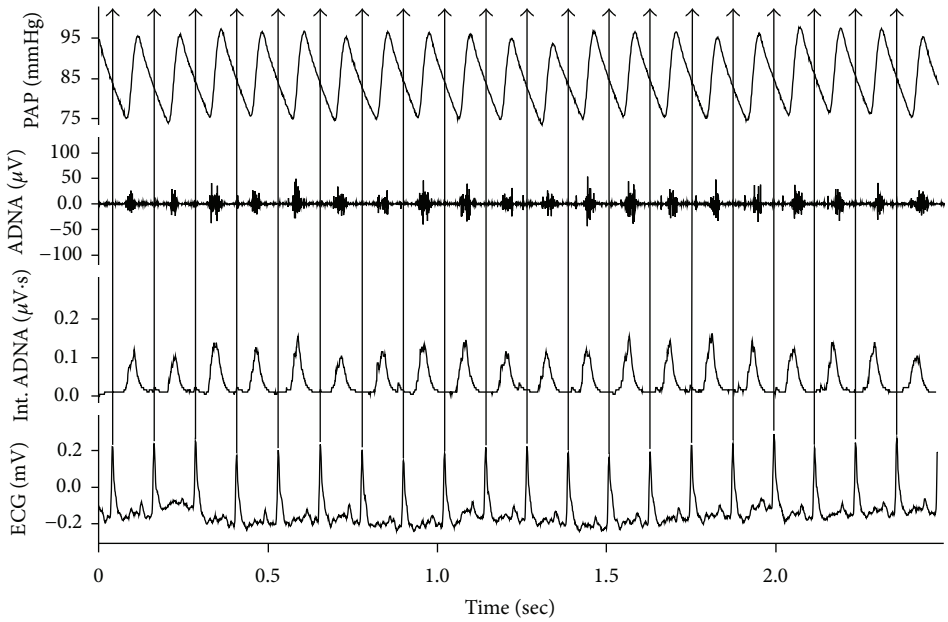

Figure 3: Original recording of PAP, ADNA (Raw ADNA), integrated ADNA (Int. ADNA), and ECG in aC57 mouse. Trace 1: PAP. Trace 2: ADNA occurred as rhythmic bursts that exhibited cardiac rhythmic patterns and was synchronous with PAP. Note: ADNA increased prior to AP increases. This is because the catheter for blood pressure measurement was inserted into the femoral artery. Trace 3: ADNA signal was integrated using a 10 ms time constant to obtain the Int. ADNA curve. The small boxes in the Int. ADNA trace enclose the intervals between ADNA bursts where signal noise can be measured. Trace 4: ECG. The R waves of the ECG signal were used to separate ADNA firing intervals automatically by Chart 5.2 (arrows).

nodose ganglia of healthy rabbits, though the effect was mild and not reversed by washout of the SOD or catalase.

4.1. hSOD1 Overexpression Did Not Change Basal Blood Pressure and Heart Rate. Superoxide radicals have profound effects in the modulation of neural activity in the brain stem [24, 59], and it is known that increases in ROS alter autonomic regulation of blood pressure [24, 60, 61]. One of the concerns of using the SOD1 mouse line is that interference with superoxide-dependent signaling in the brainstem by hSOD1 overexpression would alter basal HR and MAP. It is fairly well established that treatments with antioxidants may lead to changes of autonomic regulation in normal and disease models. hSOD1 overexpression in the paraventricular nucleus was found to reduce sympathetic activity and attenuate hypertension in spontaneously hypertensive rats, although no effect was detectable in the Wistar controls [27]. Another study found that endothelial-specific catalase overexpression caused a significant reduction in blood pressure in healthy mice [62]. Systemic administration of tempol, a SOD mimic [63], has previously been found to reduce MAP, HR, and renal sympathetic nerve activity (RSNA) in both normal and baroreceptor denervated rats [34]. The same study noted reduced spontaneous discharge rate of neurons in the paraventricular nucleus of the hypothalamus (PVN) and the rostral ventrolateral medulla (RVLM), two critical nuclei involved in sympathetic regulation of the cardiovascular system. A similar study performed on normotensive WKY and spontaneously hypertensive (SHR) rats also demonstrated reduced HR and MAP during systemic tempol administration in both groups of animals, as well as decreased splanchnic nerve activity [32]. Kawada's study determined that the reduction in blood pressure was not caused by changes in peripheral vascular tone in WKY animals, although AP reduction was associated with relaxation of vascular tone in the SHR rats. Taken together, these prior studies raise the possibility that superoxide radical scavenging may have effects on neural and vascular control of blood pressure in diseased and healthy animals.

In our study, hSOD1 overexpression had no significant effect on MAP, HR, and BRS in healthy mice. This is in agreement with a previously published report [64] showing blood pressure equivalence between C57bl/6J mice and 6-TgN(SOD1)3Cje mice with a 3-fold overexpression of hSOD1

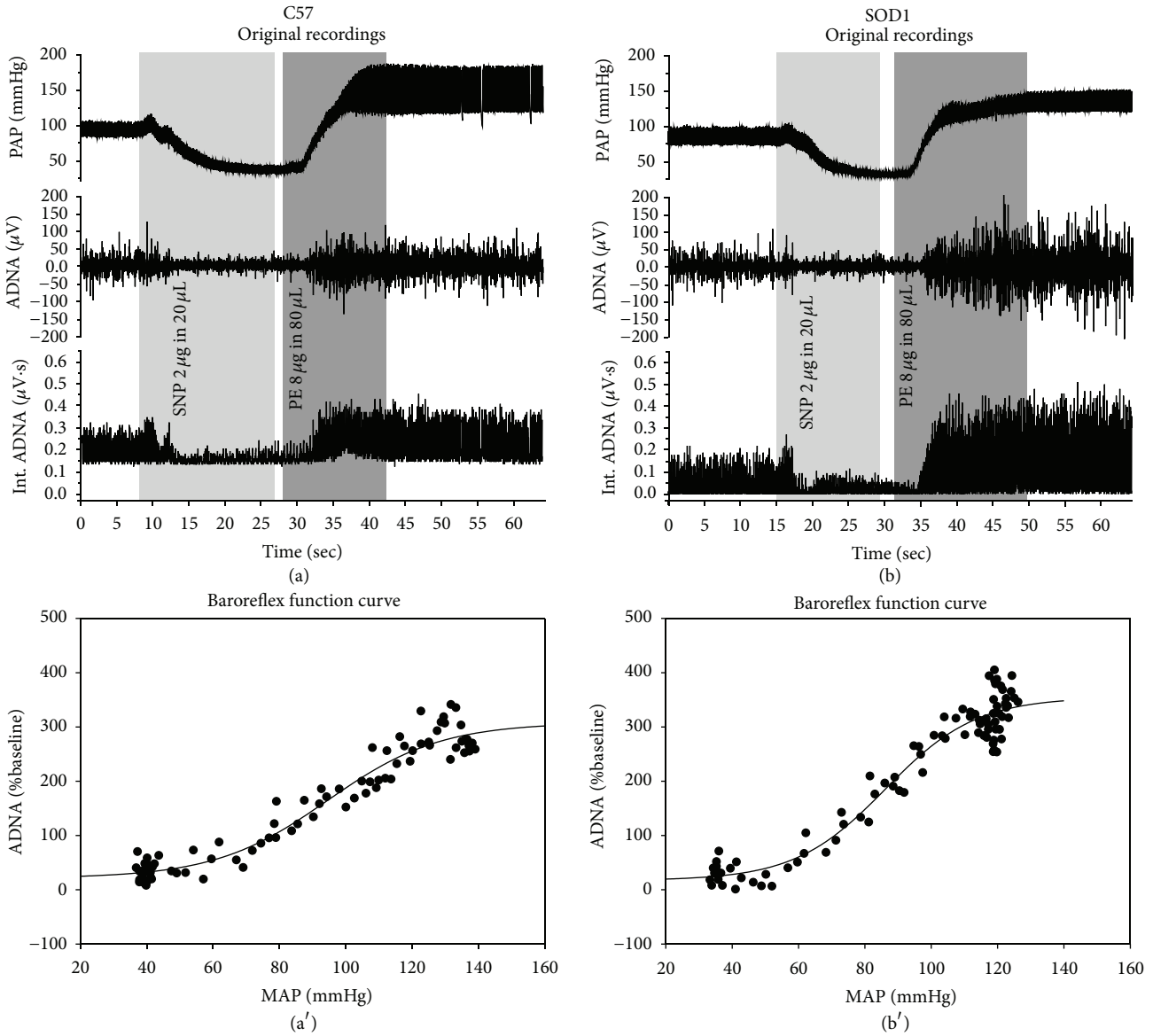

Figure 4: Baroreceptor function curve. (a and b) Original recordings showing pulse arterial pressure (PAP) and ADNA responses to sequential i.v. injections of SNP/PE in two representative C57 and SOD1 mice, respectively. (a′ and b′) Int. ADNA and MAP relationship curves of these two representative mice were fitted using logistic function, respectively (Int. ADNA: integrated ADNA).

(Jackson Catalog#: 002629). Therefore, hSOD1 overexpression in healthy animals does not seem to compromise basic hemodynamic stability as measured by HR and AP.

4.2. Baroreflex Control of Heart Rate Not Significantly Affected by hSOD1 Overexpression. Previous studies have shown that redox species modulate the activity of baroreceptor neurons [20–23], NTS [24–26], sympathetic brain stem nuclei such as the PVN [27] and RVLM [28–30], and intrinsic cardiac ganglia [65]. Perturbations in the function of any of the components of the baroreflex loop can alter baroreflex sensitivity and function. Indeed, it is well established that increased ROS levels in these components can reduce baroreflex sensitivity and response [26, 31, 61]. However, the effect of long-term antioxidant supplementation, and in particular SOD1 overexpression, on baroreflex function in healthy animals was less well documented. Li et al. [31] found that exogenous SOD1 or catalase applied to the carotid sinus caused a small but significant increase in baroreceptor activity between the pressures of 60 and 80 mmHg but did not increase the maximal baroreceptor activation. However, this study did not measure HR response to blood pressure ramps (ΔHR/ΔMAP), so it is uncertain if local application of SOD or catalase to the carotid baroreceptors would have had an appreciable effect on the baroreflex control of heart rate. Guimarães et al. [66] investigated the effects of NADPH-derived superoxide anion reductions by IV Tiron (a superoxide anion scavenger, [67]) or apocynin (NADPH oxidase inhibitor, [68]) on BRS in

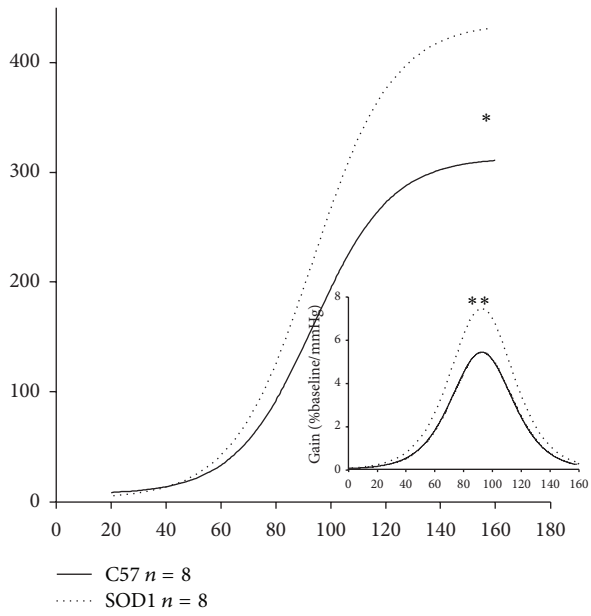

Figure 5: Baroreceptor afferent function: baroreceptor function curves for C57 ($n = 8$) and SOD1 ($n = 8$) groups were reconstructed using the averaged parameters of sigmoid logistic function curves (see Table 2). The baroreceptor discharge function curve for SOD1 mice is significantly higher for SOD mice compared to C57 ($^{*}P < 0.05$) and the gain of the baroreceptor afferent function curve was significantly higher for the SOD1 mice than for the C57 mice ($^{**}P < 0.01$).

WKY and SHR rats and found that the acute application of these agents had no significant effect on BRS in healthy animals, although they improved BRS in the hypertensive animals. Unfortunately, this still does not give any indication as to what effects long-term superoxide anion scavenging could have on BRS. The results of our investigation suggest for the first time that moderate (~3.5-fold, [69]) chronic systemic hSOD1 overexpression does not significantly impact baroreflex sensitivity in healthy animals.

4.3. Baroreceptor Afferent Function Enhanced by Overexpression of Human SOD1. As shown in Figure 5, we found that hSOD1 overexpressing mice showed significantly increased aortic baroreceptor activation slope and gain compared to C57 controls. This result is similar to the finding of Li et al. [31], who reported that carotid sinus nerve (CSN) activation in response to BP ramps was enhanced by application of SOD or catalase to the carotid sinus in rabbits.

Defining the mechanism the observed increase in baroreceptor activation is beyond the scope of this investigation, but there are certainly precedents in the literature. SOD1 is known to support nitrous oxide (NO) mediated vasorelaxation [70], which improves arterial compliance [71–73]. A high degree of vascular compliance is linked to robust baroreflex sensitivity [9, 74, 75], which decreases in step with vascular compliance. There is research that supports the hypothesis that antioxidant supplementation can improve large artery compliance [76, 77].

SOD1 may directly affect the mechanosensory properties of the aortic baroreceptor terminals by altering the expression or activity of critical ion channels in the baroreceptor terminals. There is evidence that ROS inhibit the expression of ASIC2 (Acid-Sensitive Ion Channel) which is critical to mechanotransduction of arterial pressure [78, 79]. ASIC2 expression is downregulated in SHR rats [80, 81], which show a similar diminution of baroreceptor activation to ASIC2 null mice [79]. Application of the superoxide mimetic tempol to nodose ganglia cells in either the ASIC2 null mice or SHR rats has been shown to restore baroreflex activation of baroreceptor neurons to near normal levels [78]. Hyperpolarization-activated cyclic nucleotide (HCN) channels, which are also strongly linked to mechanoreception in arterial baroreceptors, are shown to be upregulated in type 1 diabetes mellitus leading to a reduced baroreceptor function that can be rescued with tempol [22].

4.4. Perspectives. A growing body of evidence has shown that interventions based on antioxidants can be effective in reducing hypertension, increasing vascular compliance and function, and improving baroreflex-mediated control of heart rate [25, 27, 32, 33, 66, 76]. However, because ROS have a wide variety of necessary biological functions, it is important to evaluate the effect of systemic application of antioxidants on cardiac autonomic function in the absence of any other diseases. The current study uses a transgenic mouse model based on the C57bl/6j mouse line which has been engineered to express human Cu/ZnSOD (SOD1) at a level roughly 3.5-fold over normal murine SOD1 expression in cortical tissue [69]. This transgenic mouse line was originally developed in 1994 as a gene-dosage control for a mouse model of amyotrophic lateral sclerosis (ALS) overexpressing a SOD1-G93A mutation. The SOD1 mouse line used in this study showed no signs of ALS-like symptoms. In addition, Dal Canto and Gurney [39] also performed anatomical assessment of neural tissue and found that the mice overexpressing hSOD1 showed very subtle changes in the anterior portion of the anterior horn (mild swelling of motor fibers and vacuolization of dendrites) but were free of any ALS-like symptoms [39]. Functionally, there were no signs of impaired motor performance until 58 weeks of age. tgSOD1 mice in the current experiment were between 12 and 16 weeks of age, well before the window in which motor function changes are observed. In our study, we did not find any changes in AP, HR, vasoactive drugs-induced hypo- and hypertension, and BRS. Noticeably, the aortic depressor nerve function is increased in hSOD1 mice. Even though we could not interpret the mechanism for such an enhancement of aortic depressor nerve function, it appears that hSOD1 overexpression in this line of mouse did not impair but may have increased the function of baroreceptor afferent components in the baroreflex arc. Interestingly, Xu et al. [82] reported that mice overexpressing hSOD1, the same model as the one we used in present study, showed increased resistance to oxidative stress and apoptosis of cortical neurons after exposure to chronic intermittent hypoxia compared to wild-type control. hSOD1 overexpression has also been shown to protect against mitochondrial cytochrome C release and subsequent apoptosis in focal cerebral ischemia models

of stroke [83]. Since our data indicate that hSOD1 overexpression did not cause dysfunction of MAP, HR, and BRS but may increase aortic baroreceptor nerve function, we suggest that this model can be potentially used to study whether increased expression of hSOD1 protects against disease (such as chronic intermittent hypoxia and diabetes-) induced impairment of baroreflex sensitivity, vagal motor neuron death in the nucleus ambiguus, and degeneration of vagal afferent and efferent axons in the aortic arch and cardiac ganglion shown in the previous studies [51, 52, 55, 84–86]. Whether the increased baroreceptor sensitivity in healthy animals may prove advantageous in mitigating disease-induced impairment of autonomic control of the heart is a promising concept, and we are currently using our hSOD1 overexpressing mice to determine if hSOD1 overexpression can preserve normal afferent, efferent, and central components of the baroreflex arc in the CIH model of sleep apnea.

It should be pointed out that since baroreflex-mediated reduction of heart rate in response to increased arterial pressure had a trend of increase but not significantly, it appears that the increased signaling from the aortic depressor baroreceptor nerves to the brainstem is buffered by other neural components of the baroreflex loop, such as the NTS, NA, or cardiac ganglia within the heart. Whether such a buffering is a product of normal physiologic compensation or something of a more pathologic nature is undetermined. Thus, careful studies of other neural components in the baroreflex arc in addition to aortic depressor nerves are critically important to fully understand the effects of hSOD overexpression on the whole baroreflex circuitry.

Conflict of Interests

The authors declare that there is no conflict of interests regarding the publication of this paper.

References

[1] A. R. Olshan, D. T. O'connor, I. M. Cohen, J. A. Mitas, and R. A. Stone, "Baroreflex dysfunction in patients with adult-onset diabetes and hypertension," *The American Journal of Medicine*, vol. 74, no. 2, pp. 233–242, 1983.

[2] R. E. Maser and M. J. Lenhard, "Cardiovascular autonomic neuropathy due to diabetes mellitus: clinical manifestations, consequences, and treatment," *Journal of Clinical Endocrinology and Metabolism*, vol. 90, no. 10, pp. 5896–5903, 2005.

[3] A. I. Vinik, R. E. Maser, B. D. Mitchell, and R. Freeman, "Diabetic autonomic neuropathy," *Diabetes Care*, vol. 26, no. 5, pp. 1553–1579, 2003.

[4] E. D. Moreira, F. Ida, V. L. L. Oliveira, and E. M. Krieger, "Early depression of the baroreceptor sensitivity during onset of hypertension," *Hypertension*, vol. 19, no. 2, supplement, pp. II198–II201, 1992.

[5] K. Narkiewicz and V. K. Somers, "Cardiovascular variability characteristics in obstructive sleep apnea," *Autonomic Neuroscience: Basic & Clinical*, vol. 90, no. 1-2, pp. 89–94, 2001.

[6] T. B. J. Kuo, T. Lin, C. C. H. Yang, C.-L. Li, C.-F. Chen, and P. Chou, "Effect of aging on gender differences in neural control of heart rate," *American Journal of Physiology: Heart and Circulatory Physiology*, vol. 277, no. 6, part 2, pp. H2233–H2239, 1999.

[7] M. Saint Martin, F. Roche, C. Thomas-Anterion, J. C. Barthélémy, and E. Sforza, "Eight-year parallel change in baroreflex sensitivity and memory function in a sample of healthy older adults," *Journal of the American Geriatrics Society*, vol. 63, no. 2, pp. 270–275, 2015.

[8] J.-P. Fauvel, C. Cerutti, I. Mpio, and M. Ducher, "Aging process on spectrally determined spontaneous baroreflex sensitivity: a 5-year prospective study," *Hypertension*, vol. 50, no. 3, pp. 543–546, 2007.

[9] K. D. Monahan, "Effect of aging on baroreflex function in humans," *American Journal of Physiology: Regulatory Integrative and Comparative Physiology*, vol. 293, no. 1, pp. R3–R12, 2007.

[10] C. J. Lai, C. C. H. Yang, Y. Y. Hsu, Y. N. Lin, and T. B. J. Kuo, "Enhanced sympathetic outflow and decreased baroreflex sensitivity are associated with intermittent hypoxia-induced systemic hypertension in conscious rats," *Journal of Applied Physiology*, vol. 100, no. 6, pp. 1974–1982, 2006.

[11] G. A. Ford, "Ageing and the baroreflex," *Age and Ageing*, vol. 28, no. 4, pp. 337–338, 1999.

[12] M. D. Thames, T. Kinugawa, M. L. Smith, and M. E. Dibner-Dunlap, "Abnormalities of baroreflex control in heart failure," *Journal of the American College of Cardiology*, vol. 22, no. 4, supplement 1, pp. A56–A60, 1993.

[13] K. J. Osterziel, D. Hänlein, R. Willenbrock, C. Eichhorn, F. Luft, and R. Dietz, "Baroreflex sensitivity and cardiovascular mortality in patients with mild to moderate heart failure," *British Heart Journal*, vol. 73, no. 6, pp. 517–522, 1995.

[14] A. Mortara, M. T. La Rovere, G. D. Pinna et al., "Arterial baroreflex modulation of heart rate in chronic heart failure: clinical and hemodynamic correlates and prognostic implications," *Circulation*, vol. 96, no. 10, pp. 3450–3458, 1997.

[15] N. Okada, N. Takahashi, K. Yufu et al., "Baroreflex sensitivity predicts cardiovascular events in patients with type 2 diabetes mellitus without structural heart disease," *Circulation Journal*, vol. 74, no. 7, pp. 1379–1383, 2010.

[16] B. H. Machado, "Neurotransmission of the cardiovascular reflexes in the nucleus tractus solitarii of awake rats," *Annals of the New York Academy of Sciences*, vol. 940, pp. 179–196, 2001.

[17] R. A. L. Dampney, "Functional organization of central pathways regulating the cardiovascular system," *Physiological Reviews*, vol. 74, no. 2, pp. 323–364, 1994.

[18] R. A. L. Dampney, M. J. Coleman, M. A. P. Fontes et al., "Central mechanisms underlying short- and long-term regulation of the cardiovascular system," *Clinical and Experimental Pharmacology & Physiology*, vol. 29, no. 4, pp. 261–268, 2002.

[19] R. A. L. Dampney, J. Horiuchi, S. Killinger, M. J. Sheriff, P. S. P. Tan, and L. M. McDowall, "Long-term regulation of arterial blood pressure by hypothalamic nuclei: some critical questions," *Clinical and Experimental Pharmacology & Physiology*, vol. 32, no. 5-6, pp. 419–425, 2005.

[20] L. Zhang, H. Tu, and Y.-L. Li, "Angiotensin II enhances hyperpolarization-activated currents in rat aortic baroreceptor neurons: Involvement of superoxide," *American Journal of Physiology: Cell Physiology*, vol. 298, no. 1, pp. C98–C106, 2009.

[21] Y.-J. Peng, J. Nanduri, X. Zhang et al., "Endothelin-1 mediates attenuated carotid baroreceptor activity by intermittent hypoxia," *Journal of Applied Physiology*, vol. 112, no. 1, pp. 187–196, 2012.

[22] Y. L. Li, "Angiotensin II-superoxide signaling and arterial baroreceptor function in type-1 diabetes mellitus," *Journal of Diabetes & Metabolism*, vol. supplement 12, pp. 1–6, 2013.

[23] Y. Ding, Y.-L. Li, M. C. Zimmerman, R. L. Davisson, and H. D. Schultz, "Role of CuZn superoxide dismutase on carotid body function in heart failure rabbits," *Cardiovascular Research*, vol. 81, no. 4, pp. 678–685, 2009.

[24] Y. Hirooka, "Role of reactive oxygen species in brainstem in neural mechanisms of hypertension," *Autonomic Neuroscience: Basic & Clinical*, vol. 142, no. 1-2, pp. 20–24, 2008.

[25] M. Nozoe, Y. Hirooka, Y. Koga et al., "Inhibition of Rac1-derived reactive oxygen species in nucleus tractus solitarius decreases blood pressure and heart rate in stroke-prone spontaneously hypertensive rats," *Hypertension*, vol. 50, no. 1, pp. 62–68, 2007.

[26] C.-Y. Tsai, C.-H. Su, V. Baudrie et al., "Visualizing oxidative stress-induced depression of cardiac vagal baroreflex by MRI/DTI in a mouse neurogenic hypertension model," *NeuroImage*, vol. 82, pp. 190–199, 2013.

[27] N. Yuan, F. Zhang, L.-L. Zhang et al., "SOD1 gene transfer into paraventricular nucleus attenuates hypertension and sympathetic activity in spontaneously hypertensive rats," *Pflugers Archiv*, vol. 465, no. 2, pp. 261–270, 2012.

[28] T. Kishi, Y. Hirooka, Y. Kimura, K. Ito, H. Shimokawa, and A. Takeshita, "Increased reactive oxygen species in rostral ventrolateral medulla contribute to neural mechanisms of hypertension in stroke-prone spontaneously hypertensive rats," *Circulation*, vol. 109, no. 19, pp. 2357–2362, 2004.

[29] L. Gao, W. Wang, Y.-L. Li et al., "Superoxide mediates sympathoexcitation in heart failure: roles of angiotensin II and NAD(P)H oxidase," *Circulation Research*, vol. 95, no. 9, pp. 937–944, 2004.

[30] L. Gao, W. Wang, D. Liu, and I. H. Zucker, "Exercise training normalizes sympathetic outflow by central antioxidant mechanisms in rabbits with pacing-induced chronic heart failure," *Circulation*, vol. 115, no. 24, pp. 3095–3102, 2007.

[31] Z. Li, H. Z. Mao, F. M. Abboud, and M. W. Chapleau, "Oxygen-derived free radicals contribute to baroreceptor dysfunction in atherosclerotic rabbits," *Circulation Research*, vol. 79, no. 4, article 802, 1996.

[32] T. Kawada, Y. Sata, S. Shimizu, M. J. Turner, M. Fukumitsu, and M. Sugimachi, "Effects of tempol on baroreflex neural arc versus peripheral arc in normotensive and spontaneously hypertensive rats," *American Journal of Physiology—Regulatory, Integrative and Comparative Physiology*, vol. 308, no. 11, pp. R957–R964, 2015.

[33] S. Gouty, J. Regalia, F. Cai, and C. J. Helke, "α-Lipoic acid treatment prevents the diabetes-induced attenuation of the afferent limb of the baroreceptor reflex in rats," *Autonomic Neuroscience*, vol. 108, no. 1-2, pp. 32–44, 2003.

[34] S.-G. Wei, Z.-H. Zhang, Y. Yu, and R. B. Felder, "Systemically administered tempol reduces neuronal activity in paraventricular nucleus of hypothalamus and rostral ventrolateral medulla in rats," *Journal of Hypertension*, vol. 27, no. 3, pp. 543–550, 2009.

[35] H. J. Forman, M. Maiorino, and F. Ursini, "Signaling functions of reactive oxygen species," *Biochemistry*, vol. 49, no. 5, pp. 835–842, 2010.

[36] V. A. Braga, I. A. Medeiros, T. P. Ribeiro, M. S. França-Silva, M. S. Botelho-Ono, and D. D. Guimarães, "Angiotensin-II-induced reactive oxygen species along the SFO-PVN-RVLM pathway: implications in neurogenic hypertension," *Brazilian Journal of Medical and Biological Research*, vol. 44, no. 9, pp. 871–876, 2011.

[37] V. M. Campese, S. Ye, H. Zhong, V. Yanamadala, Z. Ye, and J. Chiu, "Reactive oxygen species stimulate central and peripheral sympathetic nervous system activity," *American Journal of Physiology—Heart and Circulatory Physiology*, vol. 287, no. 2, pp. H695–H703, 2004.

[38] D. Jaarsma, E. D. Haasdijk, J. A. C. Grashorn et al., "Human Cu/Zn superoxide dismutase (SOD1) overexpression in mice causes mitochondrial vacuolization, axonal degeneration, and premature motoneuron death and accelerates motoneuron disease in mice expressing a familial amyotrophic lateral sclerosis mutant SOD1," *Neurobiology of Disease B*, vol. 7, no. 6, pp. 623–643, 2000.

[39] M. C. Dal Canto and M. E. Gurney, "Neuropathological changes in two lines of mice carrying a transgene for mutant human Cu,Zn SOD, and in mice overexpressing wild type human SOD: a model of familial amyotrophic lateral sclerosis (FALS)," *Brain Research*, vol. 676, no. 1, pp. 25–40, 1995.

[40] H. J. Fullerton, J. S. Ditelberg, S. F. Chen et al., "Copper/zinc superoxide dismutase transgenic brain accumulates hydrogen peroxide after perinatal hypoxia ischemia," *Annals of Neurology*, vol. 44, no. 3, pp. 357–364, 1998.

[41] P. Amstad, A. Peskin, G. Shah et al., "The balance between Cu,Zn-superoxide dismutase and catalase affects the sensitivity of mouse epidermal cells to oxidative stress," *Biochemistry*, vol. 30, no. 38, pp. 9305–9313, 1991.

[42] O. Bar-Peled, E. Korkotian, M. Segal, and Y. Groner, "Constitutive overexpression of Cu/Zn superoxide dismutase exacerbates kainic acid-induced apoptosis of transgenic-Cu/Zn superoxide dismutase neurons," *Proceedings of the National Academy of Sciences of the United States of America*, vol. 93, no. 16, pp. 8530–8535, 1996.

[43] K. Kotulska, M. LePecheur, W. Marcol et al., "Overexpression of copper/zinc-superoxide dismutase in transgenic mice markedly impairs regeneration and increases development of neuropathic pain after sciatic nerve injury," *Journal of Neuroscience Research*, vol. 84, no. 5, pp. 1091–1097, 2006.

[44] J. M. McCord and M. A. Edeas, "SOD, oxidative stress and human pathologies: a brief history and a future vision," *Biomedicine & Pharmacotherapy*, vol. 59, no. 4, pp. 139–142, 2005.

[45] J. M. McCord, "Superoxide dismutase, lipid peroxidation, and bell-shaped dose response curves," *Dose Response*, vol. 6, no. 3, article 223, 2008.

[46] B. W. Brooksbank and R. Balazs, "Superoxide dismutase, glutathione peroxidase and lipoperoxidation in Down's syndrome fetal brain," *Brain Research*, vol. 318, no. 1, pp. 37–44, 1984.

[47] G. T. Capone, "Down syndrome: advances in molecular biology and the neurosciences," *Journal of Developmental & Behavioral Pediatrics*, vol. 22, no. 1, pp. 40–59, 2001.

[48] C. J. Epstein, K. B. Avraham, M. Lovett et al., "Transgenic mice with increased Cu/Zn-superoxide dismutase activity: animal model of dosage effects in Down syndrome," *Proceedings of the National Academy of Sciences of the United States of America*, vol. 84, no. 22, pp. 8044–8048, 1987.

[49] J. Ai, D. Gozal, L. Li et al., "Degeneration of vagal efferent axons and terminals in cardiac ganglia of aged rats," *Journal of Comparative Neurology*, vol. 504, no. 1, pp. 74–88, 2007.

[50] J. Ai, R. D. Wurster, S. W. Harden, and Z. J. Cheng, "Vagal afferent innervation and remodeling in the aortic arch of young-adult fischer 344 rats following chronic intermittent hypoxia," *Neuroscience*, vol. 164, no. 2, pp. 658–666, 2009.

[51] H. Gu, M. Lin, J. Liu et al., "Selective impairment of central mediation of baroreflex in anesthetized young adult Fischer 344 rats after chronic intermittent hypoxia," *American Journal of Physiology—Heart and Circulatory Physiology*, vol. 293, no. 5, pp. H2809–H2818, 2007.

[52] H. Gu, P. N. Epstein, L. Li, R. D. Wurster, and Z. J. Cheng, "Functional changes in baroreceptor afferent, central and efferent components of the baroreflex circuitry in type 1 diabetic mice (OVE26)," *Neuroscience*, vol. 152, no. 3, pp. 741–752, 2008.

[53] H. Gu, Z.-H. Zhang, P. N. Epstein et al., "Impaired baroreflex control of renal sympathetic nerve activity in type 1 diabetic mice (OVE26)," *Neuroscience*, vol. 161, no. 1, pp. 78–85, 2009.

[54] L. Li, C. Huang, J. Ai et al., "Structural remodeling of vagal afferent innervation of aortic arch and nucleus ambiguus (NA) projections to cardiac ganglia in a transgenic mouse model of type 1 diabetes (OVE26)," *The Journal of Comparative Neurology*, vol. 518, no. 14, pp. 2771–2793, 2010.

[55] M. Lin, R. Liu, D. Gozal et al., "Chronic intermittent hypoxia impairs baroreflex control of heart rate but enhances heart rate responses to vagal efferent stimulation in anesthetized mice," *American Journal of Physiology—Heart and Circulatory Physiology*, vol. 293, no. 2, pp. H997–H1006, 2007.

[56] M. Lin, J. Ai, L. Li et al., "Structural remodeling of nucleus ambiguus projections to cardiac ganglia following chronic intermittent hypoxia in C57BL/6J mice," *Journal of Comparative Neurology*, vol. 509, no. 1, pp. 103–117, 2008.

[57] M. Lin, J. Ai, S. W. Harden et al., "Impairment of baroreflex control of heart rate and structural changes of cardiac ganglia in conscious streptozotocin (STZ)-induced diabetic mice," *Autonomic Neuroscience: Basic & Clinical*, vol. 155, no. 1-2, pp. 39–48, 2010.

[58] B. B. Kent, J. W. Drane, B. Blumenstein, and J. W. Manning, "A mathematical model to assess changes in the baroreceptor reflex," *Cardiology*, vol. 57, no. 5, pp. 295–310, 1972.

[59] M. C. Zimmerman and R. L. Davisson, "Redox signaling in central neural regulation of cardiovascular function," *Progress in Biophysics and Molecular Biology*, vol. 84, no. 2-3, pp. 125–149, 2004.

[60] S. R. Datla and K. K. Griendling, "Reactive oxygen species, NADPH oxidases, and hypertension," *Hypertension*, vol. 56, no. 3, pp. 325–330, 2010.

[61] S. H. H. Chan and J. Y. H. Chan, "Brain stem NOS and ROS in neural mechanisms of hypertension," *Antioxidants & Redox Signaling*, vol. 20, no. 1, pp. 146–163, 2014.

[62] T. Suvorava and G. Kojda, "Reactive oxygen species as cardiovascular mediators: lessons from endothelial-specific protein overexpression mouse models," *Biochimica et Biophysica Acta*, vol. 1787, no. 7, pp. 802–810, 2009.

[63] C. Muscoli, S. Cuzzocrea, D. P. Riley et al., "On the selectivity of superoxide dismutase mimetics and its importance in pharmacological studies," *British Journal of Pharmacology*, vol. 140, no. 3, pp. 445–460, 2003.

[64] H. D. Wang, D. G. Johns, S. Xu, and R. A. Cohen, "Role of superoxide anion in regulating pressor and vascular hypertrophic response to angiotensin II," *The American Journal of Physiology—Heart and Circulatory Physiology*, vol. 282, no. 5, pp. H1697–H1702, 2002.

[65] K. A. Whyte, R. C. Hogg, J. Dyavanapalli, A. A. Harper, and D. J. Adams, "Reactive oxygen species modulate neuronal excitability in rat intrinsic cardiac ganglia," *Autonomic Neuroscience: Basic & Clinical*, vol. 150, no. 1-2, pp. 45–52, 2009.

[66] D. D. Guimarães, C. C. Carvalho, and V. A. Braga, "Scavenging of NADPH oxidase-derived superoxide anions improves depressed baroreflex sensitivity in spontaneously hypertensive rats," *Clinical and Experimental Pharmacology and Physiology*, vol. 39, no. 4, pp. 373–378, 2012.

[67] A. N. Ledenev, A. A. Konstantinov, E. Popova, and E. K. Ruuge, "A simple assay of the superoxide generation rate with Tiron as an EPR-visible radical scavenger," *Biochemistry international*, vol. 13, no. 2, pp. 391–396, 1986.

[68] M. S. Petrônio, M. L. Zeraik, L. M. Da Fonseca, and V. F. Ximenes, "Apocynin: chemical and biophysical properties of a NADPH oxidase inhibitor," *Molecules*, vol. 18, no. 3, pp. 2821–2839, 2013.

[69] M. E. Gurney, H. Pu, A. Y. Chiu et al., "Motor neuron degeneration in mice that express a human Cu,Zn superoxide dismutase mutation," *Science*, vol. 264, no. 5166, pp. 1772–1775, 1994.

[70] T. Fukai and M. Ushio-Fukai, "Superoxide dismutases: role in redox signaling, vascular function, and diseases," *Antioxidants and Redox Signaling*, vol. 15, no. 6, pp. 1583–1606, 2011.

[71] S. P. Didion, M. J. Ryan, L. A. Didion, P. E. Fegan, C. D. Sigmund, and F. M. Faraci, "Increased superoxide and vascular dysfunction in CuZnSOD-deficient mice," *Circulation Research*, vol. 91, no. 10, pp. 938–944, 2002.

[72] S. P. Didion, M. J. Ryan, G. L. Baumbach, C. D. Sigmund, and F. M. Faraci, "Superoxide contributes to vascular dysfunction in mice that express human renin and angiotensinogen," *The American Journal of Physiology—Heart and Circulatory Physiology*, vol. 283, no. 4, pp. H1569–H1576, 2002.

[73] S. M. Lynch, B. Frei, J. D. Morrow et al., "Vascular superoxide dismutase deficiency impairs endothelial vasodilator function through direct inactivation of nitric oxide and increased lipid peroxidation," *Arteriosclerosis, Thrombosis, and Vascular Biology*, vol. 17, no. 11, pp. 2975–2981, 1997.

[74] K. D. Monahan, H. Tanaka, F. A. Dinenno, and D. R. Seals, "Central arterial compliance is associated with age- and habitual exercise-related differences in cardiovagal baroreflex sensitivity," *Circulation*, vol. 104, no. 14, pp. 1627–1632, 2001.

[75] F. Michas, E. Manios, K. Stamatelopoulos et al., "Baroreceptor reflex sensitivity is associated with arterial stiffness in a population of normotensive and hypertensive patients," *Blood Pressure Monitoring*, vol. 17, no. 4, pp. 155–159, 2012.

[76] M. Shargorodsky, O. Debby, Z. Matas, and R. Zimlichman, "Effect of long-term treatment with antioxidants (vitamin C, vitamin E, coenzyme Q10 and selenium) on arterial compliance, humoral factors and inflammatory markers in patients with multiple cardiovascular risk factors," *Nutrition & Metabolism*, vol. 7, article 55, 2010.

[77] S. Ülker, P. P. McKeown, and U. Bayraktutan, "Vitamins reverse endothelial dysfunction through regulation of eNOS and NAD(P)H oxidase activities," *Hypertension*, vol. 41, no. 3, pp. 534–539, 2003.

[78] F. M. Abboud, "The Walter B. Cannon memorial award lecture, 2009. Physiology in perspective: the wisdom of the body. In search of autonomic balance: the good, the bad, and the ugly," *American Journal of Physiology—Regulatory, Integrative and Comparative Physiology*, vol. 298, no. 6, pp. R1449–R1467, 2010.

[79] Y. Lu, X. Ma, R. Sabharwal et al., "The ion channel ASIC2 is required for baroreceptor and autonomic control of the circulation," *Neuron*, vol. 64, no. 6, pp. 885–897, 2009.

[80] Y. Lu, C. A. Whiteis, M. W. Chapleau, and F. M. Abboud, "Decreased mRNA expression of ASIC2a in nodose sensory

ganglia is associated with development of hypertension in SHR (abstract)," *The FASEB Journal*, vol. 21, p. A1405, 2007.

[81] V. Snitsarev, K. Iyer, C. A. Whiteis, M. W. Chapleau, and F. M. Abboud, "Novel molecular defects in mechanosensitivity of aortic baroreceptor neurons from spontaneously hypertensive rats (Abstract)," *The FASEB Journal*, vol. 19, p. A607, 2005.

[82] W. Xu, L. Chi, B. W. Row et al., "Increased oxidative stress is associated with chronic intermittent hypoxia-mediated brain cortical neuronal cell apoptosis in a mouse model of sleep apnea," *Neuroscience*, vol. 126, no. 2, pp. 313–323, 2004.

[83] M. Fujimura, Y. Morita-Fujimura, N. Noshita, T. Sugawara, M. Kawase, and P. H. Chan, "The cytosolic antioxidant copper/zinc-superoxide dismutase prevents the early release of mitochondrial cytochrome c in ischemic brain after transient focal cerebral ischemia in mice," *Journal of Neuroscience*, vol. 20, no. 8, pp. 2817–2824, 2000.

[84] B. Yan, G. K. Soukhova-O'Hare, L. Li et al., "Attenuation of heart rate control and neural degeneration in nucleus ambiguus following chronic intermittent hypoxia in young adult Fischer 344 rats," *Neuroscience*, vol. 153, no. 3, pp. 709–720, 2008.

[85] B. Yan, H. Li, S. W. Harden et al., "Chronic intermittent hypoxia impairs heart rate responses to AMPA and NMDA and induces loss of glutamate receptor neurons in nucleus ambiguus of F344 rats," *American Journal of Physiology—Regulatory Integrative and Comparative Physiology*, vol. 296, no. 2, pp. R299–R308, 2009.

[86] B. Yan, L. Li, S. W. Harden, P. N. Epstein, R. D. Wurster, and Z. J. Cheng, "Diabetes induces neural degeneration in nucleus ambiguus (NA) and attenuates heart rate control in OVE26 mice," *Experimental Neurology*, vol. 220, no. 1, pp. 34–43, 2009.

Hindawi Publishing Corporation
Oxidative Medicine and Cellular Longevity
Volume 2016, Article ID 9802136, 9 pages
http://dx.doi.org/10.1155/2016/9802136

Research Article

Intermittent Hypoxia-Induced Carotid Body Chemosensory Potentiation and Hypertension Are Critically Dependent on Peroxynitrite Formation

Esteban A. Moya,[1] Paulina Arias,[1] Carlos Varela,[1] María P. Oyarce,[1] Rodrigo Del Rio,[2,3] and Rodrigo Iturriaga[1]

[1]*Laboratorio de Neurobiología, Departamento de Fisiología, Facultad de Ciencias Biológicas, Pontificia Universidad Católica de Chile, 8330025 Santiago, Chile*
[2]*Centro de Investigación Biomédica, Universidad Autónoma de Chile, 8900000 Santiago, Chile*
[3]*Dirección de Investigación, Universidad Científica del Sur, Lima, Peru*

Correspondence should be addressed to Rodrigo Iturriaga; riturriaga@bio.puc.cl

Received 12 August 2015; Revised 22 September 2015; Accepted 27 September 2015

Academic Editor: Hanjun Wang

Oxidative stress is involved in the development of carotid body (CB) chemosensory potentiation and systemic hypertension induced by chronic intermittent hypoxia (CIH), the main feature of obstructive sleep apnea. We tested whether peroxynitrite ($ONOO^-$), a highly reactive nitrogen species, is involved in the enhanced CB oxygen chemosensitivity and the hypertension during CIH. Accordingly, we studied effects of Ebselen, an $ONOO^-$ scavenger, on 3-nitrotyrosine immunoreactivity (3-NT-ir) in the CB, the CB chemosensory discharge, and arterial blood pressure (BP) in rats exposed to CIH. Male Sprague-Dawley rats were exposed to CIH (5% O_2, 12 times/h, 8 h/day) for 7 days. Ebselen (10 mg/kg/day) was administrated using osmotic minipumps and BP measured with radiotelemetry. Compared to the sham animals, CIH-treated rats showed increased 3-NT-ir within the CB, enhanced CB chemosensory responses to hypoxia, increased BP response to acute hypoxia, and hypertension. Rats treated with Ebselen and exposed to CIH displayed a significant reduction in 3-NT-ir levels (60.8 ± 14.9 versus 22.9 ± 4.2 a.u.), reduced CB chemosensory response to 5% O_2 (266.5 ± 13.4 versus 168.6 ± 16.8 Hz), and decreased mean BP (116.9 ± 13.2 versus 82.1 ± 5.1 mmHg). Our results suggest that CIH-induced CB chemosensory potentiation and hypertension are critically dependent on $ONOO^-$ formation.

1. Introduction

The obstructive sleep apnea (OSA) syndrome, a worldwide sleep-breathing disorder, is recognized as an independent risk factor for hypertension [1–3]. OSA is characterized by repeated episodes of complete or partial obstruction of the upper airway during sleep, resulting in chronic intermittent hypoxic and hypercapnic events. Among the disturbances produced by OSA, chronic intermittent hypoxia (CIH) is considered the main factor for the development of systemic hypertension [1–4]. Although the link between OSA and hypertension is well known, the mechanisms responsible for the hypertension are not entirely understood. OSA elicits oxidative stress, inflammation, and sympathoexcitation, which contribute to the endothelial dysfunction and hypertension [1, 2, 5–8]. Recently, it has been proposed that the carotid body (CB), the main O_2 chemoreceptor, plays a pivotal role in the development of the enhanced sympathetic activity and the generation of the hypertension following CIH [1, 2, 7, 8]. Indeed, CIH selectively enhanced CB chemosensory discharges during normoxia and hypoxia [8–12], which in turn led to a sustained potentiation of the sympathetic discharges to blood vessels, eliciting neurogenic hypertension [1, 2, 7, 12–14]. The repetitive episodes of hypoxia-reoxygenation during CIH produce oxidative stress due to the accumulation of reactive oxygen species (ROS) [1–7]. The evidence indicates that the CB chemosensory potentiation induced by CIH is mediated by oxidative stress, which increases the levels of CB

excitatory modulators such as angiotensin II and endothelin-1, and reduces the bioavailability of the inhibitory chemosensory modulator nitric oxide (NO) in the CB [15, 16]. Peng et al. [8] proposed that the superoxide radical (O_2^-) participates in the potentiation of the rat CB chemosensory responses to hypoxia since they found that pretreatment of rats for 10 days before and concomitant with the exposure to CIH with manganese (III) tetrakis (1-methyl-4-pyridyl) porphyrin pentachloride (MnTMPyP), a superoxide dismutase (SOD) mimetic, prevented the CB chemosensory potentiation. We tested the hypothesis that oxidative stress contributes to the CB chemosensory potentiation and the progression of the hypertension in rats exposed to CIH [9]. We found that ascorbic acid treatment prevented systemic and local CB oxidative stress, the potentiation of CB chemosensory responses to hypoxia, and the hypertension in rats exposed to CIH for 21 days [9]. Although these results suggest that CB chemosensory potentiation is mediated by oxidative stress, it is matter of debate whether superoxide *per se* may increase the CB chemosensory discharges [17]. Thus, it is plausible that molecules downstream ROS formation may mediate the effects of oxidative stress on CB chemoreception. It is well known that O_2^- radical reacts with NO to produce peroxynitrite ($ONOO^-$), which can nitrate several proteins residues. Indeed, we have previously shown that CIH increases 3-nitrotyrosine immunoreactivity (3-NT-ir) levels in the CB and that changes in 3-NT-ir correlate with the enhanced CB chemosensory responses to hypoxia following CIH [18]. Accordingly, it is plausible that nitrooxidative stress, through an $ONOO^-$ dependent pathway, may play a role in OSA pathophysiology. Thus, we studied if $ONOO^-$ is involved in the enhanced CB chemosensitivity and the generation and maintenance of the hypertension induced by CIH. Therefore, we tested the effects of Ebselen treatment, a potent $ONOO^-$ scavenger [19–21], on 3-NT-ir accumulation in the CBs, CB chemosensory responses to hypoxia, and arterial blood pressure (BP) in conscious rats exposed to CIH, a well stablished experimental model of OSA [7, 9, 15, 18].

2. Material and Methods

2.1. Animals and Intermittent Hypoxia Protocol. Experiments were performed on adult male Sprague-Dawley rats weighting 200 g fed with standard diet ad libitum and kept on a 12:12-hour light dark cycle. Room temperature was maintained between 23 and 25°C. All the experimental procedures were approved by the Bioethical Committee of the Biological Sciences Faculty, Pontificia Universidad Católica de Chile, Santiago, Chile, and were performed according to the National Institutes of Health Guide (NIH, USA) for the care and use of animals. Unrestrained, freely moving rats were housed in individual chambers (12 cm × 35 cm, 3 L) and exposed to hypoxic cycles of 5% inspired O_2 for 20 s, followed by 280 s of room air, 12 times per hour during 8 hours a day, or exposed to sham air-air cycles, emulating the same conditions of noise, temperature, and flow [7, 9, 10]. Rats were exposed to CIH from 8:00 AM to 16:00 PM. The O_2 level inside the chambers was continuously monitored with an oxygen analyzer (Ohmeda 5120, BOC Healthcare, Manchester, UK) and the CO_2 levels and humidity were maintained at low levels by continuous air extraction.

2.2. Carotid Body Chemosensory Recording. The CB chemosensory discharges were measured *in situ* as previously described [9, 10, 12]. Rats were anesthetized with sodium pentobarbitone (40 mg/kg) and additional doses were given to the animal when necessary to maintain a level of surgical anesthesia. Rats were placed on supine position and the body temperature was maintained at 38 ± 0.5°C with a heating pad. The trachea was cannulated for gases administration. One carotid sinus nerve was dissected and placed on a pair of platinum electrodes and covered with mineral oil. The neural signal was preamplified (Grass P511, Grass Instruments, Quincy, MA, USA), filtered (30 Hz–1 kHz), and fed to an electronic spike-amplitude discriminator, allowing the selection of action potentials of particular amplitude above the noise to be counted with a frequency meter, thus being able to measure the frequency of carotid chemosensory discharges (f_x) expressed in Hz. The carotid sinus electroneurogram was continuously monitored using an oscilloscope. Baroreceptor activity, which consisted of repetitive and rhythmic discharges synchronized with the systolic arterial blood pressure, was eliminated by crushing the baroreceptor fibers between the carotid bifurcation and the CB. This procedure resulted in the complete elimination of discharge synchronized with arterial blood pressure. 100% O_2 (Dejours test) was used to confirm that all the neural activities recorded correspond to chemosensory discharge [9, 12]. The contralateral carotid sinus nerve was cut to prevent vascular and ventilatory reflexes evoked by hypoxic activation. The CB chemosensory frequency of discharge (f_x) was measured in response to several levels of inspired PO_2 (~5–670 mmHg, applied for 20–30 s), by averaging the maximal values during the semiplateau of the chemosensory response. Thus, f_x is the absolute value of chemosensory rate of discharge. The O_2 levels were measured with an oxygen analyzer (Ohmeda 5120, BOC Healthcare, Manchester, UK).

2.3. Arterial Blood Pressure Telemetry. In a subset of rats, arterial blood pressure (BP) was recorded using radiotelemetry. Briefly, rats were anesthetized with 5% isoflurane and maintained with 1-2% isoflurane in 100% O_2 during the surgical procedure. An abdominal incision was performed to isolate the abdominal aorta. The tip of a cannula-coupled telemetry device (Telemetry Research TRM54P, Millar USA) was inserted into the abdominal aorta and fixed with methacrylate. After this procedure, the abdominal incision was sutured in layers. At the end of the surgery, rats received an i.p. injection of enrofloxacin (1%) and ketoprofen (1%) and were supplied during 3 subsequent days with the same dose of enrofloxacin in the drinking tap water. Physiological variables were acquired with an analogue-digital system (PowerLAB 8SP, ADInstruments, Australia) and analyzed with the Chart 7.2-Pro software. BP was measured after one week of recovery. For quantification of the baseline BP during normoxia, we averaged 10 minutes of BP signal, recorded 30 minutes before the beginning of the CIH protocol. To quantify ΔBP response

evoked by acute 5% O_2, we measured the difference between the maximal BP averaged for 5 s and the baseline BP values averaged for 1 min before the acute hypoxic challenge.

2.4. Experimental Procedure and Ebselen Administration. The peroxynitrite targeted antioxidant Ebselen (Enzo Life Sci, Inc., Farmingdale, NY, USA) was administrated with osmotic minipumps (2ML4, Alzet Scientific Products, Chevy Chase, MD, USA). Rats were anesthetized with isoflurane in 100% O_2, and osmotic minipumps were implanted subcutaneously on the back. Pumps were filled with 33.3 mg Ebselen in 1 mL of 80% DMSO in saline, to achieve a delivering rate of 10 mg/kg/day, a similar dose used in other studies [22, 23]. Control animals were implanted with osmotic minipumps filled with DMSO 80% in saline solution. After surgical procedures, the rats were treated with enrofloxacin and ketoprofen as mentioned before. Due to the nature of the experiments related to the study of CB chemosensory activity, a cross-sectional study was performed. Twenty-four rats were randomly divided into 3 groups: one control group, exposed to sham conditions and treated with Ebselen (Ebselen-Sham); a second group, exposed to CIH and treated with vehicle (Vehicle-CIH); and a third group, exposed to CIH and treated with Ebselen during the hypoxic protocol (Ebselen CIH). To study the therapeutic effect of Ebselen on the CIH-induced hypertension, we performed a longitudinal study. Rats with indwelling catheter from telemetry devices were exposed first to sham conditions for 7 days and then to CIH for other 7 days. At the end of the CIH 7-day exposure, an osmotic minipump filled with Ebselen was subcutaneously implanted and the rats were kept another week in CIH.

2.5. Nitrotyrosine Immunohistochemistry. At the end of the CB chemosensory studies, anesthetized rats were perfused intracardially with saline at pH 7.4 for 15 min followed by buffered 4% paraformaldehyde (PFA, Sigma, St. Louis, MO, USA). The carotid bifurcations were dissected and postfixed in the same fixative solution for 12 h to 4°C. Then, the samples were dehydrated in ethanol, included in paraffin, cut in 5 μm sections, and mounted on silanized slides. Samples were deparaffinized and exposed to antigen-retrieval solution (citrate buffer 1 M, pH 6.0) as previously described [9, 18]. Samples were then incubated in 0.3% H_2O_2 solution and blocked using normal horse serum (ABC, Vectastain kit, Vector) for 1 hour. The samples were then incubated with primary antibody against 3-NT (1 : 500, number A21285, Molecular Probes) overnight at 4°C. The immunoreactivity staining was detected using a streptavidin-peroxidase kit (ABC, Vectastain kit, Vector) and revealed at 37°C in dark chamber with 3,3′-diaminobenzidine tetrahydrochloride (DAB, Sigma). Samples were counterstained with Harris haematoxylin and mounted with Entellan (Merck, Whitehouse station, NJ, USA). Photomicrographs were taken at 100x using a CCD camera coupled to an Olympus CX 31 microscope (Olympus Corp., USA), digitized, and analyzed using ImageJ software (NIH, Betheseda, MD, USA). We measure two nonconsecutive CB sections per rat, obtaining four CB photographs from each one of those sections. The positive 3-NT-ir, averaged from the eight CB fields, was expressed as optical integrated intensity, in arbitrary units.

Table 1: Systolic, diastolic, and pulse pressure measured in normoxia in the same rats exposed to sham, CIH, or Ebselen CIH condition.

	Sham	CIH	Ebselen CIH
P_s (mmHg)	109.7 ± 2.7	138.0 ± 12.6*	110.0 ± 3.5
P_d (mmHg)	79.1 ± 2.7	106.4 ± 13.5*	71.2 ± 4.9
P_p (mmHg)	30.6 ± 1.4	31.7 ± 2.0	32.9 ± 3.0

P_s, systolic, P_d, diastolic, and P_p pulse arterial pressure ($P_s - P_d$). * $p < 0.05$, CIH versus sham and Ebselen CIH and Newman-Keuls after Repeated Measures ANOVA, $n = 4$ rats.

Table 2: Arterial blood pressure responses to 5% O_2 measured during normoxia in the same rats exposed to sham, CIH, or Ebselen CIH condition.

	Sham	CIH	Ebselen CIH
ΔP_s (mmHg)	14.6 ± 3.5	45.5 ± 4.6*	14.4 ± 5.7
ΔP_d (mmHg)	4.7 ± 4.3	19.7 ± 4.3	3.6 ± 3.5
ΔP_p (mmHg)	9.9 ± 1.9	17.2 ± 10.3	10.8 ± 4.2

ΔP_s, max-baseline systolic arterial pressure, ΔP_d, max-baseline diastolic arterial pressure, and ΔP_p, max-baseline pulse arterial pressure. * $p < 0.05$, CIH versus sham and Ebselen CIH and Newman-Keuls after Repeated Measures ANOVA, $n = 4$ rats.

2.6. Statistical Data Analysis. Data was expressed as mean ± SEM. For cross-sectional studies (Figures 1 and 2), statistical analysis was performed using one-way or two-way ANOVA tests followed by Bonferroni *post hoc* analysis. For longitudinal studies (Figures 3 and 4 and Tables 1 and 2), Repeated Measures one-way ANOVA followed by Newman-Keuls *post hoc* comparisons was used. $P < 0.05$ was set as the level of statistical significance for both studies.

3. Results

3.1. Effects of Ebselen on the CIH-Induced Increase of 3-NT-ir in the CB. The exposure to CIH for 7 days produced a marked increase in the 3-NT-ir levels in the CB (Figure 1(a)). Indeed, we found a 2.5-fold increase in 3-NT-ir in the CB from CIH-treated rats compared to the levels observed in sham rats. The administration of the peroxynitrite scavenger Ebselen to the rats during the CIH exposure prevented the CIH-induced increase of 3-NT-ir in the CB (Figure 1(b)). Figure 1(b) shows the quantification of the effects of Ebselen on the 3-NT-ir accumulation induced by CIH. Rats exposed to CIH and treated with Ebselen showed 60% of reduction in 3-NT-ir as compared with the CIH rats treated with vehicle (60.8 ± 14.9 versus 22.9 ± 4.2 a.u., $P < 0.05$, and CIH and CIH Ebselen rats, resp.).

3.2. Ebselen Prevented CB Chemosensory Potentiation Induced by CIH. To assess the effect of Ebselen on CB chemosensory activity, we measured the frequency of chemosensory discharge (f_x), from the carotid sinus nerve from rats exposed to CIH and treated with Ebselen (Figure 2). The exposure to

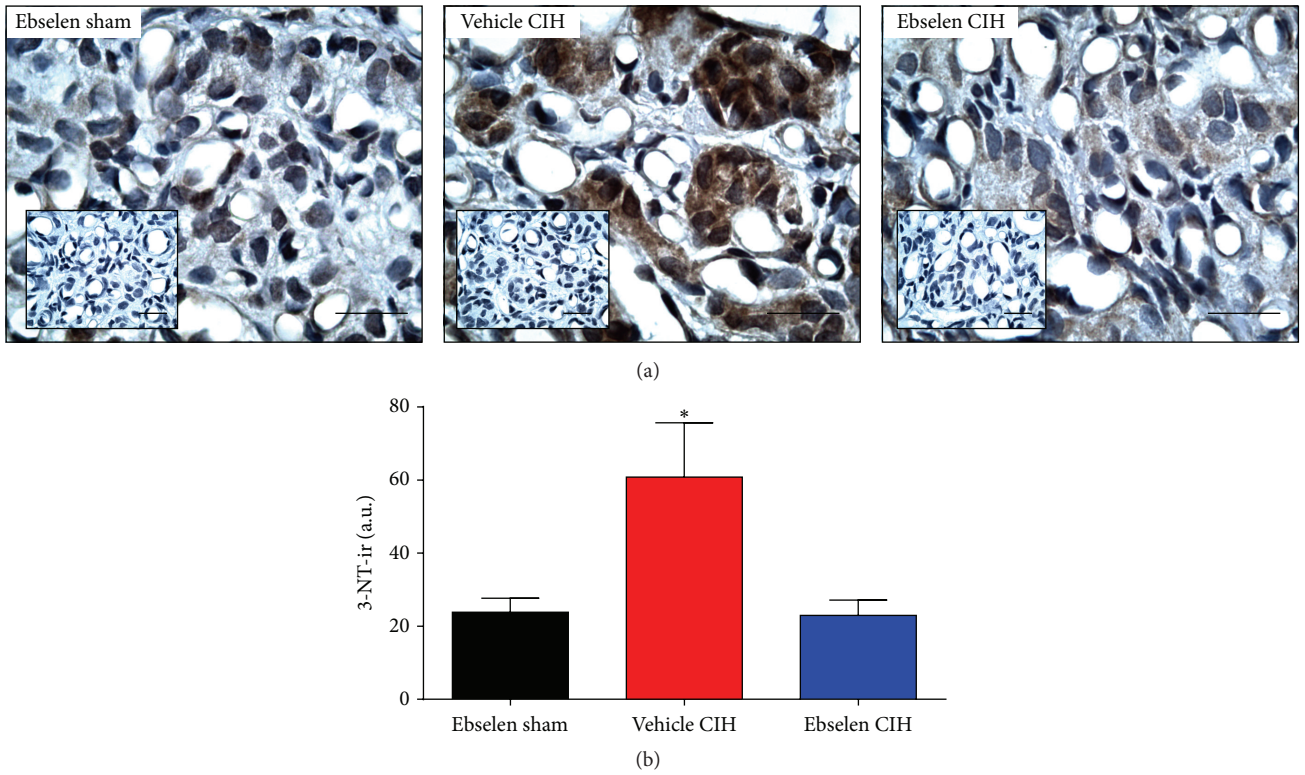

Figure 1: Ebselen treatment prevented the increased levels of 3-NT-ir. (a) Representative effects of Ebselen on positive 3-NT immunoreactivity (3-NT-ir) in CBs from rats exposed to CIH. Inset, negative controls omitted inclusion of primary antibody. Scale bars 20 μm. (b) Summary of the effects of Ebselen on 3-NT-ir measured in CBs. $^*P < 0.05$, vehicle CIH versus Ebselen sham and Ebselen CIH, and Bonferroni after one-way ANOVA, $n = 5$ rats per group.

CIH for 7 days increases the baseline CB chemosensory and the discharge evoked by hypoxia. Indeed, Ebselen treatment prevented the potentiation of the hypoxic CB chemosensory response in CIH rats (Figure 2). The two-way ANOVA analysis showed a significant increase of CB chemosensory discharge for different levels of inspired PO_2 in rats exposed to CIH ($P < 0.01$). The treatment with Ebselen during CIH exposure effectively prevented the CB increased responses to several levels of hypoxia (Figure 2(b)).

3.3. Effects of Ebselen on the CIH-Induced Hypertension. Exposure to 7 days of CIH produced a significant increase in baseline BP measured in normoxia (Figure 3). We found that, after one week of CIH exposure, the mean arterial blood pressure (MABP) increased about 25 mmHg compared to the value measured during sham condition (89.3 ± 2.5 mmHg versus 116.9 ± 13.2 mmHg, $P < 0.05$ sham versus CIH, resp.). Remarkably, Ebselen treatment normalized MABP during CIH to similar levels to those observed during sham conditions (82.1 ± 5.1 mmHg, Figure 3). The values for baseline systolic (P_s), diastolic (P_d), and pulse pressure (P_p) are summarized in Table 1. We did not find significant differences in resting heart rate (HR) between animals exposed to sham, CIH, and Ebselen CIH conditions (sham 321.9 ± 15.5, CIH 383.6 ± 20.3, and CIH Ebselen 351.8 ± 36.3 beats per minute, Figure 3(c), $P > 0.05$, one-way ANOVA). In a separate experimental series, we measured MABP and HR in 3 sham rats after one week of the implantation of osmotic pumps containing the vehicle (DMSO 80%). We did not find any differences (MABP 97.4 ± 3.9 mmHg, HR 333.1 ± 5.3 beats per minute) related to the values recorded in rats implanted with pumps containing Ebselen in DMSO in sham conditions for one week.

In addition, we measured the BP response evoked by acute hypoxia (Figure 4). Acute hypoxic episodes (5% O_2) in sham rats produced a mild increase in BP (ΔMABP = 8.0 ± 3.9 mmHg). In contrast, after one week of CIH exposure, the BP response to the same level of hypoxia was largely increased (ΔMABP = 28.1 ± 4.1 mmHg). Ebselen treatment during CIH exposure normalized BP responses to hypoxia (ΔMABP = 7.2. ± 3.9 mmHg). The mean values for ΔP_s, ΔP_d, and ΔP_p during acute hypoxic stimulus are shown in Table 2. Therefore, treatment with Ebselen effectively restores the normal arterial pressure response to hypoxia, even in the presence of CIH. The increases in BP following acute hypoxic stimulation produced a reflex bradycardia in all three conditions (sham, CIH, and Ebselen CIH). The ΔHR response to hypoxia did not reach statistical significance between the treatments ($P > 0.05$, Sham = 21.8±28.8, CIH = 90.8±54.5, and Ebselen CIH = 60.8 ± 64.8 beats per minute, Figure 4(c), $P < 0.05$, one-way ANOVA).

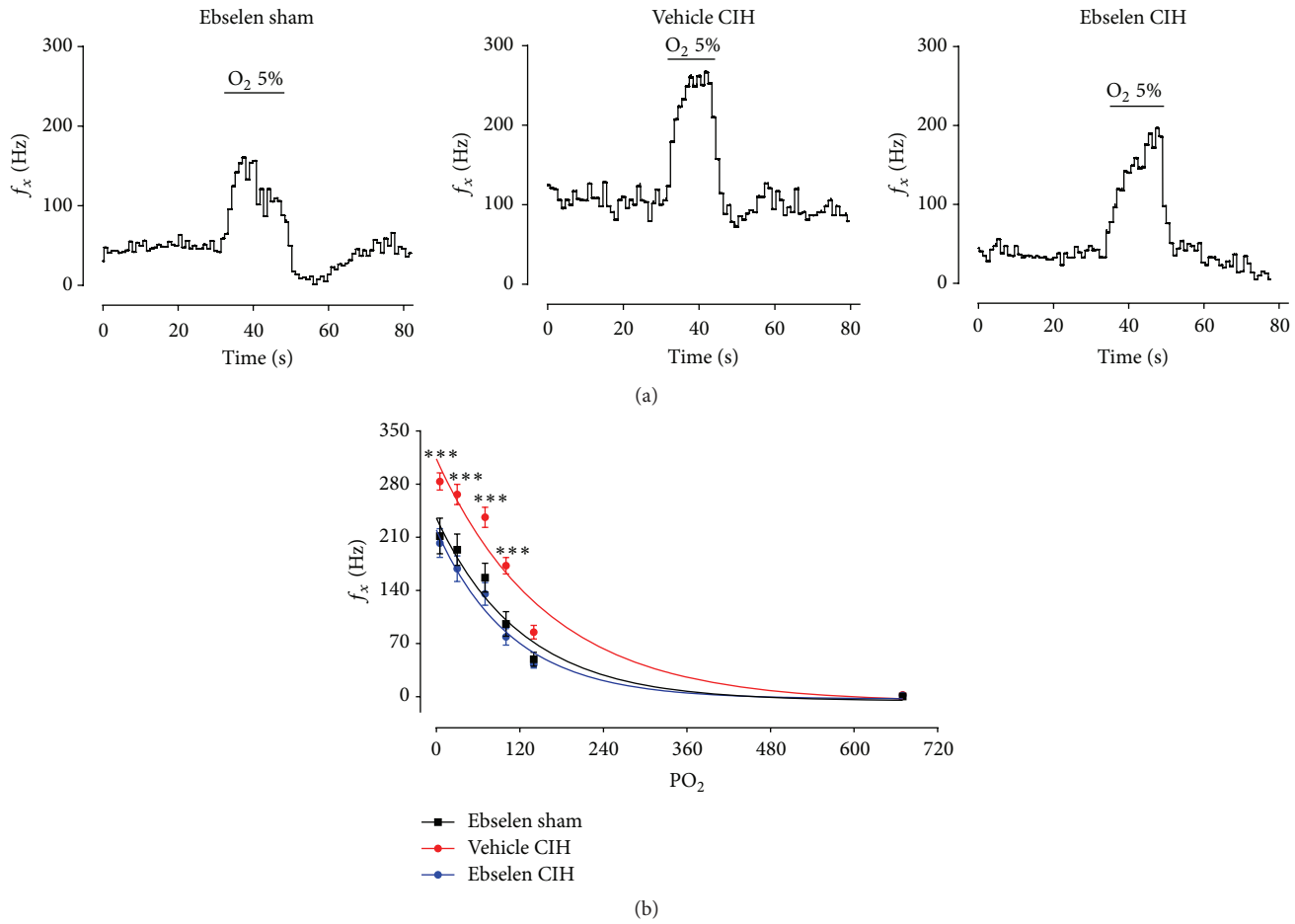

Figure 2: Ebselen treatment prevented the CB chemosensory potentiation in rats exposed to CIH. (a) Recordings of the CB frequency of chemosensory discharge (f_x) measured from the carotid sinus nerve in response to acute hypoxia (5% O_2) in rats treated with Ebselen or vehicle and exposed to sham or CIH conditions. The enhanced CB chemosensory response induced by CIH (vehicle CIH) was prevented by Ebselen (Ebselen CIH). (b) Summary of the effect of the Ebselen treatment at different levels of inspired PO_2 (mmHg) on f_x. $^{***}P < 0.001$, vehicle CIH versus Ebselen sham and Ebselen CIH, and Bonferroni after two-way ANOVA, $n = 8$ rats per group.

4. Discussion

Present results show that Ebselen prevented the accumulation of 3-NT-ir in the CB and the enhanced CB chemosensory discharges induced by CIH. Indeed, Ebselen reduced the baseline chemosensory discharge and the responses to hypoxia (Figure 2), confirming observations showing that antioxidant treatment prevents the potentiation of the rat CB chemosensory response to hypoxia induced by CIH [8, 9]. Furthermore, we found that administration of Ebselen, once rats already developed hypertension induced by CIH exposure, was able to normalize baseline BP in normoxia and the BP response to acute hypoxia. Our results suggest that increases in $ONOO^-$ in the CB contribute to the CB chemosensory potentiation induced by CIH. In addition, CIH-induced systemic hypertension is critically dependent on $ONOO^-$ since Ebselen treatment reduces BP to values similar to the ones measured in normotensive animals. Thus, it is plausible that the primary action of Ebselen reduced the exacerbation of CB chemosensory output and the sympathetic induced hypertension, but we cannot exclude other effects on the hypoxic chemoreflex pathway. To our knowledge, this is the first study that shows that an $ONOO^-$ scavenger was effective to prevent the CB chemosensory potentiation and reverses the hypertension induced by CIH.

A growing body of evidence supports the proposal that the CB contributes to the autonomic dysfunction and hypertension in OSA patients and animals exposed to CIH. Indeed, patients with recently diagnosed OSA show enhanced ventilatory, pressor, and sympathetic responses to acute hypoxia, attributed to a potentiation of the CB chemoreflexes [1, 2, 7]. Indeed, Narkiewicz et al. [13] found potentiated reflex ventilatory, tachycardic, and pressor responses to acute hypoxia in untreated normotensive patients with OSA. On the contrary, the ventilatory and pressor responses induced by hypercapnia and by the cold pressor test in OSA patients were not different from those observed in control subjects. Similarly, animals exposed to CIH show enhanced hypoxic ventilatory responses to acute hypoxia [7] for review and long-term facilitation of respiratory motor responses [8, 11]. Recording

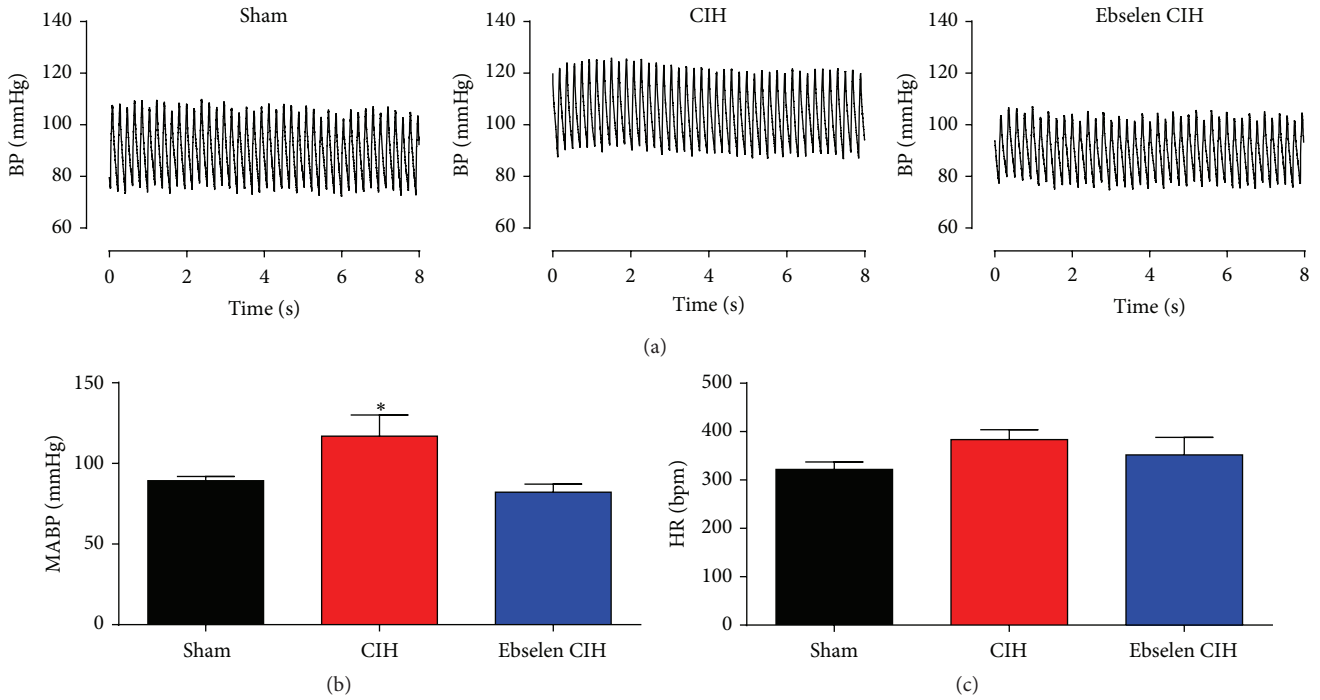

Figure 3: Ebselen reversed the increased arterial blood pressure measured during normoxia in CIH rats. Telemetric recording realized in the same rat during control condition ((a), sham), after 7 days of CIH ((a), CIH) and the effect of Ebselen after additional 7 days of CIH ((a), Ebselen CIH). Summary of the effect of Ebselen on mean arterial blood pressure (MABP, (b)) and heart rate (HR, (c)). $^{*}P < 0.05$, CIH versus sham and Ebselen CIH, and Newman-Keuls after Repeated Measures ANOVA, $n = 4$ rats.

of chemosensory discharges from the carotid sinus nerve has confirmed the idea that CIH produces facilitation of the CB chemosensory responses to hypoxia. Indeed, exposure of rats and cats to CIH for few days increases the baseline CB discharges measured in normoxia and enhances the chemosensory responses to acute hypoxia [8–12]. Peng et al. [8] reported that baseline CB discharge and chemosensory responses to acute hypoxia were higher in rats exposed to short cyclic hypoxic episodes followed by normoxia, applied during 8 hours for 10 days. Similarly, we found that cats and rats exposed to CIH for 7 days showed enhanced CB chemosensory and ventilatory responses to acute hypoxia [8, 12]. Studies performed in OSA patients and animals exposed to CIH show that OSA is associated with sympathoexcitation, mainly attributed to the enhance CB chemosensory function elicited by CIH [1, 2, 7].

Several studies have proposed that ROS are involved in the progression of the cardiovascular pathologies in patients suffering OSA and animals exposed to CIH [2, 3, 5, 7, 24]. Indeed the O_2^- radical has been proposed as the main ROS responsible for these pathological consequences, since treatment with SOD mimetic prevented the hypertension induced by CIH in rats [8, 24]. It is well known that O_2^- reacts with nitric oxide (NO) producing $ONOO^-$ with an elevated constant rate of $\sim 7 \cdot 10^9$/M s [25]. Interestingly, this rate is 3.5 times higher than its enzymatic dismutation by SOD [26]. This fast reaction explains how these particularly elusive species could rapidly react to form $ONOO^-$ [27], reducing the NO bioavailability [28, 29]. Accordingly, we previously found a reduction in the NO production in the rat CB after 7 days of CIH [30]. Since NO is considered an inhibitory modulator of CB chemosensory discharges [31], a reduced NO level may partially contribute to enhancing the baseline CB discharges and chemosensory responses to hypoxia. This interpretation agrees with the observation of Marcus et al. [32], who found that CIH decreased the expression of the nNOS in the rat CB, suggesting that the removal of the normal inhibitory NO influence contributes to enhancing the CB chemosensory responses to hypoxia.

There is evidence suggesting that $ONOO^-$ radical is involved in the development of diseases such as type I diabetes, cancer, stroke, heart failure, and neurodegenerative disorders [33, 34]. The $ONOO^-$ radical is highly unstable and produces deleterious reactions and cytotoxic effects, such as oxidation of several molecular targets like lipids, proteins, and DNA [35–37]. One of the main consequences of increased levels of $ONOO^-$ is the modification of tyrosine residues in proteins producing 3-NT [27], which has been related with many diseases and cellular damage including liver disease [38], chronic allograft nephropathy [39], and Alzheimer's and Parkinson's disease [40]. We found an increase of 3-NT-ir accumulation in the CB from rats exposed for 7 to 21 days to CIH, suggesting that $ONOO^-$ formation due to the reaction of NO with O_2^- is a critical step in the CB chemosensory potentiation induced by CIH [9, 18]. Present results agree with and extend the idea that $ONOO^-$ radical contributes to

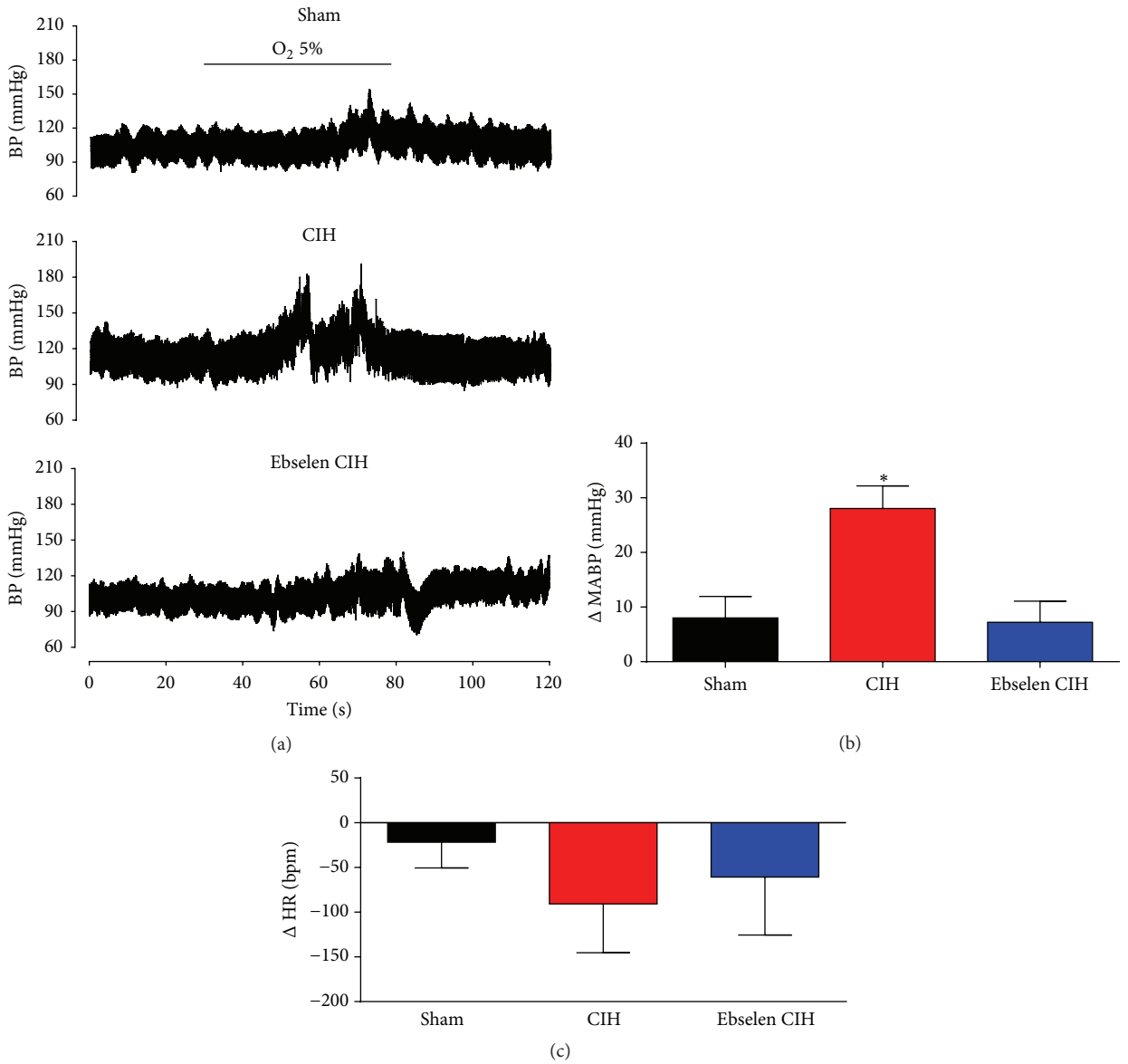

Figure 4: Ebselen reversed the CIH-induced increase in BP responses evoked by an acute hypoxic stimulus. Telemetry recordings realized in the same rat show the pressure response evoked by hypoxia (5% O_2 for 50 s), during sham conditions, after 7 days of CIH, and after additional 7 days of CIH but supplemented with Ebselen (a). Summary of the effect of Ebselen on mean arterial blood pressure (MABP, (b)) and heart rate (HR, (c)). $^*P < 0.05$, CIH versus sham and Ebselen CIH, and Newman-Keuls after Repeated Measures ANOVA, $n = 4$ rats.

the CB enhanced responses to hypoxia after CIH. Ebselen is an organoselenium compound that mimics glutathione peroxidase activity [19–21], which rapidly reacts with $ONOO^-$ [19]. The generation of 3-NT is a direct result of the $ONOO^-$ generation, and the treatment with Ebselen prevented the CIH-induced increase of 3-NT-ir levels in the CB and the chemosensory potentiation of the CB after CIH, suggesting that protein nitration may play a role in enhancing the chemoreceptor responses to acute hypoxia.

To study plausible therapeutic effects of Ebselen in an experimental model of OSA, we decide to administrate Ebselen after the development of hypertension in rats exposed to CIH. We found that Ebselen treatment effectively normalized resting BP in awake rats, even in the presence of the intermittent hypoxic stimulus (Figure 3). In addition, Ebselen abolished the potentiated BP response to acute hypoxic stimulation observed during CIH exposure (Figure 4). Taken together, Ebselen administration should be considered as a novel tool to restore normal BP adjustments following CIH. In contrast, we did not find any significant difference between the HR in response to acute hypoxia between the treatments (Figure 4). Acute hypoxia in conscious rats generates a biphasic HR response, characterized by an initial tachycardia during mild hypoxia, but bradycardia when inspired fraction of O_2 decrease below 8% [41]. Then, chronic exposure to intermittent hypoxia may affect both the tachycardic and

bradycardic responses to acute hypoxia. Future studies are needed to elucidate these questions.

5. Limitations of the Study

Our results suggest that Ebselen prevents the nitration of proteins in the CB, which contributes to normalizing the CB frequency of discharge and the sympathetic-mediated hypertension. Administration of Ebselen was achieved using subcutaneous osmotic minipumps; therefore, the treatment is delivered systemically. Thus, it is possible that Ebselen may act not only in the CB, but also in other parts of the chemosensory pathway (i.e., nucleus of the tractus solitary, rostral ventrolateral medulla), since Ebselen can cross the blood brain barrier [42]. Rats exposed to CIH show increased plasma renin activity [43], and it is known that Losartan treatment prevents the CIH-induced hypertension [43], the increased sympathetic activity induced by apnea episodes [32], and the decrease in arterial vasodilation induced by acetylcholine after 28 days of CIH [44]. Moreover, intracerebroventricular injection of Losartan prevents the hypertension induced by CIH and the neuronal activation in areas related to sympathetic activation [45]. Thus, we cannot exclude effects of Ebselen at the central nervous system, sympathetic peripheral system, or arterial vessels, which may all be involved in the antihypertensive effect of Ebselen.

6. Conclusion

Present results suggest that 3-NT accumulation contributes to the CB chemosensory potentiation through the nitration of protein residues, which in turn promotes hypertension. Ebselen treatment prevents the increased CB chemosensory activity and reverses the hypertension in rats exposed to CIH, suggesting that the CB chemosensory potentiation plays a key role in the generation and maintenance of the hypertension induced by CIH. Further development of $ONOO^-$ targeted scavengers should be of therapeutic interest in the treatment of hypertension in OSA patients.

Conflict of Interests

The authors declare that there is no conflict of interests regarding the publication of this paper.

Authors' Contribution

Esteban A. Moya, Paulina Arias, Carlos Varela, and María P. Oyarce participated in the experimental studies. Esteban A. Moya and Rodrigo Iturriaga analyzed the data and Esteban A. Moya, Rodrigo Del Rio, and Rodrigo Iturriaga wrote the paper.

Acknowledgments

This work was supported by Grants FONDECYT 1100405 and 1150040. The authors would like sincerely to thank Dr. Julio Alcayaga for his generous assistance with the design and support necessary to develop the system of intermittent hypoxia used in this study.

References

[1] V. K. Somers, D. P. White, R. Amin et al., "Sleep apnea and cardiovascular disease an American Heart Association/American College of cardiology foundation scientific statement from the American Heart Association Council for High Blood Pressure Research Professional Education Committee, Council on Clinical Cardiology, Stroke Council, and Council on Cardiovascular Nursing. In collaboration with the National Heart, Lung, and Blood Institute National Center on Sleep Disorders Research (National Institutes of Health)," *Circulation*, vol. 118, no. 10, pp. 1080–1110, 2008.

[2] J. A. Dempsey, S. C. Veasey, B. J. Morgan, and C. P. O'Donnell, "Pathophysiology of sleep apnea," *Physiological Reviews*, vol. 90, no. 1, pp. 47–112, 2010.

[3] D. Gozal and L. Kheirandish-Gozal, "Cardiovascular morbidity in obstructive sleep apnea," *American Journal of Respiratory and Critical Care Medicine*, vol. 177, no. 4, pp. 369–375, 2008.

[4] T. Young, M. Palta, J. Dempsey, J. Skatrud, S. Weber, and S. Badr, "The occurrence of sleep-disordered breathing among middle-aged adults," *The New England Journal of Medicine*, vol. 328, no. 17, pp. 1230–1235, 1993.

[5] L. Lavie, "Obstructive sleep apnoea syndrome—an oxidative stress disorder," *Sleep Medicine Reviews*, vol. 7, no. 1, pp. 35–51, 2003.

[6] J. F. Garvey, C. T. Taylor, and W. T. McNicholas, "Cardiovascular disease in obstructive sleep apnoea syndrome: the role of intermittent hypoxia and inflammation," *European Respiratory Journal*, vol. 33, no. 5, pp. 1195–1205, 2009.

[7] R. Iturriaga, E. A. Moya, and R. Del Rio, "Carotid body potentiation induced by intermittent hypoxia: implications for cardiorespiratory changes induced by sleep apnoea," *Clinical and Experimental Pharmacology and Physiology*, vol. 36, no. 12, pp. 1197–1204, 2009.

[8] Y.-J. Peng, J. L. Overholt, D. Kline, G. K. Kumar, and N. R. Prabhakar, "Induction of sensory long-term facilitation in the carotid body by intermittent hypoxia: implications for recurrent apneas," *Proceedings of the National Academy of Sciences of the United States of America*, vol. 100, no. 17, pp. 10073–10078, 2003.

[9] R. Del Rio, E. A. Moya, and R. Iturriaga, "Carotid body and cardiorespiratory alterations in intermittent hypoxia: the oxidative link," *European Respiratory Journal*, vol. 36, no. 1, pp. 143–150, 2010.

[10] R. Del Rio, E. A. Moya, M. J. Parga, C. Madrid, and R. Iturriaga, "Carotid body inflammation and cardiorespiratory alterations in intermittent hypoxia," *European Respiratory Journal*, vol. 39, no. 6, pp. 1492–1500, 2012.

[11] Y.-J. Peng and N. R. Prabhakar, "Effect of two paradigms of chronic intermittent hypoxia on carotid body sensory activity," *Journal of Applied Physiology*, vol. 96, no. 3, pp. 1236–1242, 2004.

[12] S. Rey, R. Del Rio, J. Alcayaga, and R. Iturriaga, "Chronic intermittent hypoxia enhances cat chemosensory and ventilatory responses to hypoxia," *The Journal of Physiology*, vol. 560, no. 2, pp. 577–586, 2004.

[13] K. Narkiewicz, P. J. H. van de Borne, C. A. Pesek, M. E. Dyken, N. Montano, and V. K. Somers, "Selective potentiation of peripheral chemoreflex sensitivity in obstructive sleep apnea," *Circulation*, vol. 99, no. 9, pp. 1183–1189, 1999.

[14] S. Rey, M. P. Tarvainen, P. A. Karjalainen, and R. Iturriaga, "Dynamic time-varying analysis of heart rate and blood pressure variability in cats exposed to short-term chronic intermittent hypoxia," *American Journal of Physiology—Regulatory, Integrative and Comparative Physiology*, vol. 295, no. 1, pp. R28–R37, 2008.

[15] R. Iturriaga, D. C. Andrade, and R. Del Rio, "Enhanced carotid body chemosensory activity and the cardiovascular alterations induced by intermittent hypoxia," *Frontiers in Physiology*, vol. 5, article 468, 2015.

[16] R. Iturriaga, E. A. Moya, and R. Del Rio, "Inflammation and oxidative stress during intermittent hypoxia: the impact on chemoreception," *Experimental Physiology*, vol. 100, no. 2, pp. 149–155, 2015.

[17] C. Gonzalez, G. Sanz-Alyayate, M. T. Agapito, and A. Obeso, "Effects of reducing agents on glutathione metabolism and the function of carotid body chemoreceptor cells," *Biological Chemistry*, vol. 385, no. 3-4, pp. 265–274, 2004.

[18] R. Del Rio, E. A. Moya, and R. Iturriaga, "Differential expression of pro-inflammatory cytokines, endothelin-1 and nitric oxide synthases in the rat carotid body exposed to intermittent hypoxia," *Brain Research*, vol. 1395, pp. 74–85, 2011.

[19] A. Daiber, M.-H. Zou, M. Bachschmid, and V. Ullrich, "Ebselen as a peroxynitrite scavenger in vitro and ex vivo," *Biochemical Pharmacology*, vol. 59, no. 2, pp. 153–160, 2000.

[20] Y. Nakamura, Q. Feng, T. Kumagai et al., "Ebselen, a glutathione peroxidase mimetic seleno-organic compound, as a multifunctional antioxidant. Implication for inflammation-associated carcinogenesis," *The Journal of Biological Chemistry*, vol. 277, no. 4, pp. 2687–2694, 2002.

[21] G. K. Azad and R. S. Tomar, "Ebselen, a promising antioxidant drug: mechanisms of action and targets of biological pathways," *Molecular Biology Reports*, vol. 41, no. 8, pp. 4865–4879, 2014.

[22] J.-G. Park, J.-Y. Yoo, S.-J. Jeong et al., "Peroxiredoxin 2 deficiency exacerbates atherosclerosis in apolipoprotein E-deficient mice," *Circulation Research*, vol. 109, no. 7, pp. 739–749, 2011.

[23] A. H. Bubolz, Q. Wu, B. T. Larsen, D. D. Gutterman, and Y. Liu, "Ebselen reduces nitration and restores voltage-gated potassium channel function in small coronary arteries of diabetic rats," *American Journal of Physiology: Heart and Circulatory Physiology*, vol. 293, no. 4, pp. H2231–H2237, 2007.

[24] C. M. Troncoso Brindeiro, A. Q. da Silva, K. J. Allahdadi, V. Youngblood, and N. L. Kanagy, "Reactive oxygen species contribute to sleep apnea-induced hypertension in rats," *The American Journal of Physiology—Heart and Circulatory Physiology*, vol. 293, no. 5, pp. H2971–H2976, 2007.

[25] M. Valko, D. Leibfritz, J. Moncol, M. T. D. Cronin, M. Mazur, and J. Telser, "Free radicals and antioxidants in normal physiological functions and human disease," *International Journal of Biochemistry and Cell Biology*, vol. 39, no. 1, pp. 44–84, 2007.

[26] R. A. Dweik, "Nitric oxide, hypoxia, and superoxide: the good, the bad, and the ugly!," *Thorax*, vol. 60, no. 4, pp. 265–267, 2005.

[27] G. Ferrer-Sueta and R. Radi, "Chemical biology of peroxynitrite: kinetics, diffusion, and radicals," *ACS Chemical Biology*, vol. 4, no. 3, pp. 161–177, 2009.

[28] A. G. Estévez and J. Jordán, "Nitric oxide and superoxide, a deadly cocktail," *Annals of the New York Academy of Sciences*, vol. 962, pp. 207–211, 2002.

[29] J. S. Beckman and W. H. Koppenol, "Nitric oxide, superoxide, and peroxynitrite: the good, the bad, and ugly," *The American Journal of Physiology—Cell Physiology*, vol. 271, no. 5, pp. C1424–C1437, 1996.

[30] E. A. Moya, J. Alcayaga, and R. Iturriaga, "NO modulation of carotid body chemoreception in health and disease," *Respiratory Physiology & Neurobiology*, vol. 184, no. 2, pp. 158–164, 2012.

[31] R. Iturriaga, M. Mosqueira, and S. Villanueva, "Effects of nitric oxide gas on cat carotid body chemosensory response to hypoxia," *Brain Research*, vol. 855, no. 2, pp. 282–286, 2000.

[32] N. J. Marcus, Y.-L. Li, C. E. Bird, H. D. Schultz, and B. J. Morgan, "Chronic intermittent hypoxia augments chemoreflex control of sympathetic activity: role of the angiotensin II type 1 receptor," *Respiratory Physiology and Neurobiology*, vol. 171, no. 1, pp. 36–45, 2010.

[33] P. Pacher, J. S. Beckman, and L. Liaudet, "Nitric oxide and peroxynitrite in health and disease," *Physiological Reviews*, vol. 87, no. 1, pp. 315–424, 2007.

[34] C. Szabó, H. Ischiropoulos, and R. Radi, "Peroxynitrite: biochemistry, pathophysiology and development of therapeutics," *Nature Reviews Drug Discovery*, vol. 6, no. 8, pp. 662–680, 2007.

[35] F. Yamakura and H. Kawasaki, "Post-translational modifications of superoxide dismutase," *Biochimica et Biophysica Acta*, vol. 1804, no. 2, pp. 318–325, 2010.

[36] J. T. Hancock, R. Desikan, and S. J. Neill, "Role of reactive oxygen species in cell signalling pathways," *Biochemical Society Transactions*, vol. 29, no. 2, pp. 345–349, 2001.

[37] J. J. Haddad, "Oxygen sensing and oxidant/redox-related pathways," *Biochemical and Biophysical Research Communications*, vol. 316, no. 4, pp. 969–977, 2004.

[38] L. A. MacMillan-Crow, D. L. Cruthirds, K. M. Ahki, P. W. Sanders, and J. A. Thompson, "Mitochondrial tyrosine nitration precedes chronic allograft nephropathy," *Free Radical Biology and Medicine*, vol. 31, no. 12, pp. 1603–1608, 2001.

[39] M. A. Abdelmegeed and B.-J. Song, "Functional roles of protein nitration in acute and chronic liver diseases," *Oxidative Medicine and Cellular Longevity*, vol. 2014, Article ID 149627, 21 pages, 2014.

[40] A. Martínez, M. Portero-Otin, R. Pamplona, and I. Ferrer, "Protein targets of oxidative damage in human neurodegenerative diseases with abnormal protein aggregates," *Brain Pathology*, vol. 20, no. 2, pp. 281–297, 2010.

[41] J. P. Casanova, M. Contreras, E. A. Moya, F. Torrealba, and R. Iturriaga, "Effect of insular cortex inactivation on autonomic and behavioral responses to acute hypoxia in conscious rats," *Behavioural Brain Research*, vol. 253, pp. 60–67, 2013.

[42] N. Singh, A. C. Halliday, J. M. Thomas et al., "A safe lithium mimetic for bipolar disorder," *Nature Communications*, vol. 4, article 1332, 2013.

[43] E. C. Fletcher, G. Bao, and R. Li, "Renin activity and blood pressure in response to chronic episodic hypoxia," *Hypertension*, vol. 34, no. 2, pp. 309–314, 1999.

[44] N. J. Marcus, N. R. Philippi, C. E. Bird, Y.-L. Li, H. D. Schultz, and B. J. Morgan, "Effect of AT 1 receptor blockade on intermittent hypoxia-induced endothelial dysfunction," *Respiratory Physiology and Neurobiology*, vol. 183, no. 2, pp. 67–74, 2012.

[45] W. D. Knight, A. Saxena, B. Shell, T. P. Nedungadi, S. W. Mifflin, and J. T. Cunningham, "Central losartan attenuates increases in arterial pressure and expression of FosB/ΔFosB along the autonomic axis associated with chronic intermittent hypoxia," *American Journal of Physiology—Regulatory Integrative and Comparative Physiology*, vol. 305, no. 9, pp. R1051–R1058, 2013.

Hindawi Publishing Corporation
Oxidative Medicine and Cellular Longevity
Volume 2016, Article ID 5843672, 13 pages
http://dx.doi.org/10.1155/2016/5843672

Research Article

Morin Attenuates Ovalbumin-Induced Airway Inflammation by Modulating Oxidative Stress-Responsive MAPK Signaling

Yuan Ma, Ai Ge, Wen Zhu, Ya-Nan Liu, Ning-Fei Ji, Wang-Jian Zha, Jia-Xiang Zhang, Xiao-Ning Zeng, and Mao Huang

Department of Respiratory Medicine, The First Affiliated Hospital of Nanjing Medical University, 300 Guangzhou Road, Nanjing, Jiangsu 210029, China

Correspondence should be addressed to
Xiao-Ning Zeng; zeng_xiao_ning@hotmail.com and Mao Huang; huangmao6114@126.com

Received 17 July 2015; Revised 12 September 2015; Accepted 13 September 2015

Academic Editor: Adam J. Case

Asthma is one of the most common inflammatory diseases characterized by airway hyperresponsiveness, inflammation, and remodeling. Morin, an active ingredient obtained from Moraceae plants, has been demonstrated to have promising anti-inflammatory activities in a range of disorders. However, its impacts on pulmonary diseases, particularly on asthma, have not been clarified. This study was designed to investigate whether morin alleviates airway inflammation in chronic asthma with an emphasis on oxidative stress modulation. *In vivo*, ovalbumin- (OVA-) sensitized mice were administered with morin or dexamethasone before challenge. Bronchoalveolar lavage fluid (BALF) and lung tissues were obtained to perform cell counts, histological analysis, and enzyme-linked immunosorbent assay. *In vitro*, human bronchial epithelial cells (BECs) were challenged by tumor necrosis factor alpha (TNF-α). The supernatant was collected for the detection of the proinflammatory proteins, and the cells were collected for reactive oxygen species (ROS)/mitogen-activated protein kinase (MAPK) evaluations. Severe inflammatory responses and remodeling were observed in the airways of the OVA-sensitized mice. Treatment with morin dramatically attenuated the extensive trafficking of inflammatory cells into the BALF and inhibited their infiltration around the respiratory tracts and vessels. Morin administration also significantly suppressed goblet cell hyperplasia and collagen deposition/fibrosis and dose-dependently inhibited the OVA-induced increases in IgE, TNF-α, interleukin- (IL-) 4, IL-13, matrix metalloproteinase-9, and malondialdehyde. In human BECs challenged by TNF-α, the levels of proteins such as eotaxin-1, monocyte chemoattractant protein-1, IL-8 and intercellular adhesion molecule-1, were consistently significantly decreased by morin. Western blotting and the 2′,7′-dichlorofluorescein assay revealed that the increases in intracellular ROS and MAPK phosphorylation were abolished by morin, implying that ROS/MAPK signaling contributes to the relief of airway inflammation. Our findings indicate for the first time that morin alleviates airway inflammation in chronic asthma, which probably occurs via the oxidative stress-responsive MAPK pathway, highlighting a novel profile of morin as a potent agent for asthma management.

1. Introduction

Allergic asthma, which is caused by inappropriate responses to inhaled allergens, is a heterogeneous inflammatory disorder characterized by airway hyperresponsiveness (AHR), remodeling, and inflammation [1]. Among these characteristics, chronic inflammation has attracted much attention for its contribution to asthma [2]. Conventional anti-inflammatory therapies such as glucocorticoids are merely ameliorative rather than curative and are associated with diverse unexpected side effects [3]. Some patients benefit little from these therapies and some even suffer from a series of adverse effects, including hyperglycemia, hyperlipidemia, hypertension, osteoporosis, and susceptibility to pathogens [4]. Thus, there is an urgent need for the safe and effective therapeutic options in asthma treatment.

As the first line of defense against challenges, bronchial epithelial cells (BECs) produce innate immune mediators that limit foreign antigen invasion, in addition to chemokines/cytokines that modulate immune responses under physiological conditions [5, 6]. During the development of asthma, which involves an aberrant airway immune

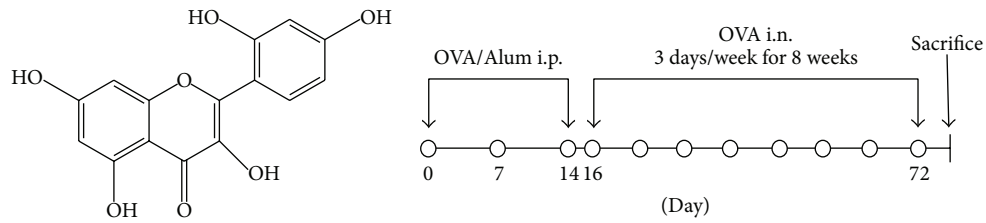

(a) Morin (b) Chronic asthma model

Figure 1: Chemical structure of morin and experimental protocol for the chronic asthma model. (a) Chemical structure of morin. (b) BALB/c mice were sensitized with OVA and aluminum hydroxide gel by intraperitoneal injection on days 0, 7, and 14 and then challenged with aerosolized 5% OVA for 30 min per day, three days per week for eight weeks, beginning on the 16th day of the experiment. The control mice were sensitized and challenged only with saline. Morin, DEX, or a vehicle (DMSO) was given by intraperitoneal injection at 30 min before each OVA challenge. i.p.: intraperitoneal injection; i.n.: inhalation.

response, insults such as infection, allergens, or environmental factors could alter the profile of BECs, initiating chronic inflammation by polarizing T-helper type 2 (Th2) lymphocytes and promoting the secretion of proinflammatory proteins, including eotaxin-1, monocyte chemoattractant protein-1 (MCP-1), interleukin- (IL-) 8, and intercellular adhesion molecule-1 (ICAM-1) [7–9]. BECs also contribute to airway remodeling by producing various extracellular matrix (ECM) proteins [10], which in turn affect inflammation, determining the outcome of asthma. Therefore, strategies targeting the modulation of BECs may represent a new option for asthma treatment.

Tumor necrosis factor alpha (TNF-α) is an important proinflammatory molecule secreted by both immunocytes and structural cells [11]. Accumulating data have shown that TNF-α is markedly increased during the process of asthma [12]. It elicits proinflammatory cytokines generation and evokes the activation of various cells, leading to an amplification of inflammatory responses [13]. Clinical trials of agents targeting TNF-α have been shown to be effective in asthma management [11]. Blockade of the activity of TNF-α notably decreases Th2 cytokines production, the serum IgE levels, and inflammatory cell infiltration [11, 14, 15]. This evidence highlights the critical role of TNF-α in the inflammation. Herein, we established an inflammatory model with TNF-α *in vitro*.

Morin (3,5,7,2′,4′-pentahydroxyflavone), which exists in high concentrations in many herbs (Figure 1(a)), such as *Cudrania tricuspidata*, Osage orange, *Artocarpus heterophyllus* Lam., fig, and other Moraceae family members, has been shown to have strong antitumor and anti-inflammatory activities. Emerging data have indicated that morin protects rats from carbon tetrachloride-induced acute liver damage [16], suppresses the growth of hepatocellular carcinoma [17], and attenuates inflammatory responses in chronic experimental colitis [18]. Although morin has gained much attention in the treatment of a number of chronic diseases, it remains unclear whether it has benefits in asthma therapy. Given that asthma is characterized by airway inflammation and that morin has anti-inflammatory activities, the aim of the present study was to determine the impact of morin on allergic airway inflammation both *in vivo* and *in vitro*. The results obtained here indicate that morin significantly attenuates allergic airway inflammation, which might be due to an inhibition of reactive oxygen species (ROS)/mitogen-activated protein kinase (MAPK) signaling.

2. Materials and Methods

2.1. Animals. Specific pathogen-free female BALB/c mice (18–22 g) aged 6 to 8 weeks were obtained from Vital River Laboratories (Beijing, China). The mice were kept in a temperature-controlled room under a 12 h dark/light cycle and were provided with food and water *ad libitum*. All experiments that involved animal and tissue samples were performed in accordance with the guidelines of the National Institutes of Health and Nanjing Medical University, and all procedures were approved by the Institutional Animal Care and Use Committee of Nanjing Medical University (Nanjing, China).

2.2. Ovalbumin (OVA) Sensitization and Challenge. Figure 1(b) schematically depicts the protocols used in this study. In total, 42 specific pathogen-free female BABL/c mice were randomly divided into 6 groups as follows: control, OVA (Grade V, Sigma-Aldrich, Milwaukee, WI, USA), OVA + ML (5 mg/kg morin, Sigma), OVA + MH (10 mg/kg morin), OVA + dexamethasone (1 mg/kg DEX, Sigma), and OVA + dimethylsulfoxide (DMSO, Biosharp, Hefei, Anhui, China). The asthmatic models were established by sensitization to OVA. Specifically, all of the mice in the OVA, OVA + ML, OVA + MH, OVA + DEX, and OVA + DMSO groups were sensitized on days 0, 7, and 14 by intraperitoneal injection of 20 μg OVA emulsified in 2 mg aluminum hydroxide gel (Invivo-Gen, San Diego, CA, USA) in a total volume of 200 μL. These sensitized mice were exposed to aerosolized 5% OVA in sterile saline for 8 weeks beginning on the 16th day of the experiment, three times a week for 30 min each time. We placed the mice in 51 × 31 × 21 cm chambers that were connected to a jet nebulizer (NE-U11B; Omron Corp., Tokyo, Japan) to create a whole-body inhalation system. Morin (5 and 10 mg/kg), DEX (1 mg/kg, positive control), and DMSO (0.4 μL in a total of 200 μL saline, solvent control) were administered by intraperitoneal injection at 30 min before

each OVA challenge. The control subjects were sensitized and challenged using the same protocol with saline alone. The mice were sacrificed at 24 h after the last challenge, and bronchoalveolar lavage fluid (BALF) and lung tissues were collected for analysis.

2.3. BALF Collection and Differential Cell Counts. Briefly, the mice were anesthetized by intraperitoneal injection of pentobarbital sodium (70 mg/kg) at 24 h after the final challenge. BALF was collected by lavage with ice-cold phosphate-buffered saline (PBS, 400 μL × 3; 85–90% of the lavage volume was recovered) via a tracheal catheter. The lavage samples from each mouse were centrifuged at 1000 rpm for 10 min at 4°C. The total number of inflammatory cells in the BALF was counted using a hemocytometer. Differential cell counts were performed using Wright's staining on the basis of morphological criteria. The number of cells in the BALF was determined by two independent investigators in a single-blind study, and at least 200 cells each were analyzed from three different random locations using a microscope. Then, the supernatant was collected and divided into four equal portions and frozen at −80°C for enzyme-linked immunosorbent assay (ELISA).

2.4. Lung Histology. After BALF samples were collected, a 20 mL syringe equipped with a 18 G needle was used to inject 10–15 mL PBS slowly into the right ventricle. Then the lungs were inflated with 4% paraformaldehyde under 20 cm pressure by a tracheal catheter and placed in 4% paraformaldehyde fixative for paraffin embedding. A series of microsections (5 μm) were cut with a microtome and stained with hematoxylin and eosin (H&E) to assess inflammatory cell infiltration. The inflammation score was determined as follows: grade 0: no inflammation; grade 1: occasional cuffing with inflammatory cells; and grades 2, 3, and 4: most bronchi or vessels which were surrounded by a thin layer (1-2 cells: grade 2), a moderate layer (3–5 cells: grade 3), or a thick layer (>5 cells: grade 4) of inflammatory cells, respectively. The total inflammation score was calculated by the addition of the peribronchial (PB) and perivascular (PV) inflammation scores. Periodic acid-Schiff (PAS) staining was used to quantify airway goblet cells, and Masson's trichrome staining was used to visualize collagen deposition and fibrosis. Both staining methods were scored as follows: 0: none; 1: <25%; 2: 25–50%; 3: 50–75%; and 4: >75% goblet cells [19–21]. Sections were also immunohistochemically stained for matrix metalloproteinase-9 (MMP-9). For the semiquantitative evaluation of MMP-9 expression, we used a scoring method modified by Sinicrope and Lu [22, 23]. The mean percentage of positive epithelial cells in the bronchi was determined in at least five areas at ×400 magnification and assigned to one of the following categories: 0: <5%; 1: 5–25%; 2: 25–50%; 3: 50–75%; and 4: >75%. The immunostaining intensity of MMP-9 was scored as 1+ (weak), 2+ (moderate), or 3+ (intense). The percentage of positive epithelial cells and the staining intensity were multiplied to produce a weighted score for each case. All of the scores were calculated by 2 independent observers who were blinded to the experiment, and at least three different fields were examined for each lung section.

2.5. Determination of Tissue Malondialdehyde (MDA) Level. The left lung tissues were homogenized on ice in normal saline. The homogenates were centrifuged at 4000 rpm at 4°C for 10 min. The MDA level in the supernatants was determined using the thiobarbituric acid reacting substances (TBARS) assay (Nanjing Jiancheng Corp., China) as previously described [23]. MDA reacts with thiobarbituric acid under acidic conditions at 95°C to form a pink-colored complex. This product can be measured at 532 nm. In this test, 1,3,3-tetraethoxypropane (TEP) was used as a standard.

2.6. Culturing and Morin Treatment of Normal Human BECs. Normal human BECs were purchased from the Beijing Institute for Cancer Research (Beijing, China). They were obtained from bronchial epithelial tissues of healthy adults who did not have a respiratory disease and did not smoke. The cells were cultured at 37°C and 5% CO_2 in RPMI 1640 medium (Invitrogen-Gibco, Paisley, Scotland) supplemented with 20 U/L penicillin, 20 μg/mL streptomycin, and 10% fetal bovine serum (Invitrogen-Gibco). Cells between passages 4 and 8 were used for the experiments. After serum starvation for 6–12 h, the cells were stimulated with 10 ng/mL TNF-α (Peprotech, Rocky Hill, USA) alone or in combination with morin (10 μM), and they were further cultured for the indicated durations. Cells were treated in the same manner with N-acetylcysteine (NAC) as a positive control.

2.7. Cell Viability Assay. The cytotoxicity of morin on BECs was examined using the CCK-8 (Dojindo Molecular Technologies Inc., Kumamoto, Japan) assay. Human BECs were cultured in a 96-well plate at a density of 5×10^3 cells per well and treated with morin at concentrations ranging from 0.1 to 200 μM for 24 h. Then, CCK-8 solution was added to the cell culture medium at a 1 : 10 dilution, and the cultures were incubated for another 1-2 h at 37°C. Absorbance at 450 nm (A450) was measured with a microplate reader (CANY, Shanghai, China).

2.8. ELISA. To explore the effect of morin on TNF-α-induced inflammation in human BECs, human eotaxin-1, MCP-1, IL-8, and ICAM-1 (R&D Systems, Abingdon, UK) levels were measured. Cells were cultured using the aforementioned procedure and were then divided into the following four treatment groups: control, T (10 ng/mL TNF-α), T + M (10 ng/mL TNF-α + 10 μM morin), and M (10 μM morin). The cells were treated for 6 h as described above, and ELISAs were performed. The total IgE (Immuno-Biological Laboratories Co., Hamburg, Germany), TNF-α, IL-4, and IL-13 levels (R&D) in the BALF of the mice were also measured by ELISA, according to the manufacturer's instructions.

2.9. Determination of Intracellular ROS Production. Intracellular ROS were measured using the 2′,7′-dichlorofluorescin diacetate (DCFH-DA) assay. Briefly, 1.5×10^4 cells were seeded into each well of a 6-well plate, cultured for 24 h, and exposed to morin (10 μM) or NAC (10 mM) with TNF-α (10 ng/mL) for 6 h. The cells were then incubated with 10 μM DCFH-DA for 30 min at 37°C in the dark. Next, they were washed twice with PBS and analyzed within 30 min using a

FACScan instrument (Becton Dickinson, San Jose, CA, USA) with an excitation setting of 488 nm. The specific fluorescence signals corresponding to DCFH-DA were determined using a 525 nm band pass filter. For consistency, 10,000 cells were analyzed for each determination. Intracellular ROS production was also measured with a laser scanning confocal microscope (Zeiss LSM 5 live, German). After incubation with DCFH-DA, the cells were fixed with 4% paraformaldehyde for 10 min and washed three times with PBS before being photographed. The excitation and emission wavelengths used were identical to those described previously, and photographs were taken. For each culture, a minimum of 5 random fields were captured.

2.10. Western Blotting. Total cellular protein was collected following lysis in lysis buffer (Cell Signaling Technology Inc., Beverly, MA, USA) on ice and centrifugation for 15 min at 14,000 rpm at 4°C. The supernatant was transferred into a fresh tube and denatured in sodium dodecyl sulfate-polyacrylamide gel electrophoresis (SDS-PAGE) Loading Buffer (Beyotime, Shanghai, China) with heating to 100°C for 5 min, and it was then stored at −80°C. The total protein concentration was determined using the BCA protein assay (Thermo, Rockford, IL, USA). Proteins were separated by 10% SDS-PAGE. After electrophoresis, the separated proteins were transferred to polyvinylidene difluoride membranes (Millipore, Billerica, MA, USA) using the wet transfer method. Nonspecific sites were blocked with 5% nonfat milk in TBS Tween 20 (TBST; 25 mM Tris [pH 7.5], 150 mM NaCl, and 0.1% Tween 20) for 2 h, and the blots were incubated with primary antibodies (Cell Signaling Technology Inc.), including anti-glyceraldehyde-3-phosphate dehydrogenase (GAPDH), anti-phospho-p38, anti-p38, anti-phospho-ERK, anti-ERK, anti-phospho-JNK, and anti-JNK antibodies, overnight at 4°C. Goat anti-rabbit horseradish peroxidase-conjugated IgG (Cell Signaling Technology Inc.) was used to detect antibody binding. After treatment of the membranes with enhanced chemiluminescence system reagents (Thermo), the binding of specific antibodies was visualized using a Bio-Rad Gel Doc/Chemi Doc Imaging System and analyzed by Quantity One software.

2.11. Statistical Analysis. The data are expressed as the mean ± standard deviation (SD). All tests were performed using Prism 6.00 (GraphPad Software, San Diego, CA, USA) and SPSS version 20 (SPSS Inc., Chicago, IL, USA). The results were analyzed by one-way analysis of variance for repeated measures, followed by Dunnett's post hoc test to determine differences among multiple comparisons. The significance level was set to $P < 0.05$.

3. Results

3.1. Morin Attenuated Allergic Airway Inflammation in OVA-Sensitized Mice. Lung sections were stained with H&E, and inflammatory cells in BALF were counted at 24 h after the last OVA challenge. Compared with the mice in the control group, those in the OVA and the vehicle group (OVA + DMSO) displayed severe airway inflammatory responses, including extensive infiltration of inflammatory cells into the BALF (Figure 2(a)) and around the respiratory tracts and vessels (Figure 2(b)). Treatment with morin or DEX suppressed the infiltration of inflammatory cells to varying degrees. Administration of morin (10 mg/kg) induced a remarkable decrease in not only the total cell counts but also the numbers of macrophages, eosinophils, and lymphocytes compared with those observed in the untreated asthmatic mice ($P < 0.05$), while the lower dose of morin (5 mg/kg) did not cause such drastic decreases in the cell numbers (Figure 2(a)). These results were further confirmed by H&E analysis and inflammation scores. Mice treated with morin (5 and 10 mg/kg) and DEX had fewer PB and PV inflammatory cells (Figure 2(b)), and the total inflammation scores were 4.1 ± 0.99, 2.5 ± 1.58, and 2.3 ± 1.64, respectively ($P < 0.05$) (Figure 2(c)). All of these findings indicated that administration of morin before the OVA aerosol challenge dose-dependently attenuated the inflammatory responses in the asthmatic airways.

3.2. Morin Abrogated Goblet Cell Hyperplasia in OVA-Sensitized Mice. The number of goblet cells and the extent of mucus production were assessed by PAS staining, and the percentage of PAS-positive cells in the bronchioles was also evaluated. We observed that the OVA-challenged mice developed marked goblet cell hyperplasia and mucus hypersecretion in the lumens of the bronchioles (Figure 2(b)). The morin- (10 mg/kg) and DEX-treated animals had fewer goblet cells in the airway epithelium, and the mucus scores in these two groups were reduced to 1.2 ± 0.79 and 1.1 ± 0.74 ($P < 0.05$), respectively, indicating the equivalent effects of the treatments (Figure 2(d)).

3.3. Morin Impaired Collagen Deposition/Fibrosis in OVA-Sensitized Mice. The area of collagen deposition/fibrosis was assessed using Masson's trichrome staining. Collagen deposition was profoundly enhanced in the interstitia of the airways and vessels of the tissues in the OVA group mice compared with the control group mice. Airway fibrosis was significantly ameliorated by administration of 10 mg/kg morin, with a score of 1.0 ± 1.05 ($P < 0.05$). The OVA + DEX group mice also showed significantly less fibrosis than the untreated asthmatic mice. However, no significant reduction in collagen deposition was observed in the OVA + ML group mice (Figures 2(b) and 2(e)).

3.4. Morin Decreased Expression of MMP-9 in OVA-Sensitized Mice. Representative photomicrographs of immunohistochemical staining for MMP-9 in the airways are shown in Figure 2(b). The densities of MMP-9 staining around the bronchioles and the infiltrated inflammatory cells in the OVA-challenged mice were higher than those in the control mice, and the score was 8.2 ± 0.92 ($P < 0.05$). These increases were dramatically reversed by the administration of DEX or the high dose of morin, with scores of 1.7 ± 1.34 and 1.5 ± 1.18, respectively ($P < 0.05$) (Figure 2(f)).

3.5. Morin Reduced Levels of IgE, TNF-α, and Th2 Cytokines in BALF. The total IgE, TNF-α, IL-4, and IL-13 levels in

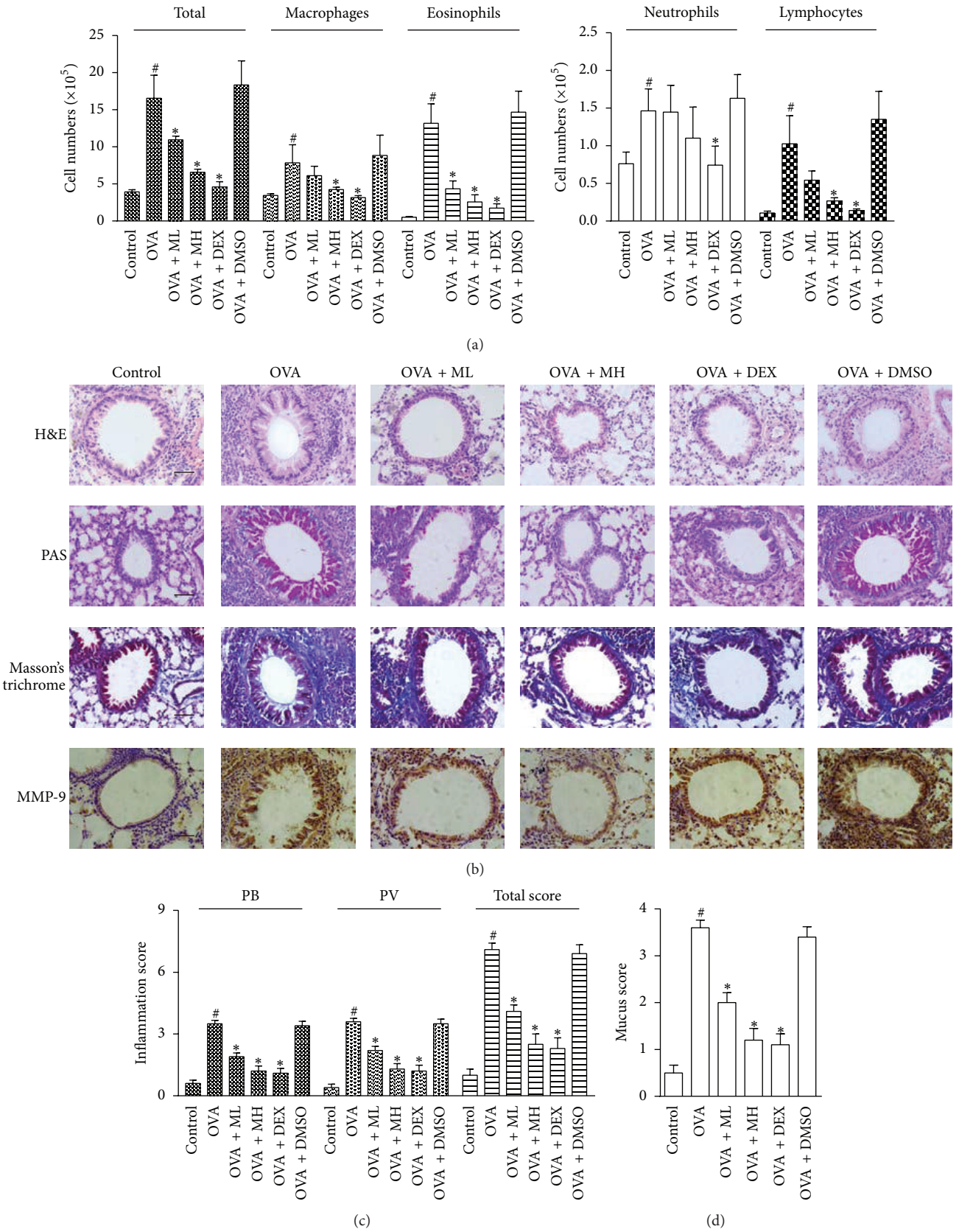

Figure 2: Continued.

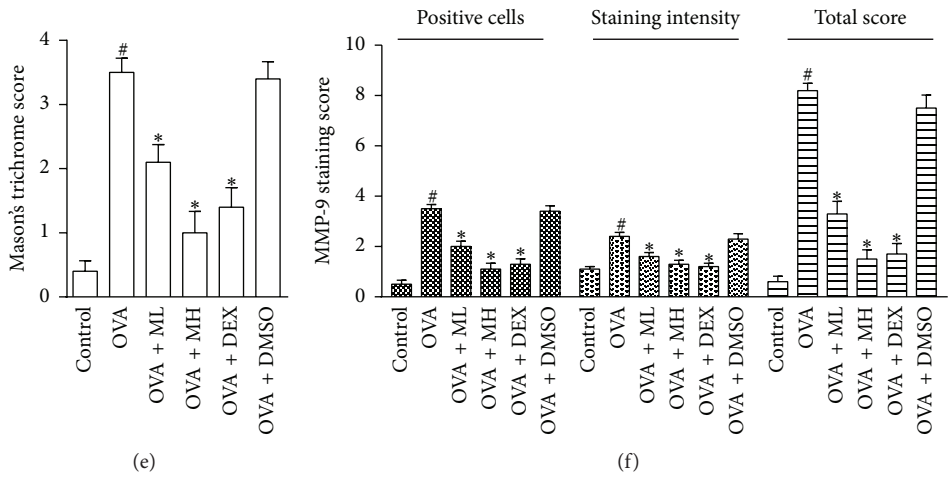

Figure 2: Treatment with morin reduced inflammatory cells infiltration, goblet cell hyperplasia, collagen deposition, and the expression of MMP-9 in lung tissue (magnification 400x). (a) Cell numbers and differentiation in BALF were determined by hemocytometer, and at least 200 cells were counted ($n = 7$ per group). (b) Lung sections were stained with H&E to analyze the infiltration of inflammatory cells, PAS to assess goblet cell hyperplasia, Masson's trichrome to evaluate the subepithelial deposition of collagen and fibrosis, and immunohistochemistry to assess the distribution of MMP-9. Scale bar: 50 μm. (c) The layers of inflammation cells were counted and the total inflammation score was summed up with peribronchial (PB) and perivascular (PV) inflammation scores. (d) PAS-positive and PAS-negative epithelial cells were counted, and the percentage of PAS-positive cells per bronchiole was calculated. (e) Masson's trichrome staining analysis of collagen deposition was calculated. (f) The MMP-9 expression was evaluated and the total MMP-9 staining score was multiplied up with percentage of positive epithelial cells and staining intensity scores. Values represented as mean ± SD ($n = 7$ per group). $^{\#}P < 0.05$ compared with the control group, and $^{*}P < 0.05$ compared with the OVA group.

the BALF were notably increased by airway challenge with OVA. Administration of morin dose-dependently reduced the levels of IgE, Th2 cytokines, and TNF-α in the BALF compared with those in the BALF of the OVA group mice ($P < 0.05$) (Figures 3(a)–3(d)). These findings indicated that morin could inhibit allergic airway reactions by modifying Th2-predominant immune activity in the OVA-induced mouse asthma model.

3.6. Morin Inhibited MDA Level in Lung Tissues. To determine whether morin inhibits OVA-induced airway inflammation by the scavenging of free radicals, we detected the MDA level in the lung tissues to evaluate the changes in OVA-induced oxidative damage. As shown in Figure 3(e), the concentrations of MDA in the lung tissues in the OVA and vehicle groups (1.638 ± 0.17 nmol/L and 1.666 ± 0.20 nmol/L, resp.) were significantly higher than that in the control group (1.189 ± 0.25 nmol/L) ($P < 0.05$). The MDA levels in the lung tissues in the DEX and morin (10 mg/kg) pretreatment groups (1.267 ± 0.21 nmol/L and 1.330 ± 0.09 nmol/L, resp.) were significantly decreased compared with that in the OVA group ($P < 0.05$).

3.7. Morin Restrained TNF-α-Induced Proinflammatory Protein Expression in Human BECs. The toxicity of morin (0.1, 1, 5, 10, 50, 100, and 200 μM) to human BECs was first determined. Cell viability was 81% ± 4% in the 10 μM group at 24 h (Figure 4(a)). BECs have been reported to release chemokines and adhesion molecules to induce an inflammatory response and stimulate eosinophil migration in asthmatic patients [5]. To further ascertain the anti-inflammatory mechanism of morin, we studied its effects on the TNF-α-induced expression of proinflammatory proteins in BECs. The results showed that morin (10 μM) dramatically blocked the TNF-α-induced upregulation of eotaxin-1, MCP-1, IL-8, and ICAM-1 expression in human BECs ($P < 0.05$) (Figures 4(b)–4(e)).

3.8. Morin Diminished TNF-α-Induced ROS Generation in Human BECs. ROS are considered to mediate the persistent inflammation that occurs in asthma [24]. Therefore, in the present study, we investigated whether it can regulate ROS generation. As shown in Figure 5, ROS production was promoted by TNF-α, which is an effective activator in BECs. Flow cytometric analysis showed that pretreatment with morin (10 μM) or NAC (10 mM) decreased the intracellular ROS levels to 85% ± 18% or 77% ± 7% ($P < 0.05$), respectively (Figure 5(a)). These significant data revealed that the antioxidant effect of morin may be similar to that of NAC, which is a potent ROS scavenger. In addition, the ROS levels in BECs were monitored using a laser scanning confocal microscope, and similar results were obtained. In brief, we found that morin could apparently suppress TNF-α-induced intracellular ROS production in BECs (Figure 5(b)), implying a significant protective effect against oxidative stress.

3.9. Morin Suppressed TNF-α-Induced MAPK Signaling Activation in Human BECs. It has been established that MAPK signaling pathways are responsible for oxidative stress-associated airway epithelial damage and that they are crucial for TNF-α-induced inflammation in BECs [25]. As shown

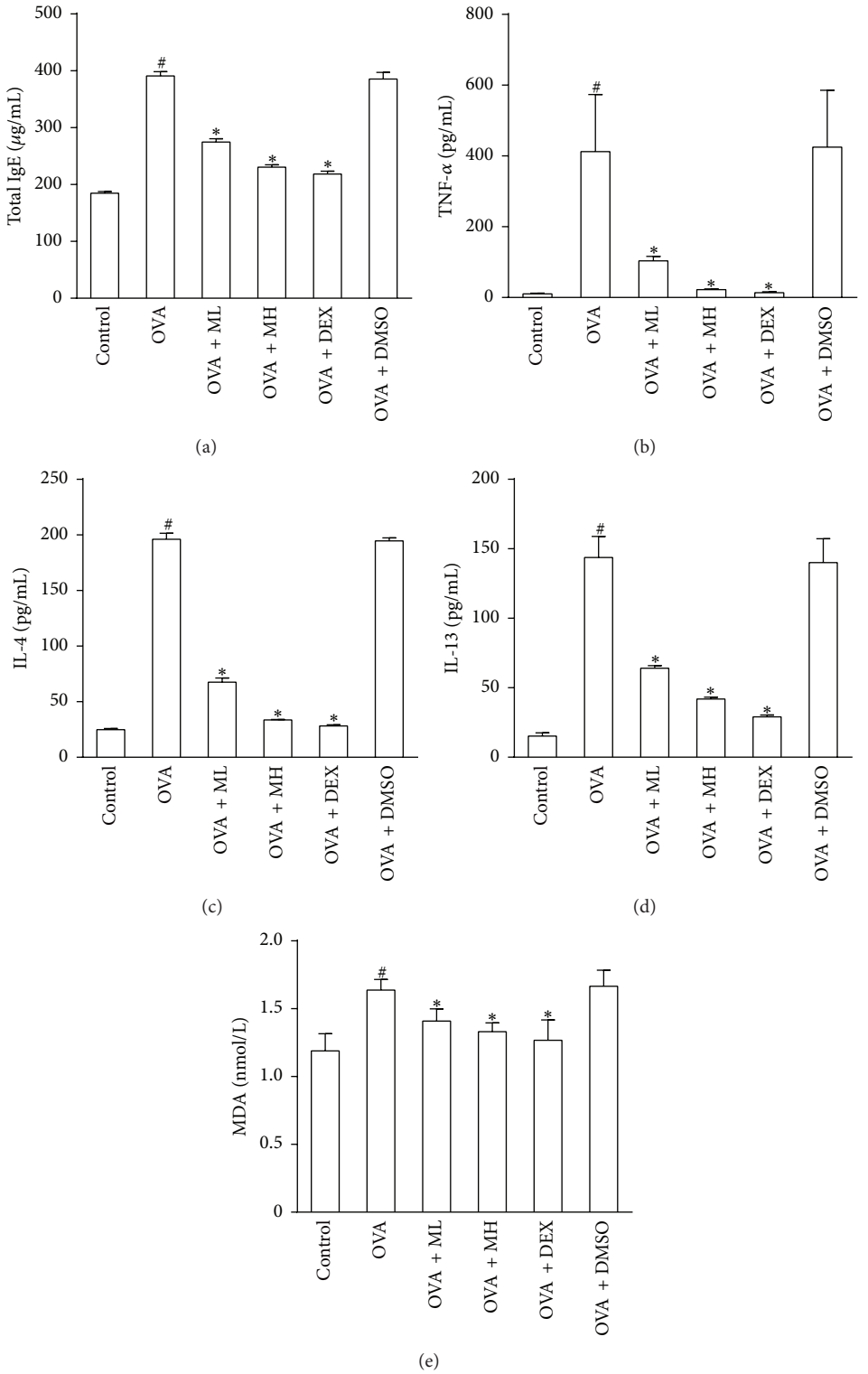

Figure 3: Treatment with morin inhibited the levels of IgE, TNF-α, and Th2 cytokines in BALF and MDA in lung tissues. (a–d) The concentrations of IgE, TNF-α, IL-4, IL-13, and MDA were measured with ELISA. Values represented as mean ± SD ($n = 7$ per group). $^{\#}P < 0.05$ compared with the control group, and $^{*}P < 0.05$ compared with the OVA group.

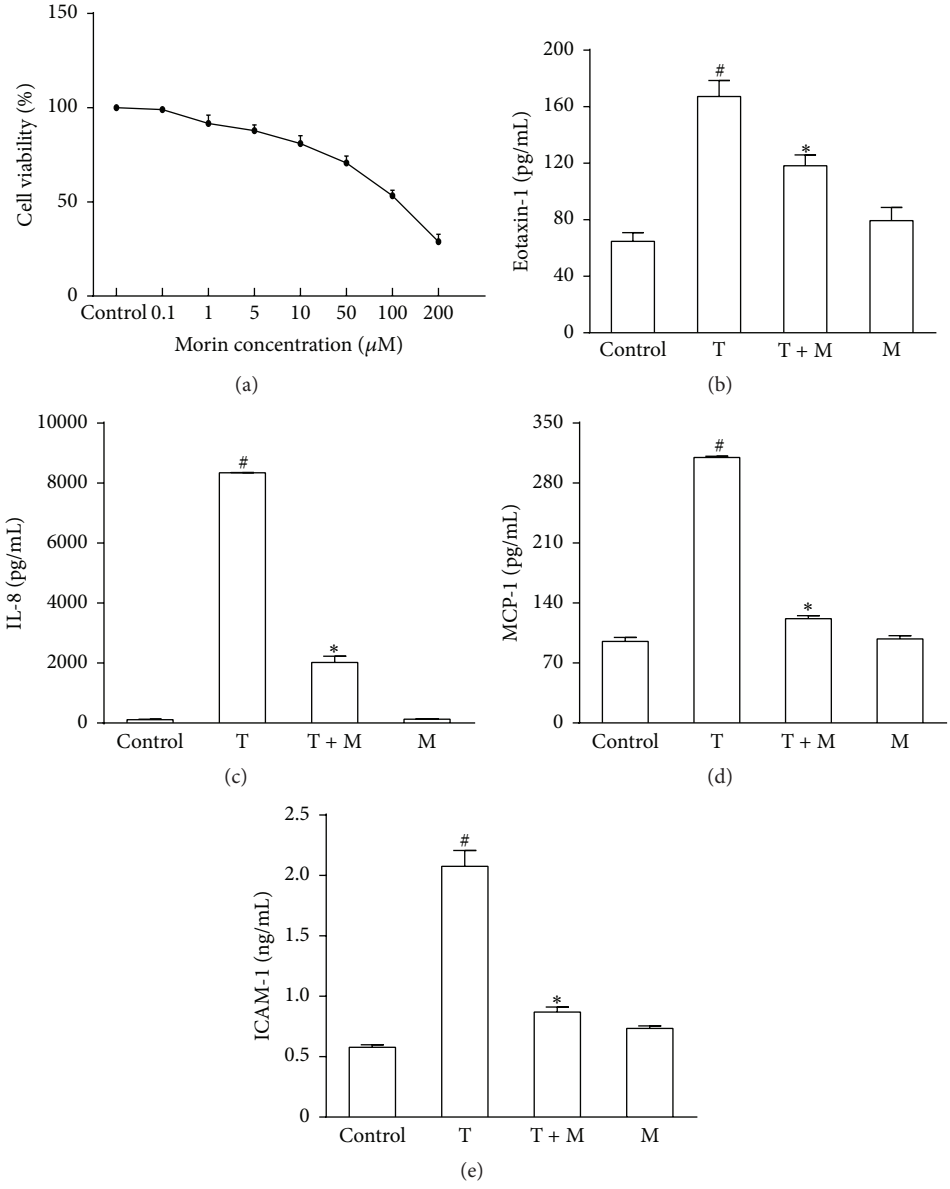

Figure 4: Treatment with morin restrained the proinflammatory proteins induced by TNF-α in BECs. (a) Effects of morin on the viability of human BECs assessed by CCK-8. (b–d) The expression levels of MCP-1 (b), eotaxin-1 (c), IL-8 (d), and ICAM-1 (e) in supernatant were measured by ELISA. Values represented as mean ± SD of at least four independent experiments performed in triplicate. $^{\#}P < 0.05$ compared with the control group, and $^{*}P < 0.05$ compared with TNF-α group. M: morin (10 μM) and T: TNF-α (10 ng/mL).

in Figure 6, we confirmed the effects of TNF-α on the activation of ERK, JNK, and p38 in the BECs within 1 h after stimulation and quantified their relative densities (phosphorylated proteins relative to total proteins). This activation was partially blunted in the morin-pretreated group. These results suggested that morin may attenuate TNF-α-induced inflammation in BECs by suppressing the activation of MAPK pathways.

4. Discussion

Over the last three decades, the prevalence of asthma has markedly increased worldwide. The high costs of asthma treatments pose an immense financial burden to society [1, 26]. Current pharmaceutical options, such as inhaled corticosteroids, long-acting β agonists, and other potential agents, have had unsatisfactory effects on controlling asthma. Thus, physicians are searching for novel therapeutic options that are both safe and effective in asthma management [27, 28].

Morin, a natural flavonol, appears to confer a protective effect in chronic inflammatory diseases. In the present study, treatment with morin inhibited the increase of inflammatory cells (including macrophages, eosinophils, and lymphocytes) and downregulated the total IgE, IL-4, and IL-13 levels in OVA-induced mice. Overexpression of IgE and the Th2

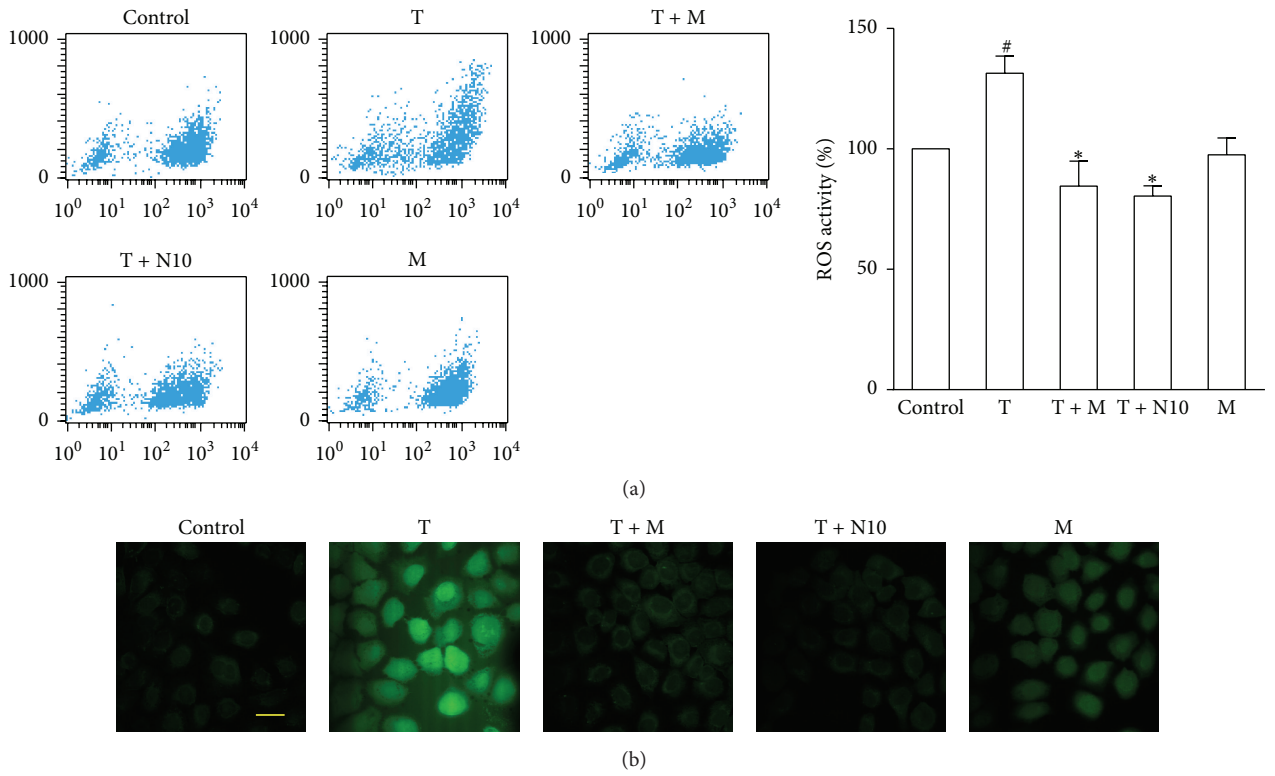

Figure 5: Treatment with morin attenuated intracellular ROS production induced by TNF-α. (a) Fluorescence-activated cell sorting profile of ROS generation by flow cytometry. Summary of the average ROS production by BECs treated with morin (10 μM) or NAC (1 and 10 mM) after TNF-α (10 ng/mL) stimulation in three independent experiments. (b) DCFH-DA fluorescence (green) imaging of ROS in BECs evaluated with a laser scanning confocal microscope. Scale bar: 50 μm. Values represented as mean ± SD of at least four independent experiments performed in triplicate. $^{\#}P < 0.05$ compared with the control, and $^{*}P < 0.05$ compared with the TNF-α group. M: morin (10 μM); T: TNF-α (10 ng/mL); N: NAC.

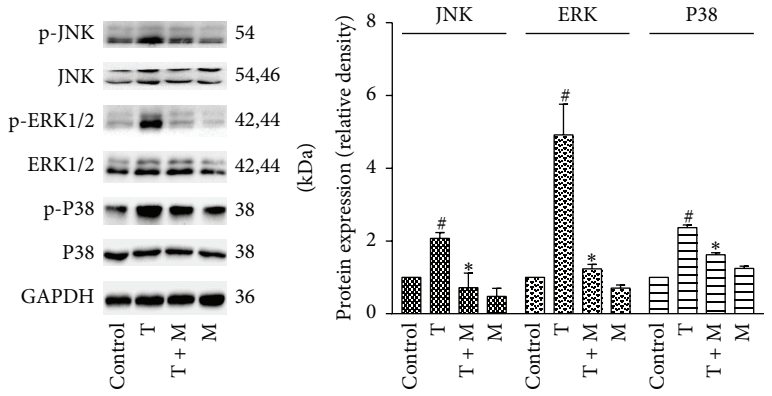

Figure 6: Treatment with morin suppressed the activation of the ERK, JNK, and p38 in BECs. The phosphorylation and total of ERK, JNK, and p38 were measured by western blotting. The relative density quantification is phosphorylated protein relative to total protein. Values represented as mean ± SD of at least four independent experiments performed in triplicate. M: morin (10 μM); T: TNF-α (10 ng/mL); $^{\#}P < 0.05$ compared with the control, and $^{*}P < 0.05$ compared with the TNF-α group.

cytokines is known to result in eosinophil-rich inflammation, mucus hypersecretion, and enhanced collagen deposition in the lungs [29, 30]. Our findings indicated that morin inhibited inflammatory cell infiltration, mucus hypersecretion, and collagen deposition/fibrosis, implying that it might be valuable as a new antiallergic and anti-inflammatory agent for asthma management.

Several studies have shown that MMP-9, an enzyme that promotes cleavage of the ECM by degrading structural proteins such as collagen, plays a crucial role in the pathogenesis of airway inflammation and remodeling in asthma [31]. The MMP-9 levels in patients with classic asthma are elevated in the serum, sputum, and BALF [32]. MMP-9-deficient animals exhibit reduced airway inflammation, and the immunoreactivity of MMP-9 has been demonstrated to be associated with the severity of asthma [33]. Anti-MMP-9 therapy has been shown to be useful for preventing airway inflammation and remodeling in murine model of asthma [34]. In the current study, we found that morin significantly attenuated MMP-9 expression, which might have contributed to the lessened ECM, thereby contributing to its positive effects on asthma.

Emerging data have provided new insights into the complex interactions that occur between MMP-9 and inflammatory cytokines such as TNF-α. The TNF-α level is increased in numerous inflammatory diseases, such as rheumatoid arthritis [35], inflammatory bowel disease [36], psoriasis [37], chronic obstructive pulmonary disease [38], and asthma [12]. Evidence obtained from recent studies indicate that the transcriptional and translational activation of MMP-9 is involved in the loss of endothelial barrier integrity induced by TNF-α [39, 40]. Airway epithelial injury also leads to an exposure to TNF-α, which induces MMP-9 expression, provoking cell migration via various pathways, including the PKC, AP-1, NF-κB, and MAPK pathways [41, 42]. Indeed, anti-TNF-α therapy has been reported to reduce the expression of MMP-9 as well as that of other inflammatory cytokines (e.g., IL-4, IL-13, and IgE), thereby hindering the recruitment of inflammatory cells and inhibiting the airway inflammation in asthma [11, 14, 15, 39]. In our study, morin markedly suppressed OVA-induced TNF-α and MMP-9 overexpression with attenuation of airway inflammation, implying that its effects might be attributed to the downregulation of TNF-α.

Asthma is a pulmonary inflammatory disorder involving excessive oxidative stress. ROS, which are known to contribute to oxidative stress, are primarily produced by eosinophils and other inflammatory cells recruited to the airways in asthma [43–45]. Moreover, stimulated BECs have been shown to generate ROS, exacerbating airway damage, including bronchial hyperreactivity, inflammatory cell infiltration, epithelial cell shedding, goblet cell metaplasia, and mucus hypersecretion [24, 46]. In the present study, severe damage was observed in the airways of the untreated asthmatic mice. Treatment with morin significantly ameliorated these asthma-related pathological injuries. Moreover, the level of MDA, a common indicator of oxidative damage to membrane lipids, in the lung tissues from the OVA-challenged rats was increased, and morin significantly attenuated this increase. This finding revealed that the protective effects of morin in chronic asthma may be partly due to its ROS scavenging activity, resulting in a reduction in OVA-induced oxidative damage.

Accumulating data have shown that ROS are also secondary messengers that are involved in intracellular signal transduction. Increased ROS levels lead to activation of the MAPK pathways [46, 47]. MAPK signaling has been implicated in the transcription of various proinflammatory cytokines (e.g., eotaxin-1, MCP-1, and IL-8) and adhesion molecules (e.g., ICAM-1 and VCAM-1) [48, 49], which contribute to a worsened airway inflammation. It has been well established that eotaxin-1 is important for the delivery of eosinophils to the airways and that it could cause tissue damage and severe inflammation. Many studies have indicated that eotaxin-1 expression is stimulated by TNF-α via p38 MAPK/NF-κB signaling [50]. MCP-1 has monocyte and lymphocyte chemotactic activities and stimulates histamine release from basophils. A recent study has confirmed that TNF-α induces MCP-1 secretion from human airway smooth muscle cells [51]. IL-8, which is perhaps best known for its proinflammatory effects on immune cells, stimulates the infiltration of neutrophils into the airways in asthma and is associated with severe asthma [52]. ICAM-1 is critical for the transmigration of leukocytes out of blood vessels and into inflamed tissues. Inhibitors of MMPs regulate inflammatory cell migration by reducing ICAM-1 expression in asthma [53]. It has been postulated that TNF-α upregulates the production of ROS, which in turn activates BECs to overexpress proinflammatory proteins, such as eotaxin-1, MCP-1, IL-8, and ICAM-1 [24, 54, 55]. These proteins are predominant agents that increase the severity of inflammatory responses. Direct or indirect oxidative stress can also induce BECs to generate TNF-α [54, 56]. Thus, a vicious feedback cycle occurs due to the cytotoxic activities of ROS. Our findings showed that morin markedly alleviated the increases in eotaxin-1, MCP-1, IL-8, and ICAM-1 in human BECs, indicating that the relief of airway inflammation might have been due to the downregulation of these proinflammatory proteins, which probably occurred via ROS.

Our findings further demonstrated that morin strongly inhibited the intracellular ROS induced by TNF-α, producing effects similar to those of NAC. As a free radical scavenger, NAC prevents oxidant-induced inflammatory mediator release [57]. It is known that ROS and MAPK are both closely related to airway inflammation, but the modulation between them is not clear so far. The previous data confirmed that ERK phosphorylation is ROS-dependent in Siglec-8-mediated eosinophil cell death [58], and JNK phosphatases were critical molecular targets of ROS in TNF-α-induced programmed cell death [59]. Pretreatment of cells with the antioxidant enzyme abrogated the thalidomide-induced p38 MAPK activation in adult erythropoiesis [60]. A recent study provided that H_2O_2 significantly increased p38 MAPK and ERK1/2 phosphorylation while NAC effectively suppressed phosphorylation of p38 MAPK and ERK1/2 [61]. Additionally, reduction of ROS has been shown to inhibit the TNF-α-mediated airway inflammation [62]. These evidences collectively suggested that ROS play key roles in MAPK signaling associated with TNF-α stimulation. Therefore,

we hypothesize that morin might suppress TNF-α-induced inflammation by inhibiting MAPK signaling via ROS.

To confirm this hypothesis, we investigated the effects of morin on the TNF-α-induced activation of MAPKs in BECs. The results showed that TNF-α induced the phosphorylation of ERK, p38, and JNK in the BECs. Morin pretreatment significantly inhibited the phosphorylation of these kinases, suggesting that morin inhibited TNF-α-induced inflammation via the oxidative stress-responsive MAPK pathways.

The present study has confirmed that morin suppresses OVA-induced airway inflammation and ROS as well as inhibiting TNF-α-induced ROS/MAPK activation. However, there are some limitations to our study. Although OVA-induced murine models closely mimic human asthma, TNF-α, as a proinflammatory cytokine, cannot completely stimulate the development of the complex alterations characteristic of asthma, such as subepithelial fibrosis, airway smooth muscle mass increases (including hypertrophy and hyperplasia), and vascular remodeling. Thus, our findings warrant further evaluations of its *in vitro* and *in vivo* functions as well as its clinical utility in the treatment of delayed allergic diseases.

5. Conclusions

In conclusion, we have demonstrated the potential therapeutic action of morin in an experimental model of asthma and its anti-inflammatory properties in human BECs. Collectively, our findings have indicated that morin (I) suppresses both the infiltration of inflammatory cells and the hyperplasia of goblet cells in the airways, (II) reduces MMP-9 expression and fibrosis in OVA-sensitized mice, (III) attenuates elevations in the total IgE, TNF-α, IL-4, and IL-13 levels in BALF, and MDA level in lung tissues, (IV) suppresses TNF-α-induced eotaxin-1, MCP-1, IL-8, and ICAM-1 expression in human BECs, and (V) inhibits TNF-α-induced ROS by regulating MAPK signaling. Taken together, our results provide direct evidence that morin might be a candidate for the adjuvant therapy for asthmatic patients.

Conflict of Interests

The authors declare that there is no conflict of interests regarding the publication of this paper.

Authors' Contribution

All authors have read and approved the final paper. Yuan Ma and Ai Ge contributed equally to this work.

Acknowledgments

This work was supported by the Jiangsu Province Special Program of Medical Science (BL2012012), the Jiangsu Province Scientific Research Innovation Project of University Graduate Students (KYZZ_0260), Project of Jiangsu Provincial Commission of Health and Family Planning (H201501), Administration of Traditional Chinese Medicine of Jiangsu Province (LZ13213), the "Six Talent Peak" Project of Jiangsu Province (2013-WSN-059), and a Project Funded by the Priority Academic Program Development of Jiangsu Higher Education Institutions (PAPD) (JX10231802).

References

[1] C. Anandan, U. Nurmatov, O. C. P. van Schayck, and A. Sheikh, "Is the prevalence of asthma declining? Systematic review of epidemiological studies," *Allergy*, vol. 65, no. 2, pp. 152–167, 2010.

[2] W.-J. Zha, Y. Qian, Y. Shen et al., "Galangin abrogates ovalbumin-induced airway inflammation via negative regulation of NF-κB," *Evidence-Based Complementary and Alternative Medicine*, vol. 2013, Article ID 767689, 14 pages, 2013.

[3] L.-P. Boulet, J. M. FitzGerald, M. L. Levy et al., "A guide to the translation of the Global Initiative for Asthma (GINA) strategy into improved care," *European Respiratory Journal*, vol. 39, no. 5, pp. 1220–1229, 2012.

[4] S. T. Holgate, "Asthma: a simple concept but in reality a complex disease," *European Journal of Clinical Investigation*, vol. 41, no. 12, pp. 1339–1352, 2011.

[5] B. N. Lambrecht and H. Hammad, "Asthma: the importance of dysregulated barrier immunity," *European Journal of Immunology*, vol. 43, no. 12, pp. 3125–3137, 2013.

[6] J. A. Hirota and D. A. Knight, "Human airway epithelial cell innate immunity: relevance to asthma," *Current Opinion in Immunology*, vol. 24, no. 6, pp. 740–746, 2012.

[7] J.-L. Malo, J. L'Archevêque, Z. Lummus, and D. Bernstein, "Changes in specific IgE and IgG and monocyte chemoattractant protein-1 in workers with occupational asthma caused by diisocyanates and removed from exposure," *Journal of Allergy and Clinical Immunology*, vol. 118, no. 2, pp. 530–533, 2006.

[8] T. Tanabe, T. Shimokawaji, S. Kanoh, and B. K. Rubin, "IL-33 stimulates CXCL8/IL-8 secretion in goblet cells but not normally differentiated airway cells," *Clinical and Experimental Allergy*, vol. 44, no. 4, pp. 540–552, 2014.

[9] S. Mukhopadhyay, P. Malik, S. K. Arora, and T. K. Mukherjee, "Intercellular adhesion molecule-1 as a drug target in asthma and rhinitis," *Respirology*, vol. 19, no. 4, pp. 508–513, 2014.

[10] Y. Wang, C. Bai, K. Li, K. B. Adler, and X. Wang, "Role of airway epithelial cells in development of asthma and allergic rhinitis," *Respiratory Medicine*, vol. 102, no. 7, pp. 949–955, 2008.

[11] K. Orihara and A. Matsuda, "Pathophysiological roles of microvascular alterations in pulmonary inflammatory diseases: possible implications of tumor necrosis factor-alpha and CXC chemokines," *International Journal of Chronic Obstructive Pulmonary Disease*, vol. 3, no. 4, pp. 619–627, 2008.

[12] D. Lykouras, F. Sampsonas, A. Kaparianos, K. Karkoulias, and K. Spiropoulos, "Role and pharmacogenomics of TNF-α in asthma," *Mini-Reviews in Medicinal Chemistry*, vol. 8, no. 9, pp. 934–942, 2008.

[13] D. Desai and C. Brightling, "Tnf-alpha antagonism in severe asthma?" *Recent Patents on Inflammation and Allergy Drug Discovery*, vol. 4, no. 3, pp. 193–200, 2010.

[14] J.-Y. Kim, J.-H. Sohn, J.-M. Choi et al., "Alveolar macrophages play a key role in cockroach-induced allergic inflammation via TNF-α pathway," *PLoS ONE*, vol. 7, no. 10, Article ID e47971, 2012.

[15] D. Laveti, M. Kumar, R. Hemalatha et al., "Anti-inflammatory treatments for chronic diseases: a review," *Inflammation & Allergy-Drug Targets*, vol. 12, no. 5, pp. 349–361, 2013.

[16] H. S. Lee, K.-H. Jung, S.-W. Hong et al., "Morin protects acute liver damage by carbon tetrachloride (CCl_4) in rat," *Archives of Pharmacal Research*, vol. 31, no. 9, pp. 1160–1165, 2008.

[17] V. Sivaramakrishnan and S. N. Devaraj, "Morin regulates the expression of NF-κB-p65, COX-2 and matrix metalloproteinases in diethylnitrosamine induced rat hepatocellular carcinoma," *Chemico-Biological Interactions*, vol. 180, no. 3, pp. 353–359, 2009.

[18] R. Kapoor and P. Kakkar, "Protective role of morin, a flavonoid, against high glucose induced oxidative stress mediated apoptosis in primary rat hepatocytes," *PLoS ONE*, vol. 7, no. 8, Article ID e41663, 2012.

[19] M. Kumar, T. Ahmad, A. Sharma et al., "Let-7 microRNA-mediated regulation of IL-13 and allergic airway inflammation," *Journal of Allergy and Clinical Immunology*, vol. 128, no. 5, pp. 1077–1085.e10, 2011.

[20] G. Gloire, S. Legrand-Poels, and J. Piette, "NF-κB activation by reactive oxygen species: fifteen years later," *Biochemical Pharmacology*, vol. 72, no. 11, pp. 1493–1505, 2006.

[21] H. Bibi, V. Vinokur, D. Waisman et al., "Zn/Ga-DFO iron-chelating complex attenuates the inflammatory process in a mouse model of asthma," *Redox Biology*, vol. 2, pp. 814–819, 2014.

[22] R. Konno, H. Yamakawa, H. Utsunomiya, K. Ito, S. Sato, and A. Yajima, "Expression of survivin and Bcl-2 in the normal human endometrium," *Molecular Human Reproduction*, vol. 6, no. 6, pp. 529–534, 2000.

[23] C.-D. Lu, D. C. Altieri, and N. Tanigawa, "Expression of a novel antiapoptosis gene, survivin, correlated with tumor cell apoptosis and p53 accumulation in gastric carcinomas," *Cancer Research*, vol. 58, no. 9, pp. 1808–1812, 1998.

[24] I.-T. Lee and C.-M. Yang, "Role of NADPH oxidase/ROS in pro-inflammatory mediators-induced airway and pulmonary diseases," *Biochemical Pharmacology*, vol. 84, no. 5, pp. 581–590, 2012.

[25] N. Baregamian, J. Song, C. E. Bailey, J. Papaconstantinou, B. M. Evers, and D. H. Chung, "Tumor necrosis factor-α and apoptosis signal-regulating kinase 1 control reactive oxygen species release, mitochondrial autophagy and c-Jun N-terminal kinase/p38 phosphorylation during necrotizing enterocolitis," *Oxidative Medicine and Cellular Longevity*, vol. 2, no. 5, pp. 297–306, 2009.

[26] J. T. Olin and M. E. Wechsler, "Asthma: pathogenesis and novel drugs for treatment," *The British Medical Journal*, vol. 349, Article ID g5517, 2014.

[27] H. McClafferty, "An overview of integrative therapies in asthma treatment," *Current Allergy and Asthma Reports*, vol. 14, no. 10, p. 464, 2014.

[28] M. del Carmen Vennera and C. Picado, "Novel diagnostic approaches and biological therapeutics for intrinsic asthma," *International Journal of General Medicine*, vol. 8, no. 7, pp. 365–371, 2014.

[29] W. W. Busse and R. F. Lemanske Jr., "Asthma," *The New England Journal of Medicine*, vol. 344, no. 5, pp. 350–362, 2001.

[30] C. H. Fanta, "Asthma," *The New England Journal of Medicine*, vol. 360, no. 10, pp. 1002–1014, 2009.

[31] A. Page-McCaw, A. J. Ewald, and Z. Werb, "Matrix metalloproteinases and the regulation of tissue remodelling," *Nature Reviews Molecular Cell Biology*, vol. 8, no. 3, pp. 221–233, 2007.

[32] K. J. Greenlee, Z. Werb, and F. Kheradmand, "Matrix metalloproteinases in lung: multiple, multifarious, and multifaceted," *Physiological Reviews*, vol. 87, no. 1, pp. 69–98, 2007.

[33] G. V. Halade, Y.-F. Jin, and M. L. Lindsey, "Matrix metalloproteinase (MMP)-9: a proximal biomarker for cardiac remodeling and a distal biomarker for inflammation," *Pharmacology and Therapeutics*, vol. 139, no. 1, pp. 32–40, 2013.

[34] Y. N. Liu, W. J. Zha, Y. Ma et al., "Galangin attenuates airway remodelling by inhibiting TGF-β1-mediated ROS generation and MAPK/Akt phosphorylation in asthma," *Scientific Reports*, vol. 9, no. 5, Article ID 11758, 2015.

[35] J. Swierkot, K. Bogunia-Kubik, B. Nowak et al., "Analysis of associations between polymorphisms within genes coding for tumour necrosis factor (TNF)-alpha and TNF receptors and responsiveness to TNF-alpha blockers in patients with rheumatoid arthritis," *Joint Bone Spine*, vol. 82, no. 2, pp. 94–99, 2015.

[36] J. C. Peng, J. Shen, and Z. H. Ran, "Novel agents in the future: therapy beyond anti-TNF agents in inflammatory bowel disease," *Journal of Digestive Diseases*, vol. 15, no. 11, pp. 585–590, 2014.

[37] K. Sato, M. Takaishi, S. Tokuoka, and S. Sano, "Involvement of TNF-α converting enzyme in the development of psoriasis-like lesions in a mouse model," *PLoS ONE*, vol. 9, no. 11, Article ID e112408, 2014.

[38] J. Ji, I. von Schéele, J. Bergström et al., "Compartment differences of inflammatory activity in chronic obstructive pulmonary disease," *Respiratory Research*, vol. 15, no. 1, article 104, 2014.

[39] G. Rajashekhar, M. Shivanna, U. B. Kompella, Y. Wang, and S. P. Srinivas, "Role of MMP-9 in the breakdown of barrier integrity of the corneal endothelium in response to TNF-α," *Experimental Eye Research*, vol. 122, no. 5, pp. 77–85, 2014.

[40] A. Yabluchanskiy, Y. Ma, R. P. Iyer, M. E. Hall, and M. L. Lindsey, "Matrix metalloproteinase-9: many shades of function in cardiovascular disease," *Physiology*, vol. 28, no. 6, pp. 391–403, 2013.

[41] M. C. Miraglia, R. Scian, C. G. Samartino et al., "*Brucella abortus* induces TNF-α-dependent astroglial MMP-9 secretion through mitogen-activated protein kinases," *Journal of Neuroinflammation*, vol. 10, article 47, 2013.

[42] S.-J. Suh, C.-H. Kwak, T.-W. Chung et al., "Pimaric acid from *Aralia cordata* has an inhibitory effect on TNF-α-induced MMP-9 production and HASMC migration via down-regulated NF-κB and AP-1," *Chemico-Biological Interactions*, vol. 199, no. 2, pp. 112–119, 2012.

[43] R. Pawliczak, "The role of radical oxygen species in airway inflammation," *Polski Merkuriusz Lekarski*, vol. 14, no. 84, pp. 493–496, 2003.

[44] L. Zuo, N. P. Otenbaker, B. A. Rose, and K. S. Salisbury, "Molecular mechanisms of reactive oxygen species-related pulmonary inflammation and asthma," *Molecular Immunology*, vol. 56, no. 1-2, pp. 57–63, 2013.

[45] W. Dröge, "Free radicals in the physiological control of cell function," *Physiological Reviews*, vol. 82, no. 1, pp. 47–95, 2002.

[46] S. Sakon, X. Xue, M. Takekawa et al., "NF-κB inhibits TNF-induced accumulation of ROS that mediate prolonged MAPK activation and necrotic cell death," *The EMBO Journal*, vol. 22, no. 15, pp. 3898–3909, 2003.

[47] H. Kamata, S.-I. Honda, S. Maeda, L. Chang, H. Hirata, and M. Karin, "Reactive oxygen species promote TNFα-induced death and sustained JNK activation by inhibiting MAP kinase phosphatases," *Cell*, vol. 120, no. 5, pp. 649–661, 2005.

[48] Y. Zhang and X. Li, "Lipopolysaccharide-regulated production of bone sialoprotein and interleukin-8 in human periodontal ligament fibroblasts: the role of toll-like receptors 2 and 4 and the MAPK pathway," *Journal of Periodontal Research*, vol. 50, no. 2, pp. 141–151, 2015.

[49] I.-T. Lee, R.-H. Shih, C.-C. Lin, J.-T. Chen, and C.-M. Yang, "Role of TLR4/NADPH oxidase/ROS-activated p38 MAPK in VCAM-1 expression induced by lipopolysaccharide in human renal mesangial cells," *Cell Communication and Signaling*, vol. 10, article 33, 2012.

[50] K.-B. Roh, E. Jung, D. Park, and J. Lee, "Fumaric acid attenuates the eotaxin-1 expression in TNF-α-stimulated fibroblasts by suppressing p38 MAPK-dependent NF-κB signaling," *Food and Chemical Toxicology*, vol. 58, no. 1, pp. 423–431, 2013.

[51] J. K. Patel, R. L. Clifford, K. Deacon, and A. J. Knox, "Ciclesonide inhibits TNFα- and IL-1β-induced monocyte chemotactic protein-1 (MCP-1/CCL2) secretion from human airway smooth muscle cells," *American Journal of Physiology: Lung Cellular and Molecular Physiology*, vol. 302, no. 8, pp. L785–L792, 2012.

[52] C. Hollander, B. Sitkauskiene, R. Sakalauskas, U. Westin, and S. M. Janciauskiene, "Serum and bronchial lavage fluid concentrations of IL-8, SLPI, sCD14 and sICAM-1 in patients with COPD and asthma," *Respiratory Medicine*, vol. 101, no. 9, pp. 1947–1953, 2007.

[53] K. S. Lee, S. M. Jin, H. J. Kim, and Y. C. Lee, "Matrix metalloproteinase inhibitor regulates inflammatory cell migration by reducing ICAM-1 and VCAM-1 expression in a murine model of toluene diisocyanate-induced asthma," *The Journal of Allergy and Clinical Immunology*, vol. 111, no. 6, pp. 1278–1284, 2003.

[54] I. Rahman and W. MacNee, "Regulation of redox glutathione levels and gene transcription in lung inflammation: therapeutic approaches," *Free Radical Biology and Medicine*, vol. 28, no. 9, pp. 1405–1420, 2000.

[55] R. F. Schwabe and D. A. Brenner, "Mechanisms of liver injury. I. TNF-α-induced liver injury: role of IKK, JNK, and ROS pathways," *American Journal of Physiology—Gastrointestinal and Liver Physiology*, vol. 290, no. 4, pp. G583–G589, 2006.

[56] I. Rahman, B. Mulier, P. S. Gilmour et al., "Oxidant-mediated lung epithelial cell tolerance: the role of intracellular glutathione and nuclear factor-kappaB," *Biochemical Pharmacology*, vol. 62, no. 6, pp. 787–794, 2001.

[57] M. Zafarullah, W. Q. Li, J. Sylvester, and M. Ahmad, "Molecular mechanisms of *N*-acetylcysteine actions," *Cellular and Molecular Life Sciences*, vol. 60, no. 1, pp. 6–20, 2003.

[58] G. Kano, M. Almanan, B. S. Bochner, and N. Zimmermann, "Mechanism of Siglec-8-mediated cell death in IL-5-activated eosinophils: role for reactive oxygen species-enhanced MEK/ERK activation," *Journal of Allergy and Clinical Immunology*, vol. 132, no. 2, pp. 437–445, 2013.

[59] C. G. Pham, S. Papa, C. Bubici, F. Zazzeroni, and G. Franzoso, "Oxygen JNKies: phosphatases overdose on ROS," *Developmental Cell*, vol. 8, no. 4, pp. 452–454, 2005.

[60] M. Sano, K. Fukuda, T. Sato et al., "ERK and p38 MAPK, but not NF-κB, are critically involved in reactive oxygen species-mediated induction of IL-6 by angiotensin II in cardiac fibroblasts," *Circulation Research*, vol. 89, no. 8, pp. 661–669, 2001.

[61] E. Youl, R. Magous, G. Cros, and C. Oiry, "MAP Kinase cross talks in oxidative stress-induced impairment of insulin secretion. Involvement in the protective activity of quercetin," *Fundamental and Clinical Pharmacology*, vol. 28, no. 6, pp. 608–615, 2014.

[62] I.-T. Lee, S.-F. Luo, C.-W. Lee et al., "Overexpression of HO-1 protects against TNF-α-mediated airway inflammation by down-regulation of TNFR1-dependent oxidative stress," *The American Journal of Pathology*, vol. 175, no. 2, pp. 519–532, 2009.

Hindawi Publishing Corporation
Oxidative Medicine and Cellular Longevity
Volume 2016, Article ID 3981790, 9 pages
http://dx.doi.org/10.1155/2016/3981790

Research Article

Central Infusion of Angiotensin II Type 2 Receptor Agonist Compound 21 Attenuates DOCA/NaCl-Induced Hypertension in Female Rats

Shu-Yan Dai,[1] Yu-Ping Zhang,[2] Wei Peng,[3] Ying Shen,[1] and Jing-Jing He[1]

[1]*Department of Obstetrics and Gynecology, Shengjing Hospital, China Medical University, Shenyang 110004, China*
[2]*Department of Pathophysiology, Hebei North University, Zhangjiakou, Hebei 075000, China*
[3]*Life Science Research Center, Hebei North University, Zhangjiakou, Hebei 075000, China*

Correspondence should be addressed to Shu-Yan Dai; daishy2014@163.com

Received 7 August 2015; Revised 11 September 2015; Accepted 13 September 2015

Academic Editor: Hanjun Wang

The present study investigated whether central activation of angiotensin II type 2 receptor (AT2-R) attenuates deoxycorticosterone acetate (DOCA)/NaCl-induced hypertension in intact and ovariectomized (OVX) female rats and whether female sex hormone status has influence on the effects of AT2-R activation. DOCA/NaCl elicited a greater increase in blood pressure in OVX females than that in intact females. Central infusion of compound 21, a specific AT2-R agonist, abolished DOCA/NaCl pressor effect in intact females, whereas same treatment in OVX females produced an inhibitory effect. Real-time RT-PCR analysis revealed that DOCA/NaCl enhanced the mRNA expression of hypertensive components including AT1-R, ACE-1, and TNF-α in the paraventricular nucleus of hypothalamus in both intact and OVX females. However, the mRNA expressions of antihypertensive components such as AT2-R, ACE-2, and IL-10 were increased only in intact females. Central AT2-R agonist reversed the changes in the hypertensive components in all females, while this agonist further upregulated the expression of ACE2 and IL-10 in intact females, but only IL-10 in OVX females. These results indicate that brain AT2-R activation plays an inhibitory role in the development of DOCA/NaCl-induced hypertension in females. This beneficial effect of AT2-R activation involves regulation of renin-angiotensin system and proinflammatory cytokines.

1. Introduction

It has been well documented that activation of angiotensin II type 2 receptor (AT2-R) plays a critical role in antagonizing AT1-R overactivity, particularly during pathological conditions [1–3]. Most of early studies looking at short-term or long-term effects of AT2-R revealed that peripheral AT2-R activation did not have an antihypertensive effect but enhanced tissue protection in various hypertensive models [1, 2]. However, recent studies implicated that AT2-R in the central nervous system (CNS) may exert more critical actions on blood pressure (BP) regulation [4]. AT2-R has been shown to reside or be in close proximity to CNS nuclei involved in cardiovascular regulation, including the solitary tract nucleus (NTS), rostral ventrolateral medulla (RVLM), subfornical organ (SFO), and paraventricular nucleus of hypothalamus (PVN) [5, 6]. In particular, within the PVN, the AT2-R-containing neuron fibres and terminals appear to synapse onto preautonomic neuron cell bodies, suggesting that AT2-R can influence sympathetic outflow and BP through these connections [6]. Central blockade of AT2-R in normal male animals attenuates baroreflex control of renal sympathetic nerve activity (RSNA) and heart rate (HR) [7]. In contrast, central activation of AT2-R by intracerebroventricular (icv) infusion of Compound 21 (C21), the first selective nonpeptide AT2-R agonist, or AT2-R overexpression in the RVLM of heart failure animals leads to sympathoinhibition [8, 9], which is accompanied with upregulation of neuronal nitric oxide synthase and downregulation of AT1-R in the several nuclei involved in regulation of BP and sympathetic activity including the PVN [9]. Moreover, central administration of C21 lowered BP and plasma norepinephrine levels in both

spontaneous hypertensive (SHR) and WKY male rats. These effects were abolished by coadministration of the AT2-R antagonist PD123319 or the nitric oxide synthase inhibitor Nω-nitro-L-arginine methyl ester (L-NAME) hydrochloride [10]. These results indicate that central AT2-R plays an important role in regulation of BP and sympathetic activity in both physiological and pathophysiological states. However, the precise mechanisms underlying the antihypertensive effect of central AT2-R activation remain unclear.

Accumulating evidence indicates that the expression and function of the AT2-R are sexually different. Female sex hormones, especially estrogen, increase the expression of the AT2-R but inhibit the AT1-R expression [11–14]. A series of studies from Denton and colleagues have shown that chronic infusion of a low dose of angiotensin (ANG) II results in an increase in BP in male rats but a decrease in BP in female rats [15]. This depressor effect of ANG II in females is via an AT2-R-mediated and an estrogen-dependent mechanism [15]. Moreover, the AT2-R mediates the normal midgestational decrease in BP and contributes to BP regulation during late gestation [16]. These findings suggest that the BP is differentially regulated by the AT2-R in females as compared with males and support an enhanced role for AT2-R in regulating BP in females. However, these studies focused on the regulating effects of AT2-R in peripheral cardiovascular tissues such as kidney and vasculature. There are few animal studies evaluating the effects of central AT2-R activation on BP regulation in female rats and the influence of female sex hormone status on the effects of central AT2-R activation.

Downregulation of renin-angiotensin system (RAS) hypertensive components, upregulation of RAS antihypertensive components, and anti-inflammation have been shown to be important features of the AT2-R underlying improved outcome in experimental disease models [16–23]. Our previous study has demonstrated that central blockade of AT2-R augments deoxycorticosterone acetate (DOCA)/NaCl-induced pressor effect in females through modulating expression of RAS components and proinflammatory cytokines in the PVN [24]. In the present study, we investigated whether central activation of AT2-R by icv infusion of C21 attenuates DOCA/NaCl-induced hypertension in female rats and whether female sex hormone status has influence on the effects of AT2-R activation. To do so, we employed *in vivo* telemetric recording of BP and real-time quantitative reverse transcription polymerase chain reaction (RT-PCR) assessing mRNA expression of several RAS components and proinflammatory cytokines in the PVN to determine the effects of central activation of AT2-R on the development of DOCA/salt-induced hypertension in intact and ovariectomized (OVX) female rats.

2. Methods

2.1. Animals. Thirty-six female rats (Wistar, 10–12 wk old) were purchased from Beijing Laboratory Animal Research Center (Beijing, China) and were maintained at an animal facility under barrier-sustained conditions with 12 h light/dark cycle at standard conditions (temperature: 23±2°C, relative humidity: 40%–80%) and free access to standard rat chow *ad libitum*. All animal procedures were reviewed and approved by the China Medical University and the Hebei North University Institutional Animal Care and Use Committee conforming to US National Institutes of Health guidelines.

The female rats were prepared with a lateral ventricular cannula, osmotic minipumps, and DOCA pellet for intracerebroventricular (icv) and subcutaneous drug infusions and with telemetry probes for continuous BP recording, as previously described [24]. Water was also changed to 1% NaCl as the sole drinking fluid. 1% NaCl intakes were measured daily. Thus, the primary study groups ($n = 6$/group) were the following: (1) intact female icv C21 (0.25 μg/h, SPS Alfachem) + 1% NaCl; (2) intact female icv vehicle (V) + DOCA/NaCl; (3) intact female icv C21 + DOCA/NaCl; (4) OVX female icv C21 (0.25 μg/h) + 1% NaCl; (5) OVX female icv vehicle (V) + DOCA/NaCl; and (6) OVX female icv C21 + DOCA/NaCl.

Animals assigned to DOCA treatment were subcutaneously implanted with a DOCA pellet (150 mg/kg, Sigma-Aldrich, USA). After the physiological studies were finished, brains were taken and PVN tissue was collected by micropunching for determining mRNA expression of RAS components and proinflammatory cytokines.

2.2. Ovariectomy. Ten days before implantation of telemetry probes, bilateral ovariectomy was performed in female rats anesthetized with pentobarbital sodium (1%, 50 mg/kg). A single 2-3 cm dorsal midline incision was made in the skin and underlying muscles. The ovaries were isolated, tied-off with sterile suture, and removed, and the incisions were closed.

2.3. Telemetry Probe Implantation. Under anesthetization with pentobarbital sodium (1%, 50 mg/kg), rats were implanted with telemetry transmitters (TA11-PA40, DSI) through the femoral artery for continuous monitoring of BP and HR.

2.4. Chronic Icv Cannula, Osmotic Pump, and DOCA Pellet Implantation. DOCA pellets were made by mixing 30–40 mg DOCA (adjusted by animal body weight) into 1 mL of silicone (Sylgard 184 silicone elastomer base; Dow Corning, Midland, MI). Once the DOCA was homogenously mixed into the silicone, silicone elastomer curing agent (0.2 mL) was added. The DOCA implants were allowed to cure at room temperature for 24 hours and were then stored at 4°C until implantation.

After baseline BP and HR recordings were made, the rats were again anesthetized with pentobarbital sodium, and the icv cannula with an osmotic pump (model 2004, 0.25 μL/h for 4 weeks, ALZET Brain Infusion Kits, Alzet Co.) was implanted into the right lateral ventricle (the coordinates 1.0 mm caudal, 1.5 mm lateral to bregma, and 4.5 mm below the skull surface) for chronic infusion of vehicle or C21 for 4 weeks. At the same time, a pellet of DOCA (150 mg/kg) was implanted subcutaneously in the back and tap water was changed to 1% NaCl.

Table 1: Sequences for primers.

Gene	Gene ID	Primers	Sequences
AT1-R	NM_030985	Forward	5′-CTCAAGCCTGTCTACGAAAATGAG-3′
		Reverse	5′-GTGAATGGTCCTTTGGTCGT-3′
AT2-R	NM_012494	Forward	5′-TGCTGTTGTGTTGGCATTCA-3′
		Reverse	5′-ATCCAAGAAGGTCAGAACATGGA-3′
ACE-1	NM_012544	Forward	5′-TTTGCTACACAAATGGCACTTGT-3′
		Reverse	5′-CGGGACGTGGCCATTATATT-3′
ACE-2	NM_001012006	Forward	5′-TTGAACCAGGATTGGACGAAA-3′
		Reverse	5′-GCCCAGAGCCTACGATTGTAGT-3′
TNF-α	NM_013693	Forward	5′-GCATGATCCGCGACGTGGAA-3′
		Reverse	5′-AGATCCATGCCGTTGGCCAG-3′
IL-10	NM_012854	Forward	5′-GTTGCCAAGCCTTGTCAGAAA-3′
		Reverse	5′-TTTCTGGGCCATGGTTCTCT-3′
GAPDH	NM_017008	Forward	5′-GCCAAAAGGGTCATCATCTC-3′
		Reverse	5′-GGCCATCCACAGTCTTCT-3′

AT-R, angiotensin receptor; ACE, angiotensin converting enzyme; TNF-α, tumor necrosis factor-α; IL-10, interleukin-10.

2.5. Real-Time RT-PCR Analysis. At the end of experiments, the animals were euthanized with an overdose of pentobarbital. The brain was removed and quickly frozen on dry ice. Six serial coronal sections (100 μm) were cut through the hypothalamus at the level of the PVN using a cryostat and the PVN region was punched using a blunt 18-gauge needle as previously described [25].

The total RNA was extracted using RNeasy Mini Kit (Qiagen, Valencia, CA, USA) and reverse transcribed into cDNA. mRNA levels for RAS components [AT1-R, AT2-R, angiotensin-converting enzyme- (ACE-) 1, and ACE-2], inflammatory cytokines [tumor necrosis factor- (TNF-)α and interleukin- (IL-)10], and GAPDH were analyzed with SYRB Green real-time PCR. The sequences for the primers are summarized in Table 1. Real-time RT-PCR was performed with the ABI prism 7300 Sequence Detection System (Applied Biosystems, Carlsbad, CA). The values were corrected by GAPDH and the final concentration of mRNA was calculated using the formula $x = 2^{-\Delta\Delta Ct}$, where x is fold difference relative to control.

2.6. Data Analysis. MAP and HR are presented as mean daily values. Differences for mean arterial pressure (MAP) and HR were calculated for each animal based on the mean of the 3-day baseline subtracted from the mean of the final 5 days of treatment. Two-way ANOVA analysis for the experimental groups was then conducted on the means of calculated differences. After establishing a significant ANOVA, *post hoc* analyses were performed with Tukey multiple comparison tests between pairs of mean changes. The same statistical methods were used to analyze the changes in HR, 1% NaCl intake, and differences in mRNA expression of the RAS components and cytokines in the PVN. All data are expressed as means ± SE. Statistical significance was set at $P < 0.05$.

3. Results

3.1. Effect of Icv C21 on DOCA/NaCl-Induced Hypertension in Intact Female Rats. Icv infusion of C21 plus 1% NaCl had no effects on basal MAP (100.9 ± 1.5 mmHg) and HR (385.6 ± 7.9 beats/min) in intact female rats. DOCA/salt treatment elicited significant increases in MAP in intact females (Δ12.1 ± 1.5 mmHg, $P < 0.05$). Icv infusion of C21 abolished this pressor effect induced by DOCA/NaCl (Δ4.0 ± 1.9 mmHg, $P < 0.05$, Figures 1(a) and 3(a)). In contrast, systemic DOCA infusion resulted in significant, comparable decrease in HR (Figures 1(b) and 3(b), $P > 0.05$) in all groups when compared to intact females receiving C21 plus 1% NaCl.

3.2. Effect of Icv C21 on DOCA/NaCl-Induced Hypertension in OVX Female Rats. OVX elicited a slight, but significant, increase in baseline MAP (105.8 ± 1.9 mmHg) but decrease in baseline HR (356.8 ± 8.1 beats/min) when compared with intact females ($P < 0.05$). Icv infusion of C21 plus 1% NaCl had no effects on these basal MAP and HR in OVX females. After 4 weeks of DOCA/salt treatment, MAP was remarkably elevated (Δ23.8 ± 2.9 mmHg, $P < 0.05$ versus baseline and intact female group with icv vehicle plus systemic DOCA). Icv infusion of C21 for 4 weeks also attenuated the DOCA/NaCl pressor effect (Δ11.6 ± 1.6 mmHg, $P < 0.05$, Figures 2(a) and 3(a)). Systemic DOCA infusions produced significant, comparable decrease in HR in all groups (Figures 2(b) and 3(b)).

3.3. Effect of DOCA Infusion on 1% NaCl Intake. There was no difference in 1% NaCl intake between intact and OVX female rats when given icv infusions of C21 alone. Systemic infusion of DOCA produced a significant, but comparable, increase in 1% NaCl intake in all groups of rats (Figure 4).

3.4. Effect of Icv C21 on mRNA Expression of RAS Components and Inflammatory Cytokines in the PVN. In PVN tissue

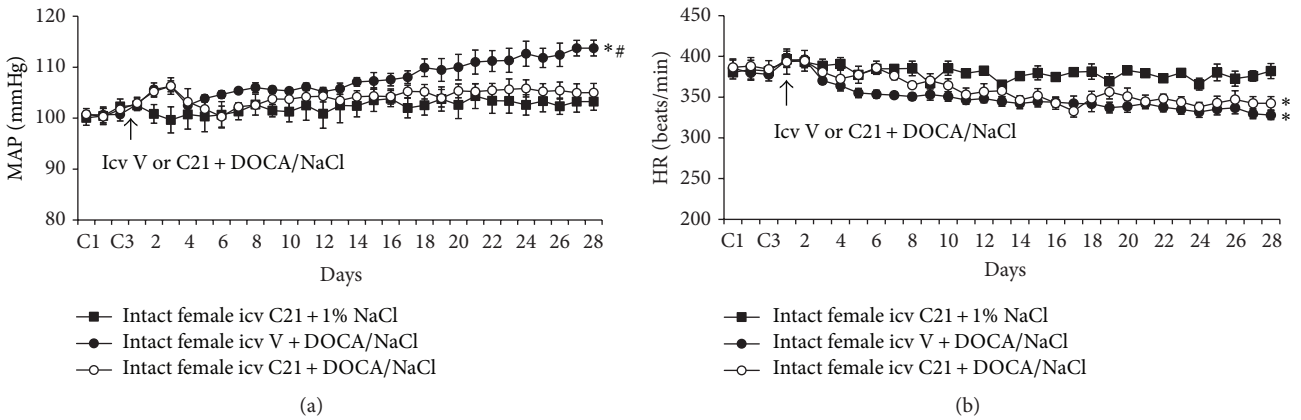

Figure 1: The effect of central infusion of AT2-R agonist, Compound 21 (C21), on DOCA/NaCl-induced increase in blood pressure in intact female rats. Daily mean arterial pressure (MAP) (a) and heart rate (HR) (b) before and during DOCA/NaCl treatment in intact females with or without central infusion of C21. $n = 6$ per group; $^{*}P < 0.05$ compared to baseline; $^{\#}P < 0.05$ compared to intact females with central infusion of C21.

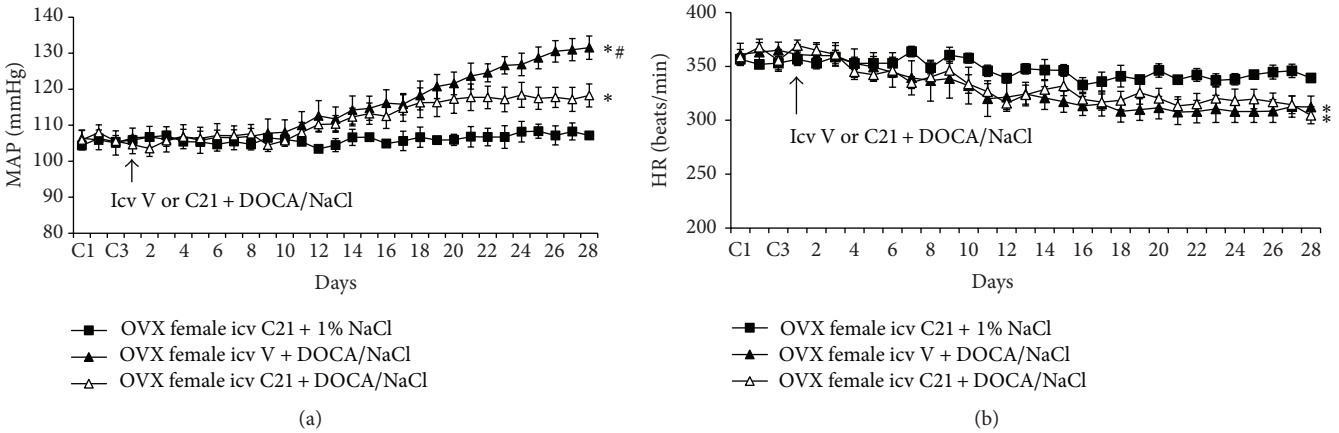

Figure 2: The effect of central infusion of AT2-R agonist, C21, on DOCA/NaCl-induced hypertension in ovariectomized (OVX) rats. Daily mean arterial pressure (MAP) (a) and heart rate (HR) (b) before and during DOCA/NaCl treatment in OVX females with or without central infusion of C21. $n = 6$ per group; $^{*}P < 0.05$ compared to baseline or central infusion of C21 alone; $^{\#}P < 0.05$ compared to OVX females with central C21 plus DOCA/NaCl.

collected from intact females, DOCA/NaCl upregulated the mRNA expression of both hypertensive components (AT1-R, ACE1, and TNF-α) and antihypertensive components (AT2-R, ACE2, and IL-10) within RAS and inflammatory cytokines when compared with controls ($P < 0.05$). Central infusion of C21 reversed the changes in mRNA expression of AT1-R, ACE1, and TNF-α. In contrast, the mRNA expressions of ACE2 and IL-10 were further increased ($P < 0.05$, Figure 5) while the mRNA expression of AT2-R remained higher.

Ovariectomy alone had no effect on the mRNA expression of RAS components and inflammatory cytokines in the PVN. In these OVX females, DOCA infusion resulted in a significant increase in the mRNA expression of AT1-R, ACE1, and TNF-α in the PVN ($P < 0.05$, Figure 5) while the expressions of AT2-R, ACE2, and IL-10 were not altered. Central infusion of C21 reduced these increased expressions of AT1-R, ACE1, and TNF-α while IL-10 expression was elevated during DOCA infusion ($P < 0.05$, Figure 5). The mRNA expression of ACE2 and AT2-R remained unchanged.

4. Discussion

The major findings of the present study are as follows: (1) central activation of AT2-R abolished DOCA/NaCl pressor effect in intact females, whereas same treatment in OVX females produced an inhibitory effect; (2) DOCA/NaCl treatment resulted in a greater increase in BP in OVX females, which was accompanied with increased mRNA expression of AT1-R, ACE1, and TNF-α, but with no altered expression of AT2-R, ACE2, and IL-10 in the PVN when compared to intact females; these changes in gene expression may be responsible for the augmentation of pressor effects induced by DOCA/NaCl in OVX females; and (3) central infusion of AT2-R agonist C21 reversed the changes in the

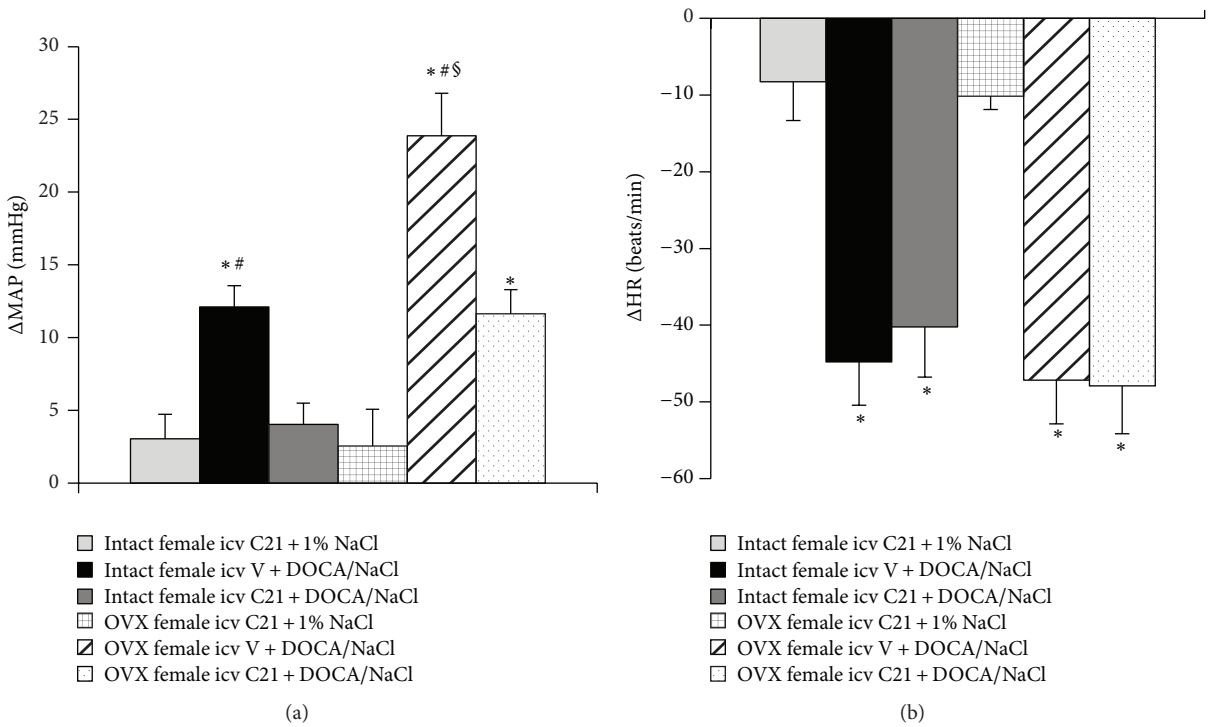

Figure 3: Average changes in MAP (a) and HR (b) produced by DOCA/NaCl treatment in intact and OVX female rats. $n = 6$ per group; $^{*}P < 0.05$ compared to intact or OVX females with central infusion of C21 alone; $^{\#}P < 0.05$ compared to intact or OVX females with central C21 plus DOCA/NaCl; $^{\S}P < 0.05$ compared to intact females with DOCA/NaCl.

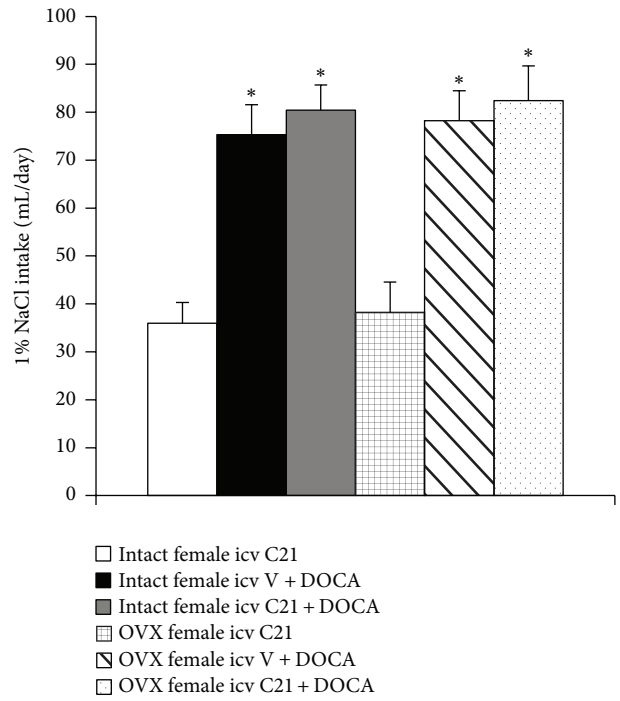

Figure 4: Mean daily 1% NaCl intake during DOCA infusions in female rats treated with central vehicle or C21. $n = 6$ per group; $^{*}P < 0.05$ compared to intact or OVX females with central infusion of C21 alone.

hypertensive components in all females, while this agonist further upregulated the expression of ACE2 and IL-10 in intact females, but only IL-10 in OVX females, suggesting different mechanism involving the AT2-R regulation of anti-hypertensive components of the RAS between intact and OVX females. These results indicate that activation of AT2-R in the CNS plays an inhibitory role in the development of DOCA/salt-induced hypertension in females and that this antihypertensive effect involves regulation of the RAS and proinflammatory cytokines.

Whether AT2-R activation alone is sufficient to lower BP has been debated. Some studies showed the antihypertensive effect of systemic AT2-R activation only in the presence of AT1-R blockers or ACE inhibitors [1, 2], whereas others demonstrated a direct depressor effect of systemic AT2-R activation [20, 23]. Hussain and colleagues reported that oral administration of C21 prevents salt-sensitive hypertension in obese Zucker rats and that this protective effect of C21 is associated with activation of renal AT2-R and improvement of renal function [23]. However, Hilliard et al. did not observe an antihypertensive effect of AT2-R activation in male SHRs [26]. Recent studies revealed that activation of AT2-R locally within the brain, without manipulating AT1-R or ACE activity, results in a BP lowering effect. Gao and colleagues reported that there is robust expression of AT2-R in the brain and that central overexpression or activation of AT2-R by C21 reduces sympathetic outflow and BP in

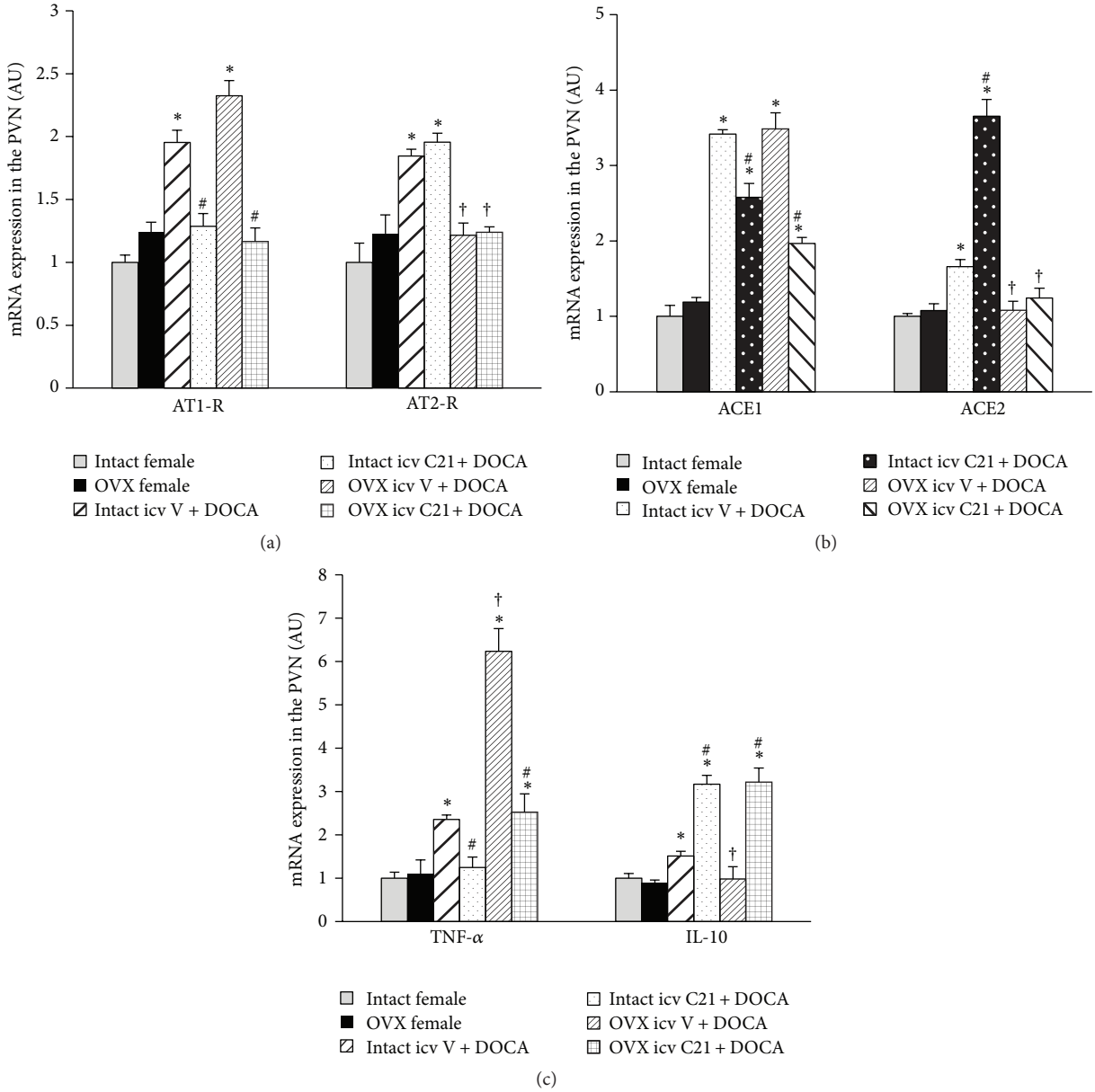

Figure 5: mRNA levels for renin-angiotensin system components (AT1-R and AT2-R (a); ACE1 and ACE2 (b)) and inflammatory cytokines (TNF-α and IL-10 (c)) in the PVN in each group of females with or without central infusion of C21 during DOCA/NaCl treatment. Values are mean ± SEM and expressed as a fold change relative to corresponding control (intact females). $n = 6$ per group; $^{*}P < 0.05$ compared to control intact females; $^{\#}P < 0.05$ compared to intact and OVX females with central vehicle plus systemic DOCA/NaCl. $^{\dagger}P < 0.05$ compared to intact females with central vehicle plus systemic DOCA/NaCl.

male rats [5, 6, 8, 9]. Brouwers and colleagues also demonstrated central administration of C21 lowered BP and plasma norepinephrine levels in both spontaneous hypertensive and WKY male rats [10]. These results suggest that central AT2-R negatively regulates neuronal function and cardiovascular activity, thereby reducing BP.

In human and animal hypertensive models, sex differences in the regulation of BP have been established, possibly through differences in the function of the RAS and in response to stimulation and inhibition of RAS between males and females. Accumulating evidence shows that the expression and function of the AT2-R are enhanced in females [11–13], suggesting that the activation of AT2-R in females may play a more potentiated role. In the female rats, the elevated BP induced by systemic ANG II infusion was markedly reduced when C21 was concomitantly infused intrarenally [27]. Hilliard et al. reported that AT2-R stimulation increases renal function in female, but not in male SHR rats [26]. Our previous studies also showed that central blockade of AT2-R augmented increase in the BP induced by DOCA/NaCl in

female while the same treatment had no effect in male rats, suggesting that central AT2-R in females plays an enhanced protective role [24]. The present study extends our previous work by showing that icv infusion of AT2-R agonist abolished and inhibited DOCA/NaCl pressor effect in intact and OVX females, respectively. This study provides direct evidence that activation of central AT2-R is also sufficient to reduce the increase in BP induced by DOCA/NaCl in females.

Within the RAS, ACE1/ANG II/AT1-R has been considered as a hypertensive axis while ACE2/ANG-(1–7)/Mas-R and ANG II/AT2-R have been viewed as an antihypertensive axis [28]. Likewise, the proinflammatory cytokines such as TNF-α are involved in the development and the maintenance of hypertension. In contrast, IL-10 plays a protective role against hypertension [29–31]. It has been established that female sex hormones play a critical role in regulating the expression of the RAS and cytokines, with downregulation of hypertensive components including AT1-R, ACE1, and TNF-α and upregulation of antihypertensive components including AT2-R, ACE2, and IL-10 [11, 16, 17]. In the present study, we found that DOCA/NaCl treatment upregulated expression of AT1-R, ACE1, and TNF-α in the PVN in both intact and OVX females, while the mRNA expression of AT2-R, ACE2, and IL-10 was upregulated only in intact females, but not in OVX females. Given the counterregulatory effects of the AT2-R, ACE2, and IL-10 on AT1-R, ACE1, and TNF-α overactivity, these results implicate that increased expression of AT2-R, ACE2, and IL-10 may play a protective role in the development of hypertension in intact females. The results also suggest that the female sex hormone status makes a different way in the RAS and cytokines where intact female and OVX female respond to physiological and pathophysiological stimulations, and female sex hormones shift the balance of the RAS and proinflammatory cytokines to favor the antihypertensive elements.

It has been shown that AT2-R is expressed to a greater extent in the kidney and vasculature of female rats and mice when compared to respective males [32]. In the CNS, Rodriguez-Perez and colleagues reported that the basal mRNA and protein expressions of AT2-R in the substantia nigra were higher in females with high level of estrogen during estrous cycle than in males. Estrogen replacement reversed ovariectomy-induced decrease in AT2-R expression in same nucleus [12, 13]. Our previous and current study showed only a slight, but not significant increase in AT2-R expression in the PVN of female rats when compared to male rats [24]. However, after DOCA/NaCl treatment, AT2-R expression in the PVN was significantly increased in intact females, but not in males and OVX females. These results suggest that female sex hormone status has an influence on the expression of AT2-R, especially under the pathophysiological condition, and that AT2-R plays a role in opposing the pressor actions induced by hypertensive component activation in females via an estrogen-dependent mechanism.

Accumulating evidence demonstrates that long-term AT2-R activation increases kidney ACE2 expression and activity, the Mas receptor (MasR), and its ligand ANG-(1–7) as well as IL-10 level but attenuates AT1-R and TNF-α expression in obese Zucker rats. Conversely, blockade of AT2-R by PD123,319 reversed the changes of these genes or agents [18–20, 23]. In *in vitro* studies, AT2-R stimulation exerts an anti-inflammatory action in renal epithelial cells, THP-1 macrophages, and human monocytic cells via reduced TNF-α and enhanced IL-10 production. IL-10 was critical for the anti-inflammatory effects of AT2-R stimulation because the IL-10-neutralizing antibody dose-dependently abolished the AT2R-mediated decrease in TNF-α level [19, 21, 22]. In the present study, we found that, in both intact and OVX female rats, central activation of AT2 not only downregulated expression of AT1-R, ACE1, and TNF-α, but also upregulated expression of IL-10 in the PVN. The changes in these gene expressions may be responsible for the AT2-R attenuation of DOCA/NaCl-induced hypertension in female rats, independent of female sex hormone status. Moreover, we found that central AT2-R activation further upregulated the expression of ACE2 while the AT2-R was kept higher in intact females, but not in OVX females, suggesting that female sex hormones are involved in the AT2-R regulation of antihypertensive components of the RAS and that the protective role of ACE2 was lost in the OVX females. These may be the explanations for the blocking effect of AT2-R activation on DOCA/NaCl-induced increase in BP in intact females and for only attenuating effect of AT2-R activation in the OVX females.

In addition, although OVX female rats showed a greater increase in BP response to DOCA than intact female rats, and central AT2-R activation altered the BP responses to DOCA infusion in all female rats in the present studies, saline intakes and decreases in HR in all groups were similar regardless of female sex hormone status or treatment condition. Thus, the differences in DOCA-induced hypertension between intact and OVX females and the effects of central AT2-R activation on DOCA-induced hypertension in the present study are unlikely to be due to saline intakes and HR changes, which is consistent with the previous studies [33].

It should be noted that there are several limitations in the present study. The present study determined the mRNA expression in a single cardiovascular autonomic nucleus, the PVN, after central C21 and DOCA/NaCl treatment. However, the protective role of central AT2-R activation in the development of DOCA-induced hypertension cannot be attributed solely to the changes in gene expression in the PVN. The central AT2-R activation-induced alterations of gene expression in other cardiovascular regulatory centers such as the nucleus of solitary tract, a nucleus with robust expression of AT2-R [6], may also contribute to the protective role of AT2-R activation in DOCA-induced hypertension. In addition, the possibility cannot be ruled out that the changes in BP produced by DOCA/NaCl and C21 treatment have an influence on the expression of the RAS components and proinflammatory cytokines in the PVN, and the studies on the time sequence of changes in mRNA expression in the PVN relative to the pressor response should be performed in the future.

Taken together, female sex hormone status has an influence on mRNA expression of central AT2-R and its regulation of antihypertensive components of the RAS such as

ACE2 expression. Nonetheless, central activation of AT2-R inhibited hypertensive components and enhanced antihypertensive components in the brain nucleus involved in regulation of cardiovascular function, thereby decreasing the BP induced by DOCA/NaCl in both intact and OVX females. The present study extends the previous studies focusing on the effect of AT2-R in peripheral tissues and provides a new central mechanism responsible for the antihypertensive effect of AT2-R activation in females.

Conflict of Interests

The authors declare that they have no competing interests.

Authors' Contribution

Shu-Yan Dai and Yu-Ping Zhang contributed equally to this work.

Acknowledgments

This work was supported by grant from Science and Technology of Shenyang (F14-158-9-41 to Shu-Yan Dai) and the funds for Major Program from Hebei North University (ZD201316 to Wei Peng).

References

[1] U. M. Steckelings, L. Paulis, P. Namsolleck, and T. Unger, "AT2 receptor agonists: hypertension and beyond," *Current Opinion in Nephrology and Hypertension*, vol. 21, no. 2, pp. 142–146, 2012.

[2] C. Sumners, A. D. de Kloet, E. G. Krause, T. Unger, and U. M. Steckelings, "Angiotensin type 2 receptors: blood pressure regulation and end organ damage," *Current Opinion in Pharmacology*, vol. 21, pp. 115–121, 2015.

[3] L. C. Matavelli and H. M. Siragy, "AT2 receptor activities and pathophysiological implications," *Journal of Cardiovascular Pharmacology*, vol. 65, pp. 226–232, 2015.

[4] L. Gao and I. H. Zucker, "AT2 receptor signaling and sympathetic regulation," *Current Opinion in Pharmacology*, vol. 11, no. 2, pp. 124–130, 2011.

[5] J. Gao, J. Chao, K.-J. K. Parbhu et al., "Ontogeny of angiotensin type 2 and type 1 receptor expression in mice," *Journal of the Renin-Angiotensin-Aldosterone System*, vol. 13, no. 3, pp. 341–352, 2012.

[6] A. D. de Kloet, L. Wang, J. A. Ludin et al., "Reporter mouse strain provides a novel look at angiotensin type-2 receptor distribution in the central nervous system," *Brain Structure and Function*, 2014.

[7] M. H. Abdulla and E. J. Johns, "Nitric oxide impacts on angiotensin AT2 receptor modulation of high-pressure baroreflex control of renal sympathetic nerve activity in anaesthetized rats," *Acta Physiologica*, vol. 210, no. 4, pp. 832–844, 2014.

[8] L. Gao, W. Wang, W. Wang, H. Li, C. Sumners, and I. H. Zucker, "Effects of angiotensin type 2 receptor overexpression in the rostral ventrolateral medulla on blood pressure and urine excretion in normal rats," *Hypertension*, vol. 51, no. 2, pp. 521–527, 2008.

[9] J. Gao, I. H. Zucker, and L. Gao, "Activation of central Angiotensin type 2 receptors by compound 21 improves arterial baroreflex sensitivity in rats with heart failure," *American Journal of Hypertension*, vol. 27, no. 10, pp. 1248–1256, 2014.

[10] S. Brouwers, I. Smolders, R. Wainford, and A. Dupont, "Hypotensive and sympathoinhibitory responses to selective central AT_2 receptor stimulation in spontaneously hypertensive rats," *Clinical Science*, vol. 129, no. 1, pp. 81–92, 2015.

[11] K. M. Denton, L. M. Hilliard, and M. Tare, "Sex-related differences in hypertension: seek and ye shall find," *Hypertension*, vol. 62, no. 4, pp. 674–677, 2013.

[12] A. I. Rodriguez-Perez, R. Valenzuela, B. Villar-Cheda, M. J. Guerra, J. L. Lanciego, and J. L. Labandeira-Garcia, "Estrogen and angiotensin interaction in the substantia nigra. Relevance to postmenopausal Parkinson's disease," *Experimental Neurology*, vol. 224, no. 2, pp. 517–526, 2010.

[13] A. I. Rodriguez-Perez, R. Valenzuela, B. Villar-Cheda, M. J. Guerra, and J. L. Labandeira-Garcia, "Dopaminergic neuroprotection of hormonal replacement therapy in young and aged menopausal rats: role of the brain angiotensin system," *Brain*, vol. 135, no. 1, pp. 124–138, 2012.

[14] L. R. Kisley, R. R. Sakai, and S. J. Fluharty, "Estrogen decreases hypothalamic angiotensin II AT1 receptor binding and mRNA in the female rat," *Brain Research*, vol. 844, no. 1-2, pp. 34–42, 1999.

[15] A. K. Sampson, L. M. Hilliard, K. M. Moritz et al., "The arterial depressor response to chronic low-dose angiotensin II infusion in female rats is estrogen dependent," *The American Journal of Physiology—Regulatory Integrative and Comparative Physiology*, vol. 302, no. 1, pp. R159–R165, 2012.

[16] K. M. Mirabito, L. M. Hilliard, Z. Wei et al., "Role of inflammation and the angiotensin type 2 receptor in the regulation of arterial pressure during pregnancy in mice," *Hypertension*, vol. 64, no. 3, pp. 626–631, 2014.

[17] C. A. McCarthy, R. E. Widdop, K. M. Denton, and E. S. Jones, "Update on the angiotensin AT_2 receptor," *Current Hypertension Reports*, vol. 15, no. 1, pp. 25–30, 2013.

[18] Q. Ali, Y. Wu, and T. Hussain, "Chronic AT2 receptor activation increases renal ACE2 activity, attenuates AT1 receptor function and blood pressure in obese Zucker rats," *Kidney International*, vol. 84, no. 5, pp. 931–939, 2013.

[19] I. Dhande, Q. Ali, and T. Hussain, "Proximal tubule angiotensin AT2 receptors mediate an anti-inflammatory response via interleukin-10: role in renoprotection in obese rats," *Hypertension*, vol. 61, no. 6, pp. 1218–1226, 2013.

[20] R. Sabuhi, Q. Ali, M. Asghar, N. R. H. Al-Zamily, and T. Hussain, "Role of the angiotensin II AT2 receptor in inflammation and oxidative stress: opposing effects in lean and obese Zucker rats," *American Journal of Physiology—Renal Physiology*, vol. 300, no. 3, pp. F700–F706, 2011.

[21] I. Dhande, W. Ma, and T. Hussain, "Angiotensin AT_2 receptor stimulation is anti-inflammatory in lipopolysaccharide-activated THP-1 macrophages via increased interleukin-10 production," *Hypertension Research*, vol. 38, no. 1, pp. 21–29, 2015.

[22] M. Menk, J. A. Graw, C. von Haefen et al., "Stimulation of the angiotensin II AT2 receptor is anti-inflammatory in human lipopolysaccharide-activated monocytic cells," *Inflammation*, vol. 38, no. 4, pp. 1690–1699, 2015.

[23] Q. Ali, S. Patel, and T. Hussain, "Angiotensin AT2 receptor agonist prevents salt-sensitive hypertension in obese Zucker rats," *The American Journal of Physiology—Renal Physiology*, vol. 308, no. 12, pp. F1379–F1385, 2015.

[24] S. Y. Dai, W. Peng, Y. P. Zhang, J. D. Li, Y. Shen, and X. F. Sun, "Brain endogenous angiotensin II receptor type 2 (AT2-R) protects against DOCA/salt-induced hypertension in female rats," *Journal of Neuroinflammation*, vol. 12, article 47, 2015.

[25] H. Zheng, N. M. Sharma, X. Liu, and K. P. Patel, "Exercise training normalizes enhanced sympathetic activation from the paraventricular nucleus in chronic heart failure: role of angiotensin II," *American Journal of Physiology—Regulatory Integrative and Comparative Physiology*, vol. 303, no. 4, pp. R387–R394, 2012.

[26] L. M. Hilliard, C. L. E. Chow, K. M. Mirabito et al., "Angiotensin type 2 receptor stimulation increases renal function in female, but not male, spontaneously hypertensive rats," *Hypertension*, vol. 64, no. 2, pp. 378–383, 2014.

[27] B. A. Kemp, N. L. Howell, J. J. Gildea, S. R. Keller, S. H. Padia, and R. M. Carey, "AT2 receptor activation induces natriuresis and lowers blood pressure," *Circulation Research*, vol. 115, no. 3, pp. 388–399, 2014.

[28] P. Xu, S. Sriramula, and E. Lazartigues, "ACE2/ANG-(1–7)/Mas pathway in the brain: the axis of good," *American Journal of Physiology—Regulatory, Integrative and Comparative Physiology*, vol. 300, no. 4, pp. R804–R817, 2011.

[29] X.-A. Song, L.-L. Jia, W. Cui et al., "Inhibition of TNF-α in hypothalamic paraventricular nucleus attenuates hypertension and cardiac hypertrophy by inhibiting neurohormonal excitation in spontaneously hypertensive rats," *Toxicology and Applied Pharmacology*, vol. 281, no. 1, pp. 101–108, 2014.

[30] S. Sriramula, J. P. Cardinale, and J. Francis, "Inhibition of TNF in the brain reverses alterations in RAS components and attenuates angiotensin II-induced hypertension," *PLoS ONE*, vol. 8, no. 5, Article ID e63847, 2013.

[31] P. J. Winklewski, M. Radkowski, M. Wszedybyl-Winklewska, and U. Demkow, "Brain inflammation and hypertension: the chicken or the egg?" *Journal of Neuroinflammation*, vol. 12, article 85, 2015.

[32] L. M. Hilliard, A. K. Sampson, R. D. Brown, and K. M. Denton, "The 'His and Hers' of the renin-angiotensin system," *Current Hypertension Reports*, vol. 15, no. 1, pp. 71–79, 2013.

[33] B. Xue, D. Badaue-Passos Jr., F. Guo, C. E. Gomez-Sanchez, M. Hay, and A. K. Johnson, "Sex differences and central protective effect of 17β-estradiol in the development of aldosterone/NaCl-induced hypertension," *American Journal of Physiology: Heart and Circulatory Physiology*, vol. 296, no. 5, pp. H1577–H1585, 2009.

Hindawi Publishing Corporation
Oxidative Medicine and Cellular Longevity
Volume 2016, Article ID 7263736, 13 pages
http://dx.doi.org/10.1155/2016/7263736

Research Article

HDAC6 Regulates the Chaperone-Mediated Autophagy to Prevent Oxidative Damage in Injured Neurons after Experimental Spinal Cord Injury

Min Su,[1,2] Huaqing Guan,[3] Fan Zhang,[3] Yarong Gao,[2] Xiaomei Teng,[4] and Weixin Yang[1]

[1]*Department of Rehabilitation, First Affiliated Hospital of Soochow University, Suzhou 215006, China*
[2]*Institute of Neuroscience, Soochow University, Suzhou 215123, China*
[3]*Department of Orthopaedics, First Affiliated Hospital of Soochow University, Suzhou 215006, China*
[4]*Institute for Cardiovascular Science, Soochow University, Suzhou 215006, China*

Correspondence should be addressed to Min Su; sumin@139.com and Weixin Yang; weixinsuda@163.com

Received 8 March 2015; Revised 10 July 2015; Accepted 22 July 2015

Academic Editor: Adam J. Case

Hypoxia-ischemia- (HI-) induced oxidative stress plays a role in secondary pathocellular processes of acute spinal cord injury (SCI) due to HI from many kinds of mechanical trauma. Increasing evidence suggests that the histone deacetylase-6 (HDAC6) plays an important role in cell homeostasis in both physiological and abnormal, stressful, pathological conditions. This paper found that inhibition of HDAC6 accelerated reactive oxygen species (ROS) generation and cell apoptosis in response to the HI. Deficiency of HDAC6 hindered the chaperone-mediated autophagy (CMA) activity to resistance of HI-induced oxidative stress. Furthermore, this study provided the experimental evidence for the potential role of HDAC6 in the regulation of CMA by affecting HSP90 acetylation. Therefore, HDAC6 plays an important role in the function of CMA pathway under the HI stress induced by SCI and it may be a potential therapeutic target in acute SCI model.

1. Introduction

Spinal cord injury (SCI) is a kind of serious and debilitating disease. The main clinical manifestations of SCI are neurological dysfunction at and/or below the level of the injury [1]. The disability and lethal rate of this disease are extremely high and at present there is no effective treatment to it [1]. Although the underlying pathocellular processes of SCI remain uncertain, secondary damage following primary SCI extends pathology beyond the site of initial trauma, characterized by neurons inflammation, demyelination, and axonal degeneration, and various degrees of oligodendrocyte and neuronal cell death [2]. Consequently, defining the mechanism of secondary damage will be important to understand neurodegenerative disorders and find the best therapeutic procedures.

Hypoxia-ischemia (HI) of the cord, resulting from various mechanical trauma, has been reported to induce the formation of active oxygen and free radicals (reactive oxygen species, ROS) which can bring irreversible secondary lesion [3, 4]. In another word, SCI is considered to be related to a vulnerability of spinal somatic and motor neurons to HI as well as the involvement of ROS [5]. However, the mechanisms underlying this vulnerability are not fully understood.

Several reports have described that autophagy occurred in SCI [6, 7]. Three different types of autophagy have been described in mammalian cells; chaperone-mediated autophagy (CMA) is one type of autophagy that was involved in resisting the ROS-induced motoneuronal death during spinal cord development [8, 9].

In addition, the recent evidence directly supports that the knockdown of histone deacetylase-6 (HDAC6) triggered a significant generation of ROS and disruption of mitochondrial membrane potential (MMP) [10]. Several investigations have demonstrated that targeting HDAC6 activity can protect neurons and glia and improve outcomes in CNS injury and disease models [11–13]. However, the role of HDAC6 in acute SCI remains unclear.

2. Materials and Methods

2.1. Animals and Surgical Procedures. A total of 30 adult female C57BL/6J mice (10–12 weeks old; Laboratory Animals Center of the Medical College of Soochow University, Suzhou, China) were used in this study. Each experimental group includes at least 5 mice. Every cage housed three or four mice and the temperature was kept at 24°C. All of the animals easily get enough water and food before and after surgery.

The mice were anesthetized with 1.25% halothane in an oxygen/nitrous oxide (30/70%) gas mixture. During surgery the rectal temperature was monitored and maintained at 37.0 ± 0.5°C by a heating pad. A sterile manner was used to preserve the skin above the thoracic vertebrae and 15 mm midline skin incision was made. Then the laminae of T7–9 were exposed, and the laminectomy was performed at T8 till the dura mater emerged. With a sharp scalpel, the spinal cord was hemitransected on the right side only [14]. Finally, the muscles and skin were closed in layers. The mice with compromised bladder function (a rare complication) received manual bladder expression twice a day until establishing reflex bladder emptying. The same surgical procedures were performed to the sham operated animals, but without the hemisection to the spinal cord. All surgical and animal handling procedures were performed following the guidelines of the National Institutes of Health for the Care of Animals, approved by the Experimental Animal Center, Soochow University, Suzhou, China.

2.2. Cell Culture and Treatments. The rat pheochromocytoma (PC12) cell line was provided by Shanghai Institute of Cell Biology, Chinese Academy of Sciences. Cells were maintained in complete Dulbecco's modified Eagle's medium (DMEM), supplemented with 10% fetal bovine serum (FBS) and 1% penicillin/streptomycin. In order to simulate hypoxia-ischemia (HI) condition, the cultures were transferred to a serum-free medium (only DMEM) preequilibrated with 95% N_2 and 5% CO_2. Then the cells were incubated in the medium and placed in the incubator equipped with 3% O_2.

2.3. Transient Transfection with HDAC6 siRNA. Three interference sequences were designed and tested for HDAC6 silencing by Shanghai Zimmer. Silencing efficiency of two interference sequences was more than 70%. The two interference sequences were chosen for further experimentation based on their ability to block HDAC6 expression. The PC12 cells were transiently transfected with HDAC6 siRNA or control sequence using Lipofectamine 2000 (Invitrogen) in accordance with the manufacturer's instructions. At 24 h after transfection, cells were subjected to Western blotting analysis. And GFP immunofluorescence was also assessed with an inverted fluorescence microscope. 48 h later, the cells with the greatest reduction of HDAC6 expression were used for further studies. Specific methods were showed in the previous publication [15].

2.4. Histological Assessments. 100 mg/kg sodium pentobarbital was injected to the mice by abdominal cavity at 24 h after the operation. The normal saline was overdosed to the mice by transcardial perfusion, followed by 4% paraformaldehyde in 0.1 M PBS, pH 7.4. Before the immunohistochemical staining, the spinal cord segments containing the injured center were collected, postfixed in the same fixative overnight at 4°C, and embedded in paraffin [14]. Serial 1 cm segment of spinal cord including the injury sites was dissected and sectioned longitudinally in the horizontal plane or transversely at 5 μm thickness on the slides. The sections were used for immunohistochemical and TUNEL staining. TUNEL staining was used to observe neuronal apoptosis, and SP staining was used to observe the HDAC6 expression in the neuron. Then the positive expression units were semiquantitatively analyzed using the Image-pro plus software which used surface density and optical density [16].

2.5. Western Blotting Analysis. Briefly, a 10 mm spinal cord segment containing the injury center was removed for protein extraction 24 h following SCI. After each indicated treatment, equal amounts of protein from the cell or tissue extracts were mixed with sodium dodecyl sulphate polyacrylamide gel electrophoresis (SDS-PAGE) sample buffer and boiled for 8 min. Equal amounts of proteins (15 μg) were loaded and separated by SDS-PAGE in Tris-glycine running buffer. After that, proteins were transferred onto a polyvinylidene difluoride membrane (Millipore, Bedford, MA, USA) and blocked with 5% nonfat milk in Tris-buffered saline for 30 min. The membranes were then incubated with anti-HDAC6 (1 : 100; Biovision), anti-LAMP-2a (1 : 1000; Abcam), anti-HSP90 (1 : 1000; Abcam), anti-HSC70 (1 : 1000; Abcam), and anti-HIF-1-alpha antibody (1 : 500; Abcam) at 4°C overnight. After washing in Tris-buffered saline containing 0.1% Tween 20 (TBST) for 3 times, the membranes were incubated with horseradish peroxidase-conjugated secondary antibodies (Vector Laboratories, Burlingame, CA) in TBST containing 3% nonfat dry milk for 2 h. Immunoreactivity was detected with enhanced chemiluminescence autoradiography (ECL kit, Amersham, Arlington Heights, IL). The densitometry of the bands was quantitatively analyzed with Sigma Scan Pro 5 software (NIH, Bethesda, MD, USA). Independent experiments were carried out in triplicate. β-actin was used as protein loading control. Repeat 3 times.

2.6. Immunoprecipitations. At the end of treatment, the culture media were aspirated and the cells were washed once with ice-cold PBS. The cells were then lysed with lysis buffer containing 20 mM Tris (pH 7.5), 150 mM NaCl, 1% Triton X-100, and sodium pyrophosphate, β-glycerophosphate, EDTA, Na_3VO_4, leupeptin, and other protease inhibitors (Sigma-Aldrich). Protein samples per 100 μg were added with 4 μL anti-HSP90 antibody (Abcam, Cambridge, UK) and shaked at 4°C overnight. 40 μL Protein A Agarose (Sigma Chemical Company) was added and incubated for 3 h at 4°C and then centrifuged at 1000 g for 5 min. After that, the supernatant was discarded and the pellet was washed 3 times with PBS. Thereafter, the precipitates were resuspended with 40 μL 1x sample buffer and heated at 96°C for 5 min. The samples were

centrifuged for 5 s and the supernatants were collected for Western blotting.

2.7. Intracellular ROS Determination. Reactive Oxygen Species Assay Kit was obtained from Sigma Chemical Company (D6883, USA). Intracellular ROS was measured using the nonfluorescent probe 2′,7′-dichlorofluorescein diacetate (DCFH-DA). PC12/siRNA PC12 cells were plated at a density of 1×10^5/well in 6-well plates. One day after plating, the cells were treated with serum-free and hypoxia (3% O_2) for 24 h. For specific method, refer to the previous publication [17]. After DCFH-DA treatment, the cells were washed with cold phosphate-buffered saline (PBS), collected, and subjected immediately to flow cytometry (Becton Dickinson FACSCalibur) analysis of DCF fluorescence at excitation wavelength of 488 nm and emission wavelength of 610 nm. The fluorescence was expressed as a percentage of total area. This process was repeated 3 times.

2.8. ELISA. ELISA kits for rat RNase A were obtained from Antibodies Company (ABIN431684, Aachen, Germany). Cells were collected after treatment, then immunoprecipitation of RNase A from cells as the manufacturer's instructions. Briefly, the supernatants were mixed with anti-RNase A antibody (1 : 5000; Rockland, PA, USA) and incubated with Protein A Agarose beads. After appropriate washing, aspirate last wash and proceed as all ELISA methods. The fluorescent properties of each sample and appropriate standards were measured using a Microplate Reader, read absorbance at 450 nm. The data were linearized by plotting the log of the RNase-A concentrations versus the log of the OD and the best fit line was determined by curve expert 13.0. This process was repeated 3 times.

2.9. Immunofluorescence Microscopy. The cells were collected and washed by PBS for 3 × 5 min, followed by being fixed for 20 min in PBS containing 4% paraformaldehyde (pH 7.4). After that, the cells were washed in PBS for 4 × 5 min and blocked in PBS containing 1% normal bovine serum albumin and 0.1% Triton-X-100 for 10 min at room temperature. Then we exposed the cells to anti-LAMP-2a (1 : 200; Abcam), anti-LAMP-1 (1 : 200; Abcam), or anti-HDAC6 (1 : 250; Abcam) antibody at 4°C overnight. Cultures were subsequently washed and incubated with mixture secondary antibody at 37°C for 1 h and then rinsed several times and incubated again with 10 mg/mL 4-6-diamidino-2-phenylindole (DAPI; Serva, Heidelberg, Germany) for 10 min at room temperature. At last, cultures were mounted on glass slides with Vectashield mounting medium (Vector Lab) and analyzed with a confocal microscope (LEICA TCS SP5II, Germany). Images were digitally analyzed by Leica microsystem software to quantify the fluorescence intensity of cells. From each group, 5 pieces of coverslips including at least 60 cells were analyzed.

2.10. Cells Apoptosis Analysis. Apoptosis was measured by flow cytometry to detect annexin V staining and propidium iodide uptake (Invitrogen Detection Technology, Eugene, OR) as described previously [15]. Three independent experiments were performed to determine the standard deviation.

2.11. Transmission Electron Microscopy. After each treatment, cells were harvested and viewed under a transmission electron microscope (JEM-1011, Japan). Specific methods were showed in the previous publication [15].

2.12. Statistical Analysis. All experiments were performed for at least three sets of independent experiments. The data are presented as mean ± SEM. Two group comparisons were performed using Student's *t*-test. Multiple group comparisons were performed using one-way analysis of variance and Fisher's least significant difference. A P value of less than 0.05 was set as statistically significant.

3. Results

3.1. The Spinal Cord Injury Activates the HDAC6 and CMA. In order to confirm the role of HDAC6 and CMA in acute SCI, a spinal cord hemitransected model in mice was set up. As indicated in Figure 1(a), after acute SCI for 24 h, HDAC6 protein expression in the damaged spinal cord tissue was dramatically increased compared with the sham operated group ($P < 0.01$). SP staining showed that the presence of brown granules was found in some neurons' cytoplasm after injury versus sham whereas the negative neurons become pyknotic (Figure 1(a)). TUNEL staining data further demonstrated the greater number of apoptosis neurons in the damaged spinal cord tissue compared to the sham operated group at 24 h after being hemitransected ($P < 0.05$). From these results, we confirmed that acute SCI caused the increased HDAC6 expression, which is associated with neuronal apoptosis in the damaged spinal cord.

In Western blot experiments, we further found that not only the protein expression of HDAC6, but also the protein expression of LAMP-2a was increased in the SCI mice compared with sham operated mice ($P < 0.05$) (Figure 1(b)). The previous studies had shown that the LAMP-2a is the speed-limiting protein of the CMA metabolic pathway [18]. Therefore, we speculated that HDAC6 affects the neuronal survival by regulating the CMA activity. In order to confirm this hypothesis, a series of *in vitro* studies were conducted.

3.2. Hypoxia-Ischemia Induced HDAC6 Expression and Oxidative Stress In Vitro. It is well known that various mechanical trauma would induce the hypoxia-ischemia (HI) which is the primary cause of secondary damage of SCI and can bring irreversible neurodegenerative changes [2]. To replicate the HI pathological state, the PC12 cells were treated with serum-free and hypoxia (3% O_2) for 24 h.

From Figure 2(a), HI cause the protein expression of hypoxia-inducible factor 1 alpha (HIF-1-alpha) dramatically increase compared with the medium-treated group ($P < 0.01$). While the reactive oxygen species (ROS) is able to promote rapid activation and stabilization of the transcription factor HIF-1-alpha, which regulates expression of genes involved in inflammation, metabolism, and cell survival [19]. Therefore these evidences suggested to us that HI triggered

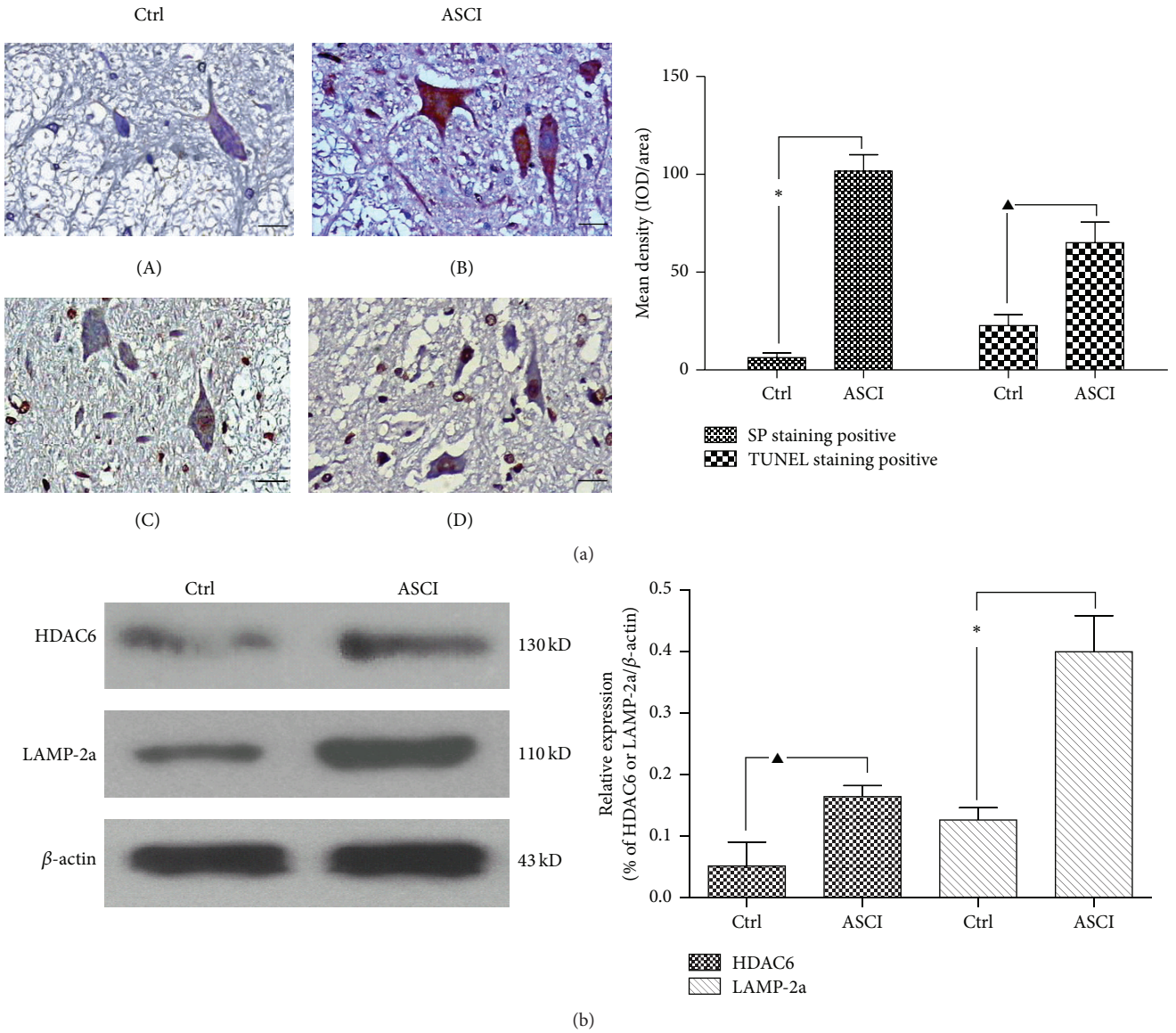

Figure 1: The expression of HDAC6 and LAMP-2a protein increased in the ASCI. 30 adult female C57BL/6J mice were divided into two groups: the T8 spinal cord hemitransected group (ASCI) and the sham operated group (Ctrl). (a) The expression of HDAC6 was analyzed by SP standing at 24 h after the operation ((A)-(B)). Brown represents HDAC6 positive expression in the cytoplasm, and its negative cell cytoplasm is light blue, while gray matter supports network negative staining; ((C)-(D)) TUNEL staining was used to observe neuronal apoptosis. (C) Field of vision is a small amount of TUNEL staining positive neurons and glial cells, which shows that only a small amount of neurons is undergoing apoptosis. Spinal cord tissue structure is basic intact, and there are few cavity formations. (D) Field of vision is more TUNEL staining positive neurons and glial cells (tan for its nucleus is positive), which shows that a large number of nerve cells are undergoing apoptosis. The structure of the spinal cord tissue is disorder, and there are more cavity formations. Scale bar: 20 μm. Semiquantitative analysis are consistent with the figure, and HDAC6 expression in ASCI was dramatically increased compared with the control group. At least 60 cells were included for analysis from five images per group. Values represent mean ± SEM, $^{*}P < 0.01$, $^{\blacktriangle}P < 0.05$ versus corresponding control group. (b) By Western blot, in the ASCI group, the protein expression of HDAC6 and LAMP-2a was significantly higher than the control group. Values represent mean ± SEM, $^{*}P < 0.01$, $^{\blacktriangle}P < 0.05$ versus corresponding control group. Each experiment repeated at least 3 times.

the generation of ROS and PC12 cells were actually experiencing hypoxia.

By exposed PC12 cell in HI condition for 24 h, the protein expression of HDAC6 was also significantly increased compared with medium-treated group ($P < 0.05$) (Figure 2(b)). It has been proved that the accumulation of ROS is an oxidative stress to which cells respond by activating various defense mechanisms; thereby we speculated that HDAC6 is involved in the process of the cells resistance to oxidative stress. This needs further study to approve the hypothesis.

3.3. Deficiency of HDAC6 Accelerates the Oxidative Stress in Response to Hypoxia-Ischemia. To investigate whether HDAC6 is essential for the cells against ROS-induced

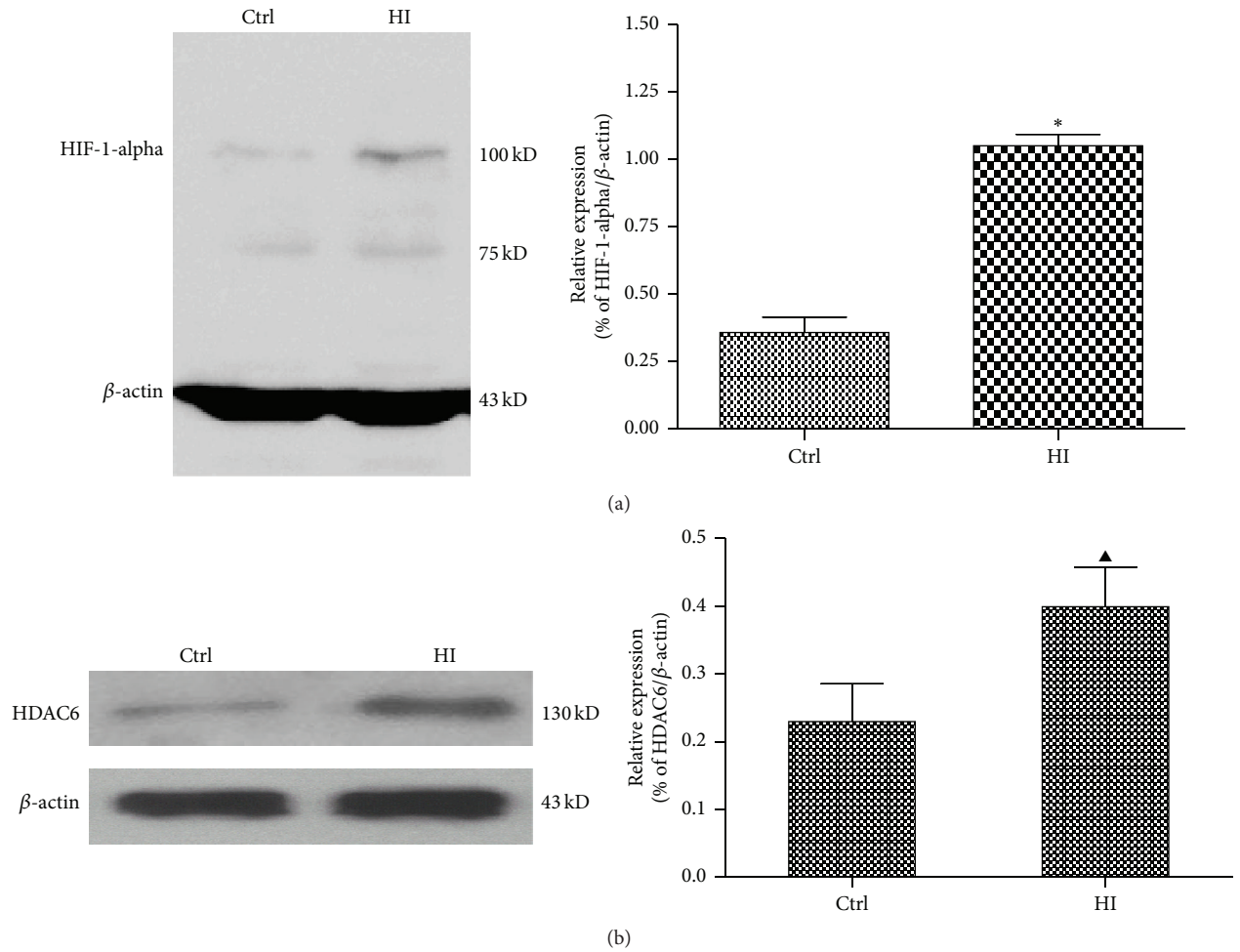

Figure 2: Hypoxia-ischemia induced HDAC6 expression and oxidative stress *in vitro*. The PC12 cells were treated with HI for 24 h. Ctrl express medium-treated group. (a) The expression of HIF-1-alpha was analyzed by Western blot. Results of the densitometric quantification are represented as mean ± SEM ($n = 3$). $^{*}P < 0.01$ versus control group. (b) The expression of HDAC6 was analyzed by Western blot. Results of the densitometric quantification are represented as mean ± SEM ($n = 3$). $^{\blacktriangle}P < 0.05$ versus control group.

cytotoxicity, *in vitro* flow cytometry studies were applied to detect the intracellular level of ROS.

As shown in Figure 3, HI induces a net increase of intracellular ROS compared with the vehicle-treated cells ($P < 0.01$), which is reflected by the DCF fluorescence value and the percentage of cell with fluorescence. After the siRNA inhibition of HDAC6, the generation of ROS was further accentuated to the HI-induced stress. These findings suggest that hypoxic stress induces accumulation of ROS in neuronal cells whereas HDAC6 deficiency induced the occurrence of the secondary oxidative stress which is considered to contribute to neural tissue damage. However, disruption of HDAC6 stimulates ROS production which may be related to the decreased cellular antioxidant activity.

3.4. Inhibition of HDAC6 Aggravates Cell Apoptosis to HI-Induced Oxidative Stress. Oxidative stress is one of the primary metabolic disorders jeopardizing cell survival [20]. To investigate whether HDAC6 is essential for the cells against ROS-induced cytotoxicity, the apoptosis of PC12 cells was analyzed by flow cytometry.

An increase in the number of apoptotic cells, especially early apoptosis, occurred after PC12 cells were exposure to HI for 24 h (Figure 4(a)). Knockdown of HDAC6 resulted in a slow but evidently increased rate of apoptosis reflected to HI (Figure 4(a)). Furthermore, the ultrastructural features of PC12 cells were examined with transmission electron microscopy (EM). Compared with vehicle-treated control cells (Figure 4(b)-(A)), HI-treated cells exhibited the initial characteristics of autophagy, such as lysosome amplification and autophagy bubbles in the cytoplasm (Figure 4(b)-(C)). EM studies confirmed that knockdown of HDAC6 further elicited cell apoptosis in response to HI. As shown in Figure 4(b)-(D), nuclear chromatin margination, cytoplasmic vacuolization, and the apoptotic bodies appeared. These results showed that HI triggered early cell apoptosis, and deficiency of HDAC6 increased the sensitivity of cells to HI-induced stress, which can exacerbate the cellular damage and

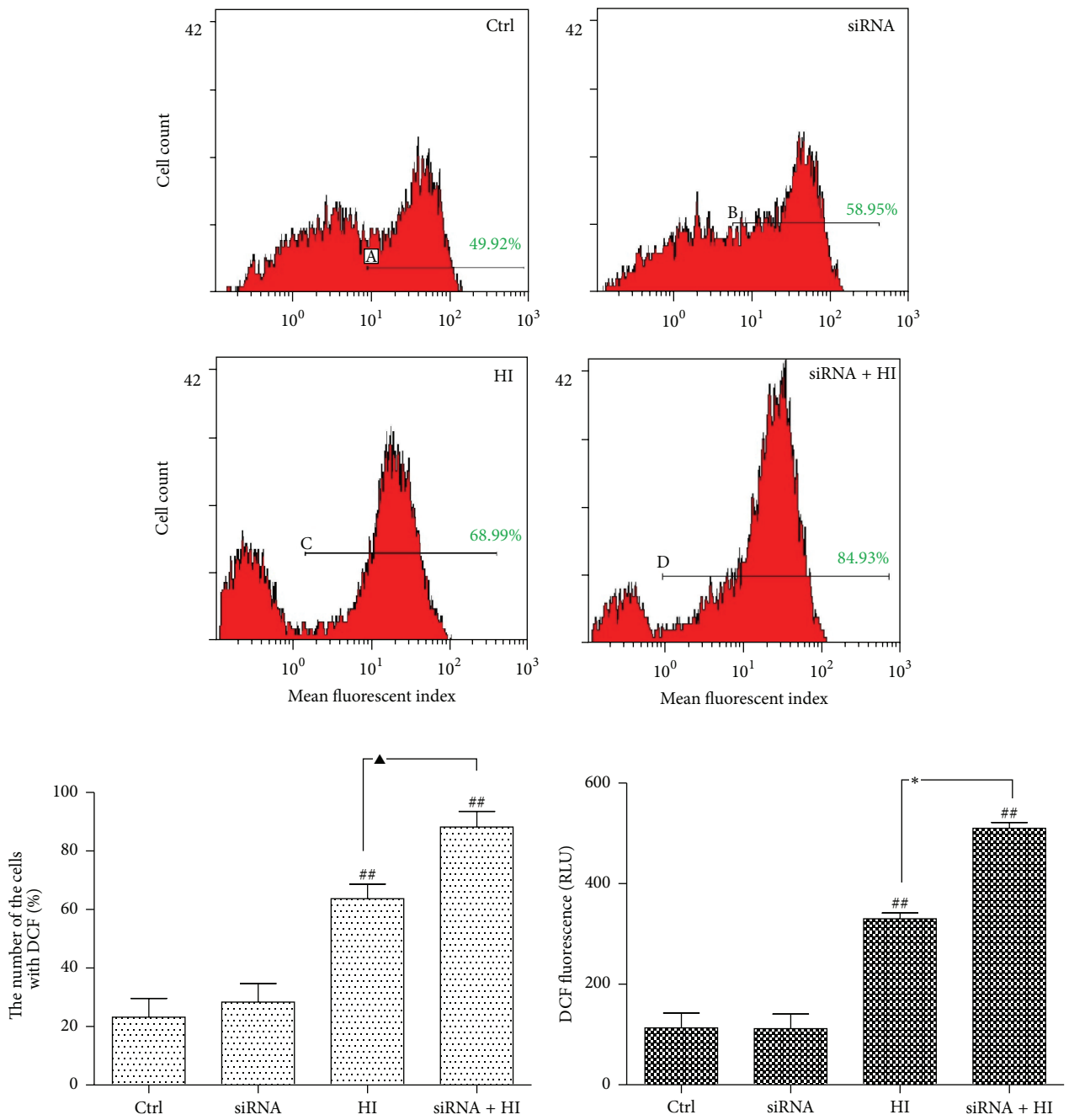

Figure 3: Deficiency of HDAC6 accelerates intracellular ROS generation in response to HI. The PC12 and PC12/siHDAC6 cells were treated with HI for 24 h. Ctrl express vehicle-treated group. Changes in the intracellular DCF fluorescence value and the percentage of cell with fluorescence can be detected by flow cytometry. The Y-axis indicates the number of cells with fluorescence; the X-axis expresses fluorescence intensity. Red indicates the level of intracellular ROS. Green indicates the figure of %Gated. Result of one representative experiment was shown. The densitometric quantification is represented as mean ± SEM ($n = 3$), $^{\#\#}P < 0.01$ versus control group; $^{*}P < 0.01$, $^{\blacktriangle}P < 0.05$ indicate the significance among the groups indicated in the bar chart.

apoptosis. Meanwhile the form of apoptosis further causes the production of ROS, eventually leading to irreversible cell death.

3.5. HDAC6 Regulates the Activity of CMA Degradation Pathway in Response to Hypoxia-Ischemia. To clarify the mechanism of deficiency of HDAC6 leading to cell apoptosis and ROS increase, the further study was made. The recent evidence directly supports the fact that the CMA was involved in resisting the ROS-induced motoneuronal death during spinal cord development [21, 22]. Thereby, we observed the effect of HDAC6 on the CMA activity.

The HSC70 and LAMP-2a, two relatively specific markers of CMA, were examined and semiquantified by Western

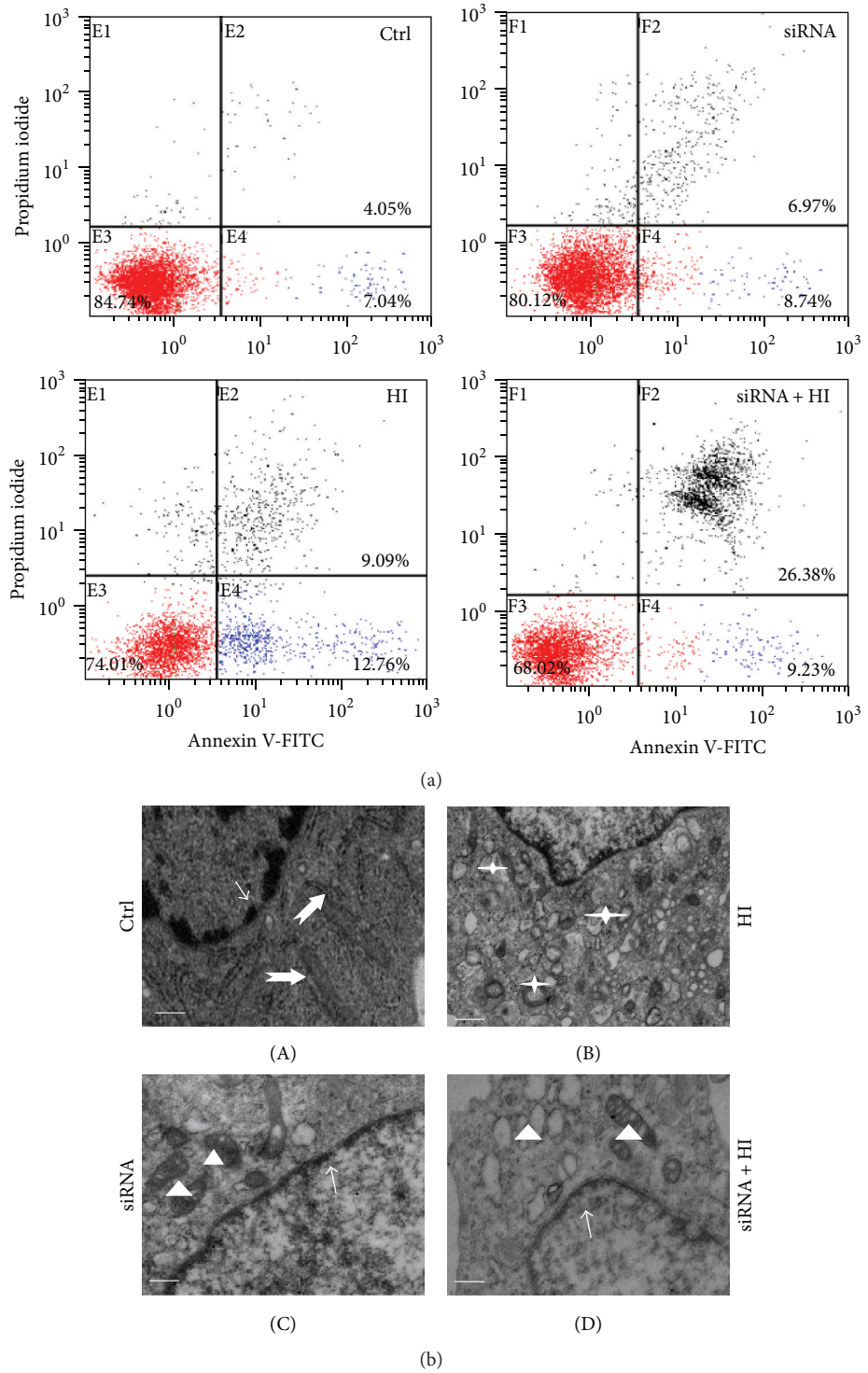

FIGURE 4: Loss of HDAC6 leads to the hypersensitivity to HI-induced stress. The PC12 and PC12/siHDAC6 cells were treated with HI for 24 h. Ctrl express vehicle-treated group. (a) Apoptotic cells were calculated by flow cytometry with simultaneous staining of annexin V-FITC and PI. (b) The ultrastructural features of PC12 cells in different groups. In control cells (A) and HDAC6-deficient cells (C), the nucleoplasm (thin arrows) remained condensed and all kinds of organelles scattered within the cytoplasm (thick arrows and triangles). HI treatment induced autophagy (B); the lysosome amplification and autophagy bubbles appear in the cytoplasm (asterisks). (D) Knockdown of HDAC6 elicited apoptotic features in cells exposure to HI. Cell swelling, cytoplasmic vacuolization (triangles), and nuclear chromatin loss and margination (thin arrows). Scale bar: 1 μm.

blotting analysis. The expression level of both proteins was significantly increased in the HI-treated cells compared with the vehicle-treated cells (Figure 5(a)). However, it was interesting that inhibition of HDAC6 by siRNA further increased the expression of LAMP-2a and HSC70 in PC12 cells exposed to HI for 24 h (Figure 5(a)). In order to confirm whether the CMA activity was consistent with the changes of LAMP-2a and HSC70, the amount of RNase A, a well-characterized protein substrate of CMA proteolytic pathway, was examined [23]. Of note, HI induced the increase in substrate degradation whereas an opposite change was observed if HDAC6 was inhibited (Figure 5(b)). These results suggest that HI may activate CMA degradation pathway which may be responsible, at least in part, for the accumulation of damaged abnormal and unnecessary proteins induced by oxidative stress in the cytoplasm. Inhibition of HDAC6 caused the reduction of CMA activity, and the increase of LAMP-2a and HSC70 may only act as a compensatory response to the ROS-induced stress.

Furthermore, we confirmed the change of LAMP-2a and LAMP-1, a marker of lysosome [24], by the immunofluorescence staining. As shown in Figure 5(c), HI treatment significantly increased the expression of LAMP-2a and also enhanced the colocalization of LAMP-2a with LAMP-1 around the nucleus. Simultaneously, the increase of LAMP-2a tends to be more notable than that of LAMP-1. Of interest, after deficiency of HDAC6, the level of LAMP-1 was shown to be further enhanced and significantly exceeded the LAMP-2a, while the colocalization of LAMP-2a with LAMP-1 did not add (Figure 5(c)). Therefore, it could be speculated that HI indeed activate CMA degradation pathway, and inhibition of HDAC6 induced LAMP-2a which is compensatory increased partially by the expansion of lysosomal membrane, instead of further improving the CMA degradation activity to resist HI-induced oxidative stress toxicity.

3.6. HDAC6 Affects the Activity of CMA by Regulating HSP90 Acetylation. Why does the inhibition of HDAC6 disrupt the activity of CMA? Previous evidence indicates that HSP90, as a constitutively and ubiquitously expressed ATP-dependent molecular chaperone, was also associated with lysosomes and, thus, may play critical roles in the functional dynamics of the CMA [25, 26]. As HDAC6 deacetylates lysine residues of HSP90 [27], the further study was continued to investigate whether HDAC6 may affect the activity of CMA by regulating the acetylation of HSP90.

To this end, the level of acetylated HSP90 and the interaction of HSP90 with HSC70 and LAMP-2a in response to HI were analyzed in combination with HDAC6 siRNA and immunoprecipitation techniques. As shown in Figure 6(a), after HI treatment for 24 h in PC12 cells, the total level of HSP90 was markedly increased, while HSP90 acetylation level did not show any significant change. However, the level of acetylated HSP90 was significantly increased by the inhibition of HDAC6. Moreover, in HDAC6 deficient cells, the interaction of HSP90 with LAMP-2a and HSC70 was markedly decreased in response to HI (Figure 6(b)). These results strongly suggest that HDAC6 may affect the activity of CMA by acting as a HSP90 deacetylase. As a key molecule chaperone to resist the oxidative stress [28], the expression of compensatory HSP90 increases after loss of HDAC6, and increased HSP90 protein synthesis may determine its greater resistance to stressor that elicits the formation of ROS-induced cellular damage.

4. Discussion

The present study firstly revealed SCI induced HDAC6 expression increase *in vivo*; simultaneously inhibition of HDAC6 accelerates ROS generation and neurons apoptosis in response to the hypoxia-ischemia (HI) *in vitro*. Second, a positive correlation between HDAC6 and CMA was represented *in vivo* and *in vitro*, and inhibition of HDAC6 hinders the CMA activity. Third, our results provided the experimental evidence for the potential role of HDAC6 in the regulation of CMA by affecting HSP90 acetylation.

Effective management of the secondary damage following primary SCI is imperative for maximizing anatomical and functional recovery [29]. Consequently, defining the mechanism of secondary damage will be important to the understanding of neurodegenerative disorders and to find the best therapeutic procedures. In recent years, several laboratories have obtained experimental evidence indicating that oxidative stress elicited by HI from all kinds of mechanical trauma is a major player in the pathogenesis of secondary damage after acute SCI [30–32]. The involvement of ROS in neuronal subsequent death has been determined, which can induce about 50% of the neuronal programmed cell death [30]. Our study shows that overproduction of ROS was correlated in a significant manner with the apoptotic index (Figures 3 and 4). High levels of ROS can oxidize cell constituents, such as lipids, proteins, and DNA, thus posing a threat to the cell integrity and viability [33]. Various defense mechanisms have been mobilized to protect cells against oxidative stress [34].

Our data had shown that both SCI and HI caused the expression increase of HDAC6 (Figures 1 and 2). As a member of the histone deacetylase family, HDAC6 is mainly localized in the cytoplasm and has two catalytic sites and an ubiquitin-binding domain at the C terminus [35]. Due to the special structure and positioning of HDAC6, it has been implicated to be involved in many cellular processes, including degradation of misfolded proteins, cell migration, and cell-cell interaction [36]. The reduction of HDAC6 activity in cultured cells may compromise cell viability when the cells are exposed to different stressors. Recently, malfunctioning of HDAC6 has been linked to a growing number of human disorders [37, 38]. In this study, we also provided the evidence that inhibition of HDAC6 accelerates ROS generation and neurons apoptosis in response to the hypoxia-ischemia (HI) *in vitro* (Figures 3 and 4).

To clarify the mechanism of HDAC6 in secondary damage following primary SCI, we observed the changes in the acetylation level of Hsp90 which is not only the exclusive substrate of HDAC6, but also a critical molecular chaperone to CMA degradation pathway. The dynamic equilibrium of protein acetylation and deacetylation plays a pivotal role in the normal physiological process of cells. Acetylation of

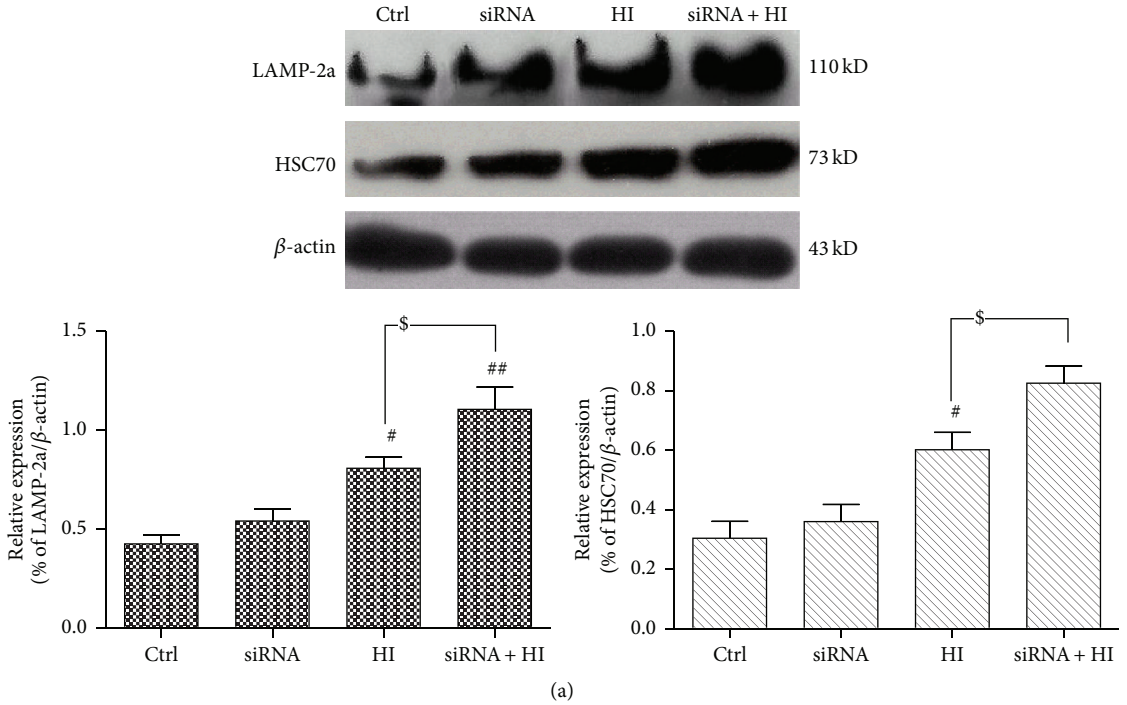

(a)

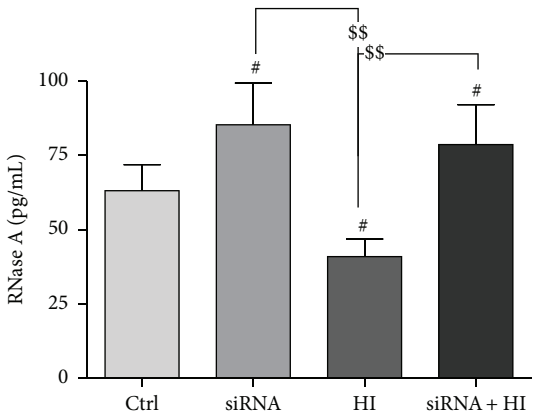

(b)

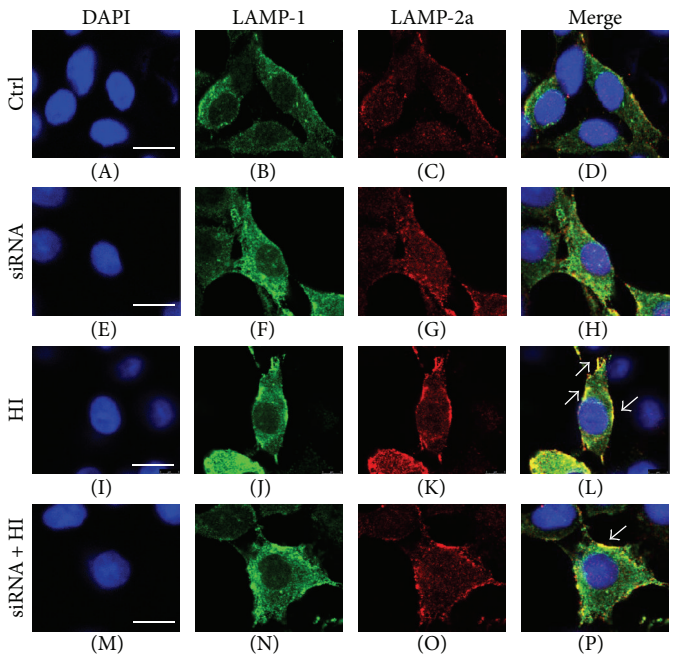

Figure 5: Continued.

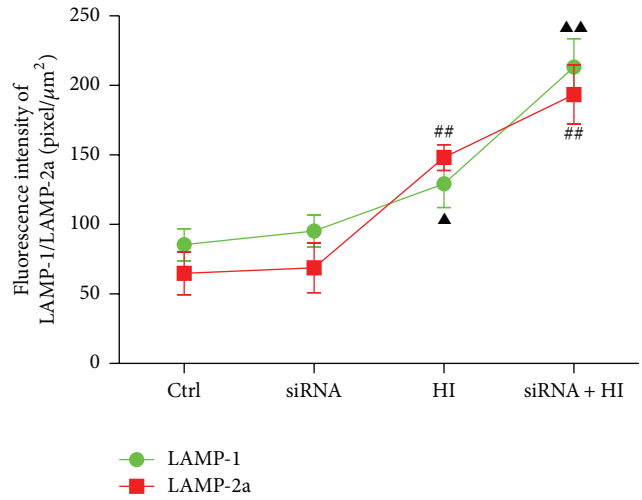

(c)

Figure 5: Deficiency of HDAC6 disrupts the CMA activity in response to HI. The PC12 and PC12/siHDAC6 cells were treated with HI for 24 h. Ctrl express vehicle-treated group. (a) The expression of LAMP-2a and HSC70 was analyzed by Western blot. The level of LAMP-2a and HSC70 was further observed in HDAC6 knockdown cells by siRNA. Results of the densitometric quantification are represented as mean ± SEM ($n = 3$). $^{\#}P < 0.05$, $^{\#\#}P < 0.01$ versus control group; $^{\$}P < 0.01$ indicates the significance among the groups indicated in the bar chart. (b) Immunoprecipitated RNase A (an identified CMA substrate) from the treated cells and then assay RNase A activity by ELISA. Group data represent mean ± SEM ($n = 3$); $^{\#}P < 0.05$ versus corresponding control group; $^{\$\$}P < 0.01$ indicates the significance among the groups indicated in the bar chart. (c) Double immunostained with antibody to LAMP-1 (green) and LAMP-2a (red) as indicated. Superimposed confocal images (merge) demonstrate the colocalization of LAMP-2a with LAMP-1 (a lysosome marker). Arrows indicate LAMP-2a mainly clustered in the perinuclear lysosomal membrane. Scale bar: 15 μm. The fluorescence intensity of LAMP-1 and LAMP-2a from experiments results shown. At least 60 cells were included for analysis from five images per group. Group data represent mean ± SEM ($n = 3$); $^{\blacktriangle}P < 0.05$, $^{\blacktriangle\blacktriangle}P < 0.01$, and $^{\#\#}P < 0.01$ versus corresponding control group.

HSP90 at lysine294 has been shown to modulate its activity by regulating client protein and cochaperone binding [39]. In addition, our study showed that the expression of compensatory HSP90 increases after loss of HDAC6 in HI condition. As a key molecule chaperone to resist the oxidative stress [28], increased HSP90 protein synthesis may determine its greater resistance to stressor that elicits the formation of ROS-induced cellular damage.

Our findings signaled that SCI increases the components of the CMA pathway and a positive correlation between HDAC6 activity and indicators of CMA pathway *in vivo* and *in vitro* (Figures 1 and 5). In mammalian cells, the pathway of CMA is constitutively and maximally activated under stressful conditions, especially oxidative stress [22]. As a cell repair mechanism, CMA was really activated during HI in our study (Figure 5). The pathway of CMA selectively degrades cytosolic proteins containing the KFERQ (five peptide sequences can be recognized by a chaperone complex containing HSC70) signal motif through direct translocation into the lysosome [40]. Oxidized substrate proteins are translocated into lysosomes more efficiently by this pathway than marcoautophagy [33]. In addition, under mild oxidative stress condition, the lysosomes bring into play a higher tendency to bind and internalize substrates transferred by CMA [7, 33]. Collectively, this shows that CMA provides the front line of defense against oxidative stress [33]. Therefore, we believe that CMA favors degradation of abnormal and unnecessary proteins against that of proteins essential for cell survival. This may also explain why CMA degradation pathway can be activated under SCI and hypoxia-ischemia condition.

The successful implementation of the CMA depends on substrates, which could be recognized by a chaperone complex containing HSC70 and delivered into lysosomes via the interactions with LAMP-2a. The cycle of HSC70-client protein complex involves successive association and dissociation with chaperone HSP90 to form various multimeric protein complexes [41]. This is dictated by the ATP-binding state of HSP90 [42]. A conformational change in HSP90 leads to the release and realignment of cochaperones HSC70 to form a mature chaperone-subtract complex [41–43]. The change of HSP90 activity is closely related to its acetylation level. Our study demonstrates for the first time that the depletion of HDAC6 levels led to the increase of HSP90 acetylation and decrease of the association between HSC70 and HSP90 in cells exposure to HI (Figure 6).

Moreover, the chaperone-substrate complex must specifically bind to LAMP-2a which located on the membrane of the lysosomal, a receptor for CMA, and the binding of substrates to LAMP-2a is the limiting step for CMA [18]. The substrate only binds with LAMP-2a monomers and promotes the organization of LAMP-2a into a high multimeric complex of approximately 700 kDa, a critical step for substrate translocation [18, 23]. When CMA is maximally activated, the level of LAMP-2a located on the lysosomal membrane may increase [23, 24]. The LAMP-2a undergoes continuous cycles of assembly/disassembly, while HSP90 is the key molecule

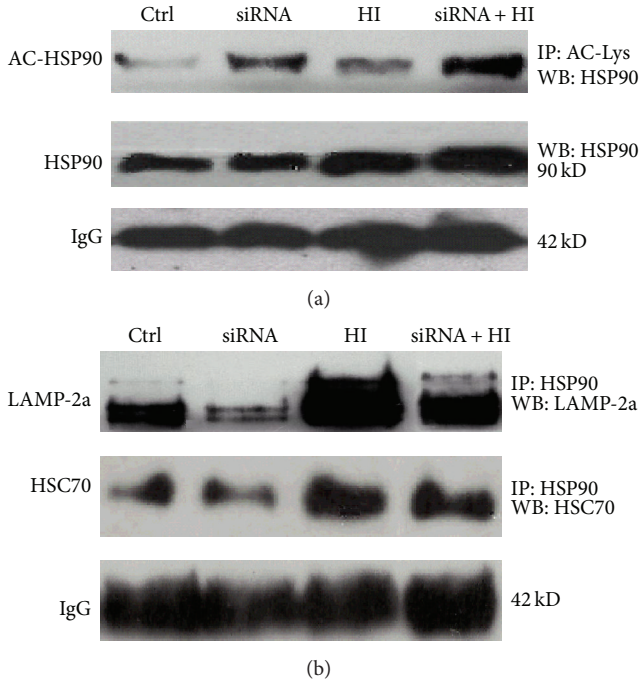

Figure 6: HDAC6 affects the activity of CMA by regulating the level of acetylated HSP90. (a) The cell lysates isolated from PC12 and PC12/siHDAC6 cells exposed to HI for 24 h. Ctrl express vehicle-treated group. The protein complexes were immunoprecipitated with anti-acetylation antibody and blotted with anti-HSP90 antibody for determination of acetylated HSP90 (Ac-Hsp90) level. The level of IgG was used as a loading control. (b) The immunocomplexes were precipitated from PC12 and PC12/siHDAC6 cells with anti-HSP90 antibody and blotted with anti-HSC70 or anti-LAMP-2a antibodies for determination of the interaction of HSP90 with HSC70 or LAMP-2a. The level of IgG was used as a loading control.

chaperone to drive the cycle. HSP90 binds to the lysosomal membrane to stabilize LAMP-2a and induce it to change from the monomeric to the multimeric state in order to efficaciously transfer substrate proteins [23, 26]. Our results showed that knockdown of HDAC6 induced irreversible hyperacetylation of HSP90 and attenuated the interaction of HSP90 with LAMP-2a. This may result in the reduction of the stability of LAMP-2a, ultimately interfering with the CMA.

In addition, the relation between the LAMP-1 and LAMP-2a was accidentally observed in our study. The LAMP-1 is a major protein component of the lysosomal membrane. The LAMP-1 has 37% amino acid sequence homology with LAMP-2, which is also the protein component of the lysosomal membrane [44]. LAMP-2a is not only an important active subtype of LAMP-2, but also the speed-limiting protein of the CMA metabolic pathway. LAMP-1 deficiency can induce overexpression of murine LAMP-2a [45], while our study showed that inhibition of HDAC6 hindered the increase of LAMP-2a; as a consequence, the number of LAMP-1 was compensatory increased to resist HI-induced oxidative stress toxicity (Figure 5(c)). Therefore, we speculated there is a regulatory balance between LAMP-2a and LAMP-1 that can further regulate the CMA pathway, which needs further study to be proven.

In this study, we provided the evidence that SCI and HI stress activated the function of CMA pathway to restrain ROS generation and alleviate cell damage, while loss of HDAC6 hindered the CMA activity increase, which could partially regulate the acetylation of HSP90. Consequently, the deacetylation of HSP90 by HDAC6 is perhaps a potential therapeutic target in acute SCI model and arouses our interests to study it in depth.

5. Conclusions

Hypoxia-ischemia- (HI-) induced oxidative stress plays a role in secondary pathocellular processes of acute SCI due to hypoxia-ischemia (HI) from many kinds of mechanical trauma. Our results showed that inhibition of HDAC6 accelerated reactive oxygen species (ROS) generation and cell apoptosis in response to the HI. Deficiency of HDAC6 hindered the CMA activity to resistance HI-induced oxidative stress. Furthermore, our results provided the experimental evidence for the potential role of HDAC6 in the regulation of CMA by affecting HSP90 acetylation. Therefore, HDAC6 plays an important role in the function of CMA pathway under the HI stress induced by SCI and arouses our interests to pursue it further in an in-depth study.

Abbreviations

SCI:	Spinal cord injury
ROS:	Reactive oxygen species
CMA:	Chaperone-mediated autophagy
HDAC6:	Histone deacetylase-6
HSP90:	Heat-shock protein of 90 kDa
HSC70:	Heat-shock cognate protein of 70 kDa
LAMP-2a:	Lysosome-associated membrane protein type 2a
LAMP-1:	Lysosome-associated membrane protein type 1
HI:	Hypoxia-ischemia
HIF-1-alpha:	Hypoxia-inducible factor 1 alpha
RNase A:	Ribonuclease A
MMP:	Mitochondrial membrane potential.

Conflict of Interests

All authors declare no conflict of interests in relation to this study.

Authors' Contribution

Min Su designed the study and wrote and reviewed the paper. Huaqing Guan and Fan Zhang contributed to the *in vivo* experimental studies. Xiaomei Teng and Yarong Gao performed the *in vitro* experimental studies. Weixin Yang analyzed data and provided research condition.

Acknowledgments

This work was supported by National Natural Science Foundation of China (no. 81301059) and Natural Science Foundation of Suzhou City of China (no. SYS201221). The authors

thank the Institute of Neuroscience of the Shanghai Institutes, Chinese Academy of Sciences, for the preparation of cell lines. They are grateful to Professor Chunfeng Liu and Professor Xinchun Jin of Institute of Neuroscience, Soochow University, for their technical help. They thank Hanjun Wang M.D. of Cellular and Integrative Physiology, University of Nebraska Medical Center, for his insightful comments and suggestions to our study.

References

[1] H.-C. Chen, T.-H. Fong, A.-W. Lee, and W.-T. Chiu, "Autophagy is activated in injured neurons and inhibited by methylprednisolone after experimental spinal cord injury," *Spine*, vol. 37, no. 6, pp. 470–475, 2012.

[2] J.-F. Wang, Y. Li, J.-N. Song, and H.-G. Pang, "Role of hydrogen sulfide in secondary neuronal injury," *Neurochemistry International*, vol. 64, no. 1, pp. 37–47, 2014.

[3] J. Y. Lee, S. Maeng, S. R. Kang et al., "Valproic acid protects motor neuron death by inhibiting oxidative stress and endoplasmic reticulum stress-mediated cytochrome c release after spinal cord injury," *Journal of Neurotrauma*, vol. 31, no. 6, pp. 582–594, 2014.

[4] S. N. Hassler, K. M. Johnson, and C. E. Hulsebosch, "Reactive oxygen species and lipid peroxidation inhibitors reduce mechanical sensitivity in a chronic neuropathic pain model of spinal cord injury in rats," *Journal of neurochemistry*, vol. 131, no. 4, pp. 413–417, 2014.

[5] Z. Jia, H. Zhu, J. Li, X. Wang, H. Misra, and Y. Li, "Oxidative stress in spinal cord injury and antioxidant-based intervention," *Spinal Cord*, vol. 50, no. 4, pp. 264–274, 2012.

[6] H. Kanno, H. Ozawa, A. Sekiguchi, and E. Itoi, "The role of autophagy in spinal cord injury," *Autophagy*, vol. 5, no. 3, pp. 390–392, 2009.

[7] E. Dohi, S. Tanaka, T. Seki et al., "Hypoxic stress activates chaperone-mediated autophagy and modulates neuronal cell survival," *Neurochemistry International*, vol. 60, no. 4, pp. 431–442, 2012.

[8] M. Dodson, V. Darley-Usmar, and J. Zhang, "Cellular metabolic and autophagic pathways: traffic control by redox signaling," *Free Radical Biology and Medicine*, vol. 63, pp. 207–221, 2013.

[9] A. Höhn, J. König, and T. Grune, "Protein oxidation in aging and the removal of oxidized proteins," *Journal of Proteomics*, vol. 92, pp. 132–159, 2013.

[10] J. Bai, Y. Lei, G. An, L. He, and S. Chen, "Down-regulation of deacetylase HDAC6 inhibits the melanoma cell line A375.S2 growth through ROS-dependent mitochondrial pathway," *PLOS ONE*, vol. 10, no. 3, Article ID e0121247, 2015.

[11] M. A. Rivieccio, C. Brochier, D. E. Willis et al., "HDAC6 is a target for protection and regeneration following injury in the nervous system," *Proceedings of the National Academy of Sciences of the United States of America*, vol. 106, no. 46, pp. 19599–19604, 2009.

[12] M. Fukada, A. Hanai, A. Nakayama et al., "Loss of deacetylation activity of Hdac6 affects emotional behavior in mice," *PLoS ONE*, vol. 7, no. 2, Article ID e30924, 2012.

[13] J. Jochems, J. Boulden, B. G. Lee et al., "Antidepressant-like properties of novel HDAC6-selective inhibitors with improved brain bioavailability," *Neuropsychopharmacology*, vol. 39, no. 2, pp. 389–400, 2014.

[14] H. Kanno, H. Ozawa, A. Sekiguchi, and E. Itoi, "Spinal cord injury induces upregulation of Beclin 1 and promotes autophagic cell death," *Neurobiology of Disease*, vol. 33, no. 2, pp. 143–148, 2009.

[15] M. Su, J.-J. Shi, Y.-P. Yang et al., "HDAC6 regulates aggresome-autophagy degradation pathway of alpha-synuclein in response to MPP^+-induced stress," *Journal of Neurochemistry*, vol. 117, no. 1, pp. 112–120, 2011.

[16] T. Hara, H. Fukumitsu, H. Soumiya, Y. Furukawa, and S. Furukawa, "Injury-induced accumulation of glial cell line-derived neurotrophic factor in the rostral part of the injured rat spinal cord," *International Journal of Molecular Sciences*, vol. 13, no. 10, pp. 13484–13500, 2012.

[17] J.-Z. Huang, Y.-Z. Chen, M. Su et al., "Dl-3-n-Butylphthalide prevents oxidative damage and reduces mitochondrial dysfunction in an MPP^+-induced cellular model of Parkinson's disease," *Neuroscience Letters*, vol. 475, no. 2, pp. 89–94, 2010.

[18] A. M. Cuervo and J. F. Dice, "Regulation of Lamp2a levels in the lysosomal membrane," *Traffic*, vol. 1, no. 7, pp. 570–583, 2000.

[19] B. Y. Chin, G. Jiang, P. J. Lee et al., "Hypoxia-inducible factor 1alpha stabilization by carbon monoxide results in cytoprotective preconditioning," *Proceedings of the National Academy of Sciences of the United States of America*, vol. 104, no. 12, pp. 5109–5114, 2007.

[20] Y.-N. Liu, Y.-X. Wang, X.-F. Liu et al., "Citreoviridin induces ROS-dependent autophagic cell death in human liver HepG2 cells," *Toxicon*, vol. 95, pp. 30–37, 2015.

[21] Q. Yang, H. She, M. Gearing et al., "Regulation of neuronal survival factor MEF2D by chaperone-mediated autophagy," *Science*, vol. 323, no. 5910, pp. 124–127, 2009.

[22] S. Kaushik and A. M. Cuervo, "Autophagy as a cell-repair mechanism: activation of chaperone-mediated autophagy during oxidative stress," *Molecular Aspects of Medicine*, vol. 27, no. 5-6, pp. 444–454, 2006.

[23] S. J. Orenstein and A. M. Cuervo, "Chaperone-mediated autophagy: molecular mechanisms and physiological relevance," *Seminars in Cell & Developmental Biology*, vol. 21, no. 7, pp. 719–726, 2010.

[24] A. M. Cuervo and J. F. Dice, "A receptor for the selective uptake and degradation of proteins by lysosomes," *Science*, vol. 273, no. 5274, pp. 501–503, 1996.

[25] S. Shen, P. Zhang, M. A. Lovchik et al., "Cyclodepsipeptide toxin promotes the degradation of Hsp90 client proteins through chaperone-mediated autophagy," *The Journal of Cell Biology*, vol. 185, no. 4, pp. 629–639, 2009.

[26] F. A. Agarraberes and J. F. Dice, "A molecular chaperone complex at the lysosomal membrane is required for protein translocation," *Journal of Cell Science*, vol. 114, no. 13, pp. 2491–2499, 2001.

[27] J. J. Kovacs, P. J. M. Murphy, S. Gaillard et al., "HDAC6 regulates Hsp90 acetylation and chaperone-dependent activation of glucocorticoid receptor," *Molecular Cell*, vol. 18, no. 5, pp. 601–607, 2005.

[28] Y. S. Kim, H. W. Seo, and G. Jung, "Reactive oxygen species promote heat shock protein 90-mediated HBV capsid assembly," *Biochemical and Biophysical Research Communications*, vol. 457, no. 3, pp. 328–333, 2015.

[29] B. Atalay, M. Bavbek, M. Cekinmez et al., "Antibodies neutralizing Nogo-A increase pan-cadherin expression and motor recovery following spinal cord injury in rats," *Spinal Cord*, vol. 45, no. 12, pp. 780–786, 2007.

[30] M. R. Sánchez-Carbente, S. Castro-Obregón, L. Covarrubias, and V. Narváez, "Motoneuronal death during spinal cord development is mediated by oxidative stress," *Cell Death and Differentiation*, vol. 12, no. 3, pp. 279–291, 2005.

[31] S. Ma, Z. Zhang, F. Yi et al., "Protective effects of low-frequency magnetic fields on cardiomyocytes from ischemia reperfusion injury *via* ros and $NO/ONOO^-$," *Oxidative Medicine and Cellular Longevity*, vol. 2013, Article ID 529173, 9 pages, 2013.

[32] Y. Miao, J. Zhou, M. Zhao et al., "Acetylcholine attenuates hypoxia/reoxygenation-induced mitochondrial and cytosolic ROS formation in H9c2 cells via M2 acetylcholine receptor," *Cellular Physiology and Biochemistry*, vol. 31, no. 2-3, pp. 189–198, 2013.

[33] R. Scherz-Shouval and Z. Elazar, "ROS, mitochondria and the regulation of autophagy," *Trends in Cell Biology*, vol. 17, no. 9, pp. 422–427, 2007.

[34] L. Jing, M.-T. He, Y. Chang et al., "Coenzyme Q10 protects astrocytes from ROS-Induced damage through inhibition of Mitochondria-Mediated cell death pathway," *International Journal of Biological Sciences*, vol. 11, no. 1, pp. 59–66, 2015.

[35] U. B. Pandey, Y. Batlevi, E. H. Baehrecke, and J. P. Taylor, "HDAC6 at the intersection of autophagy, the ubiquitin-proteasome system and neurodegeneration," *Autophagy*, vol. 3, no. 6, pp. 643–645, 2007.

[36] R. B. Parmigiani, W. S. Xu, G. Venta-Perez et al., "HDAC6 is a specific deacetylase of peroxiredoxins and is involved in redox regulation," *Proceedings of the National Academy of Sciences of the United States of America*, vol. 105, no. 28, pp. 9633–9638, 2008.

[37] A. Iwata, B. E. Riley, J. A. Johnston, and R. R. Kopito, "HDAC6 and microtubules are required for autophagic degradation of aggregated Huntingtin," *The Journal of Biological Chemistry*, vol. 280, no. 48, pp. 40282–40292, 2005.

[38] Y. Du, F. Wang, J. Zou et al., "Histone deacetylase 6 regulates cytotoxic α-synuclein accumulation through induction of the heat shock response," *Neurobiology of Aging*, vol. 35, no. 10, pp. 2316–2328, 2014.

[39] S. Sharp and P. Workman, "Inhibitors of the HSP90 molecular chaperone: current status," *Advances in Cancer Research*, vol. 95, pp. 323–348, 2006.

[40] J. F. Dice, "Chaperone-mediated autophagy," *Autophagy*, vol. 3, no. 4, pp. 295–299, 2007.

[41] P. Bali, M. Pranpat, J. Bradner et al., "Inhibition of histone deacetylase 6 acetylates and disrupts the chaperone function of heat shock protein 90: a novel basis for antileukemia activity of histone deacetylase inhibitors," *The Journal of Biological Chemistry*, vol. 280, no. 29, pp. 26729–26734, 2005.

[42] S. Aoyagi and T. K. Archer, "Modulating molecular chaperone Hsp90 functions through reversible acetylation," *Trends in Cell Biology*, vol. 15, no. 11, pp. 565–567, 2005.

[43] Y. Yang, R. Rao, J. Shen et al., "Role of acetylation and extracellular location of heat shock protein 90α in tumor cell invasion," *Cancer Research*, vol. 68, no. 12, pp. 4833–4842, 2008.

[44] W.-C. Wang, N. Lee, D. Aoki, M. N. Fukuda, and M. Fukuda, "The poly-N-acetyllactosamines attached to lysosomal membrane glycoproteins are increased by the prolonged association with the Golgi complex," *The Journal of Biological Chemistry*, vol. 266, no. 34, pp. 23185–23190, 1991.

[45] E.-L. Eskelinen, C. K. Schmidt, P. Saftig et al., "Disturbed cholesterol traffic but normal proteolytic function in LAMP-1/LAMP-2 double-deficient fibroblasts," *Molecular Biology of the Cell*, vol. 15, no. 7, pp. 3132–3145, 2004.

Hindawi Publishing Corporation
Oxidative Medicine and Cellular Longevity
Volume 2016, Article ID 2158971, 8 pages
http://dx.doi.org/10.1155/2016/2158971

Research Article

Estrogen Replacement Reduces Oxidative Stress in the Rostral Ventrolateral Medulla of Ovariectomized Rats

Fan Hao,[1] Ying Gu,[1] Xing Tan,[2] Yu Deng,[2] Zhao-Tang Wu,[2] Ming-Juan Xu,[1] and Wei-Zhong Wang[2]

[1]*Department of Obstetrics and Gynecology, Changhai Hospital, Second Military Medical University, Shanghai 200433, China*
[2]*Department of Physiology, Second Military Medical University, Shanghai 200433, China*

Correspondence should be addressed to Ming-Juan Xu; 13636373419@163.com and Wei-Zhong Wang; wangwz68@hotmail.com

Received 15 May 2015; Accepted 6 July 2015

Academic Editor: Pál Pacher

Cardiovascular disease prevalence rises rapidly after menopause, which is believed to be derived from the loss of estrogen. It is reported that sympathetic tone is increased in postmenopause. The high level of oxidative stress in the rostral ventrolateral medulla (RVLM) contributes to increased sympathetic outflow. The focus of this study was to determine if estrogen replacement reduces oxidative stress in the RVLM and sympathetic outflow in the ovariectomized (OVX) rats. The data of this study showed that OVX rat increased oxidative stress in the RVLM and sympathetic tone; estrogen replacement improved cardiovascular functions but also reduced the level of oxidative stress in the RVLM. These findings suggest that estrogen replacement decreases blood pressure and sympathoexcitation in the OVX rats, which may be associated with suppression in oxidative stress in the RVLM through downregulation of protein expression of NADPHase (NOX4) and upregulation of protein expression of SOD1. The data from this study is beneficial for our understanding of the mechanism of estrogen exerting cardiovascular protective effects on postmenopause.

1. Introduction

The prevalence and severity of cardiovascular diseases (e.g., hypertension and coronary heart disease) increase more markedly along with increasing age in postmenopausal women. A higher percentage of women than men suffer from hypertension after the age of 65 years [1, 2]. It has been indicated that estrogen possesses beneficial effects on these cardiovascular diseases [3]. Beside its well-known peripheral cardiovascular protective effects, accumulating evidence shows that estrogen is recognized as a modulator in the central nervous system (CNS) to cardiovascular regulation. For example, activation of estrogen receptors in the cardiovascular centers stimulates the release of nitric oxide but also reduces hypertension induced by L-glutamate, aldosterone, or salt [4–6].

It is well known that the rostral ventrolateral medulla (RVLM) is a key region for control of sympathetic outflow and blood pressure [7]. Overactivity of sympathetic tone is a hallmark of cardiovascular disorders including hypertension and heart failure [8]. It is interesting that sympathetic activity is also increased in the ovariectomized (OVX) rats [9–11]. Increased oxidative stress is reported to be relative to hypertension development [12]. Oxidative stress results from an imbalance of generation over degradation of the reactive oxygen species (ROS), especially superoxide [13]. It is well known that NADPH oxidase (NADPHase) transfers electron to molecular oxygen and formats superoxide [14]. Superoxide dismutase 1 (SOD1) is enzyme that alternately catalyzes the dismutation of the superoxide radical into either ordinary molecular oxygen or hydrogen peroxide [15]. Therefore, ROS production is closely relative to activity of NADPHase and SOD1. The increased sympathetic outflow in hypertension is associated with enhanced oxidative stress at the level of RVLM [16]. Interestingly, administration of estrogen counteracts oxidative stress in erythrocytes and plasma of OVX rats and in premenopausal women [17, 18]. However, it is unclear if the beneficial effect of estrogen replacement on the OVX-induced sympathetic overactivity is associated with suppression of oxidative stress in the RVLM. Therefore, the

present study was designed to determine the level of oxidative stress in the RVLM in the OVX rats and further evaluate the effect of estrogen replacement on oxidative stress.

2. Materials and Methods

2.1. Animals. Female Sprague-Dawley rats (Sino-British SIPPR/BK Laboratory Animal Ltd., Shanghai, China) were used in these experiments. All of the procedures of this study conformed to the institutional animal care guidelines and all performances were approved by the Animal Care and Use Committee of the Second Military Medical University. The rats were assigned to 4 groups: sham with vehicle (sham + vehicle), sham with 17β-estradiol injection (sham + E2), OVX with vehicle (OVX + vehicle), and OVX with 17β-estradiol injection (OVX + E2).

2.2. Ovariectomy. Ovariectomy was carried out according to previous study [19]. At 10 weeks of age, animals were anesthetized by isoflurane (induction 4%; maintenance 1.5%). The abdomen of the rat was cleaned and disinfected with 75% ethanol. An abdominal median incision was made and bilateral ovaries were removed. The rat that received the same operation without removing ovaries was regarded as the sham group. After surgery, the animals received intramuscular injection of antibiotics. One week after being OVX, rats were treated with 4-week subcutaneous injections of estrogen (17β-estradiol-water soluble, 30 μg/kg/day, Sigma, St. Louis, MO, USA) [20] and 0.9% saline was used as vehicle treatment. Finally, uterine weight and serum samples were collected for assessing the effectiveness of OVX and estrogen treatment [21]. Serum sample was diluted by 1 : 100 and performed to detect estrogen concentration by estradiol Elisa kit (BioTNT Co.).

2.3. Measurement of Cardiovascular Parameters. The procedure for general surgery was described previously [22]. Briefly, rats were anaesthetized (urethane 800 mg/kg, alpha-chloralose 40 mg/kg, i.p.) and the trachea was cannulated. The right femoral artery was catheterized for BP measurement by the PowerLab system. The mean arterial pressure (MAP) and heart rate (HR) were derived from the BP pulse. Body temperature was kept at 37°C [23]. The renal sympathetic nerve was isolated retroperitoneally and placed on a pair of silver recording electrodes. The renal sympathetic nerve activity (RSNA) signal was amplified, integrated, and recorded with the PowerLab system (AD Instruments, Australia). The maximum nerve activity (Max) and background noise level of RSNA were obtained as described previously [24]. Briefly, Max occurred 1-2 min after the rat was euthanized with an overdose of pentobarbital sodium. Baseline RSNA, subtracting the noise level from the absolute value, was expressed as a percentage of Max.

2.4. Measurement of Norepinephrine (NE) Concentration. As described previously [22], the norepinephrine (NE) in 24-h urine was detected by High-Performance Liquid Chromatography (HPLC, Model 582 pump, ESA, USA) with electrochemical detection (Model 5300, ESA, USA). Briefly, urinary samples were collected by placing rats in metabolic cages for 24-h and embalmed with glacial acetic acid. The internal standard was dihydroxybenzylamine (DHBA; Sigma). NE was absorbed onto acid-washed alumina with 1.5 mmol/L tris HCl (pH = 8.8). Then we performed shaking of NE and standing for a while before being extracted with 0.2 mol/L glacial acetic acid (400 μL). Supernatant was injected into HPLC column (reverse phase, ESA 150 × 3.2 mm, 3 μm C18 (P/N 70-0636)), and NE was eluted with mobile phase. The flow rate was 0.4 mL/min. The experiments were performed at a temperature of 22–26°C.

2.5. Western Blot Analysis. The protein expression of NOX4 and SOD1 in the RVLM was detected by Western blot, as described previously [22]. Rats were euthanized by overdose of anesthetic and the brains were removed. The RVLM tissues were punched from 100 μm coronal sections of brainstem according to the rat atlas [25]. The tissues were prepared and centrifuged. The total protein concentration was determined and equal amounts of protein (20 μg) were applied to a 10% SDS-polyacrylamide gel, followed by transferring to PVDF membrane. The membrane was blocked and incubated overnight at 4°C with NOX4 antibody (1 : 2000, Epitomics, America) or SOD-1 (1 : 2000, Epitomics, American). The following day, the membrane was incubated with goat anti-rabbit IgG (H + L) for 2 h at room temperature. Finally, the membrane was visually detected and analyzed [26]. Tubulin was severed as loading control.

2.6. Measurement of ROS Production in the RVLM. In this study, two measurements were performed to detect the ROS production in the RVLM tissue. After RVLM tissue was punched and weighed from the rat which was euthanized (pentobarbital sodium, 300 mg/kg, i.p.), 80 μL Protein Lysis Buffer (Cell Signaling Technology, USA) was added into the test tube and tissue was polished by electric homogenizer and then centrifuging for 20 min. Supernatant was collected for analysis by lucigenin chemiluminescence quantitative kit (Genmed Scientifics Inc., USA, GMS10113.5) and dihydroethidium (DHE). We can complete lucigenin chemiluminescence quantitative detecting according to the instructions. DHE, ROS sensitive fluorescent dye, brain tissues (15 μm thick) were incubated at 37°C with DHE (5 μmol/L) for 30 min. Sections were washed in 0.1 M PBS (3 × 1 min) and then examined by confocal laser scanning microscope (Fuji Film, Japan) and the image was captured at red fluorescence microscope around the RVLM and was evaluated using LAS-AF-Lite software [24].

2.7. Statistical Analysis. Data are presented as mean ± SEM. The difference of plasma estrogen concentration between sham-operated group, ovariectomized group, and ovariectomized rats with estrogen replacement group was analyzed by one-way ANOVA, followed by SNK post hoc analysis. The differences between sham-operated and ovariectomized rats with vehicle or estrogen treatment were analyzed by two-way ANOVA, followed by SNK post hoc analysis. $p < 0.05$ was considered significant.

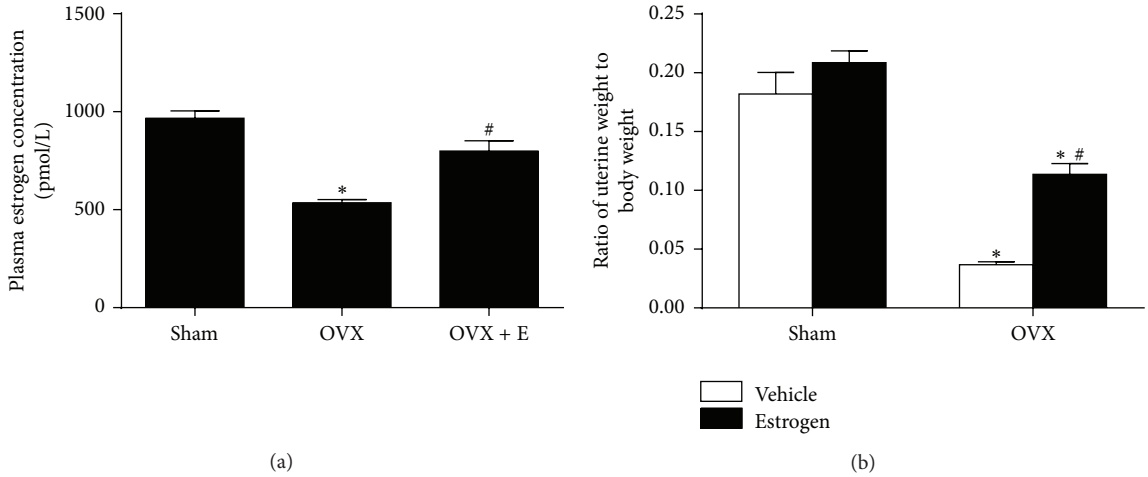

(a) (b)

Figure 1: The plasma estrogen concentration as well as relative uterine weight in sham-operated, ovariectomized rats and ovariectomized rats with estrogen treatment for 4 weeks. (a) Plasma estrogen concentration; (b) uterine weight was attenuated body weight in sham and OVX rats with vehicle or estrogen treatment. Means ± SEM, $n = 5$/group, $^{*}p < 0.05$ versus sham group, and $^{\#}p < 0.05$ versus OVX or with vehicle group.

3. Results

3.1. OVX Model Assessment. Compared with sham group, the OVX rats showed significant lower level in the relative uterine weight (0.182 ± 0.018 versus 0.037 ± 0.003 mg/g) and plasma estrogen concentration (966.7 ± 37.4 versus 535.8 ± 16.5 pmol/L), which was significantly attenuated by estrogen replacement (Figure 1).

3.2. The Cardiovascular Effect of Estrogen on OVX Rats. Levels of BP, HR, and RSNA began to be significantly increased 6 weeks after ovariectomy, which were completely prevented by subsequent injection of estrogen for 4 weeks (Figures 2(a)–2(d)). In additional, estrogen replacement also prevented the OVX-induced increase in NE in 24-h urine (Figure 2(e)).

3.3. Detection of ROS Production in the RVLM. To elucidate the effect of estrogen on ROS production in the RVLM, fluorescent labeling (DHE) was used to detect ROS production, as indicated in Figure 3. The results of DHE fluorescent staining and lucigenin chemiluminescence quantitative detection showed that the level of ROS production in the RVLM was significantly higher in the OVX group than in sham group, which was reduced by estrogen replacement.

3.4. Protein Detection of NOX4 and SOD1 in the RVLM. As indicated in Figure 4, Western blot analysis demonstrated that ovariectomy procedure significantly increased and decreased NOX4 and SOD1 protein expression in the RVLM, respectively. It was found that changes in NOX4 and SOD1 protein expression in the RVLM of VOX rats were attenuated by estrogen treatment for 4 weeks.

4. Discussion

The main finding from this study is that OVX rats show a significant increase in BP and sympathetic activity as well as ROS production in the RVLM, which can be attenuated by estrogen replacement. These data suggest that estrogen replacement decreases BP and sympathoexcitation in OVX rats, which maybe resulted from the estrogen-mediated depression of oxidative stress in the RVLM.

Accumulating evidences indicate that estrogens exert protective effects on cardiovascular disorder through actions within the CNS [4, 27]. Menopause is a cardiovascular risk factor, which is mainly related to abrupt withdrawal of estrogen, and the lack of estrogen contributes to sympathoexcitation in both human and animal models [11, 28]. The mechanism by which estrogen withdrawal increases sympathetic outflow is not clear. Several regions in CNS, including the nucleus tractus solitarius, RVLM, and the paraventricular nucleus (PVN), are known to be involved in regulation of sympathetic tone and BP [29]. Abnormalities in the RVLM neurons contribute to sympathetic overactivity, which is associated with the development and progression of cardiovascular disorders including hypertension and chronic heart failure [30, 31]. It is reported that BP, HR, and NE (an index of sympathetic nerve activity) were increased in OVX rats [11]. In this study, it has been confirmed that, under anesthesia state, OVX rats show a significant increase in BP and RSNA, which can be attenuated by estrogen replacement. This is similar to that observed previously in conscience, freely moving OVX versus sham rats [32]. Therefore, these data lead to a conclusion that withdrawal of estrogen is a major contributor to sympathoexcitation in the OVX rats.

Sympathoexcitation is closely associated with the development and progression of cardiovascular diseases [30]. High level of oxidative stress in the RVLM which is resulting from

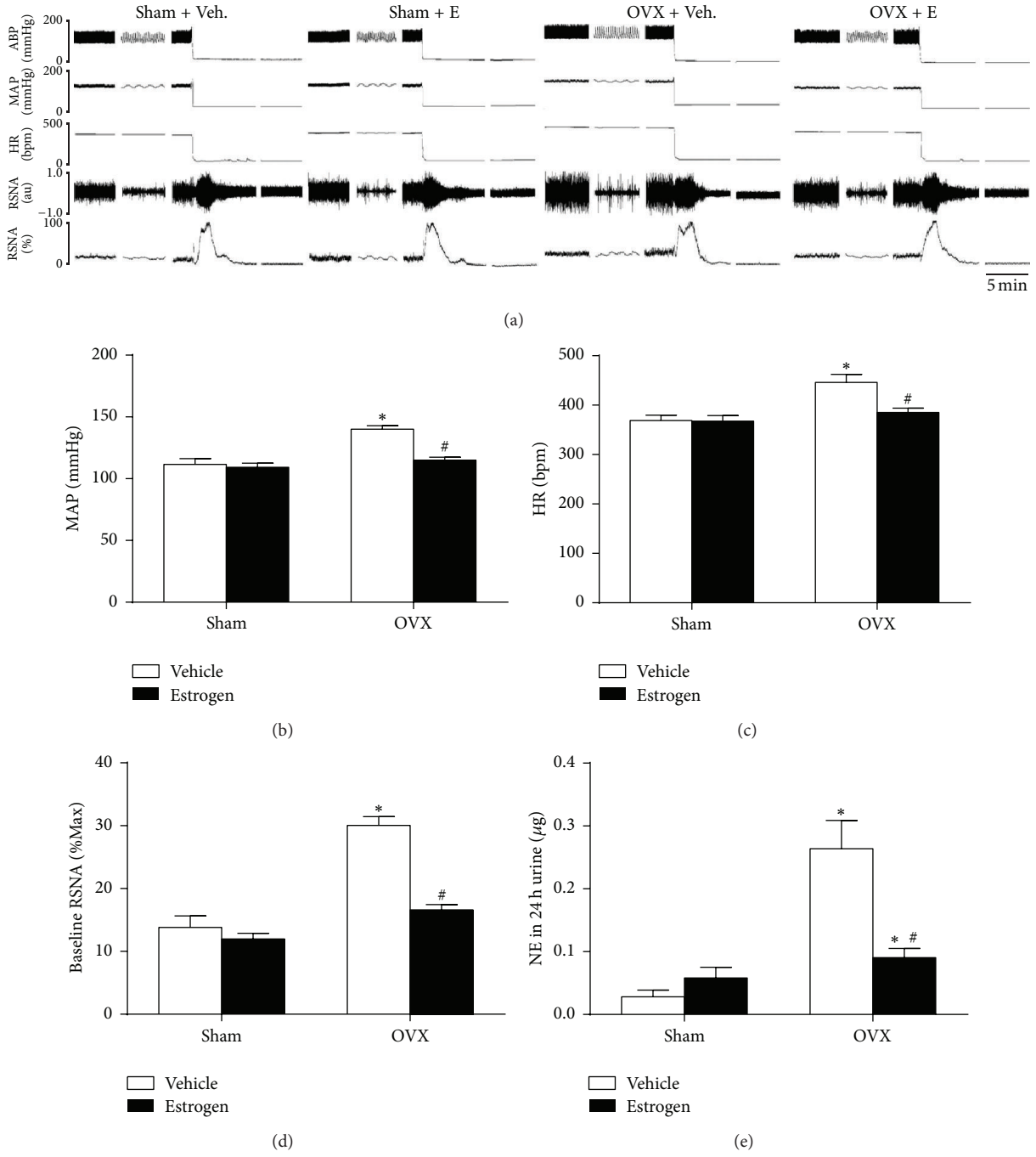

Figure 2: Cardiovascular changes in sham-operated and ovariectomized rats with vehicle or estrogen treatment for 4 weeks. (a) Representative original tracings of BP, HR, and RSNA in four groups. Maximum and background noise levels of RSNA were measured after rats were euthanized. Changes in MAP (b), HR (c), baseline RSNA (d), and NE in 24-h urine (e) were presented in four groups. Means ± SEM, n = 5/group, $^{*}p < 0.05$ versus sham + vehicle, and $^{\#}p < 0.05$ versus OVX + vehicle.

abnormalities of renin angiotensin system and proinflammatory cytokines is responsible for increased sympathetic outflow [33, 34]. In this work, β-estradiol (water soluble) was used for estrogen replacement. This drug is water soluble and belongs to steroid hormone and penetrates the blood brain barrier, so it was applied by subcutaneous injection in this work. Although we did not detect the effective concentration of estrogen in the RVLM, this dosage of subcutaneous administration led to a significant reduction in ROS production at the level of RVLM and sympathetic outflow. Therefore, the concentration of estrogen has effect on RVLM neurons. Our findings have shown that the level of ROS in the RVLM is significantly increased in OVX rats, which is effectively prevented by estrogen replacement.

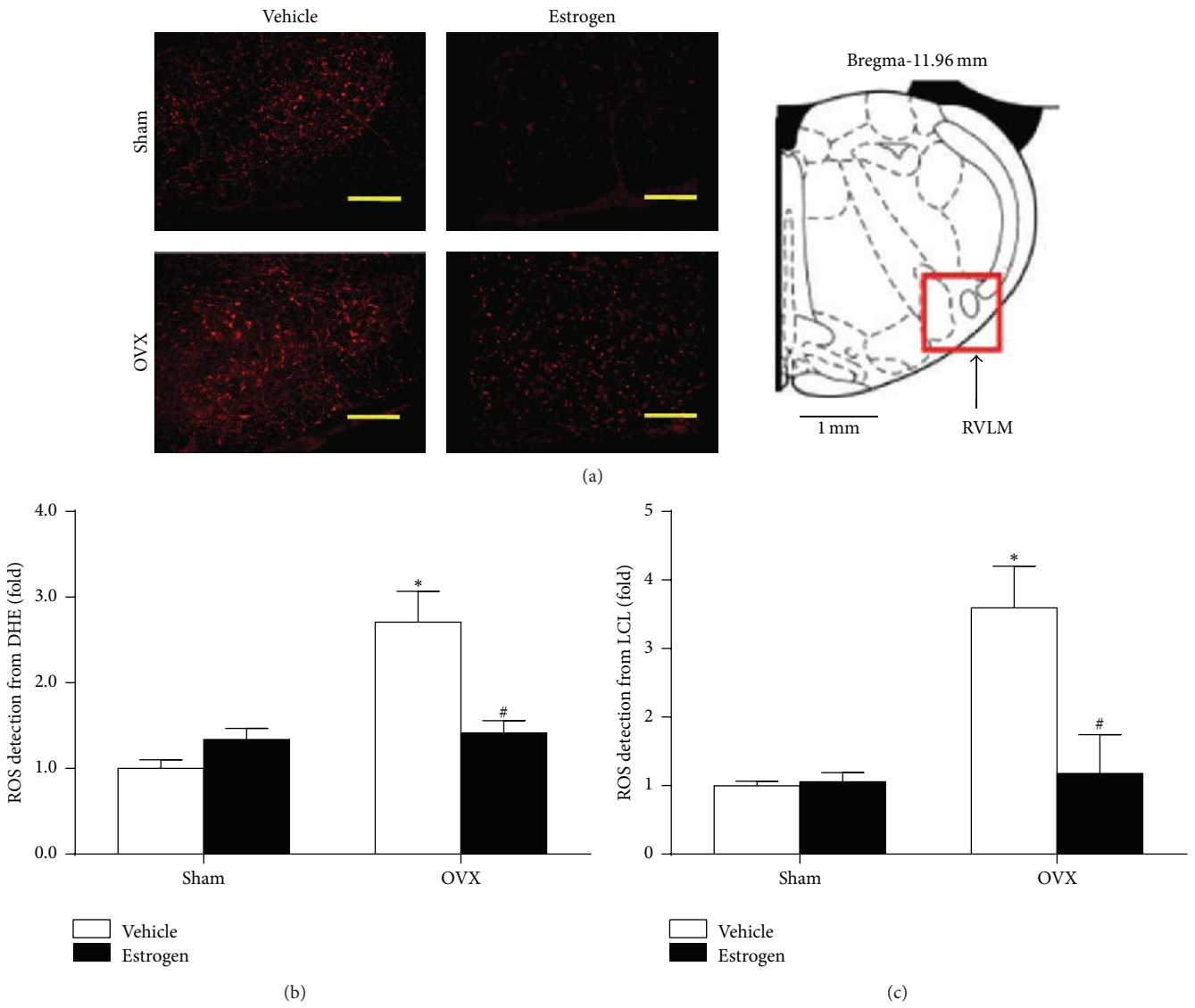

Figure 3: Estrogen attenuated the level of ROS in the RVLM of sham and OVX rats. (a) Representative confocal images of ROS (red) in the RVLM (indicated by a red square in the rat atlas) stained by fluorescent labeling (DHE). Scale bar, 200 μm. Quantification of ROS production in the RVLM from DHE fluorescent analysis (b) and lucigenin chemiluminescence (LCL) detection (c). Means ± SEM, $n = 5$/group, $^{*}p < 0.05$ versus sham vehicle, and $^{\#}p < 0.05$ versus OVX with vehicle.

Expression of NOX4 (NADPHase subtype) is increased and SOD1 is decreased in OVX rats compared with sham rats. NOX4 is predominantly involved in ROS regeneration among the NOX family in brain [35]. The antioxidant SOD catalyzes the dismutation of superoxide into hydrogen peroxide [36]. It is reported that overexpression of SOD in the RVLM attenuates the angiotensin II-induced oxidative stress [37]. Based on the present and previous work, we suggest that changes in NADPHase and SOD1 play an important role in high level of oxidative stress in the RVLM of OVX rats.

The more important finding in this work is that estrogen administration significantly reduced ROS production at the level of RVLM in OVX rats. This data supports the idea that the estrogen-mediated antioxidative stress contributes to decrease of BP and sympathoexcitation via the central mechanism. However, there are several limitations in this work. First, it is reported that serum estrogen and uterine weight were increased during prooestrus compared to dioestrus, but both of them in ovariectomized rats were decreased significantly compared with sham rats during either prooestrus or dioestrus [38]. Therefore, the success of OVX model was usually assessed by the levels of serum estrogen and relative uterine weight. In this previous study, the baseline of MAP presents fluctuation and baseline blood pressure is higher in dioestrus compared to prooestrus rats. The change difference of MAP caused by estrus cycle was an average of 7.4 mmHg in this previous study [38], which was significantly lower compared with the difference caused by ovariectomy in our

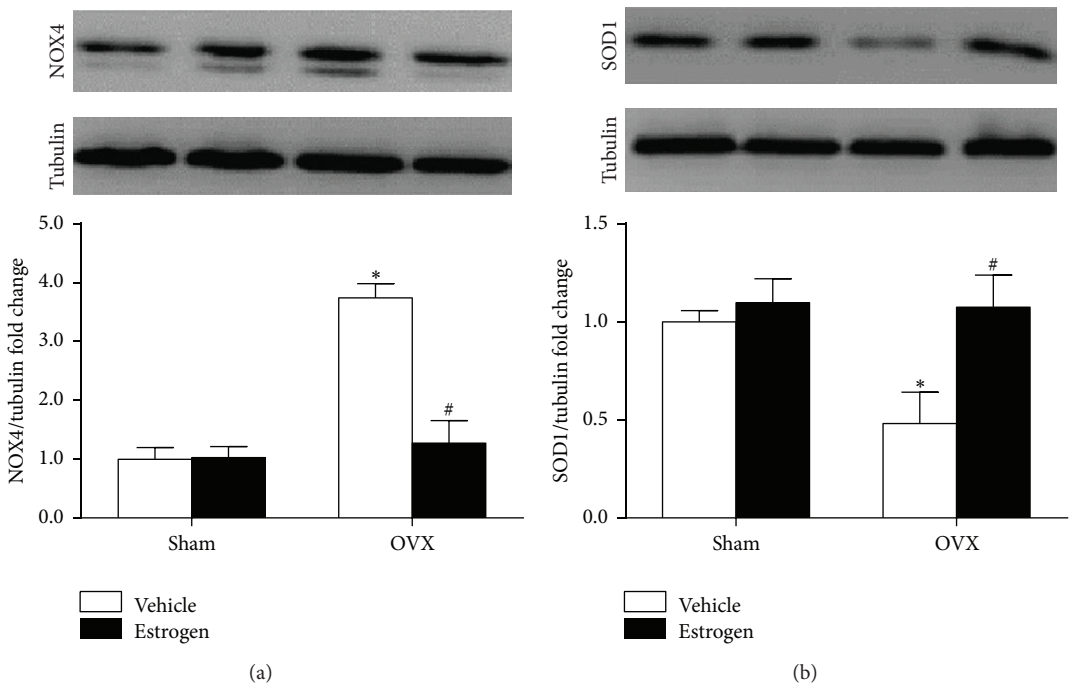

Figure 4: Representative bands (top) and quantification (bottom) of NOX4 (a) and SOD1 (b) in the RVLM of sham and OVX rats. Means ± SEM, $n = 5$/group; $^{*}p < 0.05$ versus sham + vehicle; $^{\#}p < 0.05$ versus OVX + vehicle.

work (an average of 28.5 mmHg). Moreover, there are no differences between dioestrus rats and prooestrus rats in baseline HR, lumbar, and splanchnic and renal sympathetic nerve activity. Although estrous cycle influences, at least partially, cardiovascular function, it has little impact on the conclusion of this study. Second, in addition to RVLM, the other regions such as paraventricular nucleus (PVN) also contribute to regulation of sympathetic tone [7]. Gingerich and Krukoff found that estrogen attenuated the L-glutamate-induced pressor response by microinjection into PVN mediated by ERβ receptor [5]. Site-specific injections of siRNA-ERbeta into PVN augmented aldo-induced hypertension [6]. These evidences indicate that the other centers may play a role in mediating the effect of estrogen on sympathetic outflow. Thirdly, It is not clear which receptor type in the RVLM is involved in meditating the effect of estrogen in OVX rats. Estrogen exerts its physiological effects mainly via two estrogen receptor (ER) subtypes: intracellular receptors (including ERα and ERβ) or membrane estrogen receptors (mERs). It is reported that both ERα and ERβ are expressed in the CNS [39]. Importantly, cardiovascular effects induced by injection of estrogen into the RVLM can be prevented by the ERβ antagonist but not ERα antagonist [4]. However, it is reported that ERα is centrally in the subfornical organ and is involved in the cardiovascular response to angiotensin II [40]. Thirdly, the mechanism by which estrogen regulates the ROS production in the RVLM is not further determined in this work. According to previous studies, the possible link between estrogen receptor and antioxidative stress has been indicated. For example, it is reported that treatment of OVX-SHR with conjugated equine estrogen (CEE) reduces ROS generation and NADPHase activity and enhances SOD and catalase expression in vascular and heart tissue [41, 42]. Moreover, several studies have demonstrated that estrogen is capable of regulating the transcript factor NF-KappaB, which is an important factor for regulating NADPHase expression [39, 43]. Therefore, it is possible that functional state of some transcript factor (e.g., NF-KappaB) associated with NOX4 and SOD is regulated by estrogen. In addition, the significance of estrogen-mediated antioxidative stress in protection against cardiovascular diseases needs to be further investigated. Whether estrogen could effectively reduce the incidence of hypertension and its complication in menopausal women still remains under debate. Although the beneficial effect of estrogen replacement on cardiovascular diseases in menopausal women is widely reported, it is also found that this treatment increases risk of stroke and invasive breast cancer [44].

Conflict of Interests

The authors declare that there is no conflict of interests regarding the publication of this paper.

Authors' Contribution

Fan Hao, Ying Gu, and Xing Tan contributed equally to this work.

Acknowledgment

This work was supported by the National Natural Science Foundation of China (81370363, 31100831, and 81170586).

References

[1] S. M. Harman, E. Vittinghoff, E. A. Brinton et al., "Timing and duration of menopausal hormone treatment may affect cardiovascular outcomes," *The American Journal of Medicine*, vol. 124, no. 3, pp. 199–205, 2011.

[2] L. L. Yanes and J. F. Reckelhoff, "Postmenopausal hypertension," *American Journal of Hypertension*, vol. 24, no. 7, pp. 740–749, 2011.

[3] P. Mosconi, S. Donati, C. Colombo et al., "Role of hormone therapy in the management of menopause," *Obstetrics & Gynecology*, vol. 116, no. 2, part 1, pp. 442–443, 2010.

[4] C. D. Shih, "Activation of estrogen receptor β-dependent nitric oxide signaling mediates the hypotensive effects of estrogen in the rostral ventrolateral medulla of anesthetized rats," *Journal of Biomedical Science*, vol. 16, article 60, 2009.

[5] S. Gingerich and T. L. Krukoff, "Estrogen in the paraventricular nucleus attenuates L-glutamate-induced increases in mean arterial pressure through estrogen receptor beta and NO," *Hypertension*, vol. 48, no. 6, pp. 1130–1136, 2006.

[6] B. Xue, Z. Zhang, T. G. Beltz et al., "Estrogen receptor-beta in the paraventricular nucleus and rostroventrolateral medulla plays an essential protective role in aldosterone/salt-induced hypertension in female rats," *Hypertension*, vol. 61, no. 6, pp. 1255–1262, 2013.

[7] F. R. Calaresu and C. P. Yardley, "Medullary basal sympathetic tone," *Annual Review of Physiology*, vol. 50, no. 1, pp. 511–524, 1988.

[8] G. Grassi, "Sympathetic neural activity in hypertension and related diseases," *American Journal of Hypertension*, vol. 23, no. 10, pp. 1052–1060, 2010.

[9] A. Ikeno, H. Minato, C. Kohayakawa, and J. Tsuji, "Effect of OS-0544, a selective estrogen receptor modulator, on endothelial function and increased sympathetic activity in ovariectomized rats," *Vascular Pharmacology*, vol. 50, no. 1-2, pp. 40–44, 2009.

[10] W. Zhang, M. Kanehara, Y. Zhang, X. Wang, and T. Ishida, "β-blocker and other analogous treatments that affect bone mass and sympathetic nerve activity in ovariectomized rats," *The American Journal of Chinese Medicine*, vol. 35, no. 1, pp. 89–101, 2007.

[11] M. M. El-Mas and A. A. Abdel-Rahman, "Ovariectomy alters the chronic hemodynamic and sympathetic effects of ethanol in radiotelemetered female rats," *Clinical and Experimental Hypertension*, vol. 22, no. 1, pp. 109–126, 2000.

[12] Y. Hirooka, T. Kishi, K. Sakai et al., "Imbalance of central nitric oxide and reactive oxygen species in the regulation of sympathetic activity and neural mechanisms of hypertension," *The American Journal of Physiology: Regulatory, Integrative and Comparative Physiology*, vol. 300, no. 4, pp. R818–R826, 2011.

[13] Y. Hirooka, Y. Sagara, T. Kishi, and K. Sunagawa, "Oxidative stress and central cardiovascular regulation—pathogenesis of hypertension and therapeutic aspects," *Circulation Journal*, vol. 74, no. 5, pp. 827–835, 2010.

[14] K. Bedard and K. Krause, "The NOX family of ROS-generating NADPH oxidases: physiology and pathophysiology," *Physiological Reviews*, vol. 87, no. 1, pp. 245–313, 2007.

[15] B. Halliwell, "Biochemistry of oxidative stress," *Biochemical Society Transactions*, vol. 35, no. 5, pp. 1147–1150, 2005.

[16] T. Kishi, "Regulation of the sympathetic nervous system by nitric oxide and oxidative stress in the rostral ventrolateral medulla: 2012 Academic Conference Award from the Japanese Society of Hypertension," *Hypertension Research*, vol. 36, no. 10, pp. 845–851, 2013.

[17] J. R. Munoz-Castaneda, J. Muntane, M. C. Munoz et al., "Estradiol and catecholestrogens protect against adriamycin-induced oxidative stress in erythrocytes of ovariectomized rats," *Toxicology Letters*, vol. 160, no. 3, pp. 196–203, 2006.

[18] M. Darabi, M. Ani, A. Movahedian, E. Zarean, M. Panjehpour, and M. Rabbani, "Effect of hormone replacement therapy on total serum anti-oxidant potential and oxidized LDL/β2-glycoprotein I complexes in postmenopausal women," *Endocrine Journal*, vol. 57, no. 12, pp. 1029–1034, 2010.

[19] L. Wang, H. Kitano, P. D. Hurn, and S. J. Murphy, "Estradiol attenuates neuroprotective benefits of isoflurane preconditioning in ischemic mouse brain," *Journal of Cerebral Blood Flow & Metabolism*, vol. 28, no. 11, pp. 1824–1834, 2008.

[20] S. Wang, X. Zhu, B. Cong et al., "Estrogenic action on arterial smooth muscle: permissive for maintenance of CRHR2 expression," *Endocrinology*, vol. 153, no. 4, pp. 1915–1924, 2012.

[21] M. C. Irigoyen, J. Paulini, L. J. Flores et al., "Exercise training improves baroreflex sensitivity associated with oxidative stress reduction in ovariectomized rats," *Hypertension*, vol. 46, no. 4, pp. 998–1003, 2005.

[22] Y. K. Wang, D. Shen, Q. Hao et al., "Overexpression of angiotensin-converting enzyme 2 attenuates tonically active glutamatergic input to the rostral ventrolateral medulla in hypertensive rats," *The American Journal of Physiology. Heart and Circulatory Physiology*, vol. 307, no. 2, pp. H182–H190, 2014.

[23] J. L. Wang, L. Wang, Z. T. Wu et al., "Low dose of moxonidine within the rostral ventrolateral medulla improves the baroreflex sensitivity control of sympathetic activity in hypertensive rat," *Acta Pharmacologica Sinica*, vol. 30, no. 12, pp. 1594–1600, 2009.

[24] H. J. Wang, Y. X. Pan, W. Z. Wang et al., "Exercise training prevents the exaggerated exercise pressor reflex in rats with chronic heart failure," *Journal of Applied Physiology*, vol. 108, no. 5, pp. 1365–1375, 2010.

[25] J. Peng, Y. K. Wang, L. G. Wang et al., "Sympathoinhibitory mechanism of moxonidine: role of the inducible nitric oxide synthase in the rostral ventrolateral medulla," *Cardiovascular Research*, vol. 84, no. 2, pp. 283–291, 2009.

[26] J. F. Peng, Z. T. Wu, Y. K. Wang et al., "GABAergic mechanism in the rostral ventrolateral medulla contributes to the hypotension of moxonidine," *Cardiovascular Research*, vol. 89, no. 2, pp. 473–481, 2011.

[27] A. B. Jones, E. E. Bass, L. Fan, and K. S. Curtis, "Estradiol selectively reduces central neural activation induced by hypertonic NaCl infusion in ovariectomized rats," *Physiology & Behavior*, vol. 107, no. 2, pp. 192–200, 2012.

[28] G. M. Rosano, C. Vitale, G. Marazzi, and M. Volterrani, "Menopause and cardiovascular disease: the evidence," *Climacteric*, vol. 10, supplement 1, pp. 19–24, 2007.

[29] R. Prabhushankar, C. Krueger, and C. Manrique, "Membrane estrogen receptors: their role in blood pressure regulation and cardiovascular disease," *Current Hypertension Reports*, vol. 16, no. 1, article 408, 2014.

[30] T. Kishi and Y. Hirooka, "Central mechanisms of abnormal sympathoexcitation in chronic heart failure," *Cardiology Research and Practice*, vol. 2012, Article ID 847172, 7 pages, 2012.

[31] T. Kishi and Y. Hirooka, "Oxidative stress in the brain causes hypertension via sympathoexcitation," *Frontiers in Physiology*, vol. 3, article 335, 2012.

[32] R. K. Goldman, A. S. Azar, J. M. Mulvaney, C. Hinojosa-Laborde, J. R. Haywood, and V. L. Brooks, "Baroreflex sensitivity varies during the rat estrous cycle: role of gonadal steroids," *American Journal of Physiology—Regulatory Integrative and Comparative Physiology*, vol. 296, no. 5, pp. R1419–R1426, 2009.

[33] R. J. Wang, L. J. Lu, L. B. Jin et al., "Clinicopathologic features of breast cancer patients with type 2 diabetes mellitus in southwest of China," *Medical Oncology*, vol. 31, no. 1, article 788, 2014.

[34] R. D. Feldman, "Aldosterone and blood pressure regulation: recent milestones on the long and winding road from electrocortin to KCNJ5, GPER, and beyond," *Hypertension*, vol. 63, no. 1, pp. 19–21, 2013.

[35] F. Chentli, S. Deghima, H. Zellagui, and S. Azzoug, "Volume increase in craniopharyngiomas under growth hormone and/or sex hormones substitution: role of tumors receptors or mere coincidence?" *Journal of Pediatric Neurosciences*, vol. 8, no. 2, pp. 113–116, 2013.

[36] P. Sankar, B. Zachariah, V. Vickneshwaran, S. E. Jacob, and M. Sridhar, "Amelioration of oxidative stress and insulin resistance by soy isoflavones (from *Glycine max*) in ovariectomized Wistar rats fed with high fat diet: the molecular mechanisms," *Experimental Gerontology*, vol. 63, pp. 67–75, 2015.

[37] S. H. Lindsey, A. S. da Silva, M. S. Silva, and M. C. Chappell, "Reduced vasorelaxation to estradiol and G-1 in aged female and adult male rats is associated with GPR30 downregulation," *American Journal of Physiology—Endocrinology and Metabolism*, vol. 305, no. 1, pp. E113–E118, 2013.

[38] Z. Shi and V. L. Brooks, "Leptin differentially increases sympathetic nerve activity and its baroreflex regulation in female rats: role of oestrogen," *The Journal of Physiology*, vol. 593, no. 7, pp. 1633–1647, 2015.

[39] M. H. Faulds, C. Zhao, K. Dahlman-Wright, and J. Gustafsson, "The diversity of sex steroid action: regulation of metabolism by estrogen signaling," *Journal of Endocrinology*, vol. 212, no. 1, pp. 3–12, 2012.

[40] B. Xue, Z. Zhang, T. G. Beltz, F. Guo, M. Hay, and A. K. Johnson, "Genetic knockdown of estrogen receptor-alpha in the subfornical organ augments ANG II-induced hypertension in female mice," *The American Journal of Physiology—Regulatory, Integrative and Comparative Physiology*, vol. 308, no. 6, pp. R507–R516, 2015.

[41] G. S. Ceravolo, F. P. Filgueira, T. J. Costa et al., "Conjugated equine estrogen treatment corrected the exacerbated aorta oxidative stress in ovariectomized spontaneously hypertensive rats," *Steroids*, vol. 78, no. 3, pp. 341–346, 2013.

[42] Y. Xu, S. J. Armstrong, I. A. Arenas et al., "Cardioprotection by chronic estrogen or superoxide dismutase mimetic treatment in the aged female rat," *The American Journal of Physiology—Heart and Circulatory Physiology*, vol. 287, no. 1, pp. H165–H171, 2004.

[43] E. Maloney, I. R. Sweet, D. M. Hockenbery et al., "Activation of NF-kappaB by palmitate in endothelial cells: a key role for NADPH oxidase-derived superoxide in response to TLR4 activation," *Arteriosclerosis, Thrombosis, and Vascular Biology*, vol. 29, no. 9, pp. 1370–1375, 2009.

[44] J. P. Stice, L. Chen, S.-C. Kim et al., "17β-estradiol, aging, inflammation, and the stress response in the female heart," *Endocrinology*, vol. 152, no. 4, pp. 1589–1598, 2011.

Hindawi Publishing Corporation
Oxidative Medicine and Cellular Longevity
Volume 2015, Article ID 384535, 8 pages
http://dx.doi.org/10.1155/2015/384535

Research Article

Chronic Stress Facilitates the Development of Deep Venous Thrombosis

Tao Dong,[1] Yu-Wen Cheng,[1] Fei Yang,[2] Pei-Wen Sun,[1] Chen-Jie Zhu,[1] Li Zhu,[2] and Guo-Xing Zhang[1]

[1]*Department of Physiology, Medical College of Soochow University, Suzhou 215003, China*
[2]*Cyrus Tang Hematology Center, Collaborative Innovation Center of Hematology, MOH Key Lab of Thrombosis and Hemostasis, Jiangsu Institute of Hematology, The First Affiliated Hospital, Soochow University, Suzhou 215003, China*

Correspondence should be addressed to Li Zhu; zhul@suda.edu.cn and Guo-Xing Zhang; zhangguoxing@suda.edu.cn

Received 26 February 2015; Revised 22 March 2015; Accepted 27 March 2015

Academic Editor: Hanjun Wang

The increasing pressure of modern social life intensifies the impact of stress on the development of cardiovascular diseases, which include deep venous thrombosis (DVT). Renal sympathetic denervation has been applied as one of the clinical approaches for the treatment of drug-resistant hypertension. In addition, the close relationship between oxidative stress and cardiovascular diseases has been well documented. The present study is designed to explore the mechanism by which the renal sympathetic nerve system and the oxidative stress affect the blood coagulation system in the development of DVT. Chronic foot shock model in rats was applied to mimic a state of physiological stress similar to humans. Our results showed that chronic foot shock procedure could promote DVT which may be through the activation of platelets aggregation. The aggravation of DVT and activation of platelets were alleviated by renal sympathetic denervation or antioxidant (Tempol) treatment. Concurrently, the denervation treatment could also reduce the levels of circulating oxidation factors in rats. These results demonstrate that both the renal sympathetic nerve system and the oxidative stress contribute to the development of DVT in response to chronic stress, which may provide novel strategy for treatment of clinic DVT patients.

1. Introduction

Deep venous thrombosis (DVT) is a common cardiovascular disease associated sequelae, pulmonary embolism, which is the third most common cause of death from cardiovascular diseases after heart attack and stroke. A slow blood flow, vein wall damage, and a hypercoagulable state are the three principal risk factors for DVT development. Consequently, anticoagulants and thrombolytics are the two main treatments for clinical DVT patients. The triad of risk factors predisposing to thrombus formation, postulated by Virchow, includes changes in the ratio between blood components, the integrity of the vessel wall, and the blood flow rate. The blood coagulation system plays a key role in protecting mammals against lethal bleeding. In all forms of thrombosis, coagulation and inflammation are the two principal pathways acting together to coordinate the body's responses to injury [1, 2].

Over the past few decades, psychological factors, such as stress and depression, have been recognized as important factors affecting human health [3]. Long periods of anxiety will induce the development of cardiovascular diseases. Moreover, by occurring simultaneously, depression and anxiety will aggravate the development of cardiovascular disease even further. In addition, stress and other psychological factors have been demonstrated to be closely related to the occurrence of stroke and myocardial infarction [4]. Numerous studies also have shown that stress can cause long-lasting structural damage to tissues and organs [5]. The chronic electric foot shock procedure has been characterized as a model of uncontrollable and unpredictable psychological stress [6], which has been demonstrated to be able to induce increase in systolic blood pressure [7–9]. However, there is still no report related to the effects of chronic shock on the development of DVT.

The role of sympathetic renal nerve in the development of hypertension has been demonstrated in both experimental and clinical observations [10, 11]. There are two types of sympathetic renal nerve: renal afferent nerves and renal efferent nerve. The afferent sympathetic fibers originate from the kidneys, and by modulating central sympathetic outflow they directly modify neurogenic hypertension. At the same time, the efferent nerve enhances sodium and water retention, stimulates renin release, and alters renal blood flow [10–13]. In this way, both short-term and long-term blood pressure could be influenced by renal sympathetic nerve [13]. Clinical studies have reported the beneficial effects of renal sympathetic denervation in patients with refractory hypertension [9]. In addition to the lowering effect of denervation on blood pressure, additional benefits have also been reported in cardiovascular diseases, diabetes [9], renal dysfunction, cardiac hypertrophy [1], heart failure [9], and arrhythmias [14]. Hypertension, a major risk factor for many diseases, can increase endothelial dysfunction and promote thrombosis and is also closely related to the incidence of cardiocerebral vascular diseases [9]. Therefore, renal sympathetic denervation may provide new strategy in prevention and treatment of cardiovascular diseases under high stress condition.

Recently, experiments show that oxidative stress might be responsible for the change in endothelial function [15]. The increased reactive oxygen species produced by vascular endothelium and circulating blood cells will impair vasomotor and endothelial barrier functions and enhance thrombus formation [16]. Oxidative stress was also found to be a determinant of platelet activation [17], which was the risk factor for atherothrombosis. However, whether chronic stress could affect coagulation system by increasing of oxidative stress is still unknown.

Currently, no reports are directly linking psychological stress with the coagulation system and cardiocerebral vascular diseases. Considering that the activation of the coagulation system has an important influence on both physiological hemostasis and pathological thrombosis [9], we applied foot shock stress model in rats to explore whether chronic could affect the development of DVT and the possible mechanisms involved.

2. Materials and Methods

2.1. Animal Preparation. Ten-week-old male Sprague-Dawley rats, obtained from Shanghai Laboratory Animal Center, were used in this study. Animals were maintained in a 25°C temperature-controlled environment with a 12 : 12-hour light : dark cycle. Rats exposed to the stress protocol were individually placed into a foot shock stress box, where they received a 4-hour session of electrical foot shock through an electrified grid floor delivering a 5-second long 0.15 mA shock every 30 seconds. The rat renal sympathetic nerve was surgically severed while animals were under a 10% chloral hydrate-induced anesthesia. After a one-week recovery period, the foot shock protocol was started. Tempol (10 mg/kg/day) was administered by intraperitoneal injection after the start of the stress protocol [18–20]. Venous thrombosis was induced under anaesthetized conditions with 10% chloral hydrate as previously described by Leung [21]. Briefly, the abdomen was opened, and the inferior vena cava (IVC), after being carefully separated from the surrounding tissues, was ligated tightly just below the left renal vein using a cotton thread. Then, the abdomen was closed with a double layer of sutures, closing the peritoneum with muscles first and then the skin separately. After twelve hours, the animals were anaesthetized again, the abdomen was reopened, and the plasma and thrombus were collected for further analysis [2]. The present study was performed in conformity with the European Convention for the Protection of Vertebrate Animals used for Experimental and Other Scientific Purposes (Council of Europe number 123, Strasbourg, 1985). All surgical procedures were approved by the Soochow University and performed in accordance with the guidelines for the care and use of animals established by the Soochow University.

2.2. Plasma Corticosterone Levels Measurements. Plasma corticosterone levels were measured using a commercially available enzyme-linked immunosorbent assay (ELISA) kit (TSZ Elisa, USA).

2.3. Thrombus Weight Measurements. From the reopened abdominal cavity, the ligated segment of the vena cava was removed and opened longitudinally to remove the formed thrombus, which was rinsed and weighed on filter paper.

2.4. Analysis of the Blood Coagulation Parameters. Prothrombin time (PT), activated partial thromboplastin time (APPT), and thrombin time (TT) were measured using an automated blood coagulation analyzer (Sysmex Corporation CA-50, Japan). From the reopened abdominal cavity, blood (4.5 mL) was collected from the inferior vena cava using a disposable syringe, containing 0.5 mL of a 3.8% sodium citrate solution, and transferred into autoclaved centrifuge tubes. Half of the blood was centrifuged at 3000 rpm for 10 min and the serum was collected. A 0.1 mL serum aliquot was combined to 0.1 mL of PT reagent. After preheating for 20 min, the PT was measured using an automated blood coagulation analyzer, as mentioned above. The APPT and the TT were measured using the same method as the PT.

Platelet aggregation was measured using a platelet aggregation analyzer (Chrono-Log 560 Ca, Germany). After the cavity was reopened, 4.5 mL blood was collected from the inferior vena cava by using a disposable syringe contained with 0.5 mL sodium citrate (3.8%) and then transferred to centrifuge tube. The second half of the blood was centrifuged at 1000 rpm for 10 min to obtain the platelet-rich plasma. The blood remaining in the tube was centrifuged at 3000 rpm for 10 min to prepare the platelet-poor plasma. Then, coagulation of the plasma samples was stimulated using collagen protein and adenosine diphosphate disodium (ADP) (1 mM, 10 mL) as platelet agonists.

2.5. Determination of Plasma Noradrenaline (NA) Concentration. Plasma noradrenaline (NA) levels were measured using a commercially available enzyme-linked immunosorbent assay (ELISA) kit (TSZ Elisa, USA).

Table 1: Effect of shock, denervation, and Tempol treatment on PT, APPT, and TT.

	Control	Shock	Denervation + shock	Tempol + shock
PT (s)	11.97 ± 0.47	10.4 ± 0.15*	11.03 ± 0.52	11.25 ± 0.35
APPT (s)	19.85 ± 0.14	19.05 ± 0.87	19.72 ± 1.26	18.28 ± 2.11
TT (s)	47.98 ± 0.55	64.65 ± 2.75*	56.30 ± 2.41†	53.25 ± 3.16†

PT, prothrombin time; APPT, activated partial thromboplastin time; TT, thrombin time; *$P < 0.05$ versus control group; †$P < 0.05$ versus shock group.

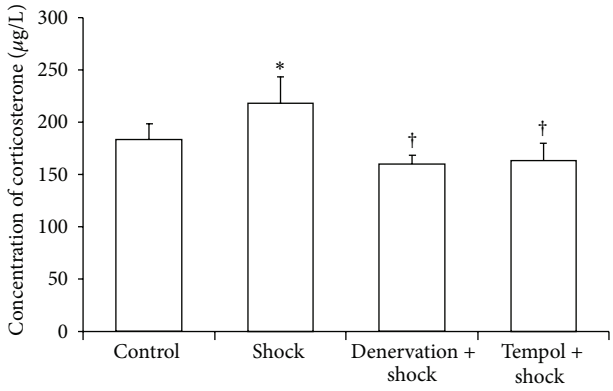

Figure 1: Plasma concentrations of corticosterone. Concentrations of corticosterone in plasma in each group after two-week stress were measured as described in Materials and Methods section. Data of each group ($n = 15$) were presented as mean ± SEM. *$P < 0.05$ compared with control group. †$P < 0.05$ compared with stress group.

2.6. Measurement of Lipid Peroxidation Levels and Plasma Superoxide Dismutase (SOD) and Glutathione Peroxidase (GSH-Px) Activity. Plasma SOD and GSH-Px activity and lipid peroxidation levels (thiobarbituric acid reactive substances, TBARS) were measured using commercially available enzyme-linked immunosorbent assay (ELISA) kits (TSZ Elisa, USA).

2.7. Statistical Analyses. All of the data were presented as the mean ± SEM. The statistical significance of the comparisons between more than two groups was tested using a two-way ANOVA followed by the Newman-Keuls test or using an unpaired two-tailed Student's t-test. P values < 0.05 were considered statistically significant.

3. Results

3.1. Effect of Shock, Denervation, and Tempol Treatment on the Plasma Corticosterone Concentrations. Plasma corticosterone levels (the marker of stress) were markedly increased in the foot shock group when compared with the control group ($P < 0.05$, Figure 1) and were markedly suppressed in both the denervation plus shock and the Tempol plus shock groups compared with the foot shock alone group ($P < 0.05$, Figure 1). This result indicated that chronic foot shock significantly increased plasma corticosterone when the body was under stress, and both of denervation and Tempol treatment could alleviate the stress state.

3.2. Effect of Shock, Denervation, and Tempol Treatment on the Weight of IVC Ligation-Induced Thrombi. Thrombi were collected 12 hours after IVC ligation and weighted. In the foot shock group, the thrombus weight was significantly increased compared with that of the control group ($P < 0.05$, Figure 2). However, the thrombus weight of the denervation plus shock and Tempol plus shock groups remained unchanged compared with the control group thrombi but was significantly decreased compared with the foot shock group thrombi ($P < 0.05$, Figure 2). These results suggest that chronic shock could facilitate the formation of DVT, while both denervation and Tempol treatment could inhibit stress-induced increase of DVT formation.

3.3. Effect of Shock, Denervation, and Tempol Treatment on Blood Coagulation Parameters. After blood collection from the IVC, blood parameters (PT, APPT, TT, and platelet aggregation) were measured. There was a significant difference in the PT, TT, and platelet aggregation parameters between the control and the foot shock groups. The PT of the foot shock group was lower than that of the control group; however, the TT and platelet aggregation parameters were higher in the foot shock group compared with the control group. In parallel, a significant decrease was observed in the TT and platelet aggregation parameters of the denervation plus shock and Tempol plus shock groups compared with the foot shock group ($P < 0.05$, Table 1 and Figure 3). These results reveal that chronic shock could enhance coagulation system by activation of platelet aggregation.

3.4. Effect of Shock, Denervation, and Tempol Treatment on the Plasma Noradrenaline (NA) Concentrations. Foot shock significantly increased the plasma noradrenaline (NA) levels compared with control group ($P < 0.05$, Figure 4). The plasma NA levels in the denervation plus shock and Tempol plus shock group were significantly suppressed compared with the foot shock group ($P < 0.05$, Figure 4). These results confirm the success of the renal denervation surgical procedure.

3.5. Effect of Shock, Denervation, and Tempol Treatment on Plasma SOD and GSH-Px Activity and on TBARS Levels. The plasma SOD activity in the stress group was markedly reduced compared with the control group ($P < 0.05$, Figure 5(a)). The plasma SOD activity in the denervation plus shock and Tempol plus shock groups was markedly elevated compared with the foot shock group ($P < 0.05$, Figure 5(a)).

The plasma GSH-Px activity in the foot shock group was also markedly higher than that of the control group ($P < 0.05$,

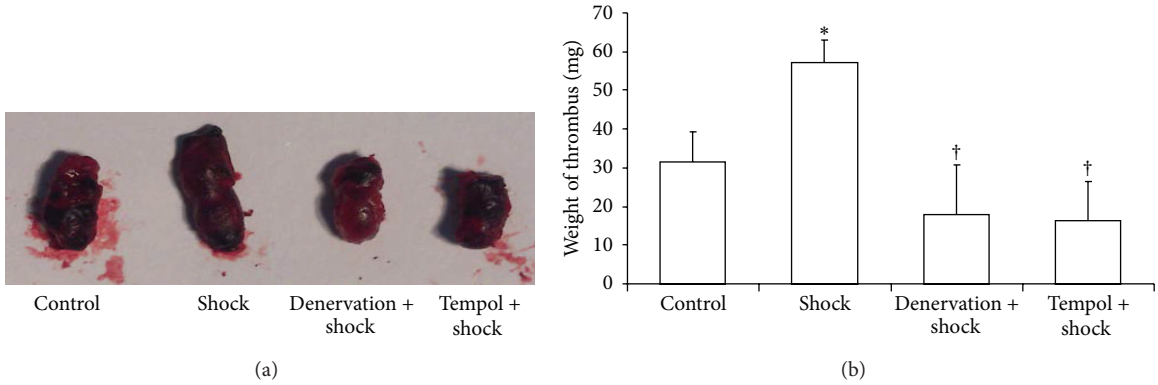

Figure 2: Weight of thrombus. (a) Representative image of thrombus in each group. (b) Weight of thrombus was measured in each group after two-week stress as described in Materials and Methods section. Data of each group ($n = 15$) were presented as mean ± SEM. $^{*}P < 0.05$ compared with control group. $^{\dagger}P < 0.05$ compared with stress group.

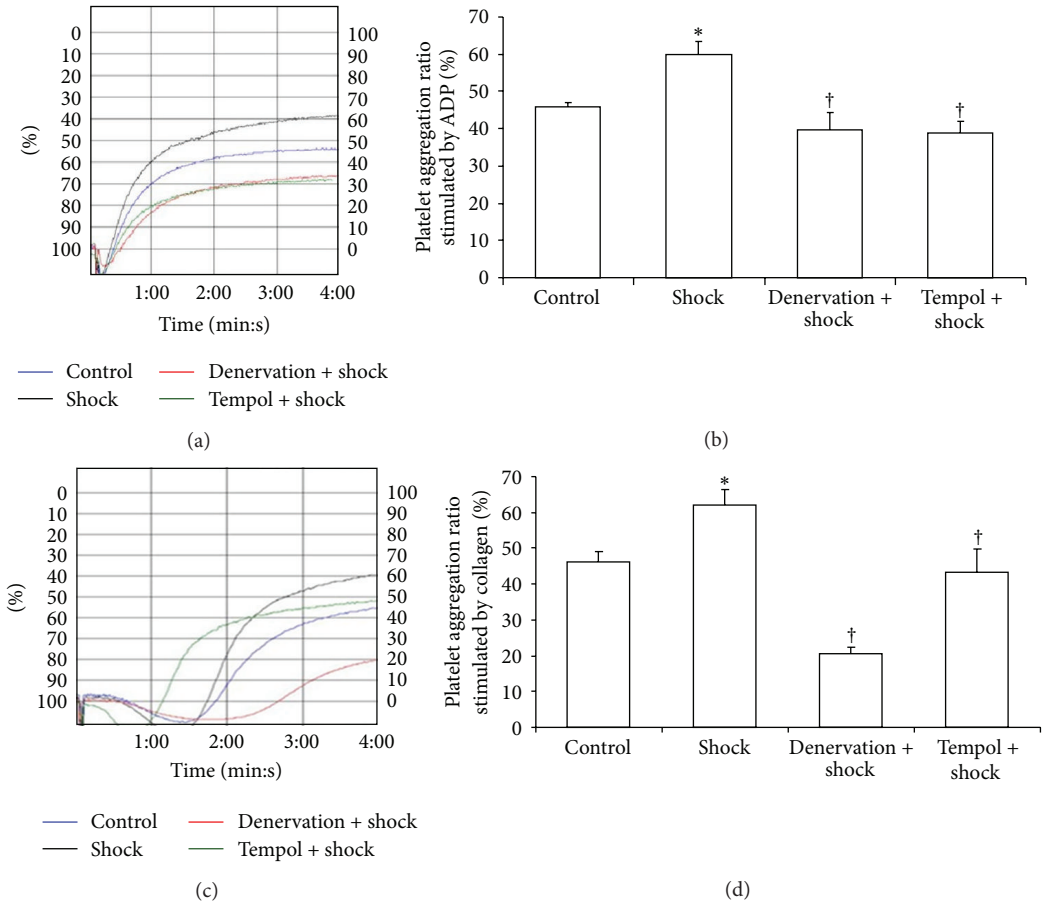

Figure 3: Platelet aggregation rate. Platelet aggregation rate stimulated by ADP (a, b) and platelet aggregation rate stimulated by collagen (c, d) were measured in each group after two-week stress as described in Materials and Methods section through platelet aggregation analyzer. (a) and (c) represent platelet aggregation trace provided by platelet aggregation analyzer. Data of each group ($n = 15$) were presented as mean ± SEM. $^{*}P < 0.05$ compared with control group. $^{\dagger}P < 0.05$ compared with stress group.

Figure 5(b)). The plasma GSH-Px activity in the denervation plus shock and Tempol plus shock groups was markedly elevated compared with the foot shock group ($P < 0.05$, Figure 5(b)).

Foot shock led to a marked increase in the levels of plasma thiobarbituric acid reactive substances (TBARS) compared with control group ($P < 0.05$, Figure 5(c)). The plasma TBARS levels in the denervation plus shock and Tempol plus

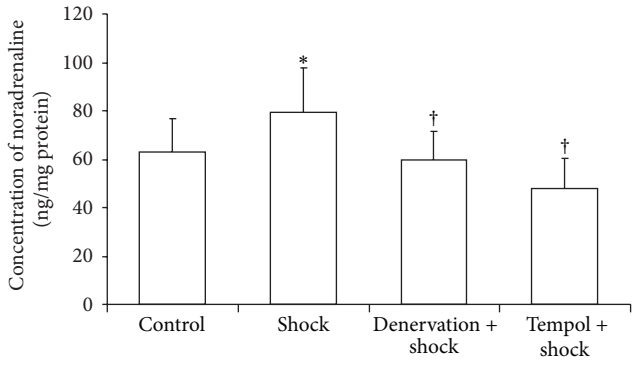

Figure 4: Plasma concentrations of noradrenaline. Concentrations of noradrenaline in plasma in each group after two-week stress were measured as described in Materials and Methods section. Data of each group ($n = 15$) were presented as mean ± SEM. $^{*}P < 0.05$ compared with control group. $^{\dagger}P < 0.05$ compared with stress group.

shock groups were markedly suppressed compared with the foot shock group ($P < 0.05$, Figure 5(c)).

4. Discussion

In this study, we identified that DVT formation is facilitated under stress conditions and that changes in the blood coagulation system are induced by stress. Accumulating data have shown that chronic psychological stress activated two systems: one is hypothalamus-pituitary-adrenal cortex (HPA) system which was mainly mediated by release of catecholamine, cortisol, vasopressin, endorphins, and aldosterone [7, 22]; the other is through activation of sympathetic-adrenal medullar system [22–25]. As shown in the data, the corticosterone levels of chronic shock group were significantly increased, indicating that HPA was activated. What is the role of sympathetic nerve system in response to stress? Since it has been demonstrated that renal sympathetic system activation is highly related to the development of hypertension, and renal denervation is a new treatment in clinical for refractory hypertension patients [26], renal sympathetic system must play an important role in cardiovascular diseases. In addition, recent observations show that high stress condition is highly related to cardiovascular diseases [4] especially cardiac and brain infarction; therefore, we speculate whether chronic stress will activate coagulation system through activation of renal sympathetic nerve system. In the present study, we firstly found that chronic stress could aggregate the DVT formation, suggesting that stress will increase the risk of cardiovascular diseases. In addition, we measured parameters defining the activity of the blood coagulation system, including PT, APPT, TT, and platelet aggregation. Our data showed that there was a significant change in platelet aggregation induced by both ADP and collagen suggesting that the aggravating effect of stress on DVT formation was mediated by activation of platelet. Our results firstly reveal the mechanism which links the high stress condition and cardiovascular diseases. Although our present data clearly demonstrated the role of renal sympathetic nerve system in the chronic shock induced development of DVT, it is hard to identify whether afferent or efferent nerve plays a major role due to the limitation of surgical procedure. We speculate that both are involved in; the reason is that afferent nerve could affect neurogenic control of blood pressure which may contribute to the development of DVT; and efferent nerve could regulate renal secretion of noradrenaline which may also contribute to the development of DVT.

The presence of damaged endothelium and activated clotting factors or platelets facilitates the development and progression of DVT [27]. Platelet aggregation (i.e., when platelets adhere to each other) occurring at sites of vascular injury has long been recognized as critical for thrombosis development [28]. In the present study, we focused mainly on platelet function in DVT. The phenomena of platelet adhesion, release, or aggregation are also known as platelet activation [29]. Activated platelets play an important role in the thrombosis process. Our data show that platelet aggregation increased after stress treatment, along with the enhancement in DVT formation. The platelet count was used to normalize the measure of platelet activity; however, no statistics on the number of platelets in each group were performed.

Our analyses of the plasma GSH-Px and SOD activity, as well as the plasma TBARS level, showed that the body is in a state of oxidative stress induced by chronic foot shock treatment, which was inhibited by renal denervation. Several reports have shown that NAD(P)H oxidase activity could be directly increased by the α1- and β2-receptors [30] through the catecholamines (CA) released by the renal sympathetic nerve. Moreover, β1-receptor antagonists were shown to reduce the vascular oxidative stress caused by NAD(P)H oxidase activation [31]. Therefore, we can say that the renal sympathetic innervation directly increases oxidative stress levels. It has been reported that platelet aggregation, an additional risk factor for thrombus, is associated with oxidative stress [32]. Oxidative stress could directly increase platelet aggregation through oxygen-free radicals located on the platelet surface [32]. Solid evidence has demonstrated that oxidative stress could directly activate platelets through a variety of ways. As the product of oxidative stress O^{2-} could react with platelet or endothelium, then NO derived from ONOO-, which is of particular importance for vascular thrombosis, also has such effects. Several studies have shown that O^{2-} could reduce the threshold for platelet activation to thrombin, collagen, or ADP and O^{2-} may even be able to induce spontaneous aggregation [33–35]. The activated platelet even could produce ROS; the role of this endogenous ROS is similar to exogenous ROS in platelet activation. Generally, several scenarios leading to stress-induced platelet aggregation exist. In the first one, the renal sympathetic nerve is activated by stress, which leads to an increased oxidative stress throughout the body that is then followed by an increase in platelet aggregation. In the other scenario, stress directly triggers the body oxidative stress production, which directly increases platelet aggregation. Renal sympathetic

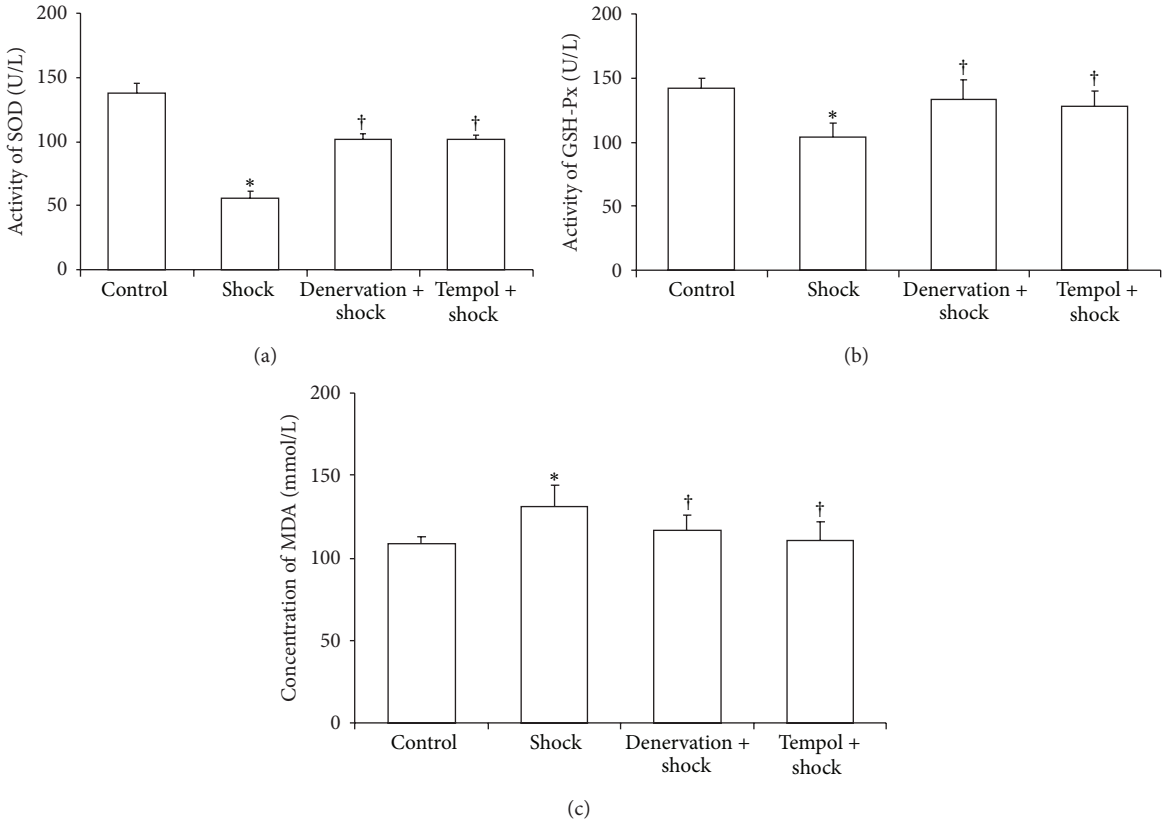

Figure 5: Plasma SOD, GSH-Px activities, and TBARS levels. Plasma SOD activity (a), GSH-Px activity (b), and TBARS levels (c) in each group after two-week stress were measured as described in Materials and Methods section. Data of each group ($n = 15$) were presented as mean ± SEM. $^{*}P < 0.05$ compared with control group. $^{\dagger}P < 0.05$ compared with stress group.

nerve denervation may affect the platelet activation directly, however, the mechanism of which remains to be explored.

Our data showed that chronic stress treatment has no significant effect on either APPT or PT, suggesting that the stress-facilitated DVT may not be associated with the extrinsic or intrinsic coagulation system. Nevertheless, chronic stress treatment could markedly increase TT, which indicates that the conversion time of fibrinogen into fibrin was prolonged because of a hyperfibrinolysis. Hence, we speculate that fibrinolytic hyperfibrinolysis was due to an enhanced blood coagulation under the condition of chronic stress. Concurrently, the renal denervation and antioxidant treatment could decrease platelet aggregation, which in turn suppressed blood coagulation. Based on our data, we could observe that the TT tended towards a normal rate in these two conditions when compared with the shock group.

It should be noted that, in our present observation, we found that Tempol treatment could reduce chronic stress-induced increase of corticosterone levels, suggesting the involvement of oxidative stress in HPA activation induced hormone release, indicating that antioxidant treatment may provide some beneficial effects in HAP activation induced organ injury. However, we did not find any difference between denervation and antioxidant treatments in any parameters, indicating that sympathetic nerve and oxidative stress may independently contribute to the development of DVT induced by chronic shock.

In conclusion, chronic stress could increase platelet aggregation directly via the activation of the renal sympathetic nerve and increase of oxidative stress. Then, DVT comes to be facilitated by the increase in platelet aggregation. A number of studies have shown that atherosclerosis and other cardiovascular diseases are closely associated with oxidative stress [36] and that patients often present with low blood antioxidant levels [37] and enhanced levels of oxidative stress markers [38]. So, in view of the cardiocerebral vascular diseases and DVT, we can prevent and treat these diseases by targeting the therapy at the hormonal and antioxidant levels. In addition to this, it is a new way of therapy through renal sympathetic nerve.

Conflict of Interests

The authors declare no competing financial interests.

Authors' Contribution

Guo-Xing Zhang conceived of and designed the experiments. Tao Dong, Yu-Wen Cheng, Pei-Wen Sun, and Chen-Jie Zhu performed the experiments. Fei Yang assisted with platelet aggregation. Guo-Xing Zhang contributed reagents/materials and analyzed data. Guo-Xing Zhang, Tao Dong, and Yu-Wen Cheng wrote the paper.

Acknowledgments

The authors are grateful to Professor Li Zhu and other members of the Zhu laboratory for experimental advice and assistance. This work was supported by the National Natural Science Foundation of China (81270316, 814170563) and the Research Program of Soochow University (Q413400111).

References

[1] P. Aranda-Lara, M. D. Martínez-Esteban, J. J. Muñoz, and D. Hernández-Marrero, "Renal sympathetic denervation: a new treatment strategy in the management of refractory arterial hypertension," *Nefrologia*, vol. 32, no. 5, pp. 555–557, 2012.

[2] J. M. Herbert, A. Bernat, and J. P. Maffrand, "Importance of platelets in experimental venous thrombosis in the rat," *Blood*, vol. 80, no. 9, pp. 2281–2286, 1992.

[3] M. Nusair, A. Al-dadah, and A. Kumar, "The tale of mind & heart: psychiatric disorders & coronary heart disease," *Missouri Medicine*, vol. 109, no. 3, pp. 199–203, 2012.

[4] S. Neelakantan, "Psychology: mind over myocardium," *Nature*, vol. 493, no. 7434, pp. S16–S17, 2013.

[5] M. R. W. Brown and A. W. Smith, "Dormancy and persistence in chronic infection: role of the general stress response in resistance to chemotherapy," *Journal of Antimicrobial Chemotherapy*, vol. 48, no. 1, pp. 141–142, 2001.

[6] M. Tanaka, "Emotional stress and characteristics of brain noradrenaline release in the rat," *Industrial Health*, vol. 37, no. 2, pp. 143–156, 1999.

[7] L. M. Lu, J. Wang, and T. Yao, "Angiotensin II participates in stress-induced high blood pressure via stimulating hypothalamic vasopressin synthesis and release," *Acta Physiologica Sinica*, vol. 52, no. 5, pp. 371–374, 2000.

[8] Z. S. Lj and X. Y. Liu, "Depressor effect of nucleus arcuatus stimulation in chronic stress-induced hypertensive rat," *Acta Physiologica Sinica*, vol. 44, no. 2, pp. 133–141, 1992.

[9] C. M. Xia, C. H. Shao, L. Xin et al., "Effects of melatonin on blood pressure in stress-induced hypertension in rats," *Clinical and Experimental Pharmacology and Physiology*, vol. 35, no. 10, pp. 1258–1264, 2008.

[10] H. Kirchheim, H. Ehmke, and P. Persson, "Sympathetic modulation of renal hemodynamics, renin release and sodium excretion," *Klinische Wochenschrift*, vol. 67, no. 17, pp. 858–864, 1989.

[11] V. Kon, "Neural control of renal circulation," *Mineral and Electrolyte Metabolism*, vol. 15, no. 1-2, pp. 33–43, 1989.

[12] P. A. Sobotka, F. Mahfoud, M. P. Schlaich, U. C. Hoppe, M. Böhm, and H. Krum, "Sympatho-renal axis in chronic disease," *Clinical Research in Cardiology*, vol. 100, no. 12, pp. 1049–1057, 2011.

[13] F. Mahfoud, T. F. Lüscher, B. Andersson et al., "Expert consensus document from the European Society of Cardiology on catheter-based renal denervation," *European Heart Journal*, vol. 34, no. 28, pp. 2149–2157, 2013.

[14] C. Ukena, A. Bauer, F. Mahfoud et al., "Renal sympathetic denervation for treatment of electrical storm: first-in-man experience," *Clinical Research in Cardiology*, vol. 101, no. 1, pp. 63–67, 2012.

[15] T. J. Guzik, N. E. West, E. Black et al., "Vascular superoxide production by NAD(P)H oxidase: association with endothelial dysfunction and clinical risk factors," *Circulation Research*, vol. 86, no. 9, pp. E85–E90, 2000.

[16] D. N. Granger, S. F. Rodrigues, A. Yildirim, and E. Y. Senchenkova, "Microvascular responses to cardiovascular risk factors," *Microcirculation*, vol. 17, no. 3, pp. 192–205, 2010.

[17] P. Minuz, P. Patrignani, S. Gaino et al., "Determinants of platelet activation in human essential hypertension," *Hypertension*, vol. 43, no. 1, pp. 64–70, 2004.

[18] G.-X. Zhang, K. Ohmori, Y. Nagai et al., "Role of AT1 receptor in isoproterenol-induced cardiac hypertrophy and oxidative stress in mice," *Journal of Molecular and Cellular Cardiology*, vol. 42, no. 4, pp. 804–811, 2007.

[19] R. J. Bolterman, M. C. Manriquez, M. C. Ortiz Ruiz, L. A. Juncos, and J. C. Romero, "Effects of captopril on the renin angiotensin system, oxidative stress, and endothelin in normal and hypertensive rats," *Hypertension*, vol. 46, no. 4, pp. 943–947, 2005.

[20] M. Yoshiyama, K. Takeuchi, T. Omura et al., "Effects of candesartan and cilazapril on rats with myocardial infarction assessed by echocardiography," *Hypertension*, vol. 33, no. 4, pp. 961–968, 1999.

[21] P. S. Leung, "The peptide hormone angiotensin II: its new functions in tissues and organs," *Current Protein and Peptide Science*, vol. 5, no. 4, pp. 267–273, 2004.

[22] R. S. Zimmerman and E. D. Frohlich, "Stress and hypertension," *Journal of Hypertension*, vol. 8, no. 4, pp. S103–S107, 1990.

[23] E. A. Anderson, C. A. Sinkey, and A. L. Mark, "Mental stress increases sympathetic nerve activity during sustained baroreceptor stimulation in humans," *Hypertension*, vol. 17, no. 4, pp. I-43–I-49, 1991.

[24] B. G. Wallin, W. Delius, and K. E. Hagbarth, "Comparison of sympathetic nerve activity in normotensive and hypertensive subjects," *Circulation Research*, vol. 33, no. 1, pp. 9–21, 1973.

[25] P. Mustacchi, "Stress and hypertension," *Western Journal of Medicine*, vol. 153, no. 2, pp. 180–185, 1990.

[26] G. Grassi, A. Mark, and M. Esler, "The sympathetic nervous system alterations in human hypertension," *Circulation Research*, vol. 116, no. 6, pp. 976–990, 2015.

[27] M. Brozovic, "Mechanisms of deep vein thrombosis: a review," *Journal of the Royal Society of Medicine*, vol. 72, no. 8, pp. 602–605, 1979.

[28] S. P. Jackson, "The growing complexity of platelet aggregation," *Blood*, vol. 109, no. 12, pp. 5087–5095, 2007.

[29] D. L. Musselman, U. Marzec, M. Davidoff et al., "Platelet activation and secretion in patients with major depression, thoracic aortic atherosclerosis, or renal dialysis treatment," *Depression and Anxiety*, vol. 15, no. 3, pp. 91–101, 2002.

[30] J. E. Faber, C. L. Szymeczek, S. S. Salvi, and H. Zhang, "Enhanced α1-adrenergic trophic activity in pulmonary artery of hypoxic pulmonary hypertensive rats," *American Journal of Physiology: Heart and Circulatory Physiology*, vol. 291, no. 5, pp. H2272–H2281, 2006.

[31] M. Oelze, A. Daiber, R. P. Brandes et al., "Nebivolol inhibits superoxide formation by NADPH oxidase and endothelial dysfunction in angiotensin II-treated rats," *Hypertension*, vol. 48, no. 4, pp. 677–684, 2006.

[32] M. Aviram, "LDL-platelet interaction under oxidative stress induces macrophage foam cell formation," *Thrombosis and Haemostasis*, vol. 74, no. 1, pp. 560–564, 1995.

[33] J. P. de la Cruz, P. J. Garcia, and F. S. de la Cuesta, "Dipyridamole inhibits platelet aggregation induced by oxygen-derived free radicals," *Thrombosis Research*, vol. 66, no. 4, pp. 277–285, 1992.

[34] R. I. Handin, R. Karabin, and G. J. Boxer, "Enhancement of platelet function by superoxide anion," *Journal of Clinical Investigation*, vol. 59, no. 5, pp. 959–965, 1977.

[35] D. Salvemini, G. De Nucci, J. M. Sneddon, and J. R. Vane, "Superoxide anions enhance platelet adhesion and aggregation," *British Journal of Pharmacology*, vol. 97, no. 4, pp. 1145–1150, 1989.

[36] H. Mangge, "Antioxidants, inflammation and cardiovascular disease," *World Journal of Cardiology*, vol. 6, no. 6, pp. 462–477, 2014.

[37] C. Murr, B. M. Winklhofer-Roob, K. Schroecksnadel et al., "Inverse association between serum concentrations of neopterin and antioxidants in patients with and without angiographic coronary artery disease," *Atherosclerosis*, vol. 202, no. 2, pp. 543–549, 2009.

[38] D. Fuchs, P. Avanzas, R. Arroyo-Espliguero, M. Jenny, L. Consuegra-Sanchez, and J. C. Kaski, "The role of neopterin in atherogenesis and cardiovascular risk assessment," *Current Medicinal Chemistry*, vol. 16, no. 35, pp. 4644–4653, 2009.